2014

NOVEL COMPOUNDS AS POTENTIAL ALZHEIMER'S DISEASE THERAPEUTICS AND INHIBITORS OF THE NLRP3 INFLAMMASOME

Jeremy E. Chojnacki
Virginia Commonwealth University

NOVEL COMPOUNDS AS POTENTIAL ALZHEIMER'S DISEASE THERAPEUTICS AND INHIBITORS OF THE NLRP3 INFLAMMASOME

A dissertation submitted in partial fulfillment of the requirements for the degree of doctor of philosophy at Virginia Commonwealth University.

by

JEREMY EDWARD CHOJNACKI, BS

Advisors:
SHIJUN ZHANG, PHD
ASSOCIATE PROFESSOR, DEPARTMENT OF MEDICINAL CHEMISTRY

GLEN KELLOGG, PHD
PROFESSOR, DEPARTMENT OF MEDICINAL CHEMISTRY

Virginia Commonwealth University
Richmond, Virginia
December, 2014

Acknowledgements

First and foremost, I would like to thank VCU for giving me the opportunity to pursue my Ph.D. in medicinal chemistry. By extension, I would like to acknowledge my alma mater, Virgina Tech, in providing me the education necessary to continue my education at the graduate level. Naturally, I would like thank my committee members, Dr. Antonio Abbate, Dr. Yan Zhang, and Dr. Darlene Brunzell, for providing me with invaluable feedback in my academic and personal pursuits. I am also very thankful for having Dr. Shijun Zhang and Dr. Glen Kellogg as my advisors. They both were highly influential in guiding me through my graduate journey and truly have a strong commitment to the education and development of their students. Again, I cannot thank them enough. I would also like to acknowledge all current and previous members of the Shijun Zhang research group, including Dr. Xing Yan, Dr. Jiangmin Chen, Dr. Ahmed Salam, Dr. Datong Zhang, Sasha Fraser, Ronak Ghandi, and Emily Wade. In addition, John Saathoff has proven a lively lab mate and great colleague, and I have thoroughly enjoyed working with him. I also could not have made it through this last year with the support and partnership of Katie Perlowski. Her ability to stick with me through thick and thin is truly a virtue, and I am forever in her debt. And of course, I would not be here without the encouragement from all my friends and family. Thank you so much. But above all, I would like to express my gratitude to Dr. Kai Liu. Kai served as a post-doc in the Zhang group and has been my personal mentor over the last four years, teaching me more about chemistry and biology than I can even remember. I would not be exaggerating when I said we've probably spent more time together in those years than with anyone else in our lives. His guidance and counsel in all things academia, and in life as well, have proven absolutely invaluable, and I am truly blessed to call him my mentor, and even more so, a dear friend.

Table of Contents

Page

List of Tables

List of Figures

List of Schemes

Abbreviations

AD	-	Alzheimer's Disease
ABC	-	ATP-Binding Cassette
ACh	-	Acetylcholine
AChE	-	Acetylcholinesterase
AChEI	-	Acetylcholinesterase Inhibitor
ACN	-	Acetonitrile
ADDL	-	Amyloid-ß Derived Diffusible Ligands
AFM	-	Atomic Force Microscopy
AIM2	-	Absent In Melanoma 2
AMI	-	Amyloid Myocardial Infarction
APP	-	Amyloid Precursor Protein
ASC	-	Apoptosis Speck-like Protein containing a CARD
Aß	-	Amyloid-ß
AßO	-	Amyloid-ß Oligomer
BBB	-	Blood Brain Barrier
CaMKII	-	Ca2+/calmodulin-dependent protein kinase II
CARD	-	Caspase-Recruitment Domain
cdk5	-	Cyclin-Dependent Kinase-5
CLR	-	C-type Lectin Receptor
COX	-	Cytochrome Oxidase

CTFß	-	C-Terminal Fragment ß
CTFγ	-	C-Terminal Fragment γ
DAMP	-	Danger-Associate Molecular Pattern
DCC	-	N,N'-Dicyclohexylcarbodiimide
DCE	-	Dichloroethane
DCFH	-	2,7-dichlorodihydrofluorescein
DCFH-DA	-	2,7-dichlorodihydrofluorescein diacetate
DCM	-	Dichloromethane
DMAP	-	4-Dimethylaminopyridine
DMEM	-	Dulbecco's Modified Eagle Medium
DMF	-	Dimethylformamide
DMSO	-	Dimethyl Sulfoxide
EDC	-	1-Ethyl-3-(3-dimethylaminopropyl)carbodiimide46
ESI	-	Electrospray Ionization
EtOAc	-	Ethyl acetate
FBS	-	Fetal Bovine Serum
FTDP-17	-	Frontotemporal Dementia with Parkinsonism linked to chromosome 17
GSK-3ß	-	Glycogen Synthase Kinase 3ß
HOBt	-	Hydroxybenzotriazole
IL-1ß	-	Interleukin-1ß
iNOS	-	Inducible Nitric-Oxide Synthase

IRI	-	Ischemia and Reperfusion Injury
LPS	-	Lipopolysaccharide
LR	-	Lipid Rafts
LRR	-	Leucine-Rich Repeat
MAPT	-	Microtubule-Associated Tau Protein
mitoROS	-	Mitochondrial Reactive Oxygen Species
mPTP	-	Mitochondrial Permeability Transition Pore
NAC	-	N-acetylcysteine
NFT	-	Neurofibrillary Tangles
NLR	-	Nucleotide-binding domain Leucine-rich Repeats
NLRP3I	-	NLRP3 Inflammasome
NMDA	-	N-methyl-D-aspartate
NMDAR	-	N-methyl-D-aspartate Receptor
NMM	-	N-methyl morpholine
NMR	-	Nuclear Magnetic Resonance
NOD	-	Nucleotide binding and Oligomerization Domain
PAMP	-	Pathogen-Associated Molecular Pattern
PC12	-	Pheochromacytoma cell 12
PMA	-	Phosphomolybdic Acid
Poly(dA:dT)	-	Poly-deoxyadenylic-deoxythymidylic acid sodium salt
PP2A	-	Protein Phosphatase 2A

PRR	-	Pathogen Recognition Receptor
PYD	-	Pyrin Domain
RLR	-	Rig-I-Like Receptor
ROS	-	Reactive Oxygen Species
sAPPß	-	Soluble Amyloid Precursor Protein ß
SAR	-	Structure-Activity Relationship
SOD	-	Superoxide Dismutase
SRM	-	Selected Reaction Monitoring
T2DM	-	Type 2 Diabetes Mellitus
TC	-	Tetracycline
TFA	-	Trifluoroacetic Acid
THF	-	Tetrahydrofuran
ThT	-	Thioflavin T
TLC	-	Thin-layer chromatography
TLR	-	Toll-Like Receptor
TMS	-	Tetramethylsilane
TPP	-	Triphenylphosphine
Trolox	-	6-hydroxy-2,5,7,8-tetramethyl chroman-2-carboxylic acid
TTC	-	2,3,5-Triphenyl-2H-tetrazolium chloride

Abstract

NOVEL COMPOUNDS AS POTENTIAL ALZHEIMER'S DISEASE THERAPEUTICS AND INHIBITORS OF THE NLRP3 INFLAMMASOME

By Jeremy Edward Chojnacki, B.S.

A dissertation submitted in partial fulfillment of the requirements for the degree of doctor of philosophy at Virginia Commonwealth University.

Virginia Commonwealth University, 2014

Advisors:
Shijun Zhang, Ph.D.
Associate Professor, Department of Medicinal Chemistry

Glen Kellogg, Ph.D.
Professor, Department of Medicinal Chemistry

Alzheimer's disease is a devastating neurodegenerative disorder and the leading cause of dementia. The disease manifests via a multitude of pathologies including neuroinflammation, oxidative stress, metal ion dyshomeostasis, and naturally, cell death. To date, no cure is available for Alzheimer's disease, and FDA approved treatments only offer symptomatic relief. To address the multifaceted nature of this disorder, the design of several diverse compounds, targeting a variety of pathological effects, was generated. First, a series of ligands based on curcumin and diosgenin were synthesized following the bivalent design strategy. These

multifunctional ligands were evaluated for their neuroprotective abilities in MC65 cells. From this series, two compounds were discovered to have neuroprotective ability, antioxidative function, and anti-Aß oligomerization (AßO) properties. A second set of molecules was also designed, wherein a hybrid compound strategy was utilized. These ligands combined pharmacophore features from two natural products known to have neuroprotective properties, curcumin and melatonin. A representative hybrid was to shown to protect MC65 cells from Aß-induced toxicity and to have significant anti-oxidative activity. Additionally, two analogs retain the same beneficial features as the representative hybrid, but are active in the low nanomolar range. Mechanistic studies propose that the primary function conferring protection is through disruption of interactions between AßOs and partner proteins associated with the mitochondria. Furthermore, one potent hybrid was also shown to be able to pass the BBB. Lastly, studies of glyburide, a common antidiabetic medication, have previously noted its off-target anti-inflammatory effects. These effects were found to be specific for the NLRP3 inflammasome, which has been implicated as an effector in AD development. Therefore, syntheses of a series of glyburide analogs were performed. From biological characterization, the initial analog synthesized was able to successfully inhibit the NLRP3 inflammasome and reduce IL-1ß expression without affecting blood glucose. Further *in vivo* studies demonstrated an ability to prevent or ameliorate adverse inflammation-related outcomes in inflammatory models of peritonitis and acute myocardial infarction. Two other analogs were also found to prevent IL-1ß release at concentrations similar to that of the initial analog. Altogether, these investigations have yielded three novel series of compounds, all capable of modifying Alzheimer's disease pathology. Results from biological assays warrant future investigations into the development,

optimization, and characterization of these analogs as potential treatments for Alzheimer's disease.

1 Introduction

1.1 Alzheimer's Disease

1.1.1 General Pathology and Statistics

Alzheimer's disease (AD) is a progressive neurodegenerative disorder, affecting an estimated 5.2 million people in the United States and up to 30 million people worldwide in 2014.[1] The National Institute of Aging defines AD as "an irreversible, progressive brain disease that slowly destroys memory and thinking skills, and eventually even the ability to carry out the simplest tasks."[2] First described in 1901 by Dr. Alois Alzheimer, for whom the disease is named, he called it the "disease of forgetfulness."[3] This is a very accurate description, as AD is typified by an accelerated decline in memory and cognitive function. As the disease progresses from mild to moderate to severe, patients diagnosed with AD will slowly lose their ability to reason properly and show increasingly poor judgment and deterioration of memory. Eventually, there may even be a complete loss of coherent communication. As motor skills decline, simple tasks become more difficult, and ultimately, daily personal assistance will become required. Minor personality changes will also become more pronounced, manifesting as irritation, agitation, anger, and paranoia. Often times, these mood swings occur in the evenings and have therefore become known as "sundowning" syndrome.[4] Over time, these effects will culminate and effectively incapacitate the patient, leaving them susceptible to secondary infections and illnesses, such as pneumonia, bladder infections, bedsores, cardiovascular disease, and complications associated with falls. Although patients with AD could eventually experience enough brain degeneration to shut down vital bodily functions, mortality is almost always caused by one of these co-morbidities.[5, 6]

Statistically, AD is the leading cause of dementia, accounting for more than 50% of all cases, and is the 6th leading cause of death in the United States. Furthermore, the number of deaths associated with AD rose 68% between 2000 and 2010, while other diseases with traditionally high mortality rates actually decreased, i.e. breast cancer, prostate cancer, heart disease, stroke, and HIV.[1] The estimated economic burden of AD for the United States for 2014 alone is $214 billion, and approximately 1 in 5 Medicare dollars is spent on caring for an individual with AD. These costs are projected to rise to $1.2 trillion by 2050.[1]

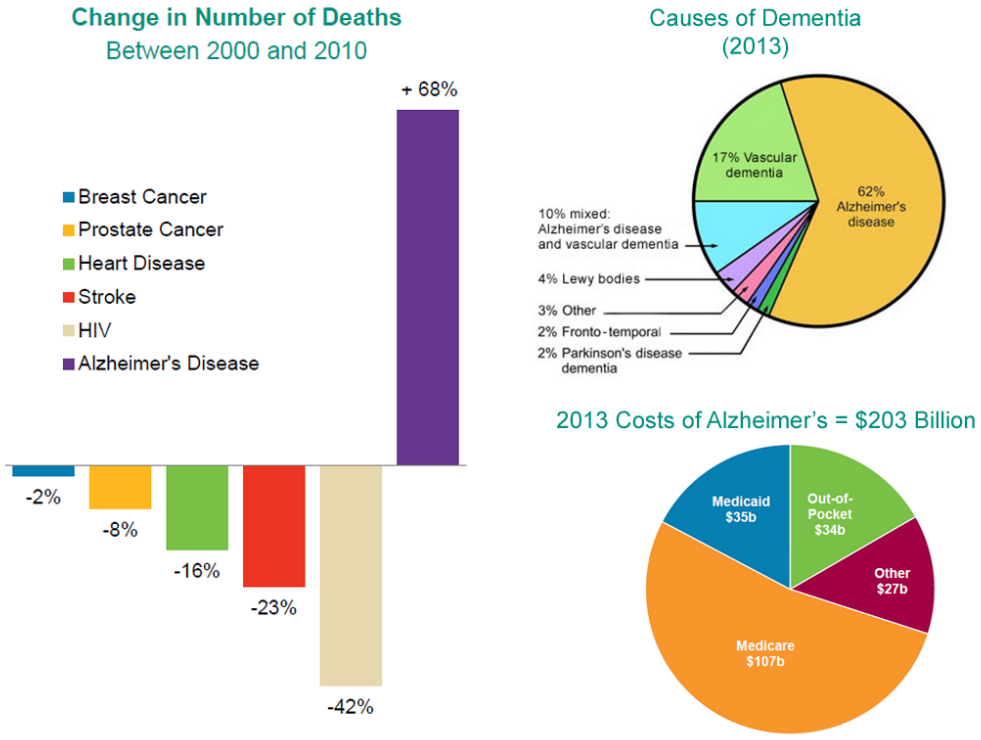

Figure 1. Facts and figures describing AD 2013. Adapted from the Alzheimer's Association.[1]

1.1.2 Molecular Etiology

Despite significant advances in the understanding of AD and its pathology, the exact etiology of the illness remains elusive. However, AD does exhibit two pathological hallmarks that are specific to the disease and are used for postmortem confirmation. These hallmarks are amyloid-ß (Aß) plaques and neurofibrillary tangles (NFT) comprised of hyperphosphorylated tau proteins.[7-9]

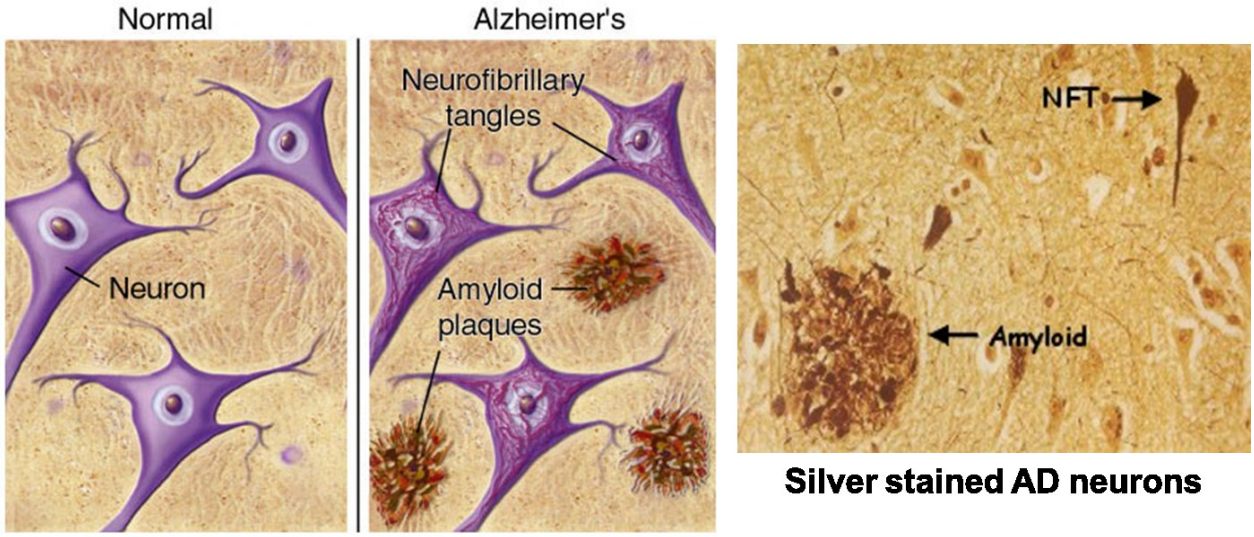

Figure 2. Cartoon and silverstain depicting Aß plaques and NFTs. Adapted from BrightFocus® Foundation.[10]

1.1.2.1 Amyloid-ß protein

Amyloid-ß are a collection of proteins around 40 amino acid residues that are the main constituents of the histological plaques found in the brains of patients with AD. While lengths can vary from 36 to 43, $Aß_{40}$ and $Aß_{42}$ are by far the two most common forms of the protein and are of the highest concentrations *in vivo*.[11-13] Notably, $Aß_{42}$ has been suggested to be the more

toxic of the two species, due to its higher degree of hydrophobicity and increased tendency to oligomerize.[14] Aß is formed by the sequential cleavage of the Amyloid precursor protein (APP), first by ß-secretase and then γ-secretase, as shown in Figure 1.

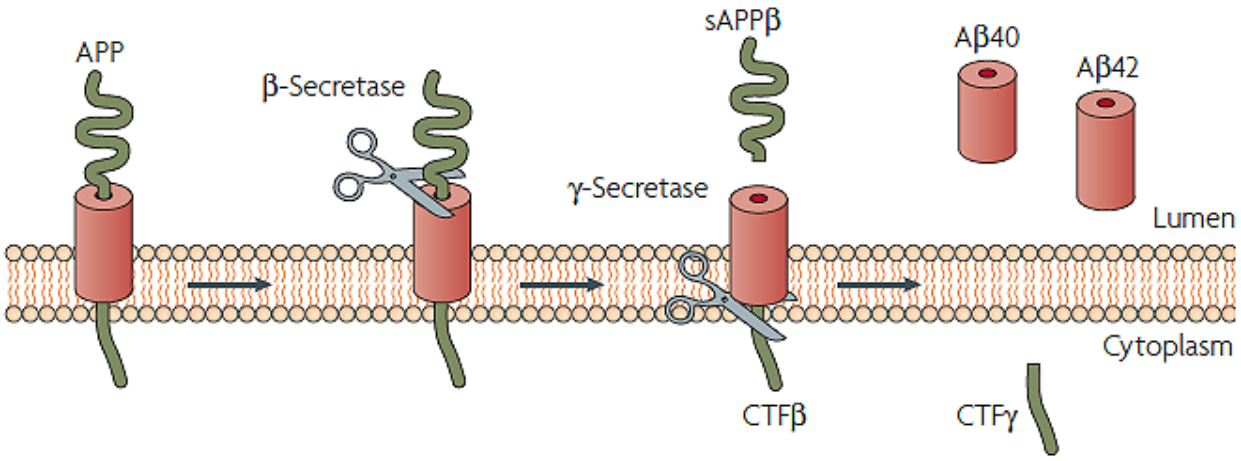

Figure 3. Proteolytic formation of Aß from APP. Abbreviations: C-terminal fragment ß (CTFß); C-terminal fragment γ (CTFγ); soluble amyloid precursor protein ß (sAPPß). Adapted from Shaw et al.[15]

Under normal physiological conditions, Aß peptides are properly metabolized and cleared by the body. However, in AD, Aß peptides are not properly cleared and can form aggregates. This increase in local Aß concentration is known as amyloidosis.[16] Aggregation of Aß follows a defined structural hierarchy. Monomers can readily oligomerize to form amyloid-ß oligomers (AßO) of varying molecular weights from low-weight soluble dimers and trimers to high-weight insoluble octamers and larger species.[17] These oligomers can then stack on each other to form long 'strings' of protofibrils. Once these protofibrils are formed, they will then twist around each other generating fully formed fibrils. Lastly, these insoluble fibrils will then self-associate and condense, leading to the creation of the fully matured plaques. The high degree of plaque formation found in AD brains compared to normal brains gave rise to the "amyloid hypothesis," which states that Aß is the primary causal protein related to AD pathology.[18, 19]

Despite the prevalence of large Aß plaques in AD brains, there is increasing evidence suggesting that it is in fact not the plaques that are responsible for the neurotoxic effects seen in AD, but rather the low-weight soluble oligomers that are causing disruption of synaptic plasticity and cognitive impairment.[17] Studies from brain samples of patients with AD show a correlation between the amount AßOs and the severity of dementia.[20, 21] Although varying sizes and assemblies of oligomers, along with their respective mechanisms, have been suggested in the literature, there is no clear consensus that represents the exact or major mechanism of toxicity *in vivo*. Only the requirement of AßOs is consistent. Aß-derived diffusible ligands (ADDLs) are globular structures of synthetic $Aß_{42}$ that represent the smallest pieces of protofibrils. Deshpande et al. examined the effects of high-weight oligomers, ADDLs, and fibrillar Aß added to primary human cortical neurons. While all three species exhibited toxicity, the oligomers caused extensive cell death within 24 hr, compared to 5 days for ADDLs and 10 days at four-fold higher concentrations for Aß fibrils.[22] In agreement, Hoshi et al. demonstrated low-weight spherical oligomeric Aß structures were significantly more toxic in cultured neurons by MTT assay, in comparison to Aß fibrils.[23] Several other studies have also indicated that non-fibrillar, oligomeric forms of Aß are quite possibly the primary toxic species.[24-30]

1.1.2.1.1 Lipid Rafts and Amyloid-ß Oligomers

Lipid rafts (LR) are densely packed microdomains of cellular membranes consisting of various types of sphingolipids, glycolipids, lipoproteins, and cholesterol.[31, 32] They serve as specific sites for the association of certain proteins and carbohydrates with the cell membrane, and influence membrane fluidity and membrane protein trafficking and regulation.[31, 33]

Recently, significant evidence has implicated LRs as a key cellular site in the formation of AßOs and the production of reactive oxygen species (ROS).[31, 32, 34] Cells enriched in LR domains exhibit an accelerated rate of oligomerization, and disruption of these domains affects Aß membrane binding and protects cells from Aß-mediated toxicity.[32, 35] Additionally, APP processing enzymes, ß- and γ-secretase, have been identified within the LR, suggesting these domains act as critical platforms for the production and oligomerization of Aß.[36-38] While a single component of the LR has not yet been recognized to be the sole mediator of the oligomerization process, formation of AßOs has been shown to be dependent on metal ions, pH, and ganglioside interactions.[35, 39-42] Due to the importance of AßOs in the development and progression of AD, LRs represent an attractive target for therapeutic intervention.

1.1.2.2 Tau proteins

Tau, also known as microtubule-associated protein tau (MAPT), is the major protein associated with microtubules. Functionally, tau's chief role is the stabilization of microtubule assemblies, which serve as cellular 'roads' in the trafficking of proteins to and from the nucleus and dendrites or axons.[43, 44] Under normal physiological conditions, tau proteins are dephosphorylated and bind tightly to microtubules. Once the tubule has served its purpose, it is disassembled, and the individual tubulin proteins will be available to form new tubules, as needed. In order to disassociate tau, the protein is phosphorylated, which decreases its binding affinity. Under pathological conditions, however, tau proteins may become hyperphosphorylated, preventing their association with microtubules, and actually promoting their self-assembly into paired helical filaments that form the base structures of NFTs.[44-46]

Several kinases have been implicated in this increase in phosphorylation, including glycogen synthase kinase 3ß (GSK-3ß), cyclin-dependent kinase-5 (cdk5), and Ca^{2+}/calmodulin-dependent protein kinase II (CaMKII). Additionally, protein phosphatase 2A (PP2A) has been shown to be the major phosphatase responsible for removal of tau phosphate groups.[7, 47, 48] Because of the strong correlation between the amount of NFTs present and the degree of cognitive decline, these enzymes have been explored as potential targets for AD-modifying therapeutics. However, there is strong evidence proposing that increases in Aß preclude the formation of NFTs in disease progression.[49-51] Additionally, the presence of NFTs has been seen in other neurodegenerative disorders, as well, collectively known as tauopathies and including frontotemporal dementia with Parkinsonism linked to chromosome 17 tau (FTDP-17 tau), Pick's disease, supranuclear palsy, chronic traumatic encephalopathy, among others.[52-55] Together, these suggest Aß oligomerization and fibrillization occur upstream from NFT formation, and are also the main toxic species responsible for AD development.

1.1.3 Oxidative Stress in AD

Oxidative imbalance occurs when the ability of endogenous antioxidants fails to adequately quench the production of oxidant species or ROS. Consequently, this leads to cellular oxidative stress, which can go on to cause molecular oxidative damage, altered cellular function, and even cell death.[56, 57] Cellular metabolic dysfunction is one contributor to oxidative stress and has been well documented in AD. For example, there is an increase in oxidative utilization for energy in comparison to glucose utilization in AD patients.[58] Furthermore, reduced metabolic function in the brain has been shown to precede any brain atrophy or

cognitive impairments.[59] One critical organelle responsible for the metabolism and ROS production is mitochondria. Improper functioning of mitochondria can lead to reduced energy production and increased oxidative stress, which are also characteristic in AD.[60, 61] Indeed, the most consistent defects in AD mitochondria are deficiencies with pyruvate dehydrogenase complex, α-keto-glutarate dehydrogenase complex, and cytochrome oxidase (COX), all of which are heavily involved in the metabolic reduction of oxygenated species.[62-64] Superoxide dismutase (SOD), an enzyme responsible for the conversion of the oxidative superoxide ion into molecular oxygen or hydrogen peroxide, also displays elevated expression levels compared to controls in AD brains and red blood cells, suggesting an innate compensatory mechanism against the rise of free radical damage from the disease pathology.[65-67] Furthermore, Aß and APP have also been shown to directly interact with mitochondria, potentially causing increases in ROS associated with AD.[68-70] Cytotoxic studies involving the addition of Aß to neuronal cell cultures demonstrated a protective effect when H_2O_2-degrading enzyme catalase was added to the media, illustrating a strong connection between Aß, ROS, and cell death.[71]

Additionally, redox-active metals have also been implicated in AD. Biometals, in particular Cu^{2+}, Fe^{3+}, and Zn^{2+}, are all capable of catalyzing the formation of the hydroxyl radical, and therefore, dyshomeostasis of these metals can lead to neuronal damage characterized by oxidative stress.[72, 73] Moreover, the concentrations of these metals have been shown to be increased in Aß senile plaques in comparison to surrounding neuropils.[74] In fact, there is evidence demonstrating the ability of Aß to bind these biometals, and in the case of Fe and Cu, convert them to their more reactive reduced states (Fe^{2+} and Cu^{+}). These reduced forms can then readily trap molecular oxygen and generate hydroxyl and peroxide free radicals via Fenton-like

redox chemistry.[75-77] These findings implicate a strong role for metal ion dyshomeostasis in oxidative stress that contributes to AD pathology.

1.1.4 Neuroinflammation in AD

In addition to oxidative stress, neuroinflammation has been shown to play an important role in the pathology of AD. Under physiological conditions, neuroinflammation is a normal part of the innate immune system, protecting the CNS from invading organisms or harmful proteins released from necrotic or apoptotic cells.[78, 79] Because of their 'defensive' nature, these types of localized, acute inflammations are generally beneficial and are quickly shut down once the stimuli have been removed. Any unintended damage is often limited and reversible.[78, 80] Under pathological conditions, however, these inflammatory reactions are not properly regulated, and excessive activation of microglia and release of pro-inflammatory signaling molecules can lead to permanent neuronal damage. This kind of pathological inflammation is typically considered a low-grade chronic inflammation, leading to a slow, progressive increase in cytokine and chemokine concentration, and consequently cellular dysfunction. Increased levels of inflammatory markers have been observed in AD brain tissue, including high levels of cytokines and chemokines, and evidence of increased microglial activation and astrocyte reactivity, both of which can also contribute to oxidative stress.[81, 82] Interestingly, epidemiological studies have shown a decreased risk of developing AD concomitant with NSAID consumption.[83-85] The exact etiology of the chronic inflammation observed in AD has not yet been fully elucidated. Significant evidence, however, has demonstrated the inflammation triggering ability of the Aß peptide, either by direct activation of microglia and astrocytes

(mentioned in a later section) or by indirectly inducing neurodegeneration, which then signals the start of an inflammatory cascade.[9, 86]

1.1.5 AD Treatments

Despite our ever-increasing understanding, there is as of yet no 'cure' for AD. Currently, the only FDA approved treatments for AD fall into two categories: acetylcholinesterase inhibitors and N-methyl D-asparate receptor antagonists.

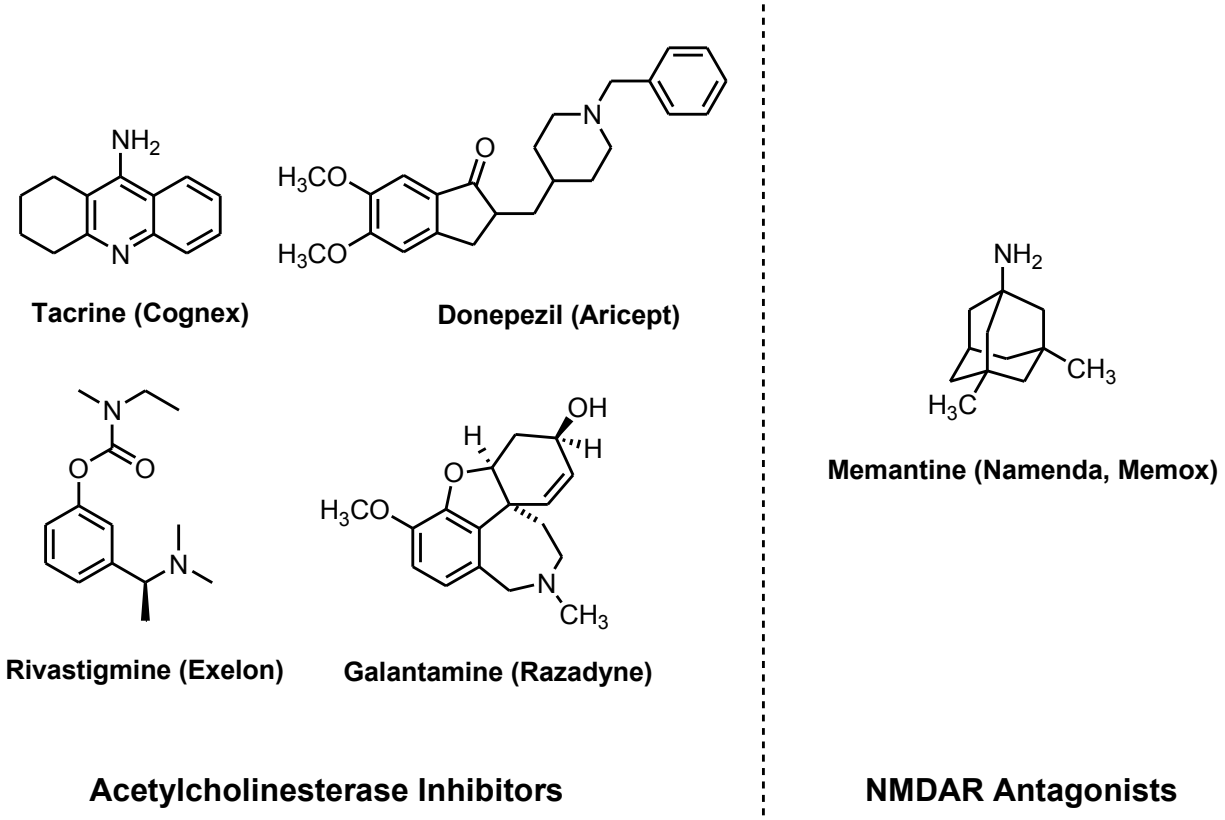

Figure 4. Current FDA approved treatments for Alzheimer's disease.

1.1.5.1 Acetylcholinesterase inhibitors

Analysis of neurotransmitters in the cerebral cortex shows a sharp reduction in a vast majority of species that correlates with neuronal loss. One of the most consistent findings in AD brain samples was a decline in cholinergic transmission that was highly correlated to the degree of severity of AD.[87] Therefore, it was hypothesized that a lack of acetylcholine was responsible for the manifested dementia seen in AD. This gave rise to the "cholinergic hypothesis," which suggests that AD dementia is caused by degeneration of cholinergic neurons, and consequently counteracting this deficiency by increasing concentrations of acetylcholine (ACh) would be beneficial in disease treatment.[88] Indeed, CNS cholinergic antagonists, such as scopolamine, can induce a befuddled state that closely resembles AD dementia.[89] Furthermore, it was proposed that the reduction of ACh may be related in part to degeneration of cholinergic neurons in the hippocampus and cerebral cortex, areas where a high degree neuronal loss is found, and the nucleus basalis of Meynert, which projects into several areas of the cortex.[90, 91] According to the "amyloid hypothesis," neurodegeneration leading to this cholinergic deficiency is caused by Aß.

By logical extension, a viable approach to treating AD by increasing levels of ACh in the synapse would be to inhibit the enzyme responsible for the breakdown and metabolism of ACh, namely acetycholinesterase (AChE). This is the primary reason why the only drugs available on the market for the treatment of mild to moderate AD are AChE inhibitors (AChEI). Presently, there are four inhibitors approved by the FDA for the treatment of AD: tacrine, donepezil, rivastigmine, and galantamine (Figure 4). Tacrine represents the first FDA approved AChEI and is a potent centrally acting inhibitor.[92] However, due to the severe side effects of use, including cramping, anorexia, nausea, vomiting, diarrhea, and liver toxicity, and the availability of later generation inhibitors, tacrine has been discontinued in the US.[93] Donepezil is a selective, long-

acting AChEI with little effect in peripheral tissues and produces modest improvements in cognitive scores in AD patients. Rivastigmine and galantamine, also second generation AChEIs, yield a similar degree of enhancement as compared with donepezil.[93-95] Adverse effects associated with donepezil, rivastigmine, and galantamine administration are comparable to those seen with tacrine, but are generally less frequent and severe. Furthermore, use of these compounds is not limited by hepatotoxicity. Due to the longer half-life of donepezil (once-daily dosing), it is generally more preferred over rivastigmine or galantamine (twice-daily dosing) and is also the only AChEI approved for moderate AD.[94, 95]

1.1.5.2 N-methyl D-aspartate receptor antagonists

Glutamate is the most prevalent neurotransmitter found in the body and the primary activator of N-methyl-D-aspartate (NMDA) receptors.[96-98] NMDA receptors (NMDAR) are ionotropic receptors, allowing the flow of Na^+, Ca^{2+}, and K^+ into and out of the cell. While moderate activation of NMDARs is critical for synaptic plasticity, learning, and memory function, excessive activation sharply increases intracellular Ca^{2+} concentrations, leading to excitotoxicity.[97, 99, 100] Dysfunction of glutaminergic neurotransmission has been associated with AD etiology, and therefore, targeting this system offers an alternative method to treatment, other than AChEIs.[100, 101] Memantine (Figure 4) is the first and only FDA approved NMDAR antagonist at present, and is also the only approved treatment for late-stage, severe AD.[102, 103] It functions by blocking NMDA channels in an activation-dependent manner, thereby limiting excessive, pathological activation without affecting normal physiological activation.[103, 104] Statistics regarding the efficacy of mematine treatment, however, are somewhat controversial.

One randomized clinical trial including 252 patients found that memantine significantly reduced mental deterioration.[104] However, another double blind, placebo-controlled trial involving 350 patients did not confirm this result. No statistically significant benefit was found after 24 weeks, the study end point, on any primary or secondary outcomes measured.[105] There is evidence although to suggest that a combination therapy with donepezil may provide greater benefits on cognition and behavior, as demonstrated in a recent 24 week trial including 322 patients.[106]

The main problem with both these classes of drugs is that they only offer symptomatic relief and are not treating the underlying pathology. Supporting synaptic transmission in a steadily degenerating neuronal network may provide temporary reprieve, but does nothing to prevent the progressive deterioration. Eventually, patients will fail to respond to these drug families as the disease advances.[93, 107] Therefore, there is a strong impetus to find novel, effective therapies that target the cause of AD.

1.1.5.3 Aß reduction approaches

One other strategy for the treatment of AD has been to find drugs that would lower levels of Aβ in the brain. To this end, ß-secretase inhibition, γ-secretase modulation, and Aß-immunization approaches have been researched.[100] Active immunization was initially explored against Aß, but has suffered significant setbacks. One of the first clinical trials for an Aß-antibody (AN1792) was conducted by Elan Pharmaceuticals, later Wyeth. Initial studies showed success in reduction of Aß plaques in animal models.[108] Phase II trials, however, were suspended due to reports of meningoencephalitis, an inflammatory reaction in the brain, from which 5 patients receiving the drug died.[109] Following these results, passive immunization using

monoclonal antibodies was attempted. So far, two monoclonal antibodies, Bapineuzumab (Pfizer and Johnson & Johnson) and Solanezumab (Eli Lilly), recently failed Phase III trials due to lack of improvement over placebo.[110, 111] Despite these negative results, there are still several monoclonal antibodies undergoing clinical trials, notably Gantenerumab (Roche, Phase III), Aducanumab (Biogen Idec, Phase Ib), and BAN2401 (Eisai and Biogen Idec, Phase II).[112-115]

Inhibition of beta secretase, also referred to as BACE, is a major therapeutic strategy, garnering a significant amount of attention and money. One reason for this intense interest is that BACE knockout mice are healthy with no detectable pathological consequences.[116] The major challenges facing BACE inhibitors are their molecular weight, which greatly affects their ability to cross the blood brain barrier.[117] Even with this hurdle, several BACE inhibitors have made it to clinical trials. Unfortunately, two of the first inhibitors to reach trials have failed. LY2811376 (Eli Lilly) was halted after Phase I trials due to high-dose toxicity.[118] LY2886721 (Eli Lilly) was stopped during Phase II trials over potential hepatotoxicity from abnormal liver tests.[119] Recently, another inhibitor from Roche (RG7129) was terminated after Phase I trials. Notably, Merck has developed an inhibitor that has reached Phase III trials (MK-8931) and is still ongoing, set to end in 2018.[120] Despite these setbacks, BACE still represents a highly pursued target by pharmaceutical companies. Inhibition of gamma secretase,[121] on the other hand, has lost a large degree support as viable strategy in Aß reduction. Notch is a transmembrane protein essential for cell differentiation, specifically in the intestine and immune system, and like Aß, is cleaved by γ-secretase.[122-126] Administration of γ-secretase inhibitors elicited severe side effects in clinical trials, including gastrointestinal toxicity and eosinophilia, presumably due to blockage on Notch processing.[123-126] Both Semagacestat (Eli Lilly) and Avagacestat (BMS) failed clinical trials, Phase III and II, respectively, after performing worse

than placebo.[127, 128] It has been suggested that γ-secretase modulators, preventing Aß cleavage with no effects on Notch, may still be a feasible strategy,[121] but focus has mostly δed to ß-secretase inhibitors.

1.2 NLRP3 Inflammasome

As previously mentioned, neuroinflammation plays a significant impact in AD pathology. Interestingly, clinical trials of NSAIDs alone as a treatment for AD have so far been largely unsuccessful.[129-132] This suggests that perhaps inflammation is primarily mediated via different pathways than those that NSAID act upon and that therapeutics targeting novel inflammatory proteins may be needed. One inflammatory complex recently linked to AD pathology is the NLRP3 (NALP3/Cyropyrin) inflammasome (NLRP3I).

1.2.1 Molecular Biology

The inflammasome, so named as a combination between "inflammation" and the Greek suffix "soma", meaning body, is a multimeric protein complex that facilitates the production of pro-inflammatory signaling factors.[133] Under normal conditions, it is an essential part of the immune response, responsible for protecting tissue from cellular damage, metabolic stress, and infection. However, excessive activation of the inflammasome can lead to acute or chronic inflammation, resulting in prolonged release of cytokines and chemokines. Formation is triggered by danger-associated molecular patterns (DAMPs), typically cellular debris, or pathogen-associated molecular patterns (PAMPs), usually from invading organisms.[134, 135] After

the complex is formed, it activates caspase-1, which rapidly produces interleukin-1ß (IL-1ß), a cytokine inducing the activation of several inflammatory cascades, from the inactive pro-form. This, in turn, leads to a form of cell death known as pyroptosis.[136]

1.2.1.1 The inflammasome complex

The inflammasome consists of three individual proteins: the sensing protein, the scaffolding protein, and caspase-1. Pattern recognition receptors (PRR) are proteins or parts of proteins that recognize DAMPs and PAMPs. In the humans, there are four families of PRRs: toll-like receptors (TLR), C-type lectin receptors (CLR), RIG-I-like receptors (RLR), and nucleotide-binding domain leucine-rich repeats (NLR). Of these, TLRs and CLRs are cell-membrane associated and respond to a variety of DAMPs and PAMPs, including peptides, glycopeptides, lipopeptides, and nucleic acids. RLRs and NLRs are cytosolic sensors. RLRs primarily respond to viral RNA and elicit an anti-viral response. NLRs, on the other hand, respond to a multitude of stimuli, including pathogens and intracellular debris.[137, 138] Notably, TLRs and NLRs can cooperate with each other to produce IL-1ß, facilitating generalized or specialized immune responses to various factors.[137] In the human genome, 22 NLR genes have been identified, although not all have been verified to form an inflammasome. Of all observed inflammasomes, three include sensing proteins from the NLR family: NLRP1, NLRP3, and NLRC4. The AIM2 (absent in melanoma 2) inflammasome is the only non-NLR complex known thus far.[139] Each sensor recognizes different stimuli. The NLRP1 protein has been shown to be active in response to anthrax lethal toxin,[140] whereas NLRC4 is specific for Gram-negative bacteria with a type III or IV secretion system and flagellin.[141, 142] It is proposed that

the AIM2 inflammasome is critical for host defense against bacterial and viral pathogens, as AIM2 recognizes dsDNA released in the cytosol.[143, 144] As for the NLRP3 protein, it is the most studied of all inflammasomes and has been associated with a numerous range of diseases and pathogens, including crystalline material, pore-forming toxins, bacteria, viruses, and localized ROS.[145, 146]

Structurally, the NLRP3 protein contains three distinct regions. The leucine rich-repeat domain (LRR) is responsible for the actual sensing of DAMPs and PAMPs. In the inactive state, the LRR region self-associates with the nucleotide binding and oligomerization domain (NOD), the second region of the protein, and locks the molecule into a 'closed' formation, preventing complex formation. Once the LRR region recognizes its partnering molecular patterns, however, it induces a conformational change in the NOD that consequently opens up the pyrin domain (PYD). Once the PYD is open, it is free to associate with its partner protein, apoptosis-associated speck-like protein containing a caspase-recruitment domain (CARD) (ASC).[147] The ASC protein primarily serves as an adapter protein, linking the NLR protein to pro-caspase-1. It consists of two domains, the PYD, which interacts and binds with the PYD of NLRP3, and a CARD, that will bind to caspase-1. Activation of ASC is characterized by aggregation of ASC to itself or NLRs upon their activation, forming the characteristic 'specks' seen in immunohistological stains.[148, 149] Some evidence has suggested that overactive ASC oligomerization can occur independently of NLR initiation in some instances, and still lead to caspase-1 binding and activation.[150] Caspase-1 is the third component of the inflammasome. Once ASC binds to NLR, its CARD can now partner to pro-caspase-1's CARD, initiating the conversion of caspase from its pro form into the fully matured form.[151, 152] Activated caspase-1 proteolytically cleaves pro-IL-1ß and pro-IL-18 into their respective mature forms. Of these, IL-

1ß is a major initiator of downstream pro-inflammatory cascades. Together, this complex represents the complete inflammasome (Figure 5).

1.2.1.2 NLRP3 inflammasome activation pathway

Activation of the NLRP3 inflammasome requires two steps. As previously mentioned, NLR proteins work in tandem with TLR proteins to tailor the inflammatory response based on the stimulus.[137] The first step is the priming step, and typically involves activation of TLR receptors. This will generate an increase in the transcription of pro-IL-1ß and NLRP3 via NF-κB stimulation, increasing their availability in the cytosol. The second step is the triggering step. Here, a specific DAMP or PAMP will interact with the NLRP3, initiating the inflammasome formation pathway and ultimately, the cleavage of pro-IL-1ß (Figure 5).[138] Notably, TLR activation alone has been known to lead to the expression of IL-1ß. However, there is also an increase in local ATP concentrations, which can activate NLRP3. Excessive ATP interacts with P2X7 receptors causing a dramatic increase in K^+ efflux, which is analogous to the action of pore-forming toxins. Recent evidence suggests that this may be acting as a previously unknown secondary potentiator in the inflammatory process, leading to NLRP3 complex formation.[153, 154] For these reasons, lipopolysaccharide (LPS) and ATP are typically used to prime and trigger NLRP3 inflammasome formation for *in vitro* analysis.[155-157]

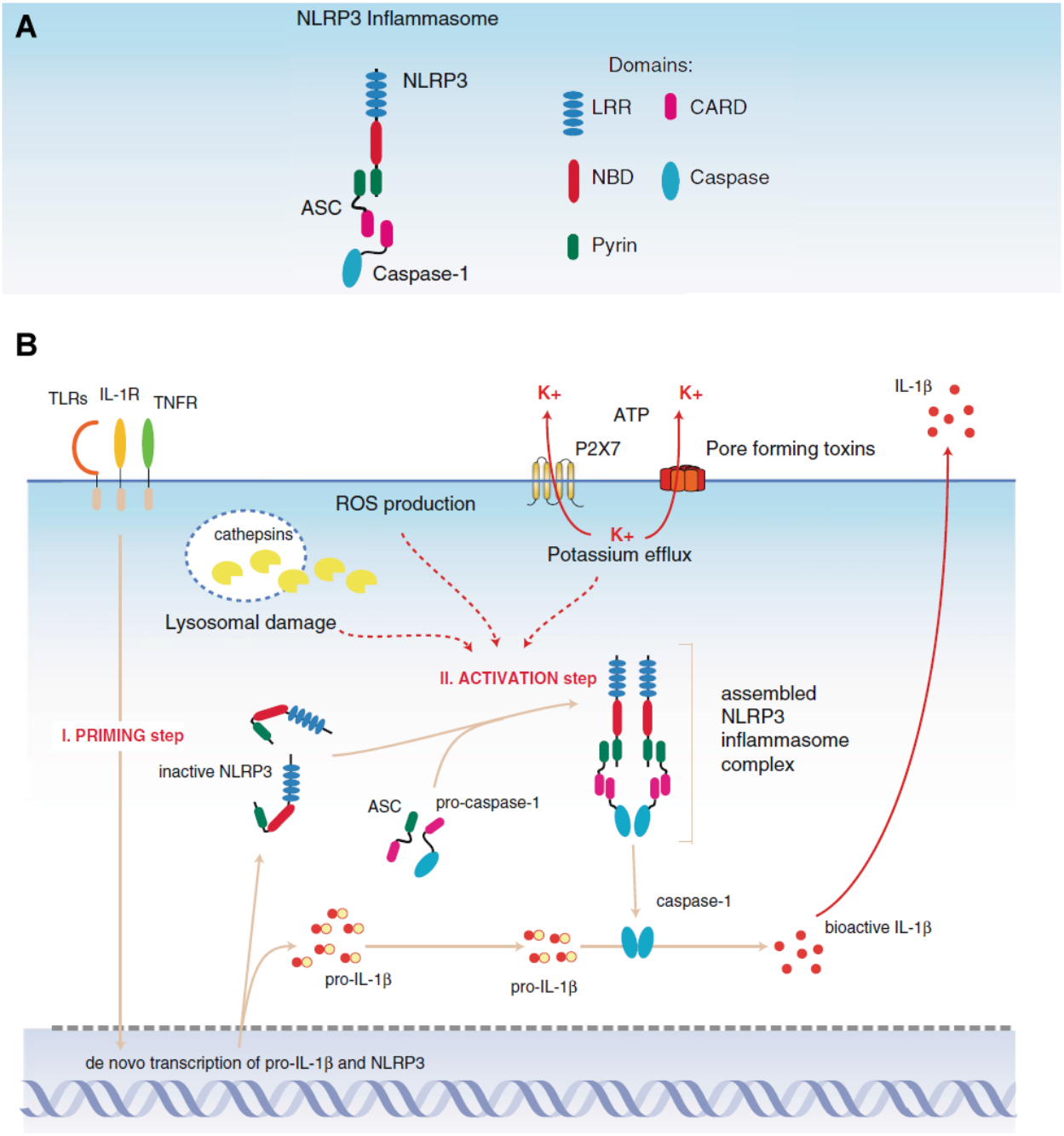

Figure 5. Activation of the NLRP3 inflammasome. A. Cartoon representing the NLRP3 inflammasome and the respective domains for each protein. B. Depiction of the NLRP3 activation pathway. Activation of TLRs induces transcription of pro-IL-1ß and NLRP3. DAMPs and PAMPs then trigger the formation of the NLRP3 inflammasome, leading to processing of IL-1ß, which potentiates the inflammatory response. Adapted from Bauernfeind et al.[138]

1.2.2 Applications

The NLRP3I specifically has been linked to the development and persistence of a number of pathologies, including AD, ischemia-reperfusion injury, obesity, and type II diabetes.[139, 158-161] There is strong evidence suggesting that activation of the NLRP3I in microglia is due to the excitatory interaction between Aß and NLRP3. Akama and Van Eldik have shown that inducible nitric-oxide synthase (iNOS) expression, a pro-inflammatory marker, is highly upregulated upon stimulation of Aß in astrocytic cells. This increase was determined to be preceded by and dependent on IL-1ß and TNF-α induction, suggesting a potential role for inflammasome formation.[162] In a related study, Halle *et al.* revealed that IL-1ß release and caspase-1 activity are greatly increased in primary microglial cells upon addition of Aß in a dose-dependent fashion. Furthermore, knock-out of ASC or NLRP3 both completely abolished this IL-1ß release, indicating that the NLRP3I is a major contributing factor to Aß-induced neuroinflammation *in vitro*.[163] This was confirmed by follow-up investigations by Heneka *et al*. in AD mouse models. NLRP3 or caspase-1 knock-outs in APP/PS1 transgenic mice resulted in significant improvements in cognitive function and reductions in IL-1ß and caspase-1 concentrations. Decreased deposition of Aß was also observed. This clearly demonstrates a correlation between NLRP3I activation and AD pathology *in vivo*.[164]

Ischemia and reperfusion injuries (IRI) occur when tissue or an organ goes through a period of ischemia, causing local deleterious effects due to hypoxia and hypoglycemia, and is then reperfused with blood flow, leading to more damage to the ischemic tissue, as well as surrounding systems, by introduction of neutrophils and the related inflammatory response to the necrotic tissue.[139] Myocardial IRI due to myocardial infarction induces profound inflammation in cardiomyocytes that has been associated with high mortality rates.[165, 166] This response has

been linked to the NLRP3 inflammasome. Kawaguchi *et al.* has demonstrated increased levels of IL-1ß in heart tissue after IRI, leading to a rise in inflammatory cell infiltration and cytokine expression. Moreover, in ASC or caspase-1 deficient mice, IL-1ß concentration, infarct size, and myocardial fibrotic tissue were all reduced following IRI.[167] Other studies have shown caspase-1 inhibition and IL-1 receptor antagonism to be protective against IRI induced apoptosis and adverse cardiac remodeling, as well.[168-171]

1.3 Hypotheses and Aims

In order to address the various effects stemming from AD and treat the underlying causes of the disease, compounds exhibiting multifunctionality may yield more promising results than current treatment strategies. To this end, two series of novel compounds were designed as multifunctional ligands, possessing anti-oxidative, anti-Aß oligomerization, and neuroprotective properties. In chapter 2, the feasibility of using a bivalent design strategy will be explored, following positive results from previous reports.[172-174] The hypothesis is that the use of compounds with a connection of a steroid analog to a multifunctional compound via a flexible linker will act as multifunctional, potent neuroprotectants. In chapter 3, a second series employing the "hybrid molecule" approach will be examined, given its success in other areas.[175] The hypothesis here is that the blending of two compounds with known protective functions into a single novel entity will confer enhanced protective abilities. Natural products curcumin **1**, melatonin **2**, and caprospinol **5**, a cholesterol **3** analog and diosgenin **4** derivative, were all incorporated in these design approaches of chapters 2 and 3 (Figure 6). The aim for these compounds was to find leads that impart significant protection in neuronal cells and to examine

their respective mechanisms of action. This will also lend credence to the application of multifunctional compounds and help guide future synthetic designs. In chapter 4, the hypothesis is that the inhibition of the NLRP3 inflammasome will provide beneficial anti-inflammatory effects that will lead to amelioration of pathological conditions. To ascertain these goals, a third series of molecules were designed and synthesized as NLRP3 inhibitors, based on the structure of glyburide, a common anti-diabetic medication. The aim for these analogs was to explore the feasibility of using this scaffold as an NLRP3 inhibitor and to discover any potential leads for further development in treating AD. Furthermore, any positive effects found would bolster the inhibition of the NLRP3 inflammasome as a potential target for therapeutic intervention. Altogether, these compounds will further validate their respective design strategies and aid in the discovery of novel, drug therapys.

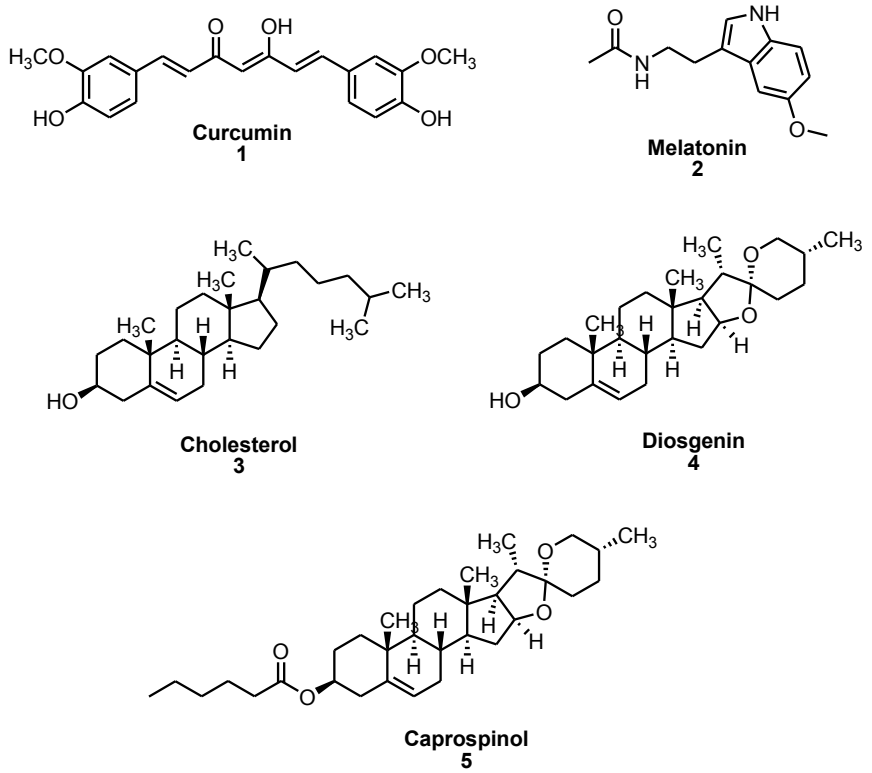

Figure 6. Natural products from which bivalent and hybrid compounds were designed.

2 Multifunctional Bivalent Compounds against Alzheimer's Disease

2.1 Project Design

Curcumin **1**, a yellow spice and pigment isolated from the rhizome of *Curcuma longa*, has been traditionally and widely used as a food coloring.[176] Recently, **1** has attracted extensive attention in biomedical research as multiple benefits of **1** have been discovered, including antioxidative, anti-inflammatory, biometal chelating, anti-proliferative, and anti-Aß activities, among others.[177, 178] Because neuroinflammation, oxidative stress, dyshomeostasis of biometals, and amyloidosis have all been implicated in the pathology of AD, **1** has been tested in various AD models. Both *in vitro* and *in vivo* studies have demonstrated the ability of **1** to prevent Aß-induced toxicity and reduce levels of Aß in the brain, as well as levels of inflammatory cytokines and reactive oxygen species, demonstrating the potential of **1** as a candidate for treatment of AD in humans.[177] However, due to its poor solubility, bioavailability, and gastrointestinal side effects, further development of **1** as an effective agent for AD has been somewhat limited.

Caprospinol **5**, a derivative based on the diosgenin **4** steroidal structure, is a natural product found in the *gynura japonica* plant.[179] It was discovered to have beneficial effects in AD models, when computational screening of potential 22R-hydroxycholesterol analogs found it had a closely related structure.[180] Biological assays have revealed 22R-hydroxycholesterol, an intermediate in the formation of pregnolone from cholesterol, was present at lower levels in AD brains than age matched controls.[181] Furthermore, once isolated, 22R-hydroxycholesterol was shown to be protective in Aß-induced toxicity of rat pheochromacytoma cells (PC12) and differentiated human NT2N neuron cells.[182] Once identified, caprospinol was shown to retain these protective functions and, in contrast to 22R-hydroxycholesterol, was devoid of any

steroidogenic activity.[180] The proposed mechanism for these effects is Aß monomer scavenging, reduction in plaque formations, and preserving proper respiratory chain function in mitochondria.[179] Together, caprospinol represents an intriguing steroidal compound against AD pathology.

The bivalent strategy approach is defined by its use of two distinct, active molecular species linked together via a spacer in order to hit dual molecular targets within close proximity with each other. The use of bivalent strategies in exploration of protein-protein interactions has been particularly successful in opioid research.[183-185] Moreover, this approach has been utilized in neurodegenerative research by development of novel acetylcholinesterase.[186] Furthermore, this concept has been successfully exploited in the creation of two previous series of bivalent, multifunctional oligomerization inhibitors for potential use in AD.[172-174] In following with these previous studies, bivalent ligands were designed utilizing curcumin as a multifunctional, oligomerization inhibitor connected to a steroid, acting as a lipid raft (LR) anchor. The idea is to localize the beneficial effects of the multifunctional inhibitor to the lipid raft area, where Aß oligomerization and production of ROS is known to occur, illustrated in Figure 7. Previous studies incorporated cholesterol and cholesterylamine as more traditional LR anchors, and polyamide linking structures. In this series, the diosgenin **4** was chosen as a new anchor due to the positive effects seen in caprospinol, a derivative of diosgenin. Additionally, the spacer was changed to a triethylene glycol structure to impart more flexibility in the linker. The length of spacer was also increased up to 28 atoms to examine any trends in increasing length. Curcumin was retained as the multifunctional inhibitor.

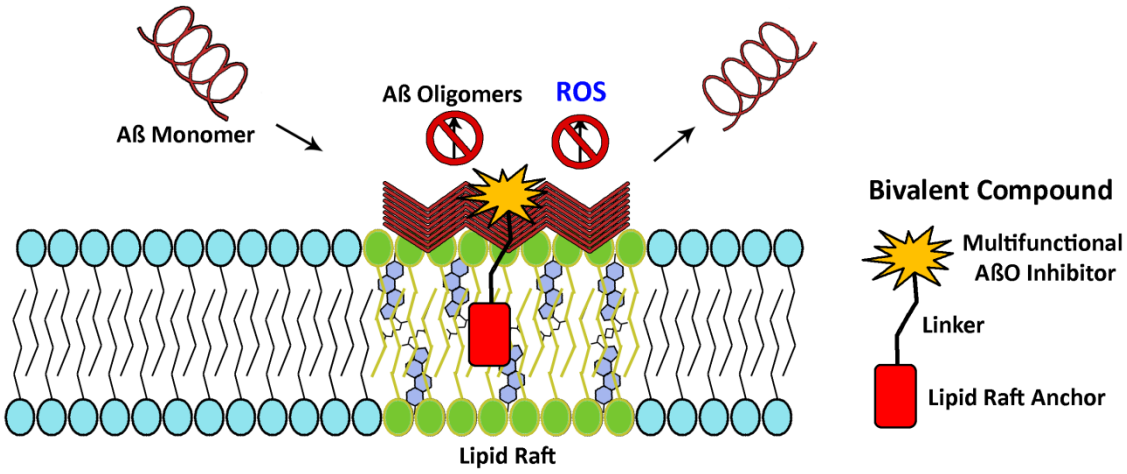

Figure 7. Cartoon representation of the proposed bivalent ligand strategy.

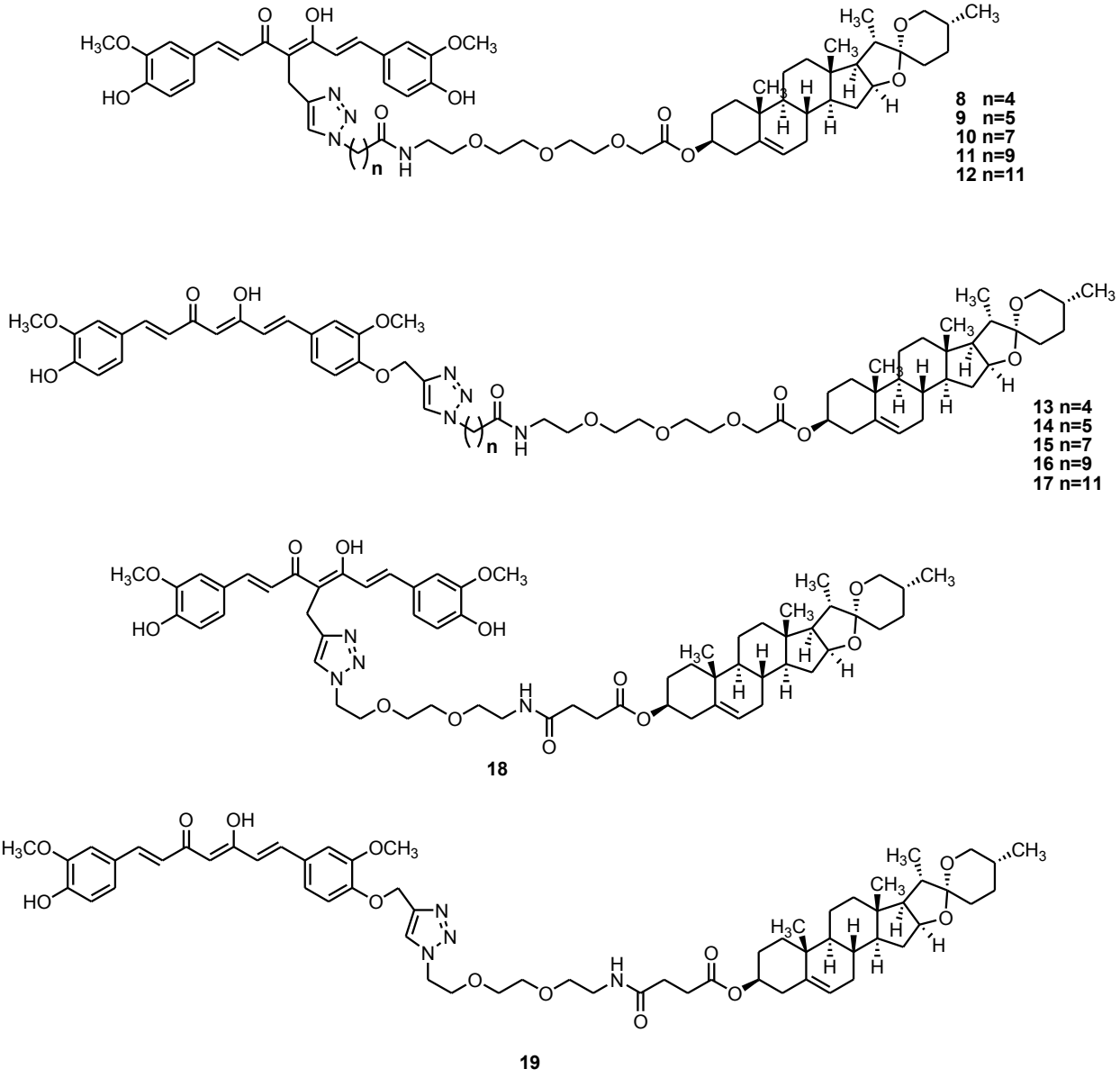

Figure 8. Designed bivalent multifunctional ligands.

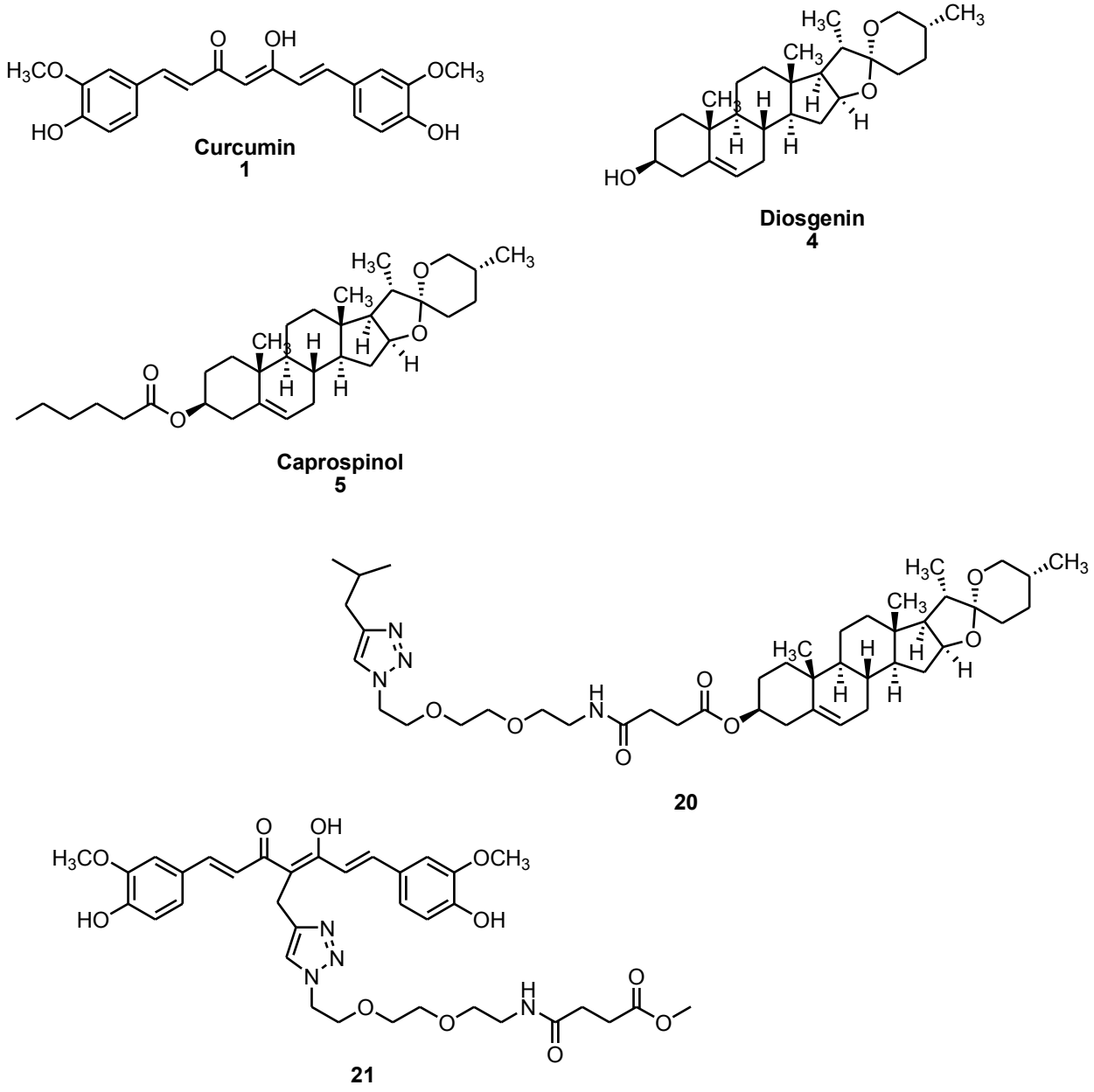

Figure 9. Control compounds for bivalent multifunctional ligands.

2.2 Chemical Design and Syntheses

As mentioned, one of the primary goals with this series of molecules was to determine the possible effects of changing linker composition, linker length, and steroid anchor. As

mentioned previously, diosgenin **4** was selected as the steroid portion of the ligand, hopefully engendering some of the positive characteristics seen in the ester derivative caprospinol **5** into the full bivalent structure. For the linker, a triethylene glycol-based linker **25** with extension by an amide-connected alkyl chain (**26-30**) was chosen. The ethylene subunit would be much more flexible than previously synthesized linkers, and the inclusion of multiple ether-connected H-bond heteroatoms could potentially influence H_2O solubility. Furthermore, linker lengths only up to 23 atoms long were explored earlier. In this series, linkers from 22 atoms up to 28 atoms (**37-40**), adding 2 atoms each time, were designed. Additionally, 17 and 21 atom spans (**50** and **36**, respectively) were also synthesized, as these represent the optimal lengths previously reported.[172, 174] Synthesis was achieved by first constructing the linker portion of the ligand, followed by coupling of the diosgenin structure **4**, and lastly, clicking on the alkyne-curcumin analogs **46** and **47**. Previous reports revealed connection of the linker to the middle position, deemed the 'M' position, of the alkyne on curcumin exhibited superior protection compared to the similar linkers connected to the phenolic oxygen position, or 'P' position.[172, 174] Attachment at both of these positions was also explored with this series. After preliminary assays were conducted, control ligands were then made incorporating the most potent linker composition connected only to diosgenin or curcumin (**20** and **21**, respectively), to insure activity was dependent on the fully formed ligand structure and not a potential substructure or metabolite.

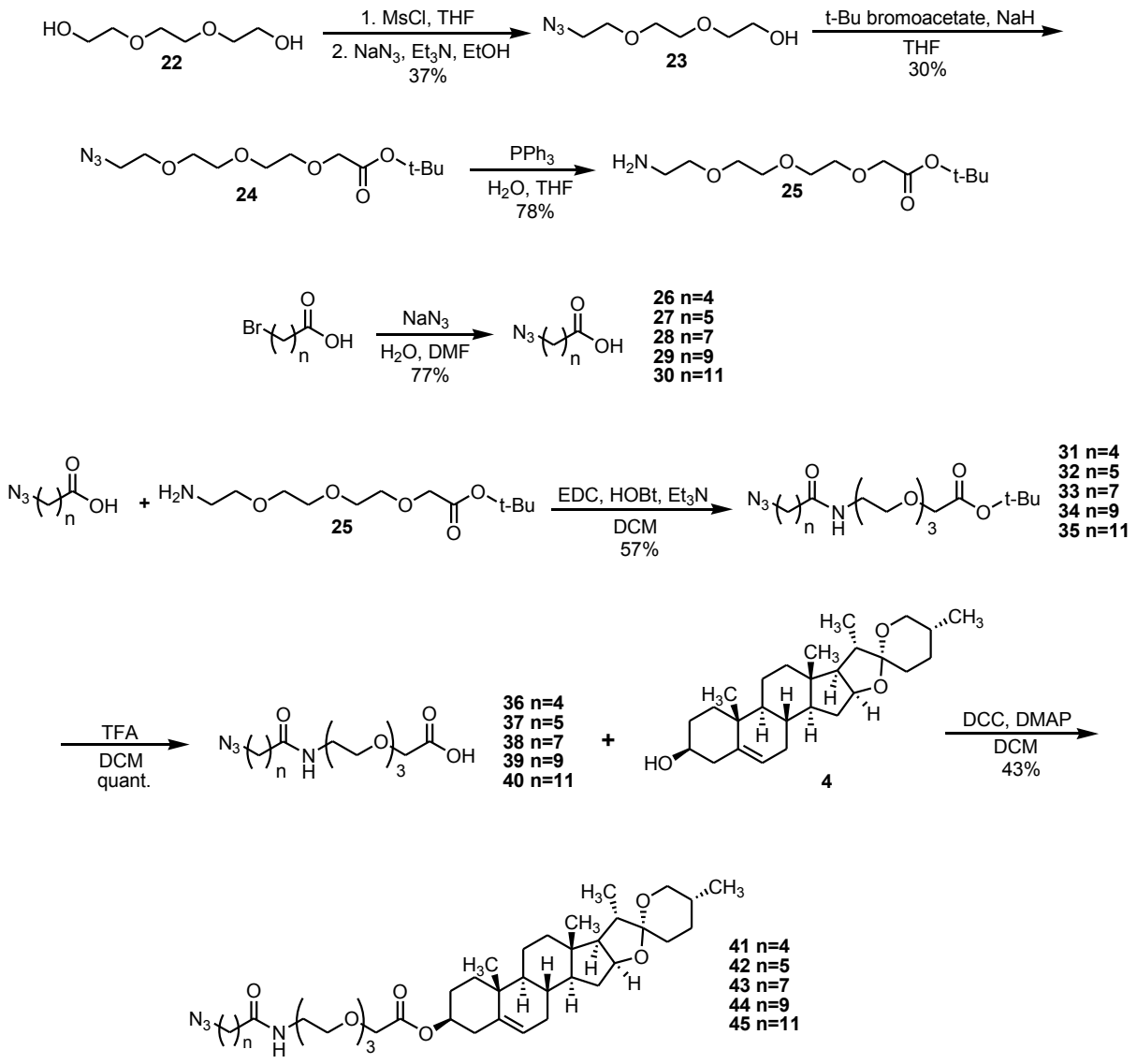

Scheme 1. Synthetic route for bivalent multifunctional ligands, part 1.

2.2.1 Azide substitution onto triethylene glycol

Linkers were synthesized through a multistep process outlined in Scheme 1. Triethylene glycol **22** was functionalized by substituting one of the hydroxyl groups for an azido group. This was accomplished by first reacting **22** with mesyl chloride to form the methanesulfonate

intermediate at one end of the glycol chain. In order to insure only one hydroxyl group was substituted, this step was conducted at low temperatures (0 °C) and in a very dilute solution. The mesyl chloride was also diluted prior to addition and was very slowly dropped into the reaction mixture, over 2 to 4 h. The methanesulfonate formed acts as a good leaving group and leaves the adjacent carbon susceptible to nucleophilic substitution, in this case by NaN_3, yielding compound **23**. Despite directing the reaction toward single substitution, inevitably some starting material will be doubly substituted, forming the double azido side product **48**. Luckily, this side product was actually later utilized in the synthesis of the 17 atom spacers.

2.2.2 Addition of the protected acetate group

Now that the azide moiety was successfully installed, the other end of the ethylene chain needed to be functionalized. Ultimately, a carboxylic acid is necessary to form an ester coupling with the diosgenin steroid **4**, but must remain protected while elongating the azido side of the linker. To accomplish this, *tert*-butyl bromoacetate was selected. NaH was added to **23** to remove the hydroxyl hydrogen (Scheme 1), forming a negatively-charged oxide ion. Next, *tert*-butyl bromoacetate was added in one portion. The bromo substituted α-carbon undergoes nucleophilic attack by the preformed oxide ion, resulting in substitution with the oxygen atom, creating the carbon-oxygen bond seen in compound **24**.

2.2.3 Staudinger reaction

First reported in 1919 by Hermann Staudinger, the Staudinger reaction involves the reaction of azides with triphenylphosphine to form phosphazides and release N_2 gas.[187] These can then be hydrolyzed with H_2O giving the related amine and triphenylphosphine oxide. Here, this reaction is utilized to reduce the relatively inert azide group to a reactive amine group. Although now typically associated with click reactions, it is interesting to note that in this case, the azide group is actually functioning as a precursor for a primary amine. To achieve this, compound **24** was reacted with triphenylphosphine (TPP) in THF, to form the phosphazide. After 4 h, H_2O was added to quench the reaction and release the primary amine **25** in good yield. Compound **25** represents half of the full linker and can now be coupled to azido-substituted fatty acids of varying lengths (**26-30**), described below.

2.2.4 Azide substitution onto long chain carboxylic acids

Naturally, different spans of atoms must be incorporated into the linker composition to obtain spacers of varying size. In order to attain the desired lengths, terminally substituted long chain carboxylic acids, more commonly known as fatty acids, were synthesized and combined with the previously created triethylene structure **25**. Because this end of the linker will be "clicking" with the alkyne-curcumin analogs **46** and **47**, an azide group needed to be installed. To accomplish this, various bromo-fatty acids were reacted with NaN_3 in DMF and H_2O. The resulting nucleophilic substitution afforded the newly substituted azido-fatty acids (**26-30**) in good yield. It is important to note that the R_f values for these compounds on TLC are near

identical, but the successful addition of the azide can be easily confirmed by IR, specifically by a characteristic absorbance band at 2100 cm^{-1}.

2.2.5 Amide coupling and deprotection

Azido-fatty acids **26-30** and compound **25** were coupled via an amide bond using the commonly employed EDC and HOBt coupling mechanism in DCM. EDC is first reacted with the carboxylic acid to give the active *O*-acylisourea intermediate that is subsequently displaced by HOBt to form the activated ester. Upon addition of the amine species **25**, HOBt is removed by nucleophilic attack, resulting in products **31-35.** Now that the linker is completely formed, the *tert*-butyl protected ester group can be unmasked in preparation for coupling with diosgenin **4**. Trifluoroacetic acid (TFA) was used to hydrolyze the *tert*-butyl group yielding the fully prepared linkers **36-40**.

2.2.6 Esterification with diosgenin

Linkers **36-40** were coupled with the diosgenin steroid **4** via ester-bond formation. Similar to the amide coupling, Steglich esterification was employed.[188] DCC, another carbodiimide species, was first reacted with the acid to form the active *O*-acyliosurea intermediate, as before. In this reaction, however, DMAP is used as a catalyst. Because alcohols are much less nucleophilic than amines, DMAP will prevent any potential intramolecular rearrangements, specifically formation of the unwanted *N*-acylisourea species that might occur due to the slower addition of an alcohol. Furthermore, the DMAP-linked intermediate can also

readily react with alcohols, efficiently transferring the acyl group forming the ester. Once esterification is complete, the DMAP is regenerated and ready to react again. The DCC derived urea side product is often difficult to remove during purificiation; however, it was easily filtered off after addition of cold EtOAc, in which compounds **41-45** were completely soluble.

2.2.7 Azide-Alkyne 'click' reaction

The last part of the ligand to be connected was the multifunctional curcumin analog. As noted, attachment at both the 'M' and 'P' positions, represented by alkyne-curcumin analogs **46** and **47**, respectively, was explored. Significant quantities of compounds **46** and **47** had been synthesized as previously described[174] and were still available for use. As such, their construction was not repeated. The classic copper-catalyzed 'click' reaction, also known as the azide-alkyne Huisgen cycloaddition, was utilized for the last step in ligand assembly. Due to the relatively inert azide and alkyne groups, 'click' reactions are so named for their high degree of specificity, lack of side products, and robust nature. Additionally, if other multifunctional effectors wished to be investigated, they need only be clicked to the alkyne, providing a high degree of interchangeability, and by extension, potential synthetic libraries. As such, compounds **41-45** were added to a THF/H_2O solution along with **46** or **47** and stirred. $CuSO_4$ and sodium ascorbate were then added to catalyze the formation of the 1,2,3-triazole ring. Ascorbate functions as a reducing agent converting Cu^{2+} into the active Cu^{+} form, necessary for catalysis. Final products **8-17** were all isolated and collected in high yield. Of particular note, after optimization of this protocol, it was found that a higher concentration of $CuSO_4$ and ascorbate were required for efficient conversion than is typically described in the literature. This could be

due to the amount and positioning of ether and carbonyl oxygen atoms in the linker that may be capable of chelating the copper, thus inhibiting its use in catalysis.

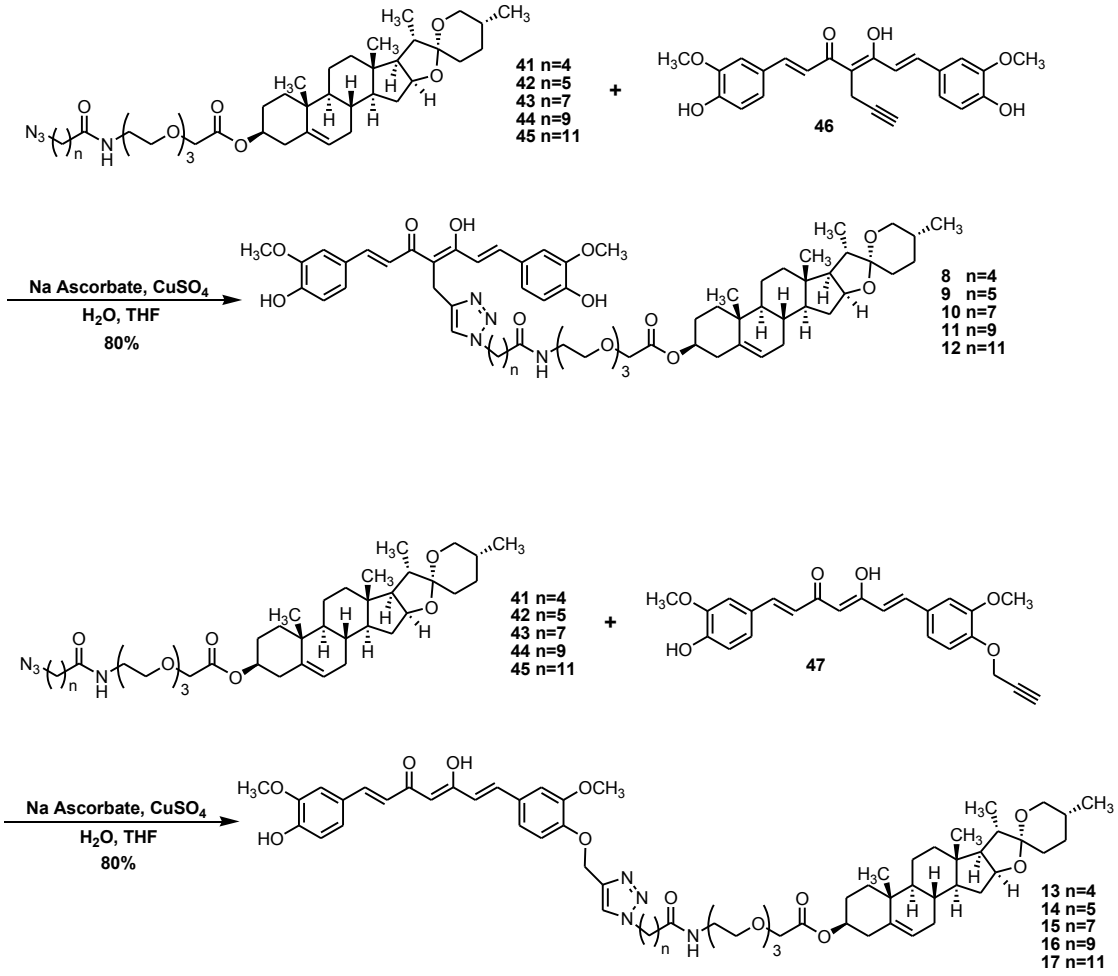

Scheme 2. Synthetic route for bivalent multifunctional ligands, part 2.

2.2.8 Synthesis of 17-atom spacer analogs 18 and 19

Compounds **8-17** correspond to linker lengths of 21 to 28. Unfortunately, reducing the alkyl portion of the linker to one atom would result in a total length of 18, one atom longer than is required. Because of this, a truncated linker composed of the same chemical structures was

necessary. To achieve this, compound **48**, a side product in the creation of **23**, was first functionalized by converting an azide to the primary amine. This reaction was run using triphenylphosphine as described before; however, in this instance, a two phase solvent system (organic EtOAc and Et_2O, and acidic water) was employed to insure only one azide would be reduced. Once the phosphazide intermediate is formed in the organic phase, it is immediately cleaved by the H_2O present in the solvent system, affording the primary amine. Due to the hydrophilic nature of the amine group, the compound now prefers to exist in the water phase, preventing a secondary interaction with triphenylphosphine in the organic phase. The newly synthesized compound **49** was then reacted with succinic anhydride. Nucleophilic ring opening created a newly formed amide bond and carboxylic acid. The resulting molecule **50** constitutes the full linker structure. From here, **50** was reacted with diosgenin **4**, and curcumin analogs **46** and **47**, as previously outlined, yielding final products **18** and **19**.

2.2.9 Synthesis of control compounds 20 and 21

After preliminary activities were assessed, control ligands were made incorporating the most potent linker composition connected only to diosgenin or curcumin. To acquire these, compound **51** was clicked to 4-methyl-1-pentyne as previously described. The product **20** includes the triazole ring, seen in all ligands, and the middle carbons of the curcumin structure. Compound **21** was obtain by coupling **49** with 3-(methoxycarbonyl)propanoic acid **53**, a methyl ester capped form of succinic acid, with EDC/HOBt, again, as previously described. The resulting product **54** was clicked together with **46** giving final product **21** in good yield.

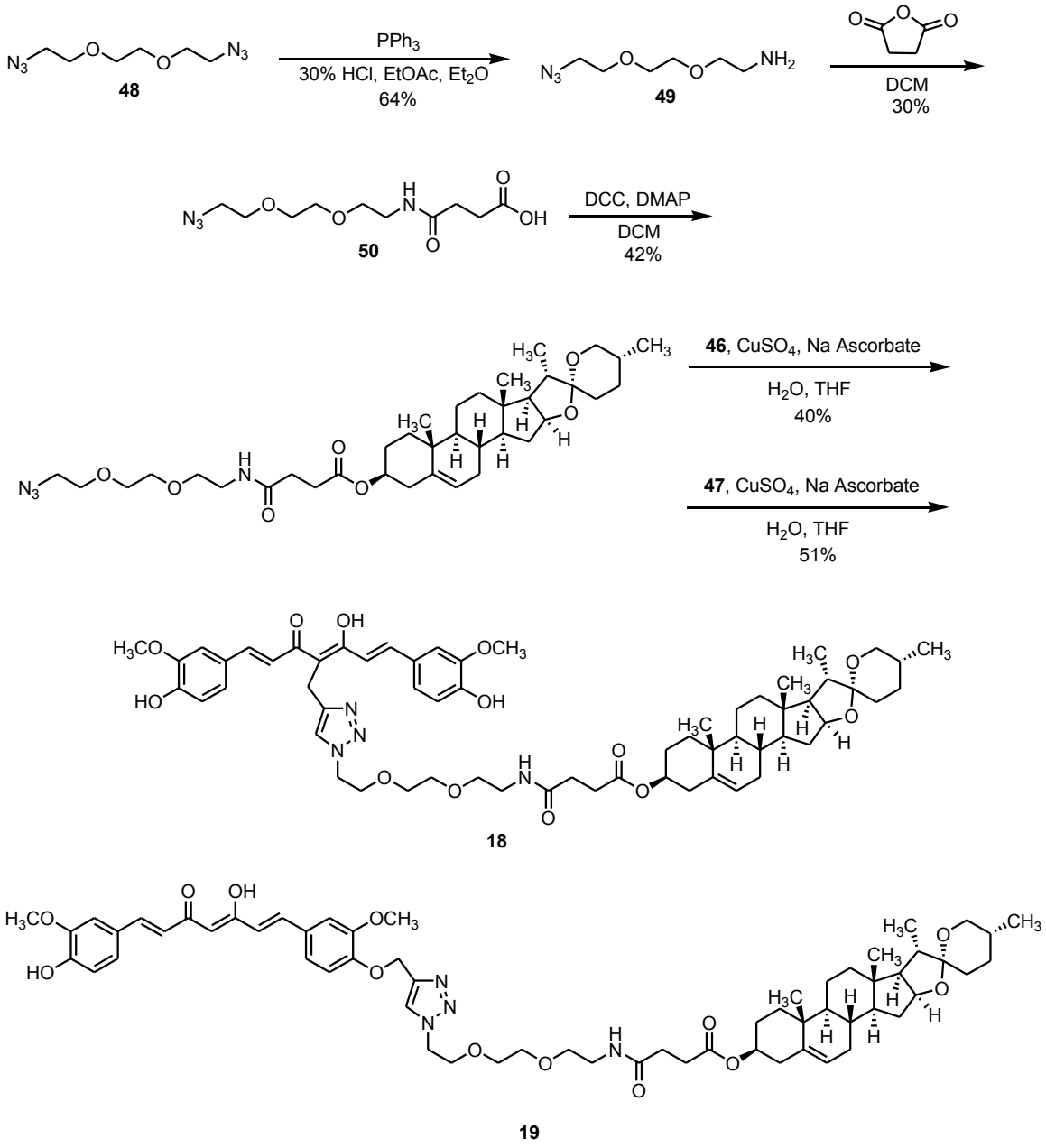

Scheme 3. Synthetic route for bivalent multifunctional ligands, part 3.

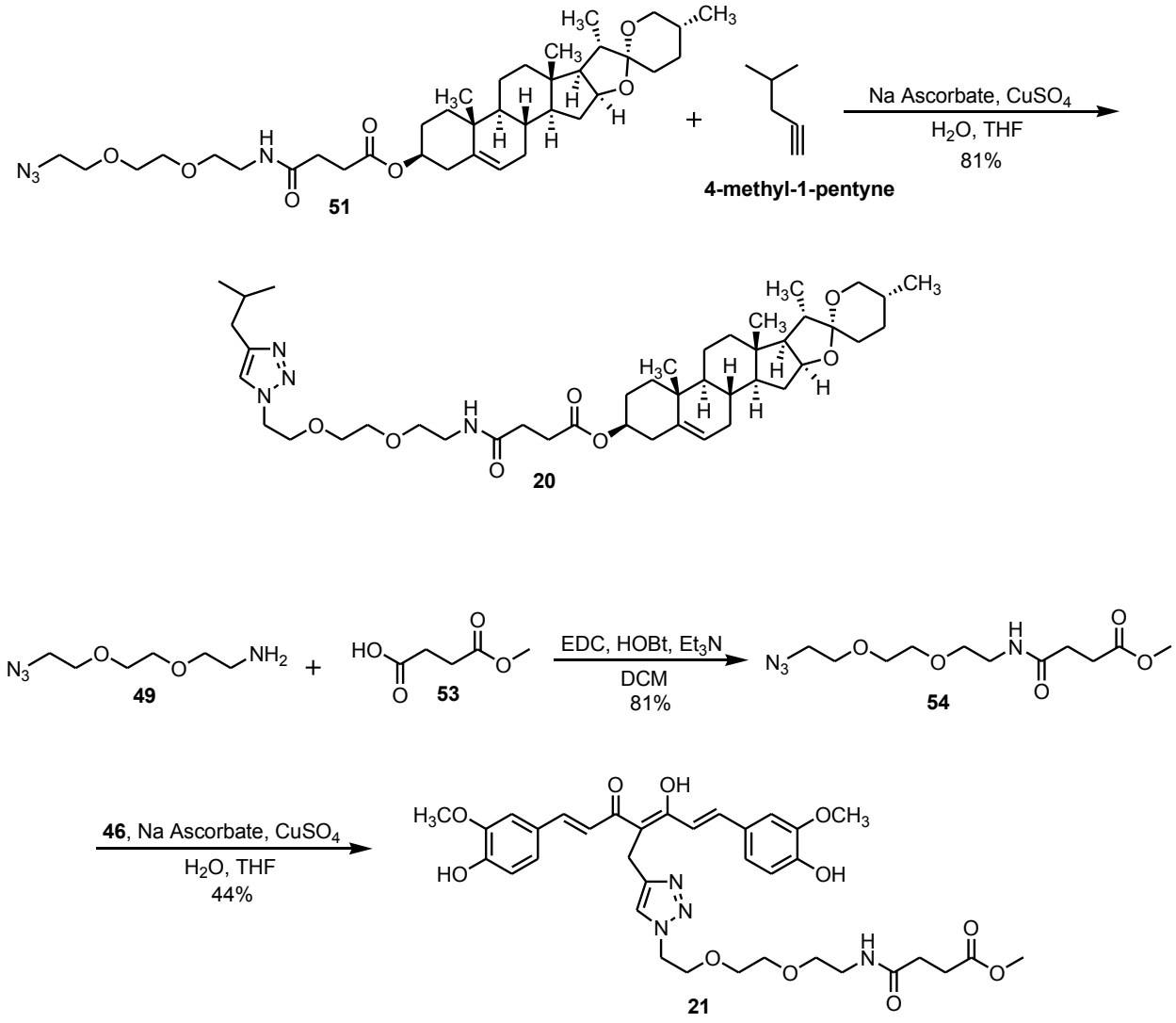

Scheme 4. Synthetic route for control compounds for bivalent series.

2.3 Biological Studies

For simplicity, compounds may be abbreviated below by their linker length, attachment site, and use of diosgenin as a steroid; for example, compound **8** may be referred to as 21-MD, denoting a 21 atom spacer, connection at the 'M' position, and 'D' for diosgenin.

2.3.1 The MC65 neuroblastoma cell model

In order to characterize the biological activities of these compounds as potential AD-modifying agents, an appropriate cell model for AD is necessary. Therefore, the MC65 cell model was selected. MC65 cells are SK-N-MC neuroblastoma cells that have been stably transfected to express the human APP-C99 fragment. Under AD pathological conditions, this fragment arises after the cleavage of APP by ß-secretase. It is then subsequently processed by γ-secretase to produce Aß. Indeed, MC65 cells have been shown to produce both the C99 protein and Aß.[189] The transfected gene in the MC65 cell line is conditionally expressed using the tetracycline (TC) responsive promoter system. Growth medium is supplemented with TC to insure the gene promoter region is blocked and cells grow normally. Upon TC removal (-TC), RNA polymerase can now freely transcribed the specified gene, leading to production of the C99 fragment and consequently, Aß. This overexpression of Aß in MC65 cells leads to aberrant cellular function, increase in oxidative stress, and ultimately, cell death, which has been well characterized.[189-191] Moreover, in this model, Aß is produced intracellularly, which better mimics AD *in vivo*, unlike other models, i.e. SH-SY5Y or PC-12, where exogenous Aß is added to the cell medium. Therefore, MC65 cells serve as a suitable model for AD *in vitro*.

2.3.2 Neuroprotective ability of bivalent ligands in MC65 cells

The full series of designed and successfully synthesized bivalent compounds were first screened for their neuroprotective ability in MC65 cells. MC65 cells were incubated with indicated compounds for 72 h in the absence of TC. Viability was then assessed by MTT assay. Briefly, cells are incubated with MTT for 4 h, after which the medium is removed and the

remaining formazan crystals produced by viable cells are dissolved in DMSO. Absorbance is then measured at 570 nm. All compounds were assayed at a concentration of 3 μM to identify active structures with reasonable potency. Ligands were plotted as pairs in ascending linker length, with the 'M' position on the left and the 'P' position on the right. As seen in Figure 10, curcumin **1** and diosgenin **2** exhibited only weak protective abilities at this concentration, and interestingly, caprospinol **5** actually showed no protection at all. Caprospinol, though protective in some cell models of AD, has not been previously characterized in MC65 cells, and may not exhibit activity at these concentrations or in this model. For all ligands, attachment at the 'M' position was significantly more protective than the 'P' position, excluding 26-PD, which was similar to the 26-MD analog. In fact, only compounds 21-MD and 26-MD imparted any significant protection compared to the -TC control, and even then, it was slight (~20% increase from -TC). This preference for the 'M' position is in agreement with the reported cholesterol and cholesterylamine series, highlighting the importance of the connection site.[172, 174] Compounds **18**, **8**, **9**, and **10** all exhibited strong neuroprotective activity, increasing viability to 80% or greater, demonstrating that these ligands can effectively rescue MC65 cell death. After 24 atoms of spacer, however, protective function dropped significantly (~25% reduction), suggesting that too long of an extension may not be positioning the curcumin and steroid structures in a proper fashion. Moreover, no protection was observed for control compounds **20** and **21**, containing just the spacer connected to only diosgenin or curcumin, respectively. This confirms that the presence of all three pieces of the ligand is required for activity and validates the bivalent design strategy. From here, dose-response studies of the 'M'-attached ligands were carried out to determine EC_{50}s. As shown in Figure 10, all ligands again showed significant protection at 3 μM that ultimately decreased to negligible values as concentration was reduced to

0.01 μM. Notably, compounds **18** and **8** (17-MD and 21-MD) were the only ligands able to raise viability to 90% or more. They exhibited the best potencies, as well, with EC_{50}s of 111.7 ± 9.0 nM and 231.7 ± 15.1 nM, respectively. Not surprisingly, these spacers were also the optimal lengths revealed from the previous series. As the linker length is increased, the general trend is a reduction in potency and efficacy, although again, 26-MD was the exception that proves the rule, with an EC_{50} of 309.0 ± 1.5 nM. Altogether, these results further substantiate the preference of the 'M' position and support the notion that optimal spacers are shorter than 22 atoms. Based on these results, compounds **18** and **8** (17-MD and 21-MD, respectively) were selected for follow-up studies of biological characterization.

2.3.3 Antioxidative properties of 18 and 8 in MC65 cells

One goal of the desired combination of **1** and **4** was to retain the antioxidative properties of the curcumin moiety and consequently reduce oxidative stress that contributes to AD pathology. Oxidative stress has also been indicated as one potential effector in imparting neurotoxicity upon the accumulation of intracellular Aß in MC65 cells.[189] Therefore, compounds **18** and **8** were evaluated for their antioxidative ability in MC65 cells. To accomplish this, a DCFH-DA (2,7-dichlorodihydrofluorescein diacetate) dye was used. *In vitro,* DCFH-DA will be de-esterified to DCFH, and then upon interaction with ROS, this will become oxidized to produce 2,7-dichlorofluorescein, which is highly fluorescent and can be measured, in this case, by flow cytometry.[192] As shown in Figure 10, removal of TC led to a significant increase in intracellular oxidative stress compared to the +TC control (108% increase), as measured by fluorescence intensity. This rise in ROS is completely prevented by addition of **18** at a

concentration as low as 0.1 μM, consistent with its EC_{50} from the MTT assay. Similarly, ligand **8** was able to significantly reduce ROS production as well, with concentrations down to 0.3 μM, also matching its EC_{50} from the MTT assay. Because the potencies for **18** and **8** in rescuing cell viability correspond closely with ROS reduction, this suggests that antioxidative ability may be the major mechanism of neuroprotection for these multifunctional compounds. Furthermore, these results also strongly correlate oxidative stress with viability for MC65 cells under -TC conditions, linking Aß production to increased ROS concentrations.

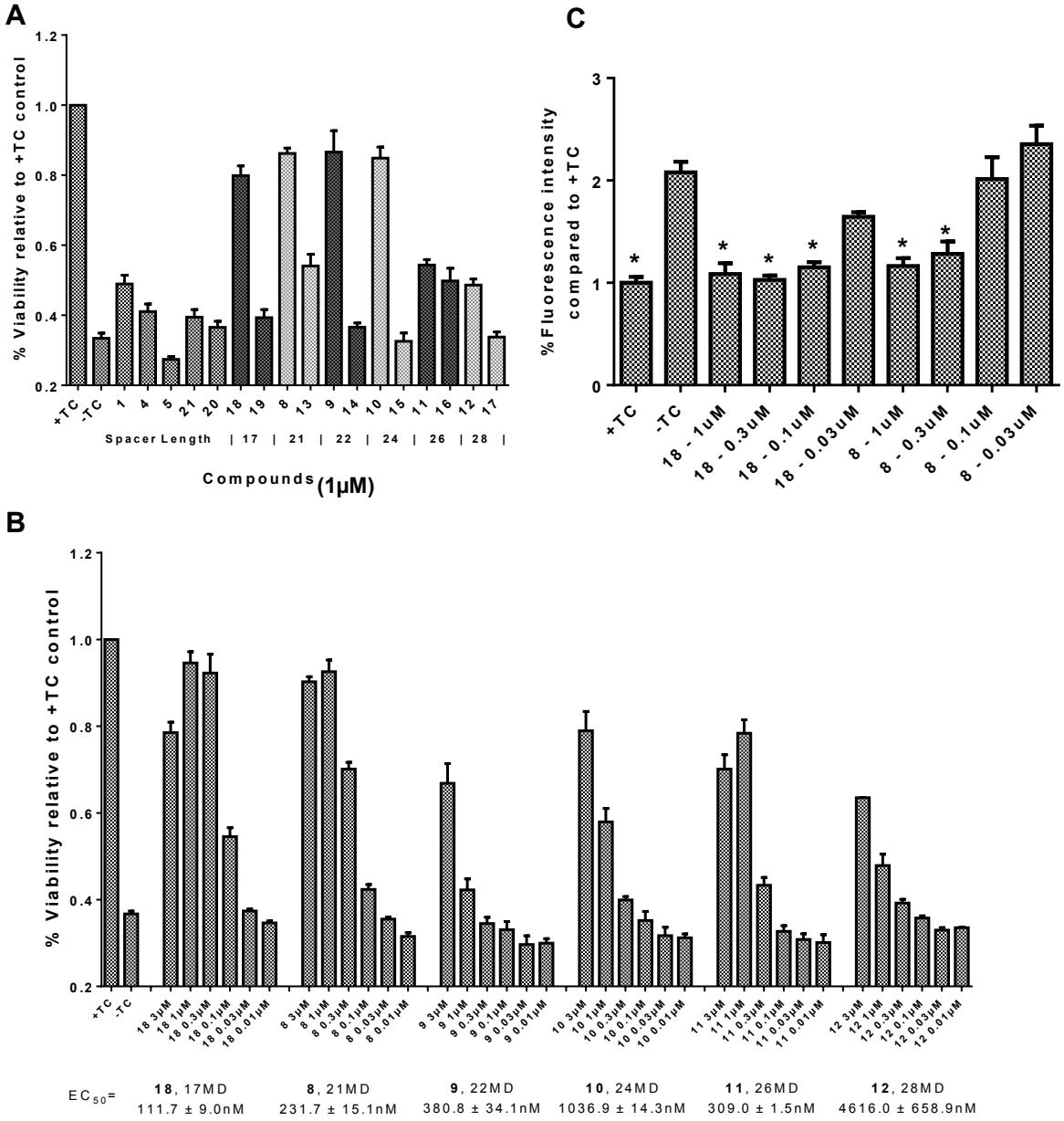

Figure 10. Screening of bivalent series in MC65 cells, MTT assay and ROS reduction. A. Neuroprotective effects of full series of bivalent ligands. MC65 cells were treated with indicated compounds at 3 μM for 72 h. Cell viability was measured by MTT assay. Data were expressed as mean percentage viability (n=3) with parallel +TC cultures set at 100% viability. Error bars represent SEM. B. Dose response of 'M' position ligands. MC65 cells were treated with indicated compounds at indicated concentrations for 72 h. Cell viability was measured by MTT assay. Data were expressed as mean percentage viability (n=3) with parallel +TC cultures set at 100% viability. Error bars represent SEM. C. Antioxidative properties of **18** and **8**. MC65 cells treated with **18** or **8** for 48 hr. ROS production was measured by DCFH-DA assay. Data were expressed as mean percentage viability (n=3) with parallel +TC cultures set at 100% viability. Error bars represent SEM. * $p < 0.05$

2.3.4 Effects of 18 and 8 on Aß oligomerization

In order to test whether these ligands are indeed having an effect on AßO formation as hypothesized, Aß oligomerization in MC65 cells was analyzed by western blot. Cells were treated with **18** and **8** for 48 h. Samples were then collected, separated by SDS-PAGE, and probed with 6E10 antibody to bind Aß oligomers. As expected, inclusion of TC in the cell medium completely blocked Aß expression, and removal of TC led to a vast increase in Aß oligomers (Figure 11). This increase was significantly suppressed by both **18** and **8** in a dose-dependent manner, confirming the anti-oligomerization properties of these ligands. In conjunction with the reduction of ROS production, this result provides additional evidence showing the close relation of oxidative stress and AßO formation. Moreover, it suggests that inhibition of Aß oligomerization is also an important mechanism of action for these ligands, and demonstrates their multifunctional nature, further supporting the bivalent design strategy.

2.3.5 Effects of 18 and 8 on overall Aß production

To provide more evidence that **18** and **8** are actually preventing oligomerization and not simply inhibiting Aß production, total Aß concentrations were calculated by ELISA. MC65 cell samples were treated with **18** or **8** for 48 h. Conditioned medium was collected and added to plates precoated with BNT77 antibody. Concentrations of both $Aß_{40}$ and $Aß_{42}$ were measured by using BA27 and BC05 antibodies, respectively. Consistent with the western blot, addition of TC to the cell medium completely blocked Aß production, and naturally, removal led to a sharp increase (Figure 11). Treatment with **18** or **8** had no significant impact on $Aß_{40}$ or $Aß_{42}$ concentrations, except **18** at 0.1 μM, which while significant, was practically negligible (< 10%

increase). These results indicate that both ligands are in fact having no effect on Aß production, and their influence on AßO formation is truly due to their anti-oligomerization properties.

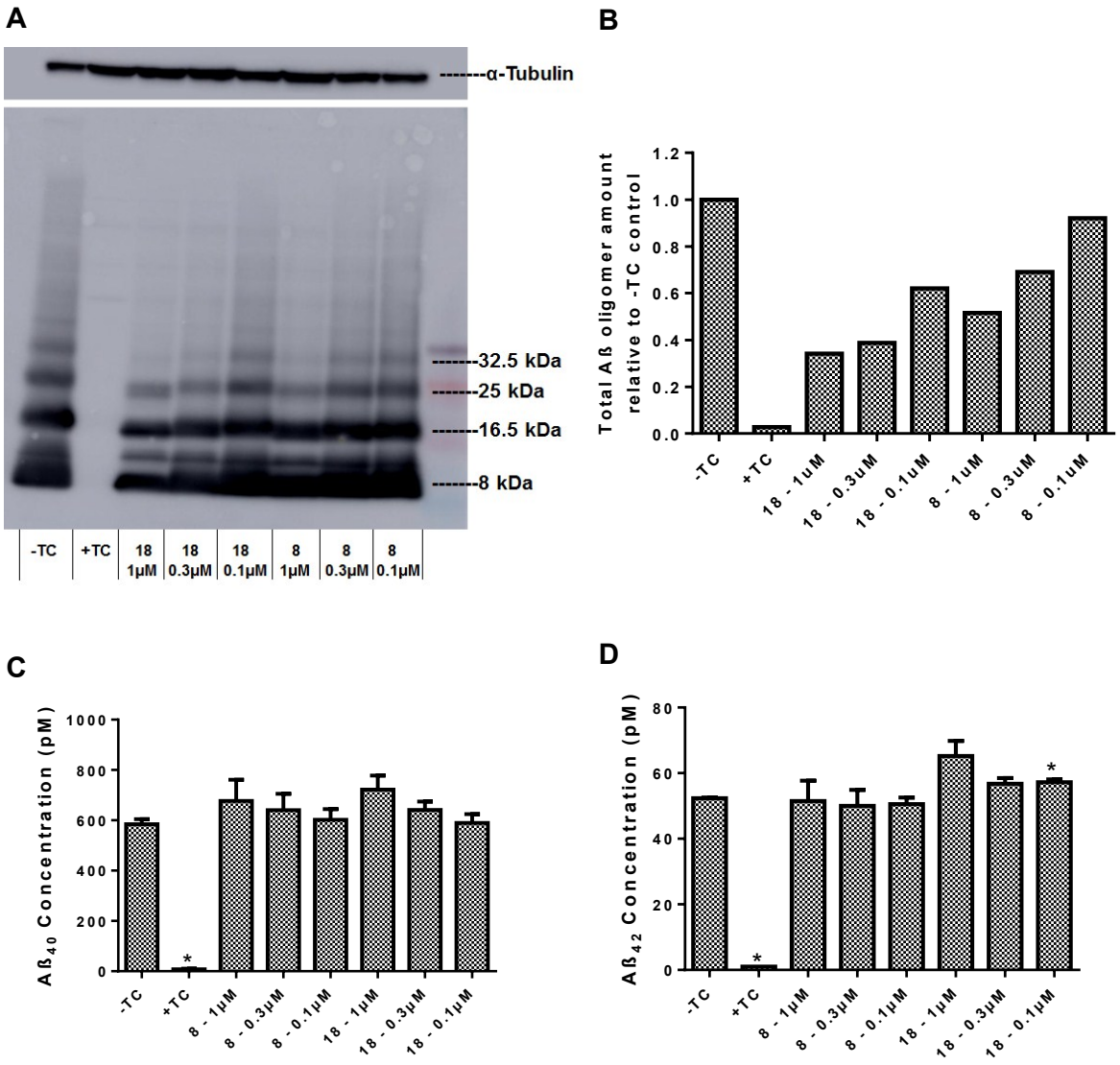

Figure 11. Effects of **18** and **8** on Aß oligomerization and production in MC65 cells. A and B. Effects of **18** and **8** on AßO formation. MC65 cells were treated **18** or **8** at indicated concentrations for 48 h. Western blot analysis (A) shows amounts of AßO for each testing condition. Total amount of AßOs as measured by total band intensity was expressed relative to the -TC control (B). Data represent a single representative assay. C and D. Total Aß concentration in MC65 cells. MC65 cells were treated with **18** or **8** at indicated concentrations for 48 h. Total $Aß_{40}$ (C) and $Aß_{42}$ (D) concentrations were calculated by ELISA. Data are expressed as mean concentration (n=3). Error bars represent SEM. * $p< 0.05$

2.4 Conclusion

A series of bivalent compounds containing curcumin **1** and diosgenin **4**, both natural products shown to have favorable properties against AD pathology, were designed and successfully synthesized. Biological screening in MC65 neuroblastoma cells revealed compounds **18** and **8** as lead compounds with strong neuroprotective activity. It was also found that the 'M' position was greatly prefered to the 'P' position, and that protection was diminished as linker length was increased past 24 atoms. Moreover, control compounds lacking either the steroid or curcumin moiety exhibited no protection, validating the bivalent design strategy. Preliminary mechanistic investigations of compounds **18** and **8** established their anti-oxidative abilities in MC65 cells, and also demonstrated their anti-Aß oligomerization properties by western blotting. This was reinforced by Aß ELISA, which confirmed that **18** and **8** have no effect on Aß production.

These results encourage further investigation and mechanistic characterization of these ligands. Evidence that these compounds are associating with lipid rafts can be addressed by fluoresence microscopy studies, due to the inherent fluorescent properties of the curcumin structure. Additionally, studies with artifical liposomes containing various LR components, namely cholesterol, sphingolipids, and gangliosides, could also be conducted to characterize LR interactions. Direct protein interactions between ligands and Aß are typically characterized by Thioflavin T binding and may offer insight into the Aß binding ability. Biometal binding should also be investigated to confirm if these ligands retain these properties from the parent compound, curcumin. Before any *in vivo* studies could be attempted, BBB penetration ability would certainly need to be assessed. Altogether, these findings support the bivalent design approach as a viable strategy in providing new chemical diagnostic tools or therapeutics.

3 Multifunctional Hybrid Compounds against Alzheimer's Disease

3.1 Project Design

Natural products have proven to be reliable resources in providing effective therapeutics for a variety of diseases. Recently, several small natural compounds with polypharmacological profiles have been shown to be of potential use in neurodegenerative disorders, among which curcumin **1** and melatonin **2** have been implicated by extensive studies as potential AD treatment agents. As described in chapter 2, curcumin exhibits a wide range of neuroprotective features in models of AD, including Aß-oligomerization, anti-oxidation, and biometal binding.[193-195] Melatonin, the major secretory product of the pineal gland, plays an essential role in the regulation of the circadian rhythm.[196] In addition, **2** can be produced in various tissues and organs, and participates in diverse functions through both receptor-dependent and independent ways, including free radical scavenging, immune response, and mood monitoring, among others.[197, 198] Notably, circadian dysfunction and the reduction of **2** have both been observed in AD, suggesting the potential of **2** in AD treatment.[199, 200] Indeed, **2** has been tested both *in vitro* and *in vivo* as a potential treatment for AD.[201] It has been demonstrated that **2** can rescue cell toxicity and death induced by Aβ via multiple mechanisms.[202] In transgenic AD mouse models, **2** has also been shown to improve cognition, reduce Aβ deposition and neuroinflammation.[201, 203] Clinical studies in AD patients with **2** also suggested beneficial effects, especially in sleep quality and reduced sundowning.[204] But more studies are needed to explore and investigate the usefulness of **2** as a treatment for AD. Furthermore, **2** has a relatively short half-life (< 30 min).[205] Therefore, novel analogs of **2** are needed for further investigation and development.

Recently, the "hybrid molecule" strategy has seen increased attention in drug design and development as previously reviewed.[175] The core idea of this strategy is the design of novel ligands by combining the known 'pharmacophoric sub-unities' of two or more bioactive compounds to achieve a new architecture with pre-selected characteristics. It has been used successfully to optimize pharmacokinetic properties, to potentially reduce undesired off-target effects, and modify drug selectivity and mode of action.[175] Given the demonstrated neuroprotective effects of **1** and **2** in various AD models and patients, the hybrid strategy should provide novel chemical scaffolds that retain the functional natures of **1** and **2**, and also provide certain advantages, such as 1) enhanced potency by self-synergy within one molecule that may not be achievable by a traditional combination of separately dosed agents; and 2) improved pharmacokinetic properties and reduced toxic side effects compared to the administration of multiple agents. Furthermore, this hybrid strategy may provide new compounds with novel mechanisms of action, thus representing an attract strategy to identify promising leads for further development.

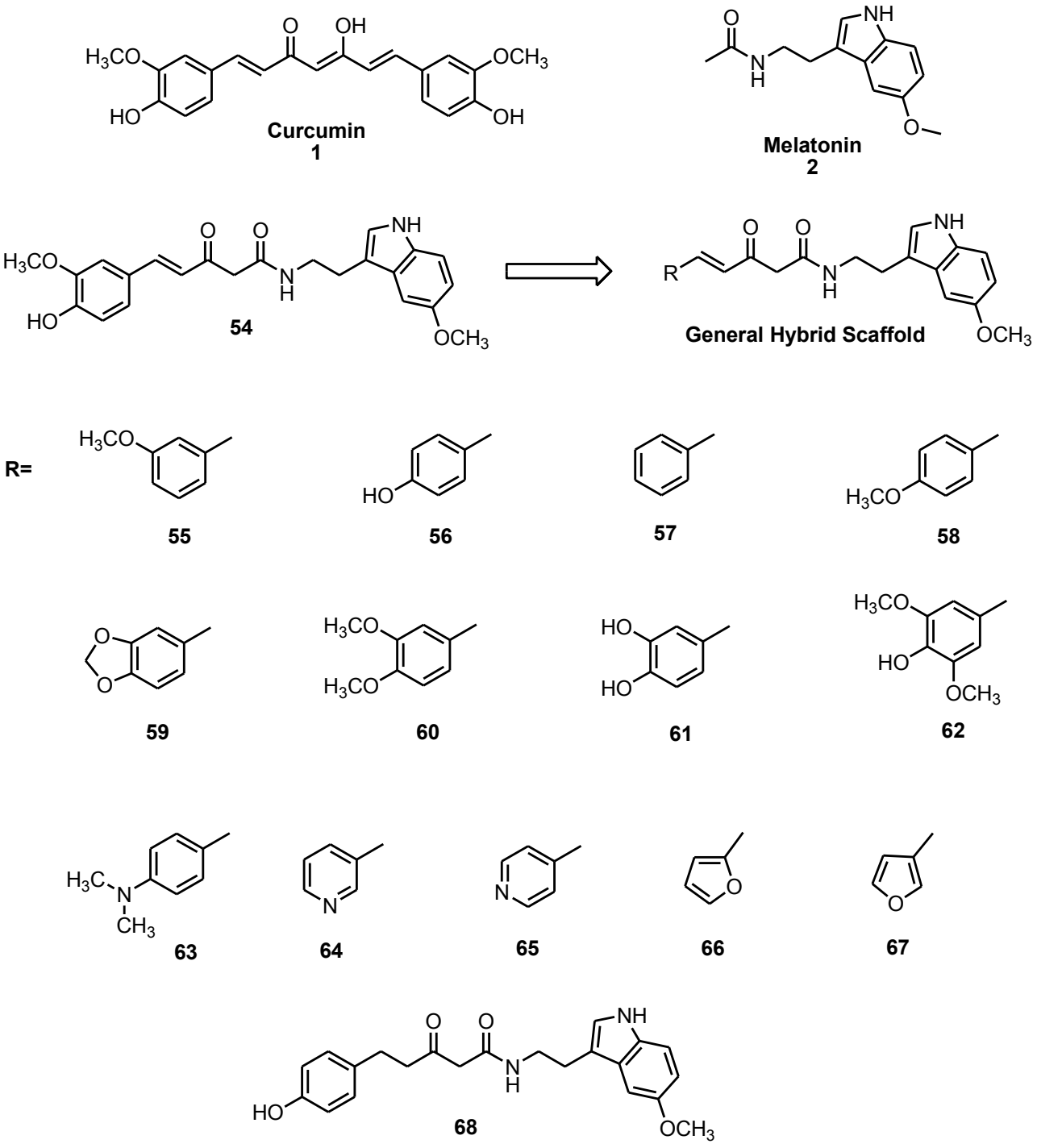

Figure 12. Designed curcumin and melatonin hybrid, and related analogs.

3.2 Chemical Design and Syntheses

This series of compounds were designed to explore the substituents of the phenyl ring in the curcumin portion of the hybrid structure. Initially, compound **54** was synthesized as the representative hybrid between curcumin and melatonin, and assayed for any *in vitro* activity. After **54** was proven to be active, its lead structure was used as the basis for the remaining series. Analogs **55-57** were used to deconstruct the ring and determine the contribution of the methoxy and hydroxyl groups individually. Compounds **58-63** contain different alkyl additions and removals to the methoxy and hydroxyl groups, as well as the phenyl ring, to examine the positional preference of these analogs and the nature of their electron-donating effects. Compounds **64-67** were used to investigate the feasibility of replacing the phenyl ring with different isoteres and to assess the preference of the heteroatoms on these rings. Finally, compound **68** was designed to determine whether the conjugation of the ketone into the ring via the alkene and its associated electronic and structural properties were integral, after initial assays revealed **56** to be fairly active.

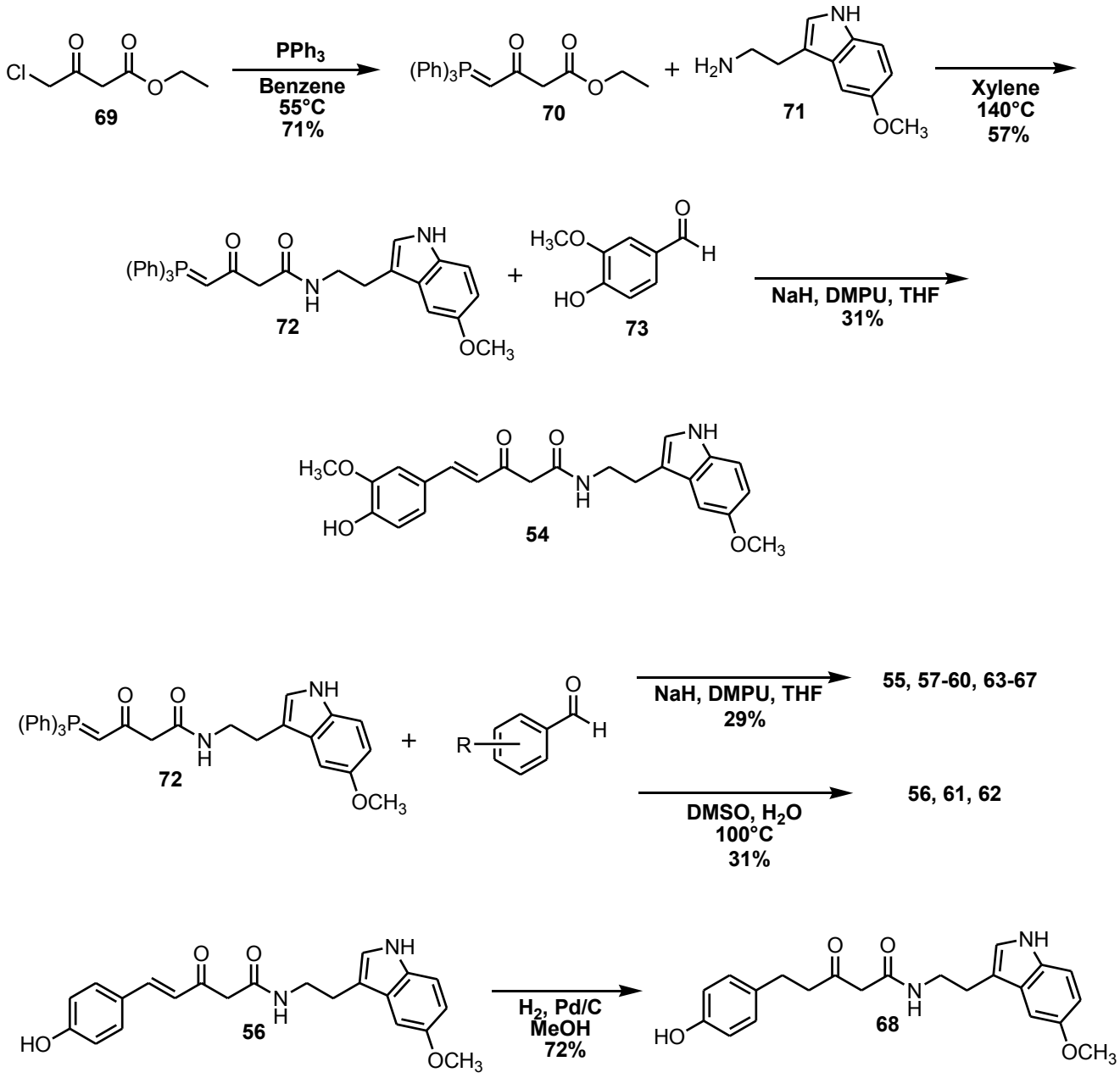

Scheme 5. Synthetic route of curcumin and melatonin hybrid compounds.

3.2.1 Phosphine addition and amide formation

Ethyl 4-chloroacetoacetate **69** was added to a solution of triphenylphosphine in benzene to create the phosphonium Wittig reagent **70**. The triphenylphosphine substituent was chosen because it would effectively 'protect' and prepare the γ-carbon for alkene formation at a later step. Next, an amine exchange reaction was performed in xylenes at high temperatures. Here, the nucleophilic primary amine of 5-methoxytryptamine **71** attacks the carbonyl carbon of **70** to form the quaternary intermediate. The ethoxy substituent becomes subsequently protonated and eliminated, forming the amide linked product **72** and ethanol. Originally, toluene was used as the solvent, but this resulted in very low yields. Use of xylenes, however, lead to the typically higher yields expected from this reaction. The more common EDC/HOBt coupling route was not chosen. Not only would this procedure introduce an extra step into the synthetic route, leading to potential losses in starting material and reduction in overall yields associated with longer synthetic schemes, but also hydrolysis of the ethyl ester to form the ß-ketocarboxylic acid could result decarboxylation, leading to formation of the methyl ketone. This is a commonly used mechanism in ketone installation, but would lead to unwanted products in this situation. Moreover, due to the nucleophilic nature of the γ-carbon in the phosphorane group, activation of the α-carbon by EDC/HOBt, following deprotection of the ethyl ester, could potentially lead to a self-reaction, forming an unwanted conjugated polymer.

3.2.2 Wittig reaction

The Wittig reaction, also known as Wittig olefination, was originally described by Georg Wittig in 1954 for whom the reaction is named.[206] It is characterized by its use of a triphenyl

phosphonium ylide, often and appropriately called a Wittig reagent, reacted with a ketone or aldehyde to give an alkene and the oxidized triphenylphosphine oxide. The negatively charged carbanion of the ylide acts a nucleophile and attacks the carbonyl carbon of the aldehyde to form a carbon-carbon bond. In this case, the NaH base aids in the formation of the carbanion, which is also stabilized by the adjacent ketone group. The steric bulk of the aldehyde and the stability of the carbanion make the carbon-carbon bond formation the rate-limiting step, which leads to preference of the *E*-isomer. As expected, virtually no *Z*-isomer is formed, as observed in the NMR of compound **54** (Figure 13). After this new bond is formed, carbon-carbon rotation gives a betaine type structure, which then leads to the oxaphosphetane intermediate. Elimination of triphenylphosphine oxide results in the fully formed alkene product. Of all compounds **55-67**, only **56, 61**, and **62** failed to react properly under the given conditions, and interestingly, all of these analogs contain a phenyl hydroxyl group. The NaH base used to form the ylide is deprotonating the phenolic oxygen, giving rise to a phenoxide anion, which consequently interferes in the reaction and prevents the Wittig reaction from occurring. For these compounds, removal of the base and changing to a DMSO/H_2O system under high heat afforded the desired products. Notably, compound **54** also contains a phenolic group and repeat reactions using DMSO/H_2O led to significantly higher yields. The newly formed alkene can be easily reduced using H_2 gas and a Pd/C catalyst in methanol to form a saturated alkane. Compound **68** was synthesized in this fashion.

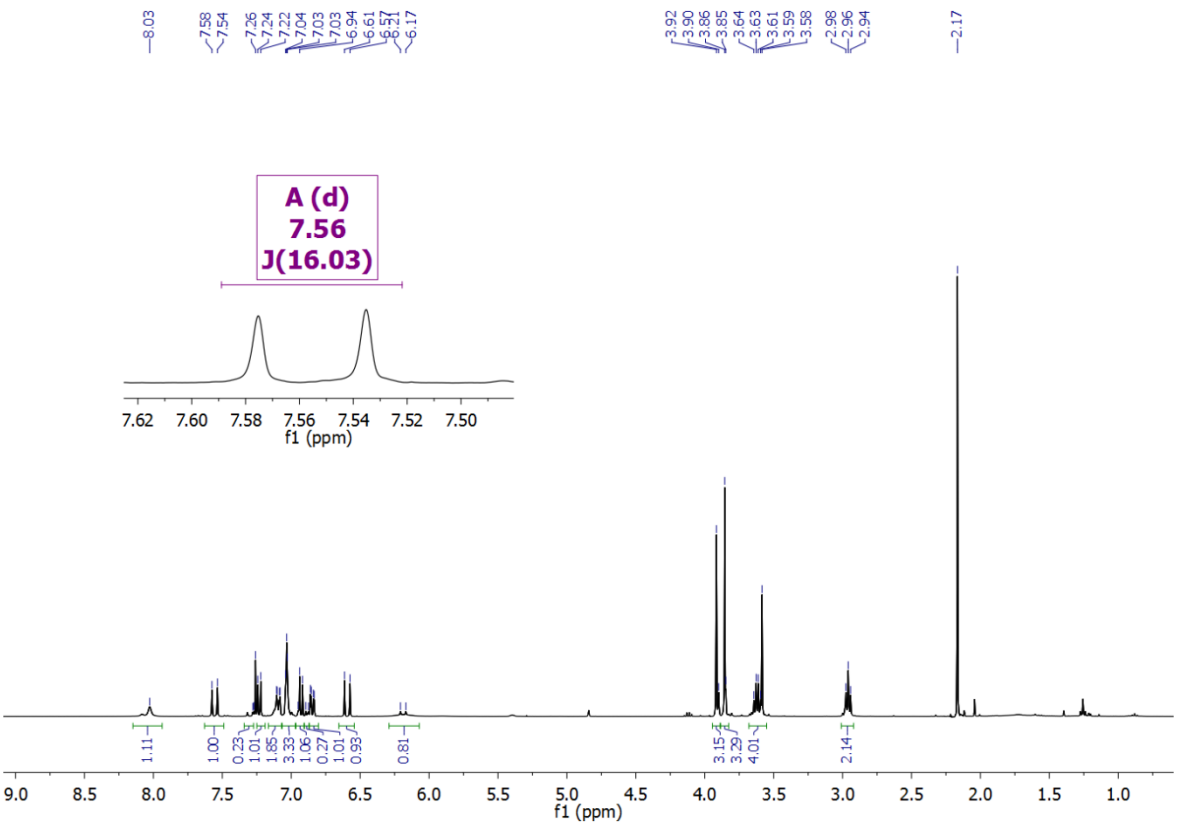

Figure 13. NMR spectrum of compound **54**. The coupling constant (*J*) between the two vicinal protons of the alkene formed in the Wittig reaction is 16 Hz, indicating a trans-conformation. Adapted from Chojnacki et al.[207]

3.3 Biological Studies

3.3.1 Neuroprotective ability of 54 in MC65 cells

Compound **54**, the representative hybrid between curcumin and melatonin, was first synthesized and evaluated for its neuroprotective activity. For this, an MTT viability assay was used in MC65 cells as previously described under TC removal conditions. Initially, we tested **54** at a concentration of 0.3 μM in order to develop active lead structures with a reasonable potency. Curcumin **1** and melatonin **2** alone, and the combination of **1** and **2** were compared as controls.

As shown in Figure 14, no neuroprotection was observed at this concentration in MC65 cells for any of the controls. These results are consistent with previously reported results of **1** in MC65 cells.[172, 174] This also indicates that although **2** has been reported to have activity in other cellular models of neurodegenerative disorders, it might not be sufficient to protect MC65 cells under these testing conditions. Notably, hybrid **54** significantly protected MC65 cells from -TC induced cell death (~61% increase in cell viability), which suggests that the combination of the essential features of **1** and **2** can provide new chemical scaffolds with novel pharmacology, and **54** could serve as a lead structure for further molecular development. Further dose-response studies of **54** established an EC_{50} of 134.2 ± 4.5 nM for its neuroprotection of MC65 cells (Figure 14).

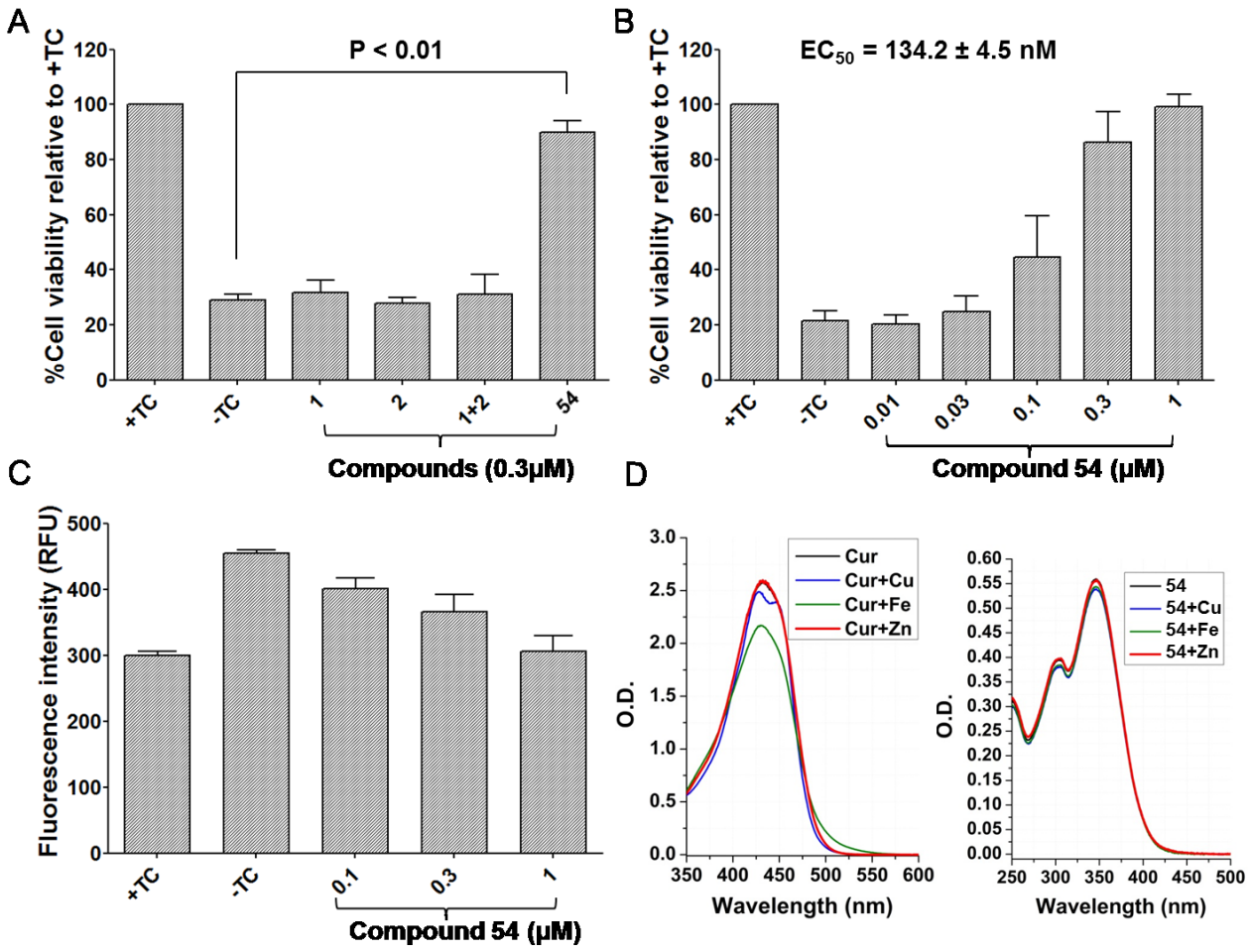

Figure 14. Biological characterization of representative hybrid compound **54**. A. Effects of **1, 2,** and **54** in MC65 cells. Cells were treated with indicated compounds at 0.3 μM under +TC or -TC conditions for 72 h. Cell viability was assessed by MTT assay. Data were expressed as mean percentage viability (n=3) with parallel +TC cultures set at 100% viability. Error bars represent SEM. B. Dose response of **54** in MC65 cells. Viability was assessed by MTT assay. Data were expressed as mean percentage viability (n=3) with parallel +TC cultures set at 100% viability. Error bars represent SEM. C. ROS inhibition of **54** in MC65 cells**.** Cells were treated with **54** for 48 h, then DCFH-DA (25 μM) was loaded and fluorescence intensity was analyzed at 485 nm (excitation) and 530 nm (emission). Data were presented as a mean percentage of fluorescence intensity (n=3). Error bars represent SEM. D. Metal chelating ability of **54.** Curcumin **1** and **54** were incubated with $CuSO_4$, $FeCl_2$, or $ZnCl_2$ at room temperature for 10 min. UV-vis spectrum was recorded from 250 nm to 600 nm. Adapted from Chojnacki et al.[207]

3.3.2 Antioxidative ability of 54 in MC65 cells

One goal of the desired hybridization of **1** and **2** was to reduce oxidative stress that contributes to AD pathology. Therefore, compound **54** was evaluated for its antioxidative activity in MC65 cells using a DCFH-DA dye and flow cytometry, as previously outlined. As shown in Figure 14, upon removal of TC, intracellular oxidative stress, as measured by fluorescence intensity, is significantly increased compared to normal growing MC65 cells in the presence of TC (52% increase). Notably, **54** suppressed intracellular oxidative stress in a dose-dependent manner with an IC_{50} of ~134 nM. Although the antioxidative activity of **54** is comparable to the previously reported antioxidative activity of **1**,[172, 174] it also significantly protected MC65 cells from cell death while **1** did not under the same experimental conditions (Figure 14). These results may suggest that the antioxidative effects of **1** and **54** are perhaps through different mechanisms, thus further supporting the hypothesis that the rational design of **1** and **2** hybrids can provide novel compounds that can both retain the activities of the parent compounds and provide superior potency and protection.

3.3.3 Metal ion chelating ability of 54

The ability of **54** to chelate biometals was also assessed, to ascertain whether changing the ß-diketone structure of **1** to a ß-ketone amide structure would affect biometal binding potential. Furthermore, dyshomeostasis of metal ions has been indicated as one of the pathologies of AD, and it has been suggested that metal ions are involved in the assembly and neurotoxicity of Aß, and may contribute to oxidative stress.[72, 73, 208] Therefore, compounds with biometal chelating properties may provide an additional layer of beneficial activity in developing

multifunctional compounds as AD-modifying agents. As shown in Figure 14, **54** did not complex with any of the tested metals (Cu^{2+}, Fe^{2+}, and Zn^{2+}), while **1** did bind to Cu^{2+} and Fe^{2+}, but not Zn^{2+} under the same conditions, consistent with the reported results from the literature.[172, 209] This suggests that the amide moiety of **54** eliminates the formation of the enol form of the ß-diketone, and consequently reduces its metal binding capacity. This also further supports the integral role of the ß-diketone structure in biometal binding ability, as demonstrated in the literature.[209] Additionally, because biometals may be playing a significant role in the production of ROS, this could account for the similarities in ROS reduction, yet differences in neuroprotection, as previously noted. Again, this suggests that the hybrid strategy not only provides novel scaffolds that retain certain properties analogous to the parent molecules, but can also produce compounds with different mechanisms of action.

3.3.4 Neuroprotective abilities of the designed analogs in MC65 cells

After confirming the neuroprotective abilities and anti-oxidative characteristics of **54,** the full series of analogs were designed and successfully synthesized, as noted before. All compounds were then screened for their protective activity in MC65 cells under -TC conditions at 0.3 μM (Figure 15) by MTT assay. Removal of the 4-OH group from **54,** as demonstrated by compound **55,** led to a complete loss of neuroprotection in MC65 cells. However, removal of 3-OCH_3 did not affect biological activity, as compound **56** exhibited significant protection at the tested concentration. Remarkably, **56** can be recognized as the hybrid of melatonin and raspberry ketone, another natural product, thus further supporting the use of the hybrid strategy. These results clearly indicate that the 4-OH is indispensable for the neuroprotective activity of

54. This notion is further demonstrated by the results of the unsubstituted analog **57**, the 4-OCH_3 analog **58**, the 3,4-methylenedioxy analog **59**, and the 3,4-dimethoxy analog **60**, all of which exhibited significantly diminished protective ability (<30% viability for all). These results could also indicate that H-bond interactions with the 4-OH group may be playing an important role in the biological activity of **54**. Interestingly, replacement of the 3-OCH_3 group of **54** with an -OH group**,** as demonstrated by **61,** led to a significant loss of neuroprotection (~60% loss) in comparison to **56.** Similarly, adding a -OCH_3 group to the 5-position of **54** (**62**) also reduced the protective abilities by about 30% compared to **54**. This may suggest that there are unfavorable H-bond or electronic interactions when an -OH group is at the 3-position. Additionally, the specific interaction site with the 4-OH moiety may not be able to tolerate steric hindrance at the 5-position, a notion further reflected by compound **63.** Compound **63** contains a -$N(CH_3)_2$ substitution at the *para*-position of the phenyl ring and showed weak neuroprotection (~20% protection compared to the -TC control). Replacement of the 4-OH-phenyl ring of **54** with a pyridine ring resulted in two compounds, with the 3-substituted pyridine analog **64** being completely inactive, while the 4-substituted pyridine analog **65** was moderately active in protecting MC65 cells (~33% increase in protection compared to the -TC control). The activity of **65** might compare somewhat to the protective activity of **56** since the nitrogen of the pyridine ring is in the same position as the 4-OH group in compound **56** and can also potentially participate in H-bond interactions. Moreover, for the furan substituted analogs **66** and **67**, no neuroprotection was observed for the 2-furan substituted analog **66**, while the 3-furan substituted analog **67** exhibited moderate protection (~48% increase in protection compared to the -TC control), which is consistent with the results of **64** and **65** considering the positions of the oxygen in the furan ring.

To investigate the contribution of the conjugated double bond between the phenyl ring and the ß-ketone, compound **68** was synthesized and assayed at a concentration of 0.3 µM. Notably, **68** also exhibited significant and comparable protection of MC65 cells with that of **56**, suggesting that the conformationally rigid double bond and the conjugation system with the phenyl ring is not necessary to produce the neuroprotection observed for these analogs. Furthermore, the electronic effects of the substitutions on the phenyl ring may not play an essential role in the biological activity of this chemotype, which is consistent with the results of **55-63**. Since compounds **56** and **68** exhibited near-full protection of MC65 cells, the dose-response of these compounds was obtained to assess their neuroprotective potency. As shown in Figure 15, the EC_{50}s for **56** and **68** to protect MC65 cells were 23.05 ± 5.23 and 27.60 ± 9.40 nM, respectively, which is about 5-fold more potent than **54**. Because **56** and **68** showed similar neuroprotective potencies in MC65 cells, either both **56** and **68,** or **68** alone, were tested in subsequent mechanistic investigations.

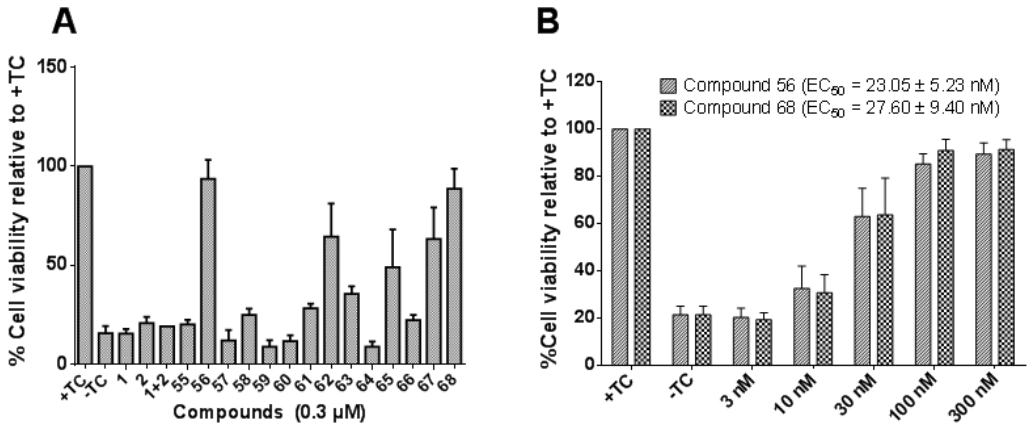

Figure 15. Full series screening of hybrid compounds and dose response of **56** and **68.** A. Neuroprotective effects of full series of hybrid compounds. MC65 cells were treated with indicated compounds at 0.3 µM under +TC or -TC conditions for 72 h. Cell viability was assessed by MTT assay. Data were expressed as mean percentage viability (n=4) with parallel +TC cultures set at 100% viability. Error bars represent SEM. B. Dose response of **56** and **68**. MC65 cells were treated with **56** or **68** at indicated concentrations under -TC conditions for 72 h. Cell viability was assessed by MTT assay. Data were expressed as mean percentage viability (n=3) with parallel +TC cultures set at 100% viability. Adapted from Chojnacki et al.[207]

3.3.5 Antioxidative ability of 56 and 68 in MC65 cells

Following the same line of reasoning with compound **54**, the anti-oxidative activity of **56** and **68** were measured using the DCFH-DA assay. As shown in Figure 16, both **56** and **68** dose-dependently suppressed ROS production with IC_{50}s of ~63 nM and ~68 nM, respectively, both of which are slightly less potent than their EC_{50}s from the MTT assay. This supports the hypothesis that these hybrids are acting in a multifunctional fashion, and that their other protective abilities may be upstream from ROS production. Furthermore, because MC65 cells express large quantities of AßOs and oxidative stress has been implicated in the death of MC65 cells, this suggests that the production of AßOs eventually funnels into ROS production, leading to cytotoxicity. In order to confirm this idea, N-acetylcysteine (NAC) and Trolox (6-hydroxy-2,5,7,8-tetramethyl chroman-2-carboxylic acid) were tested for their protection in MC65 cells under the same assay conditions as **68**. Trolox functions as a chain-breaking antioxidant and is particularly effective against lipid peroxidation.[210-212] Notably, like **68,** Trolox significantly protected MC65 cells from -TC-induced cytotoxicity at concentrations as low as 10 μM. NAC, on the other hand, acts primarily as a hydrogen peroxide scavenger, and only partially rescued viability at 8 and 16 mM concentrations (Figure 16), which is consistent with previously reported results.[172] Given the fact that Trolox and NAC have different mechanisms of antioxidation, this may suggest that ROS-induced lipid peroxidation is the major pathway involved in the death of MC65 cells. Taken together, these results strongly support the idea that oxidative stress is the convergent event after the production of AßOs in MC65 cells that ultimately leads to cell death.

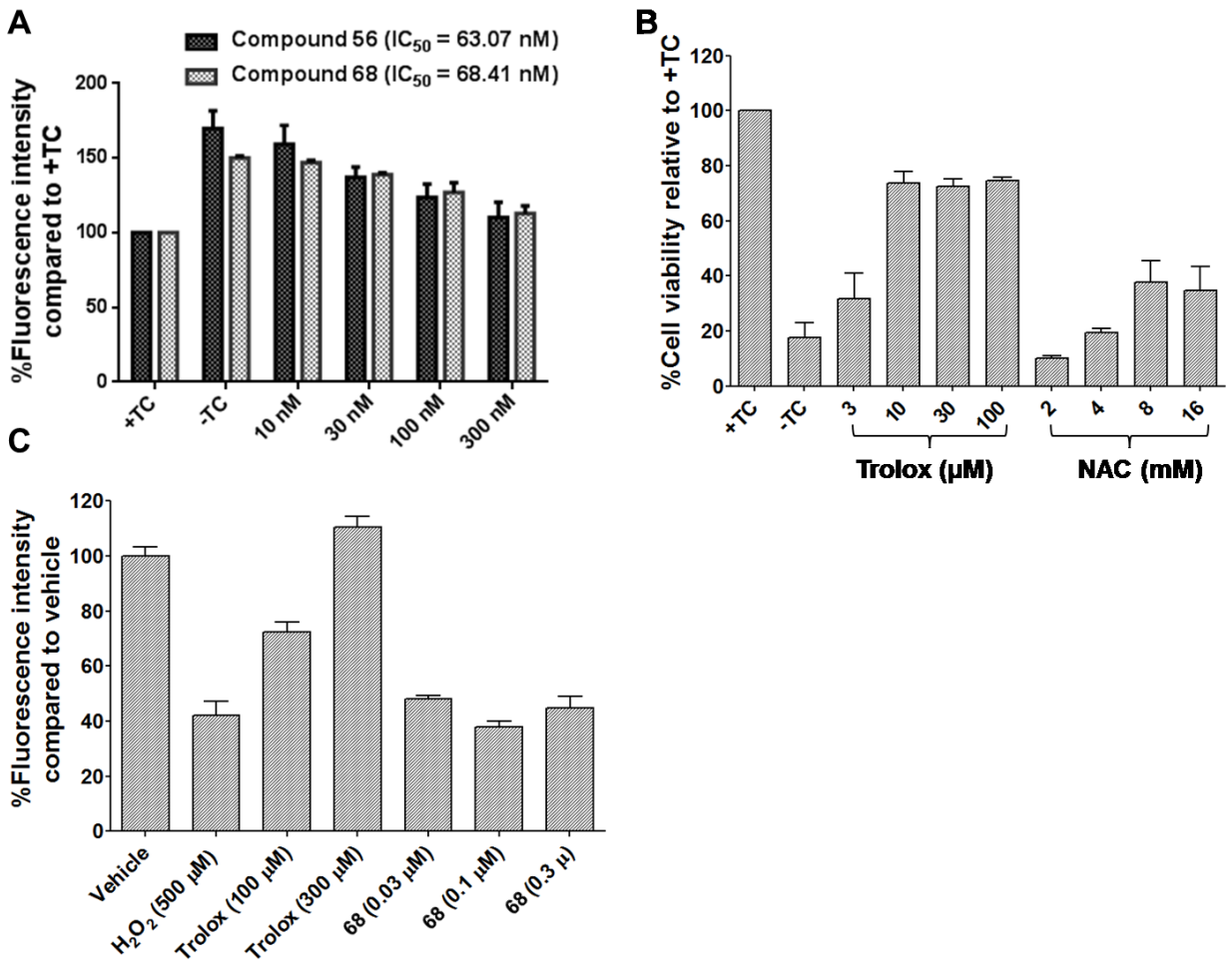

Figure 16. Antioxidative properties of Trolox, NAC, **56**, and **68** in MC65 cells**.** A. Antioxidative ability of **56** and **68**. MC65 cells were treated with **56** or **68** at indicated concentrations under -TC conditions for 48 h, then DCFH-DA (25 μM) was loaded and fluorescence intensity was analyzed at 485 nm (excitation) and 530 nm (emission). Data were presented as a mean percentage of fluorescence intensity (n=3). Error bars represent SEM. B. Neuroprotective ability of known antioxidants. MC65 cells were treated with Trolox or NAC at indicated concentrations under -TC conditions for 72 h. Cell viability was assessed by MTT assay. Data were expressed as mean percentage viability (n=3) with parallel +TC cultures set at 100% viability. Error bars represent SEM. C. Neuroprotective ability of Trolox and **68** in an oxidative stress model. HT22 cells were treated with Trolox or **68** at indicated concentrations before addition of H_2O_2 (500 μM) and incubated for 24 h. Cell viability was assessed by MTT assay. Data were expressed as mean percentage viability (n=3) with parallel H_2O_2-free cultures set at 100% viability. Error bars represent SEM. Adapted from Chojnacki et al.[207]

3.3.6 Effects of 56 and 68 on AßO production

As previously mentioned, under -TC conditions, MC65 cells can produce intracellular AßOs that eventually lead to cell death. Therefore, the inhibitory effects of **56** and **68** on the production of AβOs were investigated. As shown in Figure 17, both **56** and **68** dose-dependently suppressed the production of higher weight AßOs, including tetramers, pentamers, and heptamers. However, the potencies in suppressing AßOs were significantly lower than the potencies for protecting MC65 cells from -TC induced cytotoxicity (Figure 15). Much like the anti-oxidative ability of **56** and **68,** this may suggest that the suppression of AßOs contributes only partially to their multifunctional, neuroprotective function, and moreover, may not constitute the major mechanism of action. To further explore the effects on Aß aggregation, **68** was tested for its ability to inhibit $Aß_{42}$ fibril formation using the thioflavin T (ThT) assay. Compound **1**, known to inhibit Aß fibrillization, was tested as a positive control. As shown in Figure 17, **1** inhibited the formation of $Aß_{42}$ fibrils (25 μm or longer) by ~27% at 10 μM, consistent with reported results.[194] However, no significant inhibition was observed for **68** even at concentrations as high as 100 μM, strongly signifying that **68** cannot bind to $Aß_{42}$ directly and inhibit its fibrillization. Atomic force microscopy (AFM) studies of $Aß_{42}$ aggregation also confirmed that **68** showed no inhibition on both fibrillization and oligomerization of $Aß_{42}$ under the same assay conditions (Figure 17).

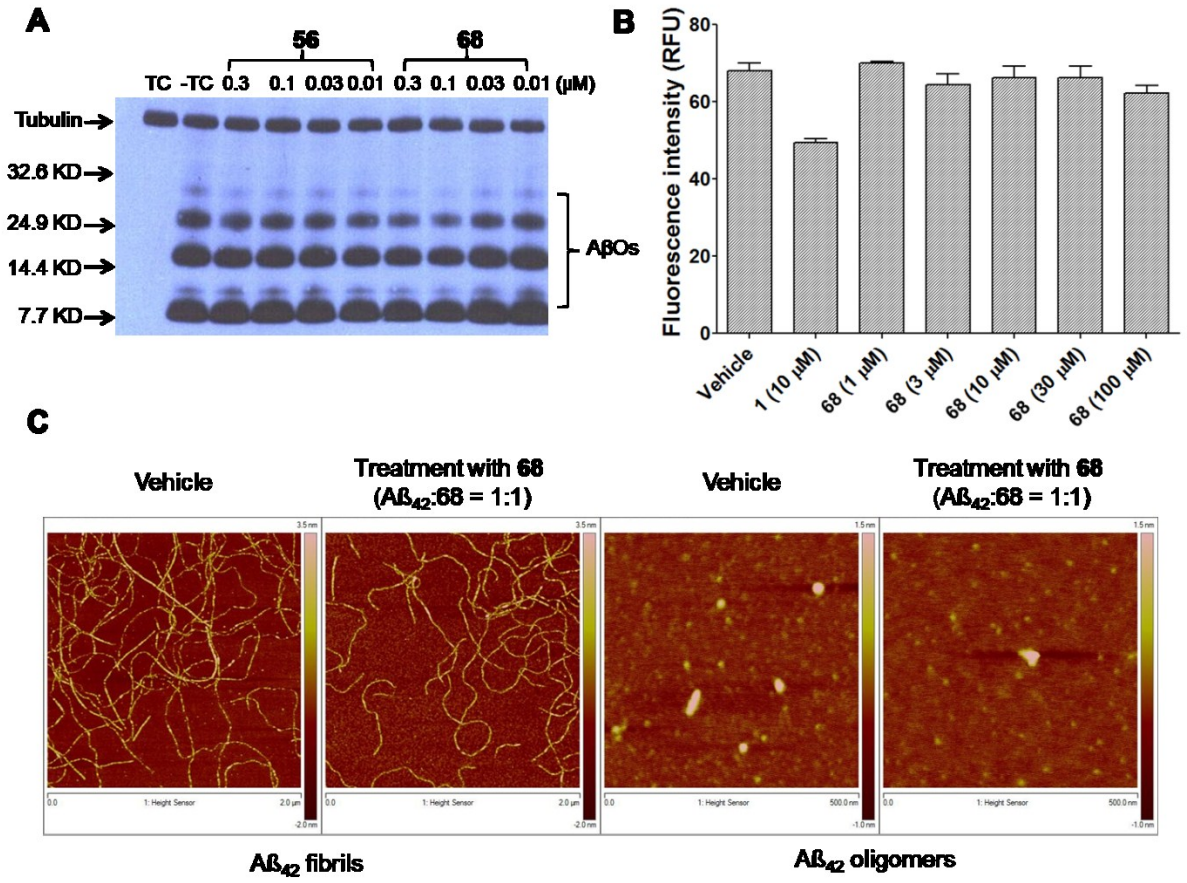

Figure 17. Effects of **54** and **68** on Aß oligomerization. A. MC65 cells were treated with indicated compounds at indicated concentrations for 24 h immediately after the removal of TC. Lysates from cultures were analyzed by Western blotting using 6E10 antibody. The image represents the results from one of three independent experiments. B. $Aß_{42}$ was added to solutions of **1** and **68** at indicated concentrations for 48 h. Thioflavin T (ThT) was then added, and fluorescence intensity was analyzed at 446 nm (excitation) and 490 nm (emission). Data were presented as a mean percentage of fluorescence intensity (n = 3). Error bars represent SEM. C. $Aß_{42}$ fibrils and oligomers were incubated with a solution of **68** in a 1:1 ratio for 24 h. Aggregate morphology was visualized by AFM. Adapted from Chojnacki et al.[207]

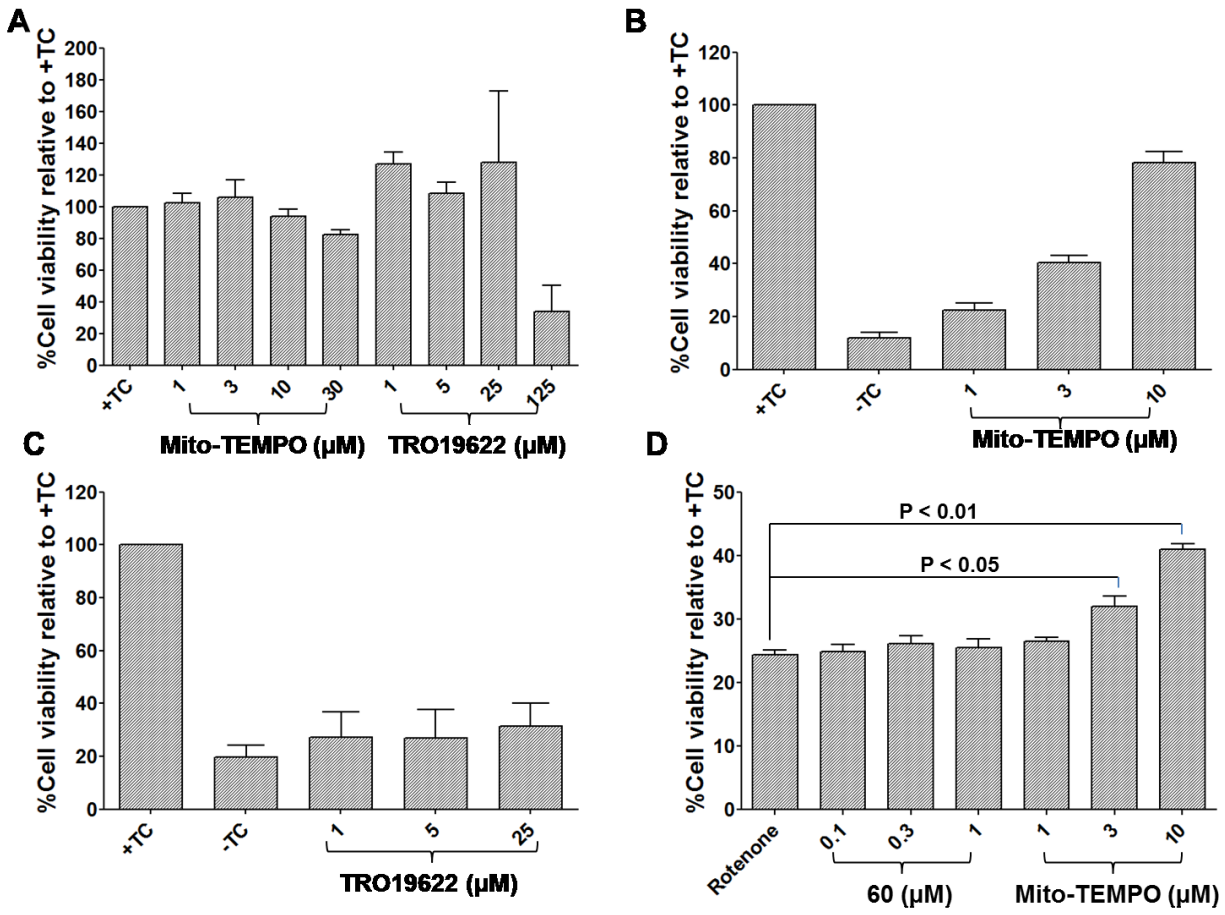

Figure 18. Effects of Mito-TEMPO, TRO19622, and **68** on ROS formation in MC65 cells. A. Effects on viability of TRO19622 and Mito-TEMPO in MC65 cells. Cells were treated with Mito-TEMPO or TRO-19622 at indicated concentrations under normal growth conditions (+TC) for 72 h. Cell viability was assessed by MTT assay. Data were expressed as mean percentage viability (n=3) with parallel +TC cultures set at 100% viability. Error bars represent SEM. B. Neuroprotective ability of Mito-TEMPO. MC65 cells were treated with Mito-TEMPO at indicated concentrations under -TC conditions for 72 h. Cell viability was assessed by MTT assay. Data were expressed as mean percentage viability (n=3) with parallel +TC cultures set at 100% viability. C. Neuroprotective ability of TRO-19622. MC65 cells were treated with TRO-19622 as described above. Data were expressed as mean percentage viability (n=3) with parallel +TC cultures set at 100% viability. D. Neuroprotective ability of Mito-TEMPO and **68** against rotenone-induced toxicity. MC65 cells were treated with indicated compounds at indicated concentrations for 2 h before addition of rotenone for 48 h. Cell viability was assessed by MTT assay. Data were expressed as mean percentage viability (n=3) with parallel +TC cultures set at 100% viability. Error bars represent SEM. Adapted from Chojnacki et al.[207]

3.3.7 Effects on H_2O_2-induced cytotoxicity in HT22 cells

As touched upon previously, the demonstrated antioxidative ability of **56** and **68** in MC65 cells could be produced through different mechanisms. Although these compounds do not directly bind Aß, as evidenced above, interference with the production of AßOs, disruption of interactions between AßOs and various partner proteins, or direct antioxidant effects could all be potential mechanisms of action. Therefore, possible mechanisms of **68**'s antioxidative properties were investigated. Since we have demonstrated that **68** does not inhibit the aggregation of Aß and inhibits the production of AßOs with a significantly lower potency compared to its neuroprotection potency, analog **68**'s ability to protect HT22 cells from H_2O_2-induced cytotoxicity was used. HT22 cells, an immortalized murine hippocampal line, are another widely used neuronal cell model, particularly for cellular oxidative stress.[213, 214] The results from this assay would help rule out the possibility of **68** acting directly as an antioxidant. As shown in Figure 18, H_2O_2 (500 μM) led to significant HT22 cell death (~58%). As expected, the known antioxidant Trolox dose-dependently protected HT22 cells from H_2O_2-induced cytotoxicity with full rescue at 300 μM. However, no protection was observed for **68** up to 0.3 μM. Altogether, these results indicate that the effects of **68** observed in MC65 cells are not through direct antioxidative ability, signifying that **68** may be functioning somewhere between the production of AßOs and the accumulation of ROS, for example, at interactions between AßO and partner proteins.

3.3.8 Effects of 68 on rotenone-induced toxicity in MC65 cells

Since mitochondria are the main sites of intracellular ROS generation,[215, 216] **68** was assayed for its ability to act inside mitochondria to exhibit its antioxidative and neuroprotective activities. Taking this into consideration, two control were first tested for their neuroprotective properties in MC65 cells under TC removal conditions: TRO-19622, a mitochondrial permeability transition pore (mPTP) inhibitor,[217] and Mito-TEMPO, a known mitochondrial ROS (mitoROS) specific scavenger.[218] Both compounds were intially tested under normal growth conditions (+TC) in MC65 cells to identify concentrations with no cytotoxic effects, ruling out any potential biased interpretation of the following assays. As shown in Figure 18, Mito-TEMPO did not show toxic effects up to 10 μM and TRO-19622 did not show cytotoxicity up to 25 μM. Therefore, these two concentrations were chosen as maximums for their respective compounds in subsequent assays. Notably, shown in Figure 18, Mito-TEMPO dose-dependently protected MC65 cells from -TC-induced cytotoxicity, while TRO-19622 did not show any protection up to 25 μM (Figure 18). Combined with the results of **68**'s antioxidative and neuroprotective effects, this may indicate that AßOs, produced upon TC removal, interact with certain mitochondrial membrane proteins to generate mitochondrial specific ROS in a mPTP-independent manner. To advance this idea further, protection of rotenone-induced cytotoxicty in MC65 cells was also explored. Rotenone is a potent neurotoxin that has been demonstrated to inhibit mitochondrial complex I and is linked to mitoROS production. As shown in Figure 18 rotenone greatly promoted death of MC65 cells (76%) at 10 μM. Mito-TEMPO significantly protected MC65 cells from cell death at 3 and 10 μM in a dose-dependent manner, while **68** did not impart any protection up to 1 μM, concentrations known to rescue MC65 cells from -TC-induced cytotoxicity. Collectively, these results propose that upon production, AßOs enter or

interact with the mitochondrial membrane to produce mitoROS that ultimately lead to the death of MC65 cells, and **68** blocks this interaction, which accounts for its antioxidative and neuprotective activities as demonstrated by the aforementioned assays. Because AßOs have been shown to promote tau hyperphosphorylation, neurofibrillary tangle formation, synaptic alteration, and neurodegeneration,[30, 219, 220] the ability of **68** to block protein-protein interactions between AßOs with its various partners implies a potential of this chemotype as a new template to develop novel, effective AD-modifying agents. Further studies are warranted to elucidate more detailed mechanisms of this compound.

3.3.9 Metal ion chelating ability of 56 and 68

Compound **54** was previously shown not to chelate biometals, including Cu^{2+}, Fe^{2+}, and Zn^{2+}, and this was ascribed to the structural change of the ß-diketone into a ß-ketone amide. To confirm this assertion and also to rule out the possible involvement of other structural moieties in biometal chelation, **56** and **68** were tested for their ability to chelate biometal ions. Consistent with **54**, both compounds failed to form complexes with any of the three biometals (Figure 19).

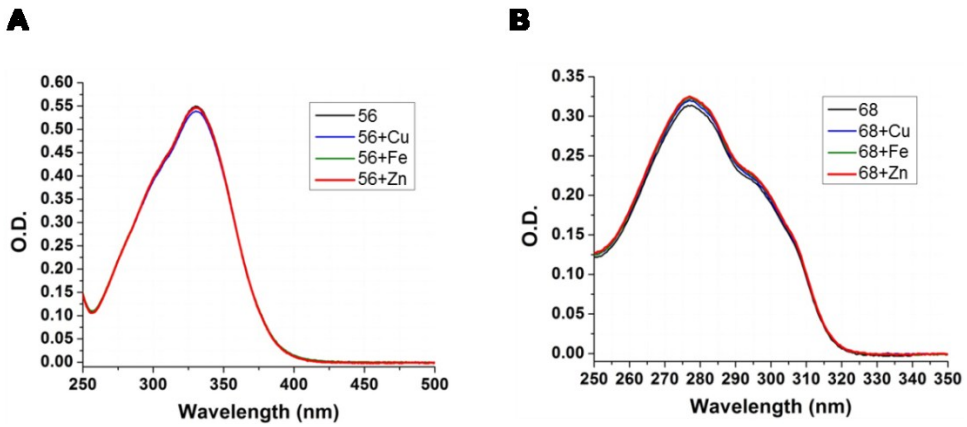

Figure 19. Metal chelating ability of **56** and **68**. Compounds **56** (A) and **68** (B) were incubated with $CuSO_4$, $FeCl_2$, or $ZnCl_2$ at room temperature for 10 min. UV-vis spectrum was recorded from 250 nm to 600 nm. Adapted from Chojnacki et al.[207]

3.3.10 BBB penetration assay

Considering AD management would be a long term care process for patients, oral administration would significantly improve patient compliance, which is sometimes just as important as drug toxicity and resistance. Based on this, compound **68** was assayed for its blood-brain barrier (BBB) permeability in male CD1 mice (n=6) by oral administration at a dose of 50 mg/kg. To quantify accurately the amount of **68** delivered into brain tissue and prevent the possibility of biased interpretation from vascular trapping, mice were perfused prior to tissue collection in order to wash out completely the vascular blood. After oral administration, plasma samples were collected at 0.25, 0.5, 1, and 24 h, and brain samples were collected at 1 and 24 h. Collected samples were analyzed by LC-MS/MS and the results are shown in Table 1. Compound **68** exhibited a quick absorption profile with plasma concentrations reaching 773 ± 309.86 nM (n=6) 15 min after oral administration and only slightly above this after 1 h. Concentrations of **68** in the plasma and brain after 1 h were 883 ± 350 nM and 555 ± 188 nM, respectively. This clearly demonstrates that **68** can quickly and efficiently reach brain tissue

after oral ingestion, confirming its BBB permeability. After 24 h, the plasma and brain concentrations dropped to 31 ± 12 nM and 47 ± 11 nM, respectively. It is important to note that the brain concentration of **68** at this time point still remains above the neuroprotective EC_{50} of **68** in MC65 cells (28 ± 10 nM), suggesting that a once daily regimen should supply a sufficient amount of compound **68** for the brain tissue to be therapeutically effective.

Table 1. Plasma and brain concentrations of **68** after oral administration in CD1 mice.

	15 min	30 min	1 h	24 h
Plasma	774 ± 310	795 ± 301	883 ± 350	31 ± 12
Brain			555 ± 188	47 ± 11

3.4 Conclusion

A series of hybrids of curcumin **1** and melatonin **2** were designed as potential multifunctional neuroprotectants for AD and successfully synthesized. Preliminary biological characterization of **54** established the feasibility of utilizing a hybrid compound strategy in providing novel chemotypes with novel pharmacology. Further SAR studies of analog **54** revealed **56** and **68** as lead compounds with potent neuroprotective properties in MC65 neuroblastoma cells. Initial mechanistic studies suggested that antioxidative effects might be a major neuroprotective mechanism, and it is likely that the observed antoxidative effects of **56** and **68** are through interference of interactions of AßOs with mitochondria in MC65 cells. Furthermore, **68** has been shown to penetrate the BBB efficiently after oral adminsitration in

intact mice, confirming that it is orally bioavailable and therapeutically relevant concentrations are attainable in the CNS.

These results strongly encourage further optimization of **68** as a new lead in the development of more potent analogs. Compounds exploring structural modification of the indole ring and ß-ketone amide are certainly warranted and would provide more comprehensive SAR data for better rational design. Due to the anti-oxidative properties of these ligands, assays examining their effects in other neurodegenerative disorders, for example Parkinson's or Huntington's diseases, could potentially be conducted. This would have the effect of either exhibiting the broader therapeutic implications of these ligands or demonstrating the specificity these ligands have toward Aß-related toxicity, providing more mechanistic insight. Naturally, *in vivo* studies must be performed to ascertain if and how these compounds affect AD pathology. AßO concentration and deposition in the brain would need to be examined, in addition to mitochondrial function and overall tissue viability. Altogether, these findings support the hybridization strategy as a novel design approach to provide effective disease-modifying agents for AD.

4 NLRP3 Inhibitors

4.1 Project Design

Glyburide (**70**) also known as Glibenclamide, was first developed in 1966 as a hypoglycemic agent, and is now the mostly used drug for the treatment of type 2 diabetes mellitus (T2DM).[221] It is of the sulfonylurea class of anti-diabetics and works by inhibiting ATP-sensitive K^+ (K_{ATP}) channels in pancreatic ß cells causing membrane depolarization that opens voltage-gated Ca^{2+} channels. This calcium influx leads to the secretion of insulin, which ultimately reduces blood glucose.[222] Mechanistically, glyburide binds the ATP-binding cassette (ABC) transporter domain of the K^+ channel, which is sensitive to sulfonylurea moieties. In addition to K_{ATP} channels, ABC transporter ABCA1 has also been suggested to be a potential target for glyburide.[223, 224] Notably, glyburide has also been known to exhibit anti-inflammatory activity. Recent epidemiological studies have revealed that T2DM patients were protected from death associated with pulmonary bacterial-associated sepsis, and this increase in survival was correlated to a rise in anti-inflammatory gene expression profiles in blood leukoctyes.[225] In fact, glyburide was first shown to decrease IL-1ß production and release in 1997.[226] Follow up studies have determined that this effect is specific to the NLRP3 inflammasome. Unfortunately, the use of glyburide as a NLRP3 inhibitor *in vivo* would require several hundred-fold higher doses than those used in diabetes to achieve significant anti-inflammatory activity, which would inevitably lead to lethal hypoglycemia.[227]

Because the sulfonylurea moiety in the glyburide molecule is chiefly involved in the binding of K_{ATP} channels, one study by Lamkanfi *et al.* explored the effects of removing this group. Interestingly, it was shown that removal of the cyclohexylurea moiety abolishes

glyburide's insulin secretion ability, yet retains some activity on NLRP3 inhibition.[227] The analog described in the report, **74**, contains a sulfonyl chloride group, which is highly susceptible to nucleophilic attack. Therefore, this compound would likely be unstable in a physiological environment. Notably, no further studies were pursued. Based on these findings, however, we hypothesize that glyburide analogs free of the cyclohexylurea group containing stable sulfonyl moieties could exhibit NLRP3 inhibition without affecting blood glucose levels.

To this end, a series of novel compounds based on analog **74**'s scaffold were designed and synthesized (Figure 20). Inhibition of IL-1ß, the major cytokine produced from NLRP3 inflammasome activation, was used as the primary metric of activity and for elucidation of any structure-activity relationships (SAR). Additionally, various aspects of NLRP3 formation and function, including ASC aggregation, caspase-1 activity, and cellular viability, were also investigated, both *in vitro* and *in vivo*.

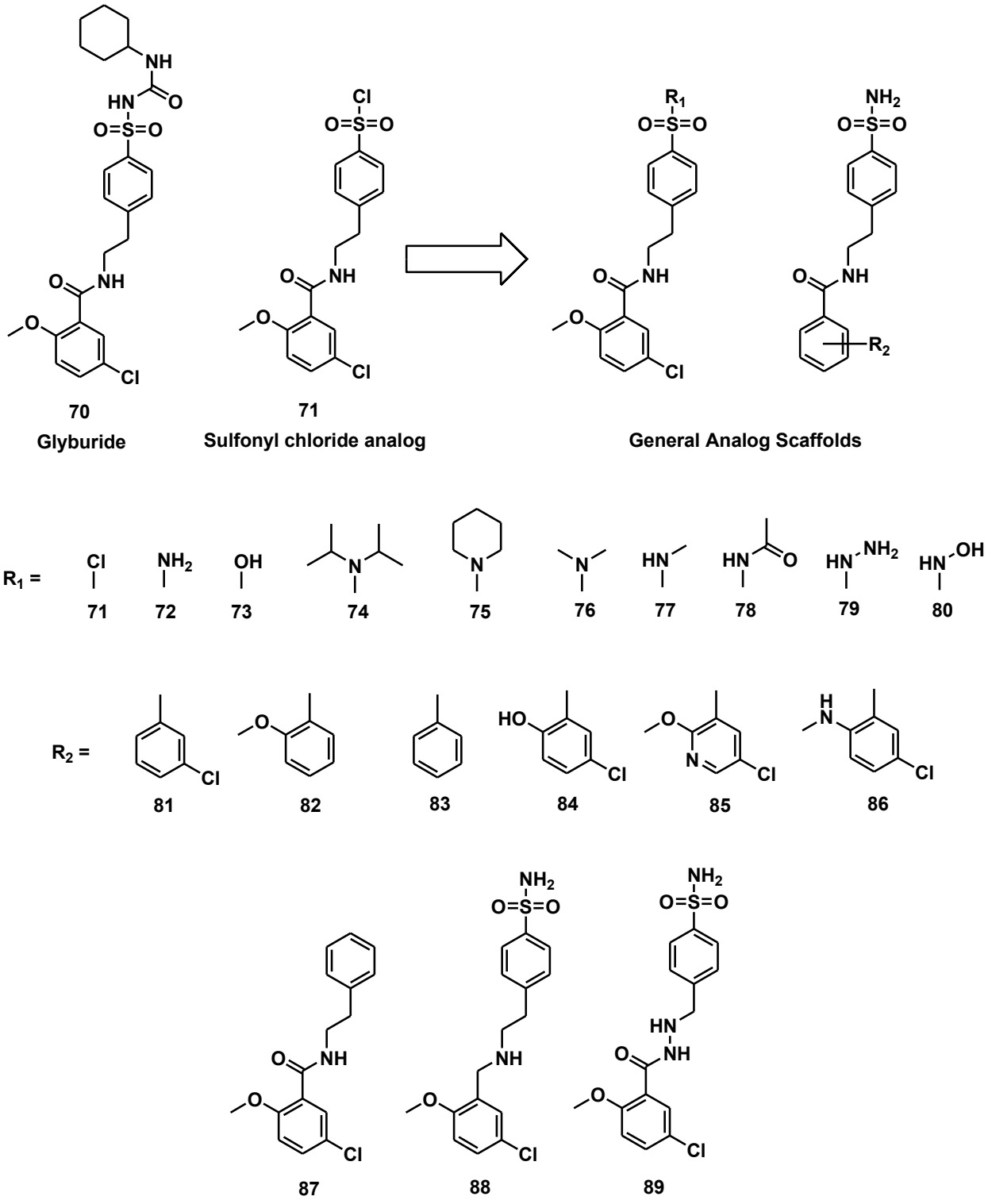

Figure 20. Synthesized glyburide analogs as potential inhibitors of the NLRP3I.

4.2 Chemical Design and Syntheses

Compounds **71, 72, 73,** and **87** were initially designed to examine the necessity of the sulfonyl group and the effectiveness of stabilizing the sulfonyl chloride, reported by Lamkanfi et al.[227] After preliminary biological characterization, compound **72** was found to be highly active. From here, the remaining analogs were based on **72'**s structure. Compounds **74-80** were designed to explore the space around the sulfonamide and determine the effects of various substitutions of the nitrogen atom. Compounds **81-86** were synthesized to deconstruct the benzamide ring and investigate the effects of altering substituents to the ring. Lastly, compounds **88** and **89** contain changes in the alkyl chain linking the two rings: **88** with a reduced carbonyl carbon to examine the necessity of the amide group and **89** with the addition an extra amine to explore its hydrogen bonding capabilities and to increase potentially water solubility.

4.2.1 Amide coupling

The synthetic route for this series of glyburide analogs is outlined in Scheme 6. Initially, compounds **87, 71, 72,** and **73** were synthesized. The remaining analogs were synthesized after preliminary assays for the first compounds were conducted. 5-chloro-2-methoxybenzoic acid **90** and phenethylamine **91** were coupled via an amide bond using EDC and HOBt as carboxyl activating agents, and Et_3N as an acid trap. The resulting product **87** contains the general scaffold of glyburide lacking the sulfonyl substituent, and later was actually used as a negative control in some assays. A reaction utilizing thionyl chloride to create an acid chloride intermediate was also used to create the amide bond seen in a majority of the designed analogs. Here, thionyl chloride was added to different benzoic acids and refluxed to form the acid

chloride intermediate. Because this substituent is highly susceptible to nucleophilic attack, even from weak nucleophiles, it was not isolated. Removal of thionyl chloride via rotary evaporation followed by addition of the amine species yielded the amide species in good yield. Typically, 4-(2-aminoethyl)benzenesulfonamide **92**, with the sulfonamide group already installed, was used as the starting material, affording analogs **81, 82, 83,** and **85** in one step. For analogs **84** and **86**, this protocol was not used, as the unprotected hydroxyl group leads to unwanted intramolecular reactions. Instead the EDC/HOBt protocol was used.

4.2.2 Aromatic sulfonation

Addition of the sulfonyl chloride group to the unsubstituted phenyl ring was accomplished by aromatic sulfonation. Compound **87** was dissolved in concentrated chlorosulfonic acid and heated to 75 °C for 1~2 h. After cooling back to room temperature, the reaction was slowly poured onto a crushed ice and water solution, due to the strong reactivity of the excess acid. The sulfonyl chloride product **71** was then extracted into DCM for purification. Substitution at the para position is greatly preferred over the ortho position due to steric hindrance, giving isomeric ratios of 95:5 or more. Initial reactions were heated to 100 °C, as originally reported, but this actually leads to increased formation of the unwanted ortho product. Purification of the para-substituted product was performed by column chromatography. Despite some of the instabilities of the sulfonyl chloride group and the high ratio of para product, it is preferable to isolate the desired isomer at this step and not continue directly to subsequent steps. This is because it was later discovered that separation of isomers of the various sulfonamides

final products was more difficult to achieve, often accomplished by recrystallization, which can significantly reduce product yield.

4.2.3 Sulfonamide formation

Adding various amines to **71**, often at room temperature, readily converts the sulfonyl chloride group into a sulfonamide moiety, through nucleophilic substitution. Reactions containing amines in hydrochloride salt form were premixed with an acid trap base, typically triethlyamine or N-methylmorpholine, to give the free base form of the amine. Compound **73** was accomplished through a similar mechanism to form the sulfonic acid derivative. However, because the oxygen in water is a significantly weaker nucleophile than the other amines used, the reaction needed to be heated (~100 °C) to provide enough energy for substitution.

4.2.4 Reductive amination

Compounds **88** and **89** were designed to explore the amide and alkyl chains linking the two phenyl rings of compound **72**. Compound **88** lacks the carbonyl oxygen, effectively changing the amide to an amine. Compound **89** has an added secondary amine linked to the amide in order to potentially increase water solubility. Both analogs were successfully synthesized by reductive amination. Here, the individual aldehyde and amine starting materials were added together in the presence of acetic acid to form the respective imine *in situ*. $NaCNBH_3$ in MeOH was then added as a reducing agent, directly reducing the imine to the desired amine in good yield.

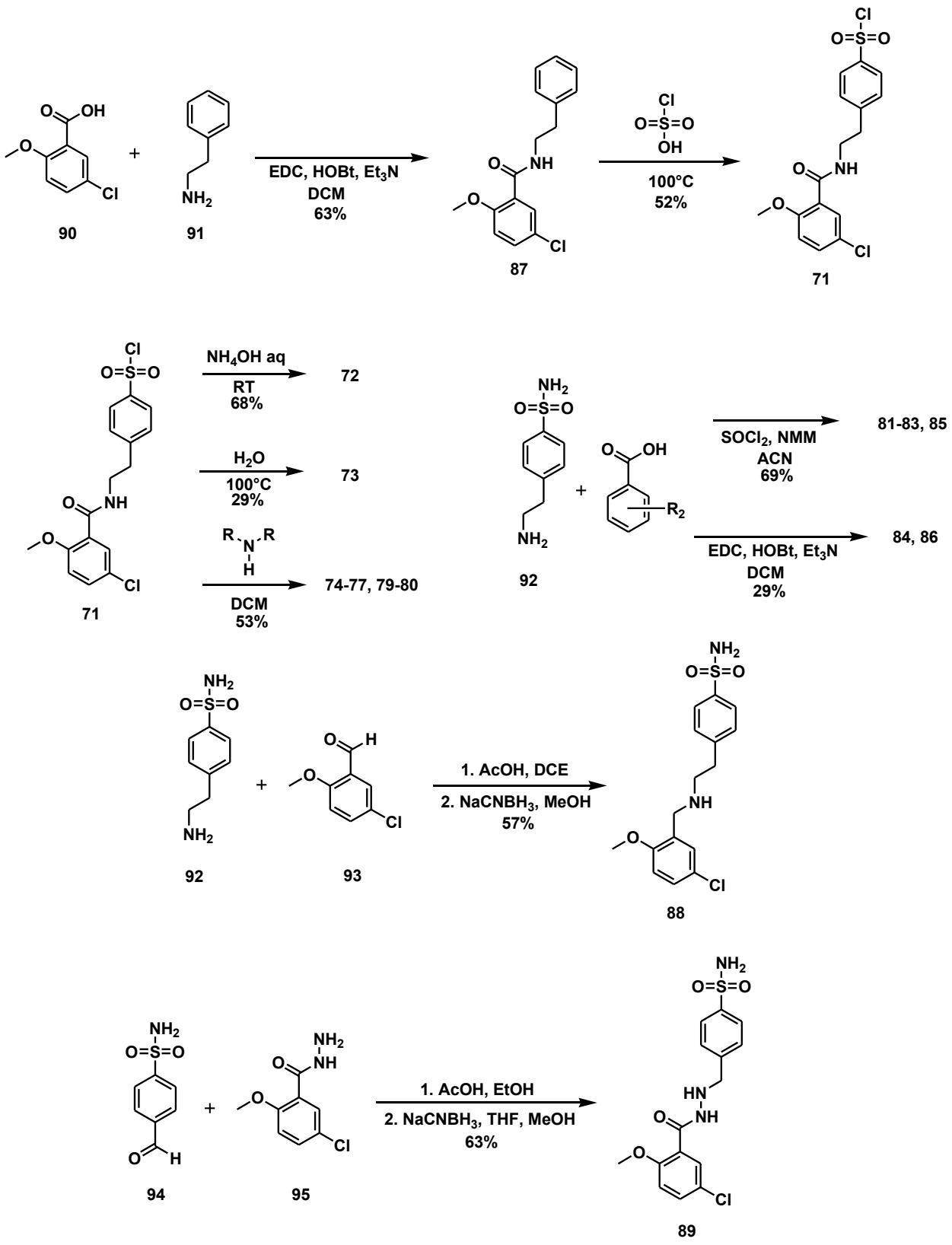

Scheme 6. Synthetic route for designed glyburide analogs.

4.3 Biological Studies

As mentioned previously, the NLRP3 inflammasome has been implicated in a variety of diseases and disorders. In particular, it plays a major role in AD, but also cardiac related inflammation, namely myocardial infarction, ischemia-reperfusion injury, and peritonitis. Due to the availability of animal resources, murine models of amyloid myocardial infarction (AMI) and peritonitis were chosen for biological screening *in vivo*. Additionally, two cell lines, both expressing the NLRP3 inflammasome, were chosen for *in vitro* studies: J774.A1 murine macrophages and HL-1 cardiomyocytes. As previously mentioned, compounds **71, 72, 73,** and **87** were initially synthesized and biologically characterized for their effects on cell viability in HL-1 cardiomyocytes. From here, lead compound **72** was assayed extensively for its anti-inflammatory properties. The remaining series were then synthesized and screened for IL-1ß reduction in J774.A1 macrophages.

4.3.1 Effects on HL-1 cell viability

To examine compounds **71, 72, 73,** and **87** for their effects on NLRP3 inflammasome-induced cell death, HL-1 cardiomyocytes were used. HL-1 cells were treated with LPS and ATP to induce inflammasome formation, which subsequently leads to a decrease in cell viability. The amount of cell death was measured by the Trypan Blue exclusion method (Figure 21). Compounds were dosed before administration of ATP at 400 μM, in accordance with Lamkanfi's report. Compound **71** showed some protection from LPS/ATP induced cell death, consistent with its reported effects on NLRP3 inhibition.[227] Notably, compound **72** exhibited the

strongest protection. Due to this and the inherent instabilities of the sulfonyl chloride group previously mentioned, compound **72** was chosen for further testing.

4.3.2 NLRP3 inflammasome formation prevention *in vitro*

Cultured J774.A1 mouse macrophages were treated with LPS followed by ATP to induce the formation of the NLRP3 inflammasome, and the release of mature IL-1ß in the supernatant was measured (Figure 21). Treatment with compound **72** significantly limited IL-1ß release after LPS and ATP challenge (Figure 21). To determine whether **72** also inhibited the formation of the inflammasome in cardiomyocytes, cultured adult HL-1 cardiomyocytes were treated with LPS and ATP, which induces the formation of the NLRP3 inflammasome. Inflammasome activation was measured by immunocytochemistry for ASC aggregates, caspase-1 activity, and inflammatory cell death. All of these effects were prevented or significantly reduced by treatment with **72** (Figure 21). ATP binding to P2X7 receptors leads to K^+ efflux from the cell and subsequent activation of the NLRP3 inflammasome. Accordingly, addition of nigericin, a pore forming toxin allowing for K^+ efflux, along with LPS also leads to NLRP3 activation, independent of the P2X7 receptor. This pathway of activation was prevented by compound **72**, as well (Figure 21). The activation of inflammasomes that use sensors other than NLRP3, but are still complexed with caspase-1 (AIM2, triggered by exogenous dual strand DNA; NLRC4, triggered by flagellin), were not inhibited by compound **72** (Figure 22). Together, this demonstrates **72**s specificity for the NLRP3 inflammasome and shows that its effects are neither due to P2X7 interaction nor caspase-1 inhibition.

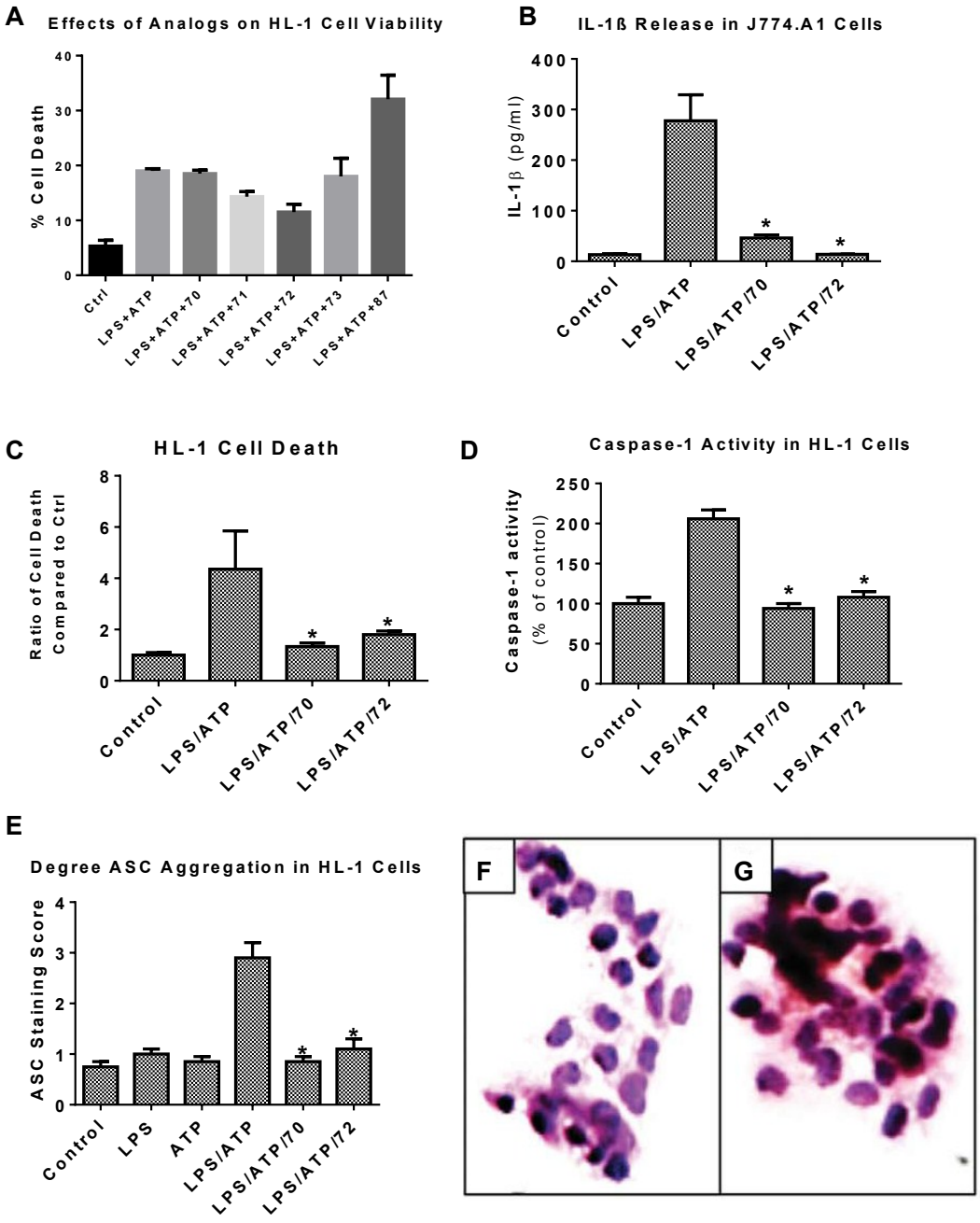

Figure 21. Various effects of glyburide and **72** on markers of inflammasome activation. A. Compounds **71** and **72** show better protection of cell death in HL-1 cardiomyocytes compared to glyburide **70**. B. LPS/ATP stimulates IL-1ß release in J774.A1 macrophages that is inhibited by **70** and **72**. C. Comparative ratio of protection of **70** and **72** in HL-1 cells. D. Caspase-1 activity is increased in response to LPS/ATP, which is prevented by **70** and **72**. E. Compounds **70** and **72** prevent ASC aggregation upon LPS/ATP stimulation. F and G. Example stains of ASC aggregates without LPS/ATP (F) and with LPS/ATP (G). *$p<0.05$ Adapted from Marchetti et al.[228]

4.3.3 Effects on blood glucose *in vivo*

Compared to the glyburide structure, **72** lacks the cyclohexylurea moiety involved in the activation of the release of insulin. As such compound **72** was well tolerated when given at doses as high as 500 mg/kg for 7 days, showing no significant effects on survival, body weight, appetite, or behavior. Compound **72** also exhibited no effects on plasma glucose levels, whereas glyburide led to a significant reduction in glucose levels as early as 2 h. Additionally, glyburide was lethal within 3 days in 50% of mice treated with 100 mg/kg every 6 h for 3 doses, and in 100% of mice after daily doses of 500 mg/kg, due to severe hypoglycemia in all cases (Figure 22). This further confirms the importance of the cyclohexylurea group for K_{ATP} binding and the insulin secreting effects of glyburide, which are not seen for **72**.

4.3.4 Inhibition of the NLRP3 inflammasome in acute myocardial infarction in mouse

To determine whether compound **72** inhibited the NLRP3 inflammasome *in vivo*, a model of severe regional myocardial ischemia due to surgical coronary ligation (30 min) followed by reperfusion (24 h) was used. Treatment with **72** led to a significant (>90%) reduction in caspase-1 activity in heart tissue measured 24 h after ischemia (Figure 24). A significant reduction in the infarct size, measured with TTC (>40% reduction) or troponin I levels (>70% reduction), was also observed when compared with vehicle alone (Figure 24). This demonstrates compound **72**'s effectiveness *in vivo*.

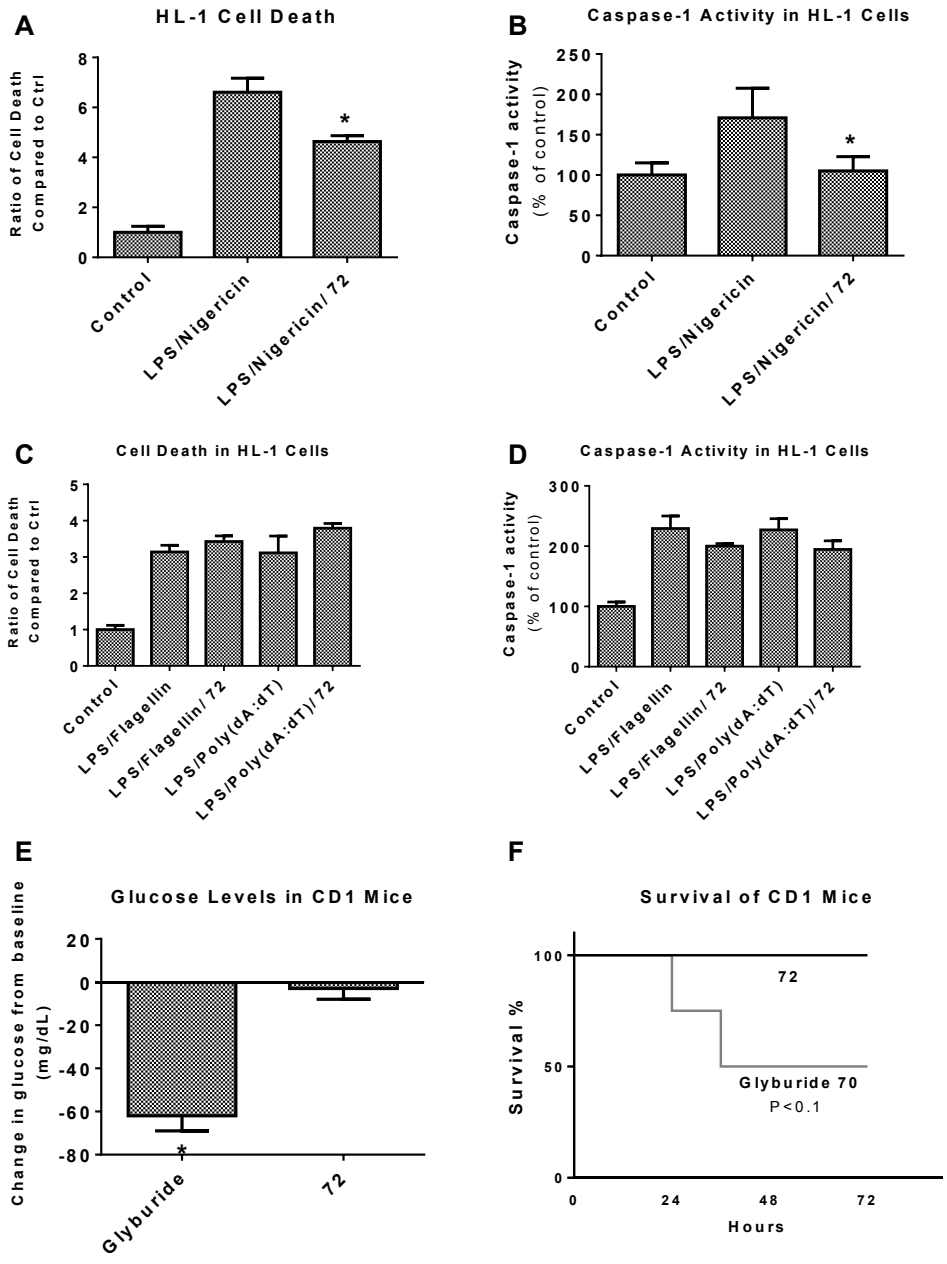

Figure 22. Effects of **72** on NLRC4 and AIM2 inflammasome stimulation and blood glucose. A and B. Compound **72** prevents cell death and reduces caspase-1 activity in HL-1 cardiomyocytes stimulated with LPS/Nigericin, which activates the NLRP3 inflammasome. C and D. Flagellin and Poly:dAdT induce cell death and caspase-1 activation in HL-1 through the NLRC4 and AIM2 inflammasomes, respectively, both of which are unaffected by addition of **72**. E. Compound **72** does not significantly change glucose levels after 2 h after a single dose (100 mg/kg), compared to glyburide (132.5 mg/kg equimolar to **72**). F. Glyburide shows 50% mortality in healthy CD1 mice after 48 h. Compound **72** exhibited no effects mortality. Both were dosed every 6 h for 24 h total. *$p<0.05$ Adapted from Marchetti et al.[228]

4.3.5 Inhibition of the NLRP3 inflammasome in a model of acute peritonitis in mouse

Inflammation of the peritoneum, known as peritonitis, is known to be dependent on NLRP3 activation. In order to determine if compound **72** can inhibit the NLRP3 inflammasome *in vivo* independent of the effects of myocardial ischemia/infarction, zymosan A was used to induce peritonitis in the mouse. Pre-treatment with **72** (5, 20, and 100 mg/kg) limited the severity of the peritonitis in a dose-dependent manner, as measured by the intensity of leukocyte infiltration in the peritoneal cavity (Figure 23). Together with the AMI results, these further exhibit compound **72**'s activity on the NLRP3 inflammasome *in vivo*, independent of the inflammatory stimulus.

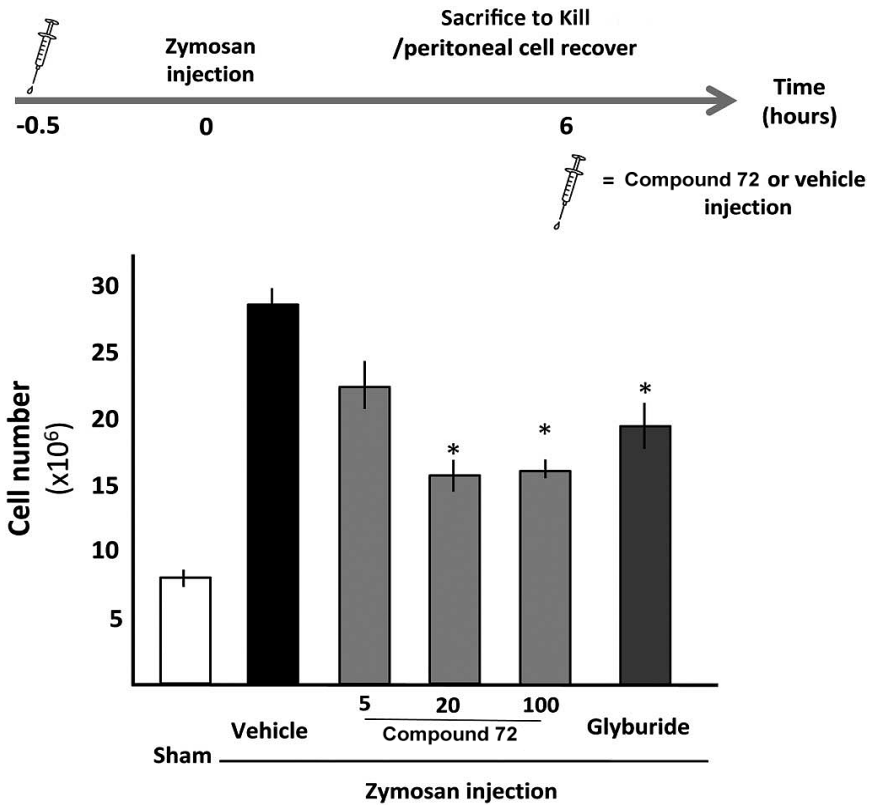

Figure 23. Effects of **72** in a model of acute peritonitis in the mouse. A schematic of the study design is provided. A significant increase in the number of cells recovered from the peritoneal cavity was examined 6 h after treatment with zymosan, which was significantly reduced by treatment with **72** or glyburide. Adapted from Marchetti et al.[228]

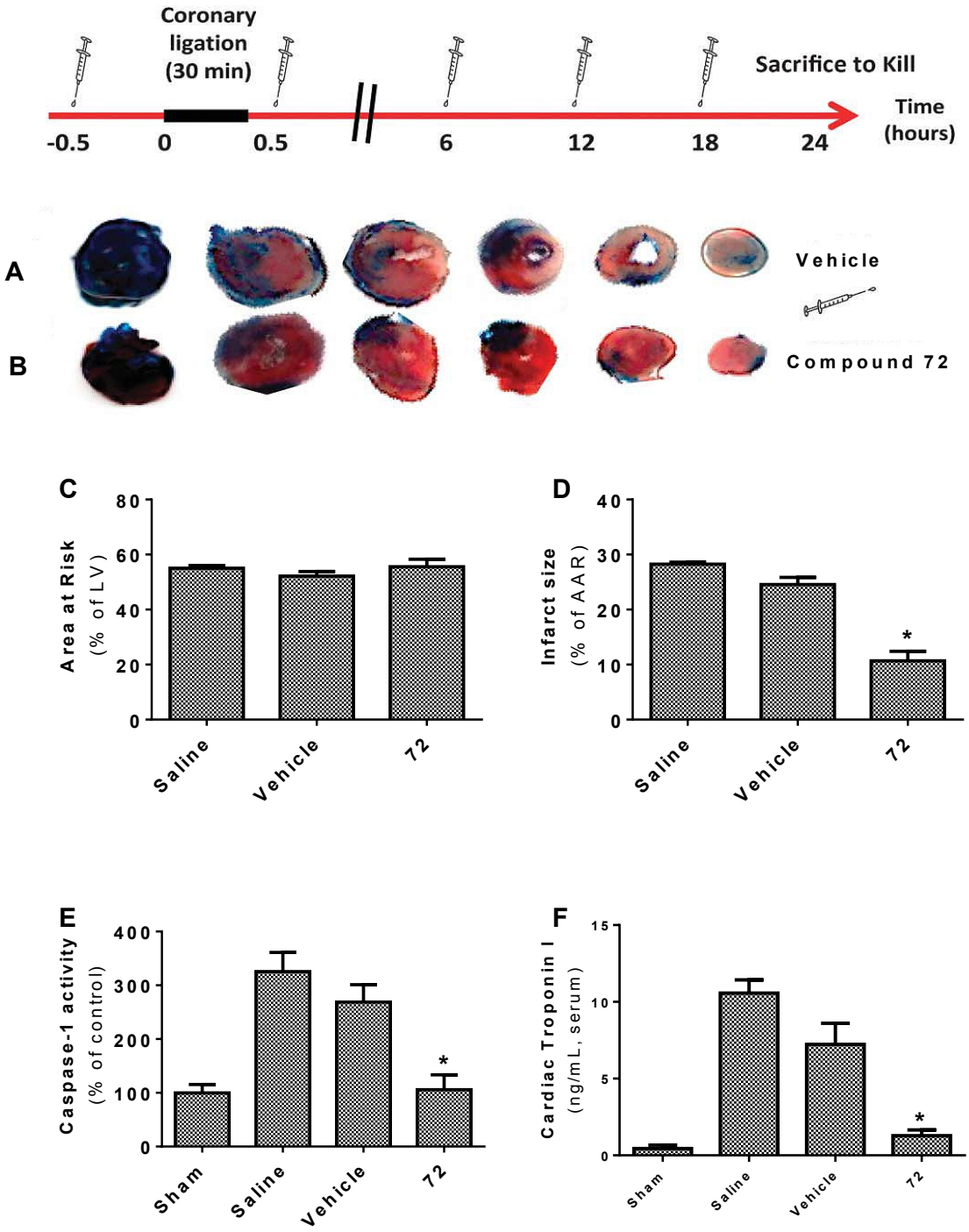

Figure 24. Effects of **72** in a model of acute myocardial infarction in the mouse. A and B. Representative images of the TTC staining for infarct size, and a representative scheme of the AMI assay. C and D. Compound **72** shows significant reduction in infarct size without difference in area-at-risk. E. Compound **72** reduces caspase-1 activity in the heart 24 h after ischemia-reperfusion. F. Serum cardiac troponin I levels are greatly increased after ischemia-reperfusion, which is significantly prevented by **72**. * $p < 0.05$ Adapted from Marchetti et al.[228]

4.3.6 Inhibition of IL-1ß production in J774.A1 murine macrophages

Compounds **71**-**89** were assayed for their ability to reduce IL-1ß release in J774.A1 cells upon stimulation with LPS and ATP (Figure 25 and Table 2). Cells were treated with LPS and ATP as previously described, and all compounds were dosed at 50 μM. The relative ability of compounds to reduce IL-1ß release compared to the LPS/ATP control is given in Table 2. Notably, all compounds exhibit some activity in decreasing of IL-1ß concentration, the worst being compound **84** reducing to only 66%. The top compounds, **76, 87,** and **80,** showed slightly higher inhibitory ability compared to **72**. Structurally, these compounds are very similar to **72**. Addition of methyl groups to the sulfonamide, compounds **76** and **77,** both exhibited protection greater than 70% and seem to be well tolerated. Larger substituents, **74** and **75**, significantly decreased activity, indicating too much bulk cannot be added to the sulfonamide portion of the compound. Interestingly, the hydrazine analog **79** was less effective than **72**, whereas the hydroxamate analog **80** displayed stronger activity than **72**. This may suggest that **80** is acting as a pro-drug, masking compound **72**, or that the electronic properties of the oxygen atom is preferable to the nitrogen. The sulfonic acid **73** also decreased IL-1ß, although it was not effective in rescuing cell death in HL-1 cells, shown in Figure 21. Compounds **81** and **83**, both lacking the methoxy group, were much less active than **72**. Compound **82**, without the chloro group, while not as active as **72**, was still more effective than **81** and **83**. The hydroxy analog **84** exhibited the lowest degree of activity, and the methylamine analog **86** showed moderate activity. Together, these indicate the importance of the methoxy group to activity. Incorporation of a nitrogen atom into the ring **85** also led to a loss of inhibition. Addition of an amine group into the chain linking the two rings **89** had no effect on function, while reduction of the amide to an amine **88** significantly reduced activity. Despite **87**'s apparent effectiveness, it was

previously shown to have no effect in prior assays (Figure 21), highlighting the importance of the sulfonamide moiety.

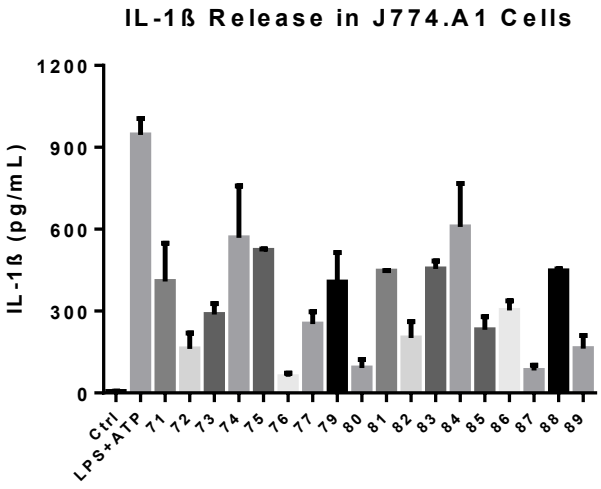

Figure 25. Screening of full series of glyburide analogs against IL-1ß release. The full series of glyburide analogs assayed for their prevention of IL-1ß release in J774.A1 cells stimulated with LPS and ATP. Compounds were dosed at 50 µM.

Table 2. Inhibition of IL-1ß release expressed as % inhibition compared to control. Data as seen in Figure 25 are expressed as percent inhibition compared to the LPS/ATP control with SEM.

Compound	% Inhibition	SEM
Ctrl	0.59%	0.03%
LPS+ATP	100.00%	6.35%
71	44.29%	17.69%
72	17.56%	7.23%
73	30.85%	6.12%
74	61.68%	23.94%
75	55.54%	4.07%
76	6.44%	1.75%
77	27.11%	6.50%
79	43.95%	14.19%
80	9.91%	3.99%
81	47.46%	3.25%
82	21.81%	7.68%
83	48.13%	0.07%
84	65.70%	20.97%
85	24.91%	6.69%
86	31.88%	1.65%
87	8.92%	2.55%
88	47.58%	3.77%
89	17.63%	6.17%

4.4 Conclusion

The NLRP3 inflammasome is a central mediator in inflammatory response in a variety of diseases and pathologies, including myocardial infarction and AD.[229] Glyburide, a common anti-diabetic medication, has been known to have anti-inflammatory properties, specifically reducing the production IL-1ß.[227] Here, a series of glyburide analogs were synthesized and screened for their NLRP3 inhibiting effects. Compound **72** was shown to inhibit production of IL-1ß, prevent ASC aggregation, and reduce caspase-1 activity, all of which are related to formation of the NLRP3 inflammasome. Furthermore, compound **72** reduced infarct size and prevented leukocyte migration in the peritoneum *in vivo*. In addition to compound **72**, compounds **76, 80,** and **89** all showed a similar, if not stronger, efficacy in reducing IL-1ß production in J774.A1 macrophages.

Further exploration into optimization for more potent analogs is certainly warranted. Compounds incorporating groups with the potential to form covalent bonds could aid in structural biology assays investigating the exact binding mode and position of these analogs. This would provide value information aiding in the rational optimization of this scaffold. Additionally, assays looking at microglial inflammasome activation would confirm the potential of these compounds for use in neuroinflammatory models. BBB penetration would also need to be addressed. Based on the positive *in vivo* results seen here, formal toxicology studies are necessary, as well, if further preclinical studies are to be conducted. Altogether, these analogs represent the first class of NLRP3 inhibitors reported to have activity both *in vitro* and *in vivo*.

5 Experimental Methods

5.1 Chemical Syntheses

Reagents and solvents were obtained from commercial suppliers and used as received unless otherwise indicated. Reactions were monitored by thin-layer chromatography (TLC) (precoated silica gel 60F254 plates, EMD Chemicals) and visualized with UV light or by treatment with phosphomolybdic acid (PMA), ninhydrin, or iodine. Column chromatography was performed on silica gel (200-300 mesh, Fisher Scientific) using solvents as indicated. ^{1}H NMR and ^{13}C NMR spectra were routinely recorded on a Bruker ARX 400 spectrometer. The NMR solvent used was CDCl3 or d6-DMSO as indicated. Tetramethylsilane (TMS) was used as the internal standard. Infrared spectra were obtained on a Thermo Nicolet FT-IR with a Smart iTR attachment. Exact masses were identified using a PerkinElmer AxION 2 TOF mass spectrometer. The purity of target compounds was determined by HPLC using a Varian 100-5 C18 250×4.6 mm column with UV detection (280 nm and 360 nm for hybrid compounds, and 350nm and 440nm for bivalent compounds and NLRP3 inhibitors) (50% H_2O in acetonitrile and 0.1% TFA, and 30-50% H_2O in methanol and 0.1% TFA, for hybrid compounds; 30% acetonitrile in methanol, for bivalent compounds; 50% acetonitrile in H_2O, for NLRP3 inhibitors) to be ≥ 95%.

5.1.1 Bivalent Compounds

2-(2-(2-azidoethoxy)ethoxy)ethanol (**23**). Triethylene glycol **22** (50 g, 333 mmol) was added to THF (450 mL) and Et_3N (69.6 mL, 499 mmol), and cooled to 0 °C for 30 min. To this, mesyl chloride (12.8 mL, 166 mmol) diluted in THF (50 mL) was added slowly, dropwise, over 3 h. The solution was then allowed to warm to room temperature and stirred for another 3 h.

The solution was then concentrated under reduced pressure. The resulting concentrate was then dissolved in a 95% EtOH/5% H_2O solution (200 mL). To this solution, NaN_3 (16.2 g, 249 mmol) was added, and the solution was refluxed overnight. The solution was then concentrated again under reduced pressure, and then dissolved in Et_2O and washed thrice with H_2O. The ether layer was then dried and concentrated. The crude residue was purified by column chromatography (EtOAc/Hexanes: 10/90 to 60/40) to give **23** (21.5 g, 37%) as a yellow oil. The double substituted side product 1,2-bis(2-azidoethoxy)ethane **48** (4.1 g, 5%) was also collected as a yellow oil. ^{1}H NMR (400 MHz, $CDCl_3$) δ 3.74 (t, J = 5.30 Hz, 2H), 3.67 - 3.71 (m, 6H), 3.61 (t, J = 4.50 Hz, 2H), 3.41 (t, J = 5.20 Hz, 2H).

tert-butyl 2-(2-(2-(2-azidoethoxy)ethoxy)ethoxy) acetate (**24**). Compound **23** (10 g, 57 mmol) was dissolved in THF and cooled to 0 °C. To this, NaH (1.5 g, 63 mmol) was added and the reaction was stirred for 30 min, and then allowed to warm to room temperature. Then *tert*-butyl bromoacetate (10.52 mL, 71.25 mmol) was added, and the reaction was heated to reflux for 4 h. The reaction was then cooled to room temperature and quenched with H_2O. The solution was then concentrated, and more H_2O was added. The product was then extracted into EtOAc, and the organic layer was concentrated under reduced pressure. The crude residue was purified by column chromatography (EtOAc/Hexanes: 20/80 to 60/40) to give **24** (1.51 g, 30%) as a yellow oil. ^{1}H NMR (400 MHz, $CDCl_3$) δ 4.03 (s, 2H), 3.65 - 3.74 (m, 10H), 3.39 (t, J = 5.02 Hz, 2H), 1.48 (s, 9H).

tert-butyl 2-(2-(2-(2-aminoethoxy)ethoxy)ethoxy) acetate (**25**). Compound **24** (1.5 g, 5.2 mmol) was dissolved in THF (10 mL) and then triphenylphosphine (2.72 g, 10.4 mmol) was added, and the reaction was stirred for 4 h at room temperature. H_2O was then added to quench the reaction. THF was removed under reduced pressure, and the remaining water layer was

basified to pH 10. The product was then extracted into DCM. The organic layer then concentrated, and the resulting residue was purified by column chromatography (EtOAc/Hexanes: 50/50 to 95/5) to afford **25** (1.1 g, 78%) as a viscous oil. ^{1}H NMR (400 MHz, $CDCl_3$) δ 4.02 (s, 2H), 3.68 - 3.73 (m, 4H), 3.62 - 3.68 (m, 4H), 3.51 (t, J = 5.20 Hz, 2H), 2.86 (t, J = 5.20 Hz, 2H).

Procedure A. 5-azidopentanoic acid (**26**). 5-bromovaleric acid (2 g, 11.0 mmol) was dissolved in DMF (40 mL) and H_2O (10 mL), and cooled to 0 °C. NaN_3 (1.79 g, 27.5 mmol) was then added, and the reaction was stirred for 30 min. The reaction was then allowed to warm to room temperature and stirred overnight. The reaction was then acidified to pH 3, and the product was extracted into Et_2O. The organic layer was then washed extensively with acidified H_2O, and concentrated to give **26** (740 mg, 47%) as a clear oil. Azide was confirmed by IR absorbance band at 2100 cm^{-1}. ^{1}H NMR (400 MHz, $CDCl_3$) δ 10.27 (br. s, 1H), 3.31 (t, J = 6.53 Hz, 2H), 2.40 (t, J = 7.00 Hz, 2H), 1.63 - 1.76 (m, 4H).

6-azidohexanoic acid (**27**). 6-bromohexanoic acid (4 g, 20.5 mmol) was reacted with NaN_3 (2.67 g, 41.0 mmol) following Procedure A to give **27** (3.2 g, 90%). ^{1}H NMR (400 MHz, $CDCl_3$) δ 6.72 (br. s, 1H), 3.28 (t, J = 6.90 Hz, 2H), 2.33 (t, J = 7.40 Hz, 2H), 1.59 - 1.70 (m, 4H), 1.38 - 1.50 (m, 2H).

8-azidooctanoic acid (**28**). 8-bromooctanoic acid (2 g, 8.96 mmol) was reacted with NaN_3 (1.17 g, 17.9 mmol) following Procedure A to give **28** (1.49 g, 89%). ^{1}H NMR (400 MHz, $CDCl_3$) δ 10.44 (br. s, 1H), 3.26 (t, J = 6.90 Hz, 2H), 2.34 (t, J = 7.53 Hz, 2H), 1.54 - 1.69 (m, 4H), 1.30 - 1.43 (m, 6H).

10-azidodecanoic acid (**29**). 10-bromodecanoic acid (1 g, 4.00 mmol) was reacted with NaN_3 (648 mg, 10.0 mmol) following Procedure A to give **29** (760 mg, 90%). ^{1}H NMR (400 MHz, $CDCl_3$) δ 10.89 (br. s, 1H), 3.26 (t, J = 7.03 Hz, 2H), 2.35 (t, J = 7.53 Hz, 2H), 1.54 - 1.69 (m, 4H), 1.28 - 1.37 (m, 10H).

12-azidododecanoic acid (**30**). 12-bromododecanoic acid (1 g, 3.59 mmol) was reacted with NaN_3 (583 mg, 8.97 mmol) following Procedure A to give **30** (590 mg, 68%). ^{1}H NMR (400 MHz, $CDCl_3$) δ 10.92 (br. s, 1H), 3.26 (t, J = 7.03 Hz, 2H), 2.35 (t, J = 7.53 Hz, 2H), 1.55 - 1.68 (m, 4H), 1.27 - 1.38 (m, 14H).

Procedure B. *tert*-butyl 2-(2-(2-(2-(5-azidopentanamido)ethoxy)ethoxy)ethoxy) acetate (**31**). Compound **26** (300 mg, 1.14 mmol) and Et_3N (318 µL, 2.28 mmol) were dissolved in DMF (25 mL), and cooled to 0 °C. EDC (328 mg, 1.71 mmol) was then added. After 30 min, HOBt (231 mg, 1.71 mmol) was then added. After another 30 min, compound **25** was then added. The reaction was then allowed to warm to room temperature and stirred overnight. The solution was then concentrated under reduced pressure. H_2O was then added and the product was extracted into EtOAc. The organic layer was then concentrated, and the crude residue was purified by column chromatography (DCM/MeOH: 100/0 to 95/5) to afford **31** (330 mg, 75%) as a viscous oil. ^{1}H NMR (400 MHz, $CDCl_3$) δ 6.30 (br. s, 1H), 4.02 (s, 2H), 3.68 - 3.74 (m, 4H), 3.61 - 3.68 (m, 4H), 3.56 (t, J = 5.00 Hz, 2H), 3.45 (q, J = 5.20 Hz, 2H), 3.29 (t, J = 6.80 Hz, 2H), 2.23 (t, J = 7.20 Hz, 2H), 1.69 - 1.75 (m, 2H), 1.61 - 1.67 (m, 2H), 1.48 (s, 9H).

tert-butyl 2-(2-(2-(2-(6-azidohexanamido)ethoxy)ethoxy)ethoxy) acetate (**32**). Compound **27** (239 mg, 1.52 mmol) was reacted with compound **25** (400 mg, 1.52 mmol) following Procedure B to give **32** (376 mg, 62%). ^{1}H NMR (400 MHz, $CDCl_3$) δ 6.21 (br. s, 1H), 4.02 (s,

2H), 3.68 - 3.74 (m, 4H), 3.61 - 3.68 (m, 4H), 3.56 (t, J = 5.14 Hz, 2H), 3.45 (q, J = 5.19 Hz, 2H), 3.27 (t, J = 6.90 Hz, 2H), 2.20 (t, J = 7.40 Hz, 2H), 1.57 - 1.72 (m, 4H), 1.48 (s, 9H), 1.38 - 1.45 (m, 2H).

tert-butyl 2-(2-(2-(2-(8-azidooctanamido)ethoxy)ethoxy)ethoxy) acetate (**33**). Compound **28** (282 mg, 1.52 mmol) was reacted with compound **25** (400 mg, 1.52 mmol) following Procedure B to give **33** (170 mg, 26%). ^{1}H NMR (400 MHz, $CDCl_3$) δ 6.19 (br. s, 1H), 4.04 (s, 2H), 3.70 - 3.77 (m, 4H), 3.63 - 3.70 (m, 4H), 3.58 (t, J = 5.02 Hz, 2H), 3.47 (q, J = 5.35 Hz, 2H), 3.27 (t, J = 6.90 Hz, 2H), 2.20 (t, J = 7.53 Hz, 2H), 1.57 - 1.70 (m, 4H), 1.50 (s, 9H), 1.32 - 1.43 (m, 6H).

tert-butyl 2-(2-(2-(2-(10-azidodecanamido)ethoxy)ethoxy)ethoxy) acetate (**34**). Compound **29** (325 mg, 1.52 mmol) was reacted with compound **25** (400 mg, 1.52 mmol) following Procedure B to give **34** (490 mg, 70%). ^{1}H NMR (400 MHz, $CDCl_3$) δ 6.27 (br. s, 1H), 4.02 (s, 2H), 3.68 - 3.75 (m, 4H), 3.61 - 3.68 (m, 4H), 3.56 (t, J = 5.00 Hz, 2H), 3.45 (q, J = 5.27 Hz, 2H), 3.25 (t, J = 6.90 Hz, 2H), 2.18 (t, J = 7.65 Hz, 2H), 1.52 - 1.66 (m, 4H), 1.48 (s, 9H), 1.27 - 1.37 (m, 10H).

tert-butyl 2-(2-(2-(2-(12-azidododecanamido)ethoxy)ethoxy)ethoxy) acetate (**35**). Compound **30** (366 mg, 1.52 mmol) was reacted with compound **25** (400 mg, 1.52 mmol) following Procedure B to give **35** (400 mg, 54%). ^{1}H NMR (400 MHz, $CDCl_3$) δ 6.14 (br. s, 1H), 4.02 (s, 2H), 3.68 - 3.75 (m, 4H), 3.61 - 3.68 (m, 4H), 3.56 (t, J = 5.00 Hz, 2H), 3.45 (q, J = 5.02 Hz, 2H), 3.25 (t, J = 7.03 Hz, 2H), 2.17 (t, J = 7.50 Hz, 2H), 1.56 - 1.67 (m, 4H), 1.48 (s, 9H), 1.25 - 1.35 (m, 14H).

Procedure C. 2-(2-(2-(2-(5-azidopentanamido)ethoxy)ethoxy)ethoxy) acetic acid (**36**). Compound **31** (330 mg, 0.85 mmol) was dissolved in a 10% TFA in DCM solution (5 mL) and stirred overnight at room temperature. The solution was concentrated under reduced pressure, and then washed extensively with Heptane to remove any residual TFA. After the final concentration, compound **36** was left as a viscous oil in quantitative yield. ^{1}H NMR (400 MHz, $CDCl_3$) δ 6.99 (br. s., 1H), 6.30 (br. s., 1H), 4.19 (s, 2H), 3.78 - 3.82 (m, 2H), 3.68 - 3.75 (m, 4H), 3.63 - 3.66 (m, 2H), 3.57 (t, J = 4.70 Hz, 2H), 3.50 (q, J = 4.85 Hz, 2H), 3.29 (t, J = 6.65 Hz, 2H), 2.39 (t, J = 7.40 Hz, 2H), 1.68 - 1.77 (m, 2H), 1.59 - 1.68 (m, 2H).

2-(2-(2-(2-(6-azidohexanamido)ethoxy)ethoxy)ethoxy) acetic acid (**37**). Compound **32** (367 mg, 0.91 mmol) was deprotected following Procedure C giving compound **37** as a viscous oil in quantitative yield. ^{1}H NMR (400 MHz, $CDCl_3$) δ 7.93 (br. s., 1H), 7.11 (br. s., 1H), 4.20 (s, 2H), 3.78 - 3.83 (m, 2H), 3.69 - 3.75 (m, 4H), 3.64 - 3.68 (m, 2H), 3.59 (t, J = 4.70 Hz, 2H), 3.48 - 3.54 (m, 2H), 3.27 (t, J = 6.78 Hz, 2H), 2.39 (t, J = 7.50 Hz, 2H), 1.55 - 1.72 (m, 4H), 1.35 - 1.47 (m, 2H).

2-(2-(2-(2-(8-azidooctanamido)ethoxy)ethoxy)ethoxy) acetic acid (**38**). Compound **33** (170 mg, 0.45 mmol) was deprotected following Procedure C giving compound **38** as a viscous oil in quantitative yield. ^{1}H NMR (400 MHz, $CDCl_3$) δ 6.77 (br. s., 2H), 4.18 (s, 2H), 3.77 - 3.81 (m, 2H), 3.68 - 3.73 (m, 4H), 3.62 - 3.66 (m, 2H), 3.57 (t, J = 4.70 Hz, 2H), 3.48 (q, J = 4.68 Hz, 2H), 3.25 (t, J = 6.90 Hz, 2H), 2.30 (t, J = 7.40 Hz, 2H), 1.54 - 1.68 (m, 4H), 1.31 - 1.38 (m, 6H).

2-(2-(2-(2-(10-azidodecanamido)ethoxy)ethoxy)ethoxy) acetic acid (**39**). Compound **34** (490 mg, 1.22 mmol) was deprotected following Procedure C giving compound **39** as a viscous oil in quantitative yield. ^{1}H NMR (400 MHz, $CDCl_3$) δ 6.97 (br. s., 2H), 4.19 (s, 2H), 3.78 - 3.82

(m, 2H), 3.68 - 3.74 (m, 4H), 3.63 - 3.66 (m, 2H), 3.58 (t, J = 4.80 Hz, 2H), 3.50 (q, J = 4.80 Hz, 2H), 3.25 (t, J = 7.03 Hz, 2H), 2.35 (t, J = 7.78 Hz, 2H), 1.48 - 1.67 (m, 4H), 1.25 - 1.35 (m, 10H).

2-(2-(2-(2-(12-azidododecanamido)ethoxy)ethoxy)ethoxy) acetic acid (**40**). Compound **35** (400 mg, 0.82 mmol) was deprotected following Procedure C giving compound **40** as a viscous oil in quantitative yield. ^{1}H NMR (400 MHz, $CDCl_3$) δ 7.00 (br. s., 1H), 6.80 (br. s., 1H), 4.18 (s, 2H), 3.78 - 3.81 (m, 2H), 3.68 - 3.74 (m, 4H), 3.62 - 3.66 (m, 2H), 3.57 (t, J = 4.80 Hz, 2H), 3.49 (q, J = 4.77 Hz, 2H), 3.25 (t, J = 7.03 Hz, 2H), 2.32 (t, J = 7.60 Hz, 2H), 1.54 - 1.67 (m, 4H), 1.25 - 1.36 (m, 14H).

Procedure D. (1'S,2R,2'S,4'S,5R,7'S,8'R,9'S,12'S,13'R,16'S)-5,7',9',13'-tetramethyl-5'-oxaspiro[oxane-2,6'-pentacyclo[10.8.0.0^{2,9}.0^{4,8}.0^{13,18}]icosan]-18'-en-16'-yl 2-(2-(2-(2-(5-azidopentanamido)ethoxy)ethoxy)ethoxy)acetate (**41**). Compound **36** (250 mg, 0.75 mmol) and DCC (171 mg, 0.83 mmol) were dissolved in DCM (10 mL) and cooled to 0 °C. To this solution, diosgenin **4** (344 mg, 0.83 mmol) was added. DMAP (46 mg, 0.38 mmol) was then added, and the reaction was allowed to warm to room temperature and stirred overnight. The organic layer was concentrated under reduced pressure. The remaining solid was dissolved in EtOAc and cooled to 4 °C for 2 h. Then solution was then filtered again to remove residual DCC. The remaining solution was purified by column chromatography (1. EtOAc/Hexanes: 50/50; 2. DCM/MeOH: 100/0 to 97/3) giving compound **41** (140 mg, 25%) as a white solid. ^{1}H NMR (400 MHz, $CDCl_3$) δ 6.25 (br. s., 1H), 5.38 (d, J = 4.52 Hz, 1H), 4.64 - 4.75 (m, 1H), 4.41 (q, J = 7.50 Hz, 1H), 4.12 (s, 2H), 3.68 - 3.76 (m, 4H), 3.61 - 3.67 (m, 4H), 3.56 (t, J = 5.00 Hz, 2H), 3.45 (q, J = 5.20 Hz, 2H), 3.37 (t, J = 11.00 Hz, 1H), 3.29 (t, J = 6.78 Hz, 2H), 2.34 (d, J =

7.78 Hz, 2H), 2.22 (t, J = 7.28 Hz, 2H), 1.94 - 2.05 (m, 2H), 1.82 - 1.92 (m, 3H), 1.41 - 1.81 (m, 19H), 1.24 - 1.28 (m, 2H), 1.04 (s, 3H), 0.97 (d, J = 7.03 Hz, 4H), 0.79 (t, J = 3.14 Hz, 6H).

(1'S,2R,2'S,4'S,5R,7'S,8'R,9'S,12'S,13'R,16'S)-5,7',9',13'-tetramethyl-5'-oxaspiro[oxane-2,6'-pentacyclo[10.8.0.$0^{2,9}$.$0^{4,8}$.$0^{13,18}$]icosan]-18'-en-16'-yl 2-(2-(2-(2-(6-azidohexanamido)ethoxy)ethoxy)ethoxy)acetate (**42**). Compound **37** (423 mg, 1.22 mmol) was reacted with diosgenin **4** (556 mg, 1.34 mmol) following Procedure D yielding compound **42** (276 mg, 30%) as a white solid. ^{1}H NMR (400 MHz, $CDCl_3$) δ 6.14 (br. s., 1H), 5.38 (d, J = 4.52 Hz, 1H), 4.63 - 4.74 (m, 1H), 4.41 (q, J = 7.40 Hz, 1H), 4.11 (s, 2H), 3.68 - 3.75 (m, 4H), 3.61 - 3.67 (m, 4H), 3.56 (t, J = 5.02 Hz, 2H), 3.45 (q, J = 5.02 Hz, 2H), 3.37 (t, J = 11.00 Hz, 1H), 3.27 (t, J = 6.90 Hz, 2H), 2.34 (d, J = 8.03 Hz, 2H), 2.19 (t, J = 7.53 Hz, 2H), 1.95 - 2.05 (m, 2H), 1.83 - 1.92 (m, 3H), 1.62 - 1.80 (m, 9H), 1.36 - 1.55 (m, 7H), 1.07 - 1.34 (m, 7H), 1.04 (s, 3H), 0.97 (d, J = 6.78 Hz, 4H), 0.79 (t, J = 3.14 Hz, 6H).

(1'S,2R,2'S,4'S,5R,7'S,8'R,9'S,12'S,13'R,16'S)-5,7',9',13'-tetramethyl-5'-oxaspiro[oxane-2,6'-pentacyclo[10.8.0.$0^{2,9}$.$0^{4,8}$.$0^{13,18}$]icosan]-18'-en-16'-yl 2-(2-(2-(2-(8-azidooctanamido)ethoxy)ethoxy)ethoxy)acetate (**43**). Compound **38** (151 mg, 0.40 mmol) was reacted with diosgenin **4** (182 mg, 0.44 mmol) following Procedure D yielding compound **43** (213 mg, 68%) as a white solid. ^{1}H NMR (400 MHz, $CDCl_3$) δ 6.12 (br. s., 1H), 5.38 (d, J = 5.02 Hz, 1H), 4.64 - 4.74 (m, 1H), 4.41 (q, J = 7.50 Hz, 1H), 4.11 (s, 2H), 3.68 - 3.75 (m, 4H), 3.61 - 3.68 (m, 4H), 3.56 (t, J = 5.00 Hz, 2H), 3.45 (q, J = 4.50 Hz, 2H), 3.37 (t, J = 11.00 Hz, 1H), 3.25 (t, J = 6.90 Hz, 2H), 2.34 (d, J = 7.53 Hz, 2H), 2.18 (t, J = 7.40 Hz, 2H), 1.94 - 2.03 (m, 2H), 1.82 - 1.92 (m, 3H), 1.61 - 1.81 (m, 11H), 1.07 - 1.53 (m, 16H), 1.04 (s, 3H), 0.97 (d, J = 7.03 Hz, 4H), 0.79 (t, J = 3.14 Hz, 6H).

(1'S,2R,2'S,4'S,5R,7'S,8'R,9'S,12'S,13'R,16'S)-5,7',9',13'-tetramethyl-5'-oxaspiro[oxane-2,6'-pentacyclo[10.8.0.0^{2,9}.0^{4,8}.0^{13,18}]icosan]-18'-en-16'-yl 2-(2-(2-(2-(10-azidodecanamido)ethoxy)ethoxy)ethoxy)acetate (**44**). Compound **39** (545 mg, 1.35 mmol) was reacted with diosgenin **4** (618 mg, 1.49 mmol) following Procedure D yielding compound **44** (405 mg, 37%) as a white solid. ^{1}H NMR (400 MHz, $CDCl_3$) δ 6.09 (br. s., 1H), 5.38 (d, J = 4.02 Hz, 1H), 4.64 - 4.74 (m, 1H), 4.41 (q, J = 6.53 Hz, 1H), 4.11 (s, 2H), 3.68 - 3.76 (m, 4H), 3.60 - 3.68 (m, 4H), 3.56 (t, J = 5.02 Hz, 2H), 3.45 (q, J = 5.27 Hz, 2H), 3.34 - 3.41 (m, 1H), 3.25 (t, J = 6.90 Hz, 2H), 2.34 (d, J = 7.28 Hz, 2H), 2.14 - 2.21 (m, J = 7.40, 7.40 Hz, 2H), 1.93 - 2.06 (m, 2H), 1.83 - 1.89 (m, 3H), 1.50 - 1.80 (m, 17H), 1.08 - 1.38 (m, 14H), 1.04 (s, 3H), 0.97 (d, J = 7.03 Hz, 4H), 0.79 (t, J = 2.80 Hz, 6H).

(1'S,2R,2'S,4'S,5R,7'S,8'R,9'S,12'S,13'R,16'S)-5,7',9',13'-tetramethyl-5'-oxaspiro[oxane-2,6'-pentacyclo[10.8.0.0^{2,9}.0^{4,8}.0^{13,18}]icosan]-18'-en-16'-yl 2-(2-(2-(2-(12-azidododecanamido)ethoxy)ethoxy)ethoxy)acetate (**45**). Compound **40** (381 mg, 0.89 mmol) was reacted with diosgenin **4** (402 mg, 0.97 mmol) following Procedure D yielding compound **45** (391 mg, 53%) as a white solid. ^{1}H NMR (400 MHz, $CDCl_3$) δ 6.09 (br. s., 1H), 5.38 (d, J = 5.02 Hz, 1H), 4.64 - 4.74 (m, 1H), 4.41 (q, J = 7.50 Hz, 1H), 4.11 (s, 2H), 3.68 - 3.75 (m, 4H), 3.61 - 3.68 (m, 4H), 3.56 (t, J = 5.00 Hz, 2H), 3.45 (q, J = 5.20 Hz, 2H), 3.37 (t, J = 11.00 Hz, 1H), 3.25 (t, J = 7.03 Hz, 2H), 2.34 (d, J = 7.53 Hz, 2H), 2.17 (t, J = 7.50 Hz, 2H), 1.94 - 2.03 (m, 2H), 1.83 - 1.92 (m, 3H), 1.53 - 1.81 (m, 16H), 1.12 - 1.36 (m, 19H), 1.04 (s, 3H), 0.97 (d, J = 6.78 Hz, 4H), 0.79 (t, J = 3.14 Hz, 6H).

Procedure E. (1'S,2R,2'S,4'S,5R,7'S,8'R,9'S,12'S,13'R,16'S)-5,7',9',13'-tetramethyl-5'-oxaspiro[oxane-2,6'-pentacyclo[10.8.0.0^{2,9}.0^{4,8}.0^{13,18}]icosan]-18'-en-16'-yl 2-(2-(2-[2-(5-(4-[(2Z,4E)-2-[(2E)-1-hydroxy-3-(4-hydroxy-3-methoxyphenyl)prop-2-en-1-ylidene]-5-(4-

hydroxy-3-methoxyphenyl)-3-oxopent-4-en-1-yl]-1H-1,2,3-triazol-1-yl)pentanamido)ethoxy]ethoxy)ethoxy)acetate (**8**). Compound **41** (30 mg, 0.041 mmol) and compound **46** (18 mg, 0.045 mmol) were added together in a 50/50 THF/H_2O solution (2 mL). $CuSO_4$ (6.5 mg, 0.041 mmol) and sodium ascorbate (8.1 mg, 0.041 mmol) were then added, and the reaction was stirred at 35 °C for 24 h. More H_2O was added, and the product was extracted into EtOAc. The organic layer was then concentrated under reduced pressure. The remaining solid was purified by column chromatography (DCM/MeOH: 100/0 to 95/5) to afford compound **8** (45 mg, 96%) as a dark orange solid. ^{1}H NMR (400 MHz, $CDCl_3$) δ 7.69 (d, J = 15.31 Hz, 1H), 7.59 (d, J = 15.81 Hz, 1H), 7.35 (s, 1H), 7.09 (dd, J = 1.76, 8.28 Hz, 2H), 7.02 (dd, J = 1.76, 7.03 Hz, 2H), 6.93 (s, 1H), 6.90 (dd, J = 0.75, 8.28 Hz, 2H), 6.69 (d, J = 16.06 Hz, 1H), 6.31 (br. s., 1H), 5.36 (br. s., 1H), 4.67 (s, 1H), 4.41 (q, J = 7.53 Hz, 1H), 4.27 (t, J = 7.15 Hz, 2H), 4.06 (s, 1H), 4.08 (d, J = 9.29 Hz, 2H), 3.93 (s, 3H), 3.91 (s, 3H), 3.60 - 3.73 (m, 8H), 3.54 (t, J = 4.89 Hz, 2H), 3.34 - 3.50 (m, 6H), 2.33 (d, J = 7.03 Hz, 2H), 2.09 (s, 2H), 1.95 - 2.01 (m, 2H), 1.83 - 1.89 (m, 4H), 1.47 - 1.75 (m, 18H), 1.19 - 1.28 (m, 3H), 1.02 (d, J = 2.26 Hz, 3H), 0.97 (d, J = 6.78 Hz, 4H), 0.76 - 0.81 (m, 6H); ^{13}C NMR (100 MHz, $CDCl_3$) δ 194.5, 183.2, 169.9, 148.8, 148.2, 147.0, 147.0, 145.1, 142.4, 139.4, 127.9, 126.8, 124.2, 123.3, 122.7, 122.2, 118.0, 115.0, 109.9, 109.3, 80.8, 70.9, 70.6, 70.2, 69.9, 66.9, 62.2, 56.5, 56.2, 56.1, 50.0, 41.7, 40.3, 39.8, 39.3, 38.1, 36.9, 36.8, 35.3, 32.1, 31.9, 31.5, 30.3, 29.7, 28.9, 27.8, 24.8, 22.4, 20.9, 19.3, 17.1, 16.3, 14.5.

(1'S,2R,2'S,4'S,5R,7'S,8'R,9'S,12'S,13'R,16'S)-5,7',9',13'-tetramethyl-5'-oxaspiro[oxane-2,6'-pentacyclo[10.8.0.0^{2,9}.0^{4,8}.0^{13,18}]icosan]-18'-en-16'-yl 2-(2-(2-[2-(6-(4-[(2Z,4E)-2-[(2E)-1-hydroxy-3-(4-hydroxy-3-methoxyphenyl)prop-2-en-1-ylidene]-5-(4-hydroxy-3-methoxyphenyl)-3-oxopent-4-en-1-yl]-1H-1,2,3-triazol-1-yl)hexanamido)ethoxy]ethoxy)ethoxy)acetate (**9**).

Compound **42** (35 mg, 0.047 mmol) was reacted with compound **46** (21 mg, 0.052 mmol) following Procedure D affording compound **9** (32 mg, 59%) as a dark orange solid. ^{1}H NMR (400 MHz, $CDCl_3$) δ 7.69 (d, J = 15.31 Hz, 1H), 7.58 (d, J = 15.81 Hz, 1H), 7.33 (s, 1H), 7.07 (dd, J = 1.51, 8.28 Hz, 2H), 7.01 (dd, J = 1.63, 8.41 Hz, 2H), 6.90 (dd, J = 2.26, 8.28 Hz, 2H), 6.88 (d, J = 15.06 Hz, 1H), 6.68 (d, J = 15.81 Hz, 1H), 6.01 - 6.24 (m, 1H), 5.36 (br. s., 1H), 4.66 (t, J = 9.29 Hz, 1H), 4.41 (q, J = 6.90 Hz, 1H), 4.25 (q, J = 6.86 Hz, 2H), 4.04 - 4.12 (m, 3H), 3.92 (s, 3H), 3.89 (s, 3H), 3.60 - 3.75 (m, 9H), 3.54 (q, J = 4.80 Hz, 2H), 3.36 - 3.46 (m, 4H), 2.32 (t, J = 6.80 Hz, 2H), 2.06 (t, J = 7.53 Hz, 1H), 1.92 - 2.03 (m, 3H), 1.73 - 1.89 (m, 7H), 1.43 - 1.64 (m, 12H), 1.05 - 1.33 (m, 8H), 1.02 (d, J = 2.26 Hz, 4H), 0.97 (dd, J = 1.40, 6.80 Hz, 3H), 0.94 - 0.99 (m, 1H), 0.75 - 0.81 (m, 6H); ^{13}C NMR (100 MHz, $CDCl_3$) δ 194.5, 183.1, 169.8, 148.9, 148.3, 147.1, 147.1, 145.0, 142.3, 139.4, 127.8, 126.7, 124.1, 123.3, 122.7, 122.2, 117.9, 115.1, 115.0, 110.0, 109.2, 80.8, 74.7, 70.8, 70.5, 70.2, 70.0, 69.9, 68.7, 66.8, 62.2, 56.4, 56.1, 56.0, 50.1, 50.0, 41.6, 40.3, 39.7, 39.2, 38.1, 36.9, 36.7, 36.0, 35.7, 32.0, 31.8, 31.4, 30.3, 29.9, 29.7, 28.8, 27.7, 26.0, 25.9, 24.8, 24.7, 20.8, 19.3, 17.1, 16.2, 14.5.

(1'S,2R,2'S,4'S,5R,7'S,8'R,9'S,12'S,13'R,16'S)-5,7',9',13'-tetramethyl-5'-oxaspiro[oxane-2,6'-pentacyclo[10.8.0.0^{2,9}.0^{4,8}.0^{13,18}]icosan]-18'-en-16'-yl 2-(2-(2-[2-(8-(4-[(2Z,4E)-2-[(2E)-1-hydroxy-3-(4-hydroxy-3-methoxyphenyl)prop-2-en-1-ylidene]-5-(4-hydroxy-3-methoxyphenyl)-3-oxopent-4-en-1-yl]-1H-1,2,3-triazol-1-yl)octanamido)ethoxy]ethoxy)ethoxy)acetate (**10**). Compound **43** (67.5 mg, 0.068 mmol) was reacted with compound **46** (30.4 mg, 0.075 mmol) following Procedure D affording compound **10** (67 mg, 84%) as a dark orange solid. ^{1}H NMR (400 MHz, $CDCl_3$) δ 7.69 (d, J = 15.31 Hz, 1H), 7.58 (d, J = 15.81 Hz, 1H), 7.31 (s, 1H), 7.06 (d, J = 8.28 Hz, 2H), 7.00 (dd, J = 1.76, 10.54 Hz, 2H), 6.90 (d, J = 8.03 Hz, 2H), 6.85 (s, 1H), 6.68 (d, J = 15.81 Hz, 1H), 6.32 (t, J = 5.14 Hz, 1H), 5.36 (br. s., 1H), 4.62 - 4.72 (m, 1H), 4.34 - 4.44

(m, 1H), 4.19 - 4.28 (m, 2H), 4.10 (s, 1H), 4.06 (s, 2H), 3.89 (s, 3H), 3.91 (s, 3H), 3.60 - 3.75 (m, 9H), 3.52 - 3.58 (m, 2H), 3.33 - 3.47 (m, 4H), 2.33 (t, J = 5.65 Hz, 2H), 2.10 (t, J = 7.53 Hz, 1H), 1.93 - 2.04 (m, 3H), 1.42 - 1.89 (m, 21H), 1.06 - 1.23 (m, 10H), 1.02 (d, J = 2.01 Hz, 4H), 0.97 (dd, J = 2.13, 6.90 Hz, 3H), 0.95 - 0.99 (m, 1H), 0.76 - 0.81 (m, 6H); ^{13}C NMR (100 MHz, $CDCl_3$) δ 194.6, 183.1, 169.8, 148.3, 147.2, 145.1, 142.4, 139.4, 127.7, 124.1, 123.1, 122.7, 122.2, 117.7, 115.2, 110.1, 109.3, 107.7, 80.8, 74.6, 70.8, 70.8, 70.5, 70.2, 70.0, 68.8, 66.8, 62.1, 56.4, 56.1, 56.0, 50.0, 41.6, 40.3, 39.7, 39.2, 38.1, 36.9, 36.7, 36.4, 32.0, 31.8, 31.4, 30.3, 30.1, 29.7, 29.0, 28.8, 28.7, 27.7, 26.2, 25.6, 20.8, 19.3, 17.1, 16.2, 14.5.

(1'S,2R,2'S,4'S,5R,7'S,8'R,9'S,12'S,13'R,16'S)-5,7',9',13'-tetramethyl-5'-oxaspiro[oxane-2,6'-pentacyclo[10.8.0.0^{2,9}.0^{4,8}.0^{13,18}]icosan]-18'-en-16'-yl 2-(2-(2-[2-(10-(4-[(2Z,4E)-2-[(2E)-1-hydroxy-3-(4-hydroxy-3-methoxyphenyl)prop-2-en-1-ylidene]-5-(4-hydroxy-3-methoxyphenyl)-3-oxopent-4-en-1-yl]-1H-1,2,3-triazol-1-yl)decanamido)ethoxy]ethoxy)ethoxy)acetate (**11**). Compound **44** (11 mg, 0.014 mmol) was reacted with compound **46** (6.3 mg, 0.015 mmol) following Procedure D affording compound **11** (18 mg, 95%) as a dark orange solid. ^{1}H NMR (400 MHz, $CDCl_3$) δ 7.70 (d, J = 15.30 Hz, 1H), 7.58 (d, J = 16.06 Hz, 1H), 7.19 - 7.32 (m, 1H), 7.05 - 7.09 (m, 2H), 7.00 (dd, J = 1.80, 12.60 Hz, 2H), 6.90 (d, J = 8.28 Hz, 2H), 6.85 (s, 1H), 6.68 (d, J = 15.81 Hz, 1H), 6.30 (s, 1H), 5.37 (br. s., 1H), 4.69 (br. s., 1H), 4.39 - 4.45 (m, 1H), 4.22 - 4.29 (m, 2H), 4.05 - 4.12 (m, 3H), 3.89 - 3.94 (m, 6H), 3.59 - 3.76 (m, 9H), 3.52 - 3.59 (m, 2H), 3.34 - 3.48 (m, 4H), 2.33 (d, J = 8.03 Hz, 2H), 2.14 (t, J = 7.40 Hz, 1H), 2.00 (dd, J = 5.90, 13.43 Hz, 3H), 1.81 (br. s., 21H), 1.10 - 1.18 (m, 14H), 1.02 - 1.04 (m, 4H), 0.97 (s, 4H), 0.77 - 0.80 (m, 6H); ^{13}C NMR (100 MHz, $CDCl_3$) δ 193.3, 181.4, 174.7, 147.6, 131.6, 130.9, 128.9, 124.0, 122.7, 113.6, 110.8, 109.3, 93.1, 90.4, 87.0, 82.5, 81.8, 80.8, 70.5, 70.2, 66.9, 62.1, 61.6, 56.4, 41.6, 40.3, 38.1, 36.9, 36.7, 31.9, 31.4, 30.3, 30.2, 29.4, 28.8, 22.7, 19.3, 17.1, 16.3, 14.1.

(1'S,2R,2'S,4'S,5R,7'S,8'R,9'S,12'S,13'R,16'S)-5,7',9',13'-tetramethyl-5'-oxaspiro[oxane-2,6'-pentacyclo[10.8.0.0^{2,9}.0^{4,8}.0^{13,18}]icosan]-18'-en-16'-yl 2-(2-(2-[2-(12-(4-[(2Z,4E)-2-[(2E)-1-hydroxy-3-(4-hydroxy-3-methoxyphenyl)prop-2-en-1-ylidene]-5-(4-hydroxy-3-methoxyphenyl)-3-oxopent-4-en-1-yl]-1H-1,2,3-triazol-1-yl)dodecanamido)ethoxy]ethoxy)ethoxy)acetate (**12**). Compound **45** (30 mg, 0.036 mmol) was reacted with compound **46** (16.1 mg, 0.040 mmol) following Procedure D affording compound **12** (36.4 mg, 82%) as a dark orange solid. ^{1}H NMR (400 MHz, $CDCl_3$) δ 7.70 (d, J = 15.31 Hz, 1H), 7.59 (d, J = 15.81 Hz, 1H), 7.19 - 7.33 (m, 1H), 7.07 (dd, J = 1.88, 8.16 Hz, 2H), 7.00 (dd, J = 1.63, 11.42 Hz, 2H), 6.90 (d, J = 8.03 Hz, 2H), 6.86 (s, 1H), 6.69 (d, J = 15.81 Hz, 1H), 6.32 (br. s., 1H), 5.37 (br. s., 1H), 4.68 (d, J = 5.27 Hz, 1H), 4.40 (td, J = 7.59, 14.93 Hz, 1H), 4.20 - 4.29 (m, 2H), 4.11 (d, J = 2.76 Hz, 2H), 4.06 (s, 1H), 3.91 (d, J = 5.77 Hz, 6H), 3.60 - 3.76 (m, 8H), 3.56 (dd, J = 2.26, 5.02 Hz, 2H), 3.33 - 3.49 (m, 5H), 2.33 (d, J = 7.28 Hz, 2H), 2.17 (t, J = 7.65 Hz, 2H), 1.93 - 2.04 (m, 3H), 1.40 - 1.91 (m, 24H), 1.06 - 1.21 (m, 14H), 1.03 (s, 4H), 0.97 (d, J = 6.78 Hz, 4H), 0.78 (m, 6H); ^{13}C NMR (100 MHz, $CDCl_3$) δ 183.1, 148.4, 147.1, 147.0, 126.6, 124.1, 123.3, 122.7, 115.0, 109.9, 109.3, 80.8, 70.8, 70.5, 70.2, 68.8, 66.9, 62.1, 56.4, 56.0, 50.0, 41.6, 40.3, 39.7, 38.1, 36.9, 36.7, 32.0, 31.8, 31.4, 30.3, 29.7, 29.3, 28.8, 27.7, 20.8, 19.3, 17.1, 16.3, 14.5.

(1'S,2R,2'S,4'S,5R,7'S,8'R,9'S,12'S,13'R,16'S)-5,7',9',13'-tetramethyl-5'-oxaspiro[oxane-2,6'-pentacyclo[10.8.0.0^{2,9}.0^{4,8}.0^{13,18}]icosan]-18'-en-16'-yl 2-[2-(2-(2-[5-(4-(4-[(1E,3Z,6E)-3-hydroxy-7-(4-hydroxy-3-methoxyphenyl)-5-oxohepta-1,3,6-trien-1-yl]-2-methoxyphenoxymethyl)-1H-1,2,3-triazol-1-yl)pentanamido]ethoxy)ethoxy)ethoxy]acetate (**13**). Compound **41** (30 mg, 0.041 mmol) was reacted with compound **47** (18 mg, 0.045 mmol) following Procedure D affording compound **13** (41 mg, 89%) as a dark orange solid. ^{1}H NMR (400 MHz, $CDCl_3$) δ 7.69 (s, 1H), 7.59 (d, J = 15.06 Hz, 1H), 7.09 (dd, J = 6.70, 22.00 Hz, 2H),

7.03 - 7.16 (m, 1H), 6.94 (d, J = 7.28 Hz, 1H), 6.49 (d, J = 15.81 Hz, 1H), 6.39 (s, 1H), 5.36 (d, J = 3.00 Hz, 1H), 4.68 (d, J = 8.03 Hz, 1H), 4.32 - 4.45 (m, 3H), 4.11 (s, 2H), 3.95 (s, 2H), 3.88 - 3.94 (m, 3H), 3.71 (d, J = 8.03 Hz, 4H), 3.61 - 3.66 (m, 4H), 3.55 (t, J = 4.70 Hz, 2H), 3.41 - 3.51 (m, 4H), 3.37 (t, J = 11.00 Hz, 2H), 2.33 (d, J = 7.53 Hz, 2H), 2.19 - 2.26 (m, 2H), 1.94 - 2.03 (m, 4H), 1.83 - 1.90 (m, 4H), 1.75 - 1.79 (m, 2H), 1.45 - 1.73 (m, 16H), 1.26 (d, J = 1.00 Hz, 3H), 1.06 - 1.20 (m, 4H), 1.02 (s, 3H), 0.97 (d, J = 6.78 Hz, 4H), 0.77 - 0.82 (m, 6H); ^{13}C NMR (100 MHz, $CDCl_3$) δ 172.3, 169.9, 139.4, 122.7, 109.3, 80.8, 74.7, 70.8, 70.5, 70.5, 70.1, 69.9, 68.7, 66.8, 62.1, 56.4, 55.9, 49.9, 41.6, 40.3, 39.7, 39.2, 38.0, 36.9, 36.7, 35.3, 32.0, 31.8, 31.4, 30.3, 29.6, 28.8, 27.7, 22.4, 20.8, 19.3, 17.1, 16.3, 14.5.

(1'S,2R,2'S,4'S,5R,7'S,8'R,9'S,12'S,13'R,16'S)-5,7',9',13'-tetramethyl-5'-oxaspiro[oxane-2,6'-pentacyclo[10.8.0.0^{2,9}.0^{4,8}.0^{13,18}]icosan]-18'-en-16'-yl 2-[2-(2-(2-[6-(4-(4-[(1E,3Z,6E)-3-hydroxy-7-(4-hydroxy-3-methoxyphenyl)-5-oxohepta-1,3,6-trien-1-yl]-2-methoxyphenoxymethyl)-1H-1,2,3-triazol-1-yl)hexanamido]ethoxy)ethoxy)ethoxy]acetate (**14**). Compound **42** (100 mg, 0.135 mmol) was reacted with compound **47** (60.2 mg, 0.148 mmol) following Procedure D affording compound **14** (101 mg, 65%) as a dark orange solid. ^{1}H NMR (400 MHz, $CDCl_3$) δ 7.64 (s, 1H), 7.59 (dd, J = 3.14, 15.69 Hz, 2H), 7.04 - 7.15 (m, 5H), 6.93 (d, J = 8.03 Hz, 1H), 6.49 (dd, J = 4.77, 15.81 Hz, 2H), 6.19 (br. s., 1H), 5.86 (s, 1H), 5.81 (s, 1H), 5.36 (br. s., 1H), 4.67 (br. s., 1H), 4.38 - 4.46 (m, 1H), 4.34 (t, J = 7.03 Hz, 2H), 4.10 (s, 2H), 3.95 (s, 3H), 3.92 (s, 3H), 3.60 - 3.75 (m, 10H), 3.52 - 3.56 (m, 2H), 3.33 - 3.47 (m, 5H), 2.33 (d, J = 6.78 Hz, 2H), 2.14 - 2.20 (m, 3H), 1.62 - 2.06 (m, 18H), 1.22 - 1.49 (m, 8H), 1.03 (s, 3H), 0.97 (d, J = 6.78 Hz, 4H), 0.77 - 0.81 (m, 6H); ^{13}C NMR (100 MHz, $CDCl_3$) δ 183.6, 182.9, 169.8, 149.8, 149.6, 148.0, 146.9, 140.7, 140.1, 139.4, 128.9, 127.7, 122.9, 122.7, 122.5, 122.2, 121.8, 114.9, 113.9, 110.6, 109.7, 109.3, 101.2, 80.8, 74.7, 70.8, 70.5, 70.5, 70.2, 69.9, 68.8,

66.9, 63.1, 62.1, 56.4, 56.0, 53.4, 50.2, 50.0, 41.6, 40.3, 39.7, 39.2, 38.1, 36.9, 36.7, 36.0, 35.9, 32.0, 31.8, 31.4, 30.3, 30.0, 29.7, 28.8, 27.7, 26.1, 24.8, 20.8, 19.3, 17.1, 16.2, 14.5.

(1'S,2R,2'S,4'S,5R,7'S,8'R,9'S,12'S,13'R,16'S)-5,7',9',13'-tetramethyl-5'-oxaspiro[oxane-2,6'-pentacyclo[10.8.0.0^{2,9}.0^{4,8}.0^{13,18}]icosan]-18'-en-16'-yl 2-[2-(2-(2-[8-(4-(4-[(1E,3Z,6E)-3-hydroxy-7-(4-hydroxy-3-methoxyphenyl)-5-oxohepta-1,3,6-trien-1-yl]-2-methoxyphenoxymethyl)-1H-1,2,3-triazol-1-yl)octanamido]ethoxy)ethoxy)ethoxy]acetate (**15**). Compound **43** (100 mg, 0.130 mmol) was reacted with compound **47** (58 mg, 0.143 mmol) following Procedure D affording compound **15** (109 mg, 71%) as a dark orange solid. ^{1}H NMR (400 MHz, $CDCl_3$) δ 7.55 - 7.64 (m, 1H), 7.59 (dd, J = 3.51, 16.06 Hz, 2H), 7.03 - 7.15 (m, 5H), 6.93 (d, J = 8.53 Hz, 1H), 6.49 (dd, J = 4.52, 15.81 Hz, 2H), 6.14 (br. s., 1H), 5.86 (s, 1H), 5.81 (s, 1H), 5.38 (br. s., 1H), 4.70 (br. s., 1H), 4.37 - 4.44 (m, 1H), 4.33 (t, J = 7.15 Hz, 2H), 4.11 (s, 2H), 3.95 (s, 3H), 3.92 (s, 3H), 3.60 - 3.76 (m, 10H), 3.53 - 3.57 (m, 2H), 3.33 - 3.47 (m, 5H), 2.34 (d, J = 7.53 Hz, 2H), 2.16 (t, J = 7.53 Hz, 3H), 1.61 - 2.02 (m, 18H), 1.12 - 1.38 (m, 12H), 1.03 (s, 3H), 0.97 (d, J = 6.78 Hz, 4H), 0.76 - 0.81 (m, 6H); ^{13}C NMR (100 MHz, $CDCl_3$) δ 183.5, 182.9, 173.1, 169.8, 149.7, 149.6, 148.0, 146.9, 140.7, 140.1, 139.4, 128.9, 127.7, 122.9, 122.8, 122.7, 122.4, 122.2, 121.8, 120.7, 114.9, 113.9, 110.6, 109.7, 109.3, 101.2, 80.8, 74.7, 70.8, 70.5, 70.5, 70.2, 70.0, 68.8, 66.9, 63.1, 62.1, 56.4, 56.0, 56.0, 50.4, 50.0, 41.6, 40.3, 39.7, 39.2, 38.1, 36.9, 36.7, 36.4, 32.0, 31.8, 31.4, 30.3, 30.1, 28.9, 28.8, 28.6, 27.7, 26.3, 25.4, 20.8, 19.3, 17.1, 16.3, 14.5.

(1'S,2R,2'S,4'S,5R,7'S,8'R,9'S,12'S,13'R,16'S)-5,7',9',13'-tetramethyl-5'-oxaspiro[oxane-2,6'-pentacyclo[10.8.0.0^{2,9}.0^{4,8}.0^{13,18}]icosan]-18'-en-16'-yl 2-[2-(2-(2-[10-(4-(4-[(1E,3Z,6E)-3-hydroxy-7-(4-hydroxy-3-methoxyphenyl)-5-oxohepta-1,3,6-trien-1-yl]-2-methoxyphenoxymethyl)-1H-1,2,3-triazol-1-yl)decanamido]ethoxy)ethoxy)ethoxy]acetate (**16**).

Compound **44** (100 mg, 0.125 mmol) was reacted with compound **47** (56 mg, 0.138 mmol) following Procedure D affording compound **16** (128 mg, 85%) as a dark orange solid. ^{1}H NMR (400 MHz, $CDCl_3$) δ 7.64 (br. s., 1H), 7.59 (dd, J = 3.89, 15.69 Hz, 2H), 7.05 - 7.14 (m, 5H), 6.81 (d, J = 7.53 Hz, 1H), 6.49 (dd, J = 3.89, 15.69 Hz, 2H), 6.17 (br. s., 1H), 5.37 (d, J = 4.52 Hz, 2H), 4.63 - 4.74 (m, 1H), 4.41 (q, J = 7.40 Hz, 1H), 4.33 (t, J = 7.28 Hz, 2H), 4.11 (s, 2H), 3.95 (s, 3H), 3.92 (s, 3H), 3.60 - 3.76 (m, 10H), 3.52 - 3.58 (m, 2H), 3.33 - 3.50 (m, 5H), 2.34 (d, J = 7.78 Hz, 2H), 2.16 (t, J = 7.53 Hz, 2H), 1.67 - 2.05 (m, 20H), 1.33 - 1.56 (m, 9H), 1.06 - 1.23 (m, 7H), 1.03 (s, 3H), 0.97 (d, J = 7.03 Hz, 4H), 0.79 (t, J = 3.01 Hz, 6H); ^{13}C NMR (100 MHz, $CDCl_3$) δ 154.8, 149.1, 122.7, 109.3, 95.8, 80.8, 77.2, 74.7, 70.8, 70.5, 70.2, 68.8, 66.9, 62.1, 56.4, 49.9, 41.6, 40.3, 39.7, 39.2, 36.7, 32.0, 31.4, 30.3, 29.7, 29.2, 28.8, 20.8, 19.3, 17.1, 16.3, 14.5.

(1'S,2R,2'S,4'S,5R,7'S,8'R,9'S,12'S,13'R,16'S)-5,7',9',13'-tetramethyl-5'-oxaspiro[oxane-2,6'-pentacyclo[10.8.0.0^{2,9}.0^{4,8}.0^{13,18}]icosan]-18'-en-16'-yl 2-[2-(2-(2-[12-(4-(4-[(1E,3Z,6E)-3-hydroxy-7-(4-hydroxy-3-methoxyphenyl)-5-oxohepta-1,3,6-trien-1-yl]-2-methoxyphenoxymethyl)-1H-1,2,3-triazol-1-yl)dodecanamido]ethoxy)ethoxy)ethoxy]acetate (**17**). Compound **45** (100 mg, 0.121 mmol) was reacted with compound **47** (54 mg, 0.133 mmol) following Procedure D affording compound **17** (103 mg, 69%) as a dark orange solid. ^{1}H NMR (400 MHz, $CDCl_3$) δ 7.64 (s, 1H), 7.59 (dd, J = 3.89, 15.69 Hz, 2H), 7.03 - 7.15 (m, 5H), 6.93 (d, J = 8.28 Hz, 1H), 6.50 (d, J = 3.51 Hz, 2H), 6.12 (br. s., 1H), 5.86 (s, 1H), 5.81 (s, 1H), 5.38 (br. s., 1H), 4.70 (br. s., 1H), 4.38 - 4.44 (m, 1H), 4.33 (t, J = 7.40 Hz, 2H), 4.11 (s, 2H), 3.95 (s, 3H), 3.92 (s, 3H), 3.59 - 3.76 (m, 10H), 3.53 - 3.57 (m, 2H), 3.34 - 3.47 (m, 5H), 2.34 (d, J = 8.28 Hz, 2H), 2.16 (t, J = 7.53 Hz, 3H), 1.61 - 2.02 (m, 18H), 1.21 - 1.33 (m, 20H), 1.03 (s, 3H), 0.97 (d, J = 7.03 Hz, 4H), 0.79 (t, J = 3.14 Hz, 6H); ^{13}C NMR (100 MHz, $CDCl_3$) δ 183.6, 182.9, 173.3,

169.8, 149.8, 149.6, 148.0, 146.9, 140.7, 140.1, 139.4, 128.9, 127.7, 122.9, 122.7, 122.5, 122.2, 121.8, 114.9, 114.0, 110.7, 109.8, 109.3, 101.2, 80.8, 74.7, 70.8, 70.5, 70.5, 70.2, 70.0, 68.8, 66.9, 63.2, 62.2, 58.4, 56.4, 56.0, 56.0, 50.5, 50.0, 41.6, 40.3, 39.7, 39.2, 38.1, 36.9, 36.7, 36.7, 32.0, 31.8, 31.4, 30.3, 30.2, 29.7, 29.4, 29.4, 29.3, 29.3, 28.9, 28.8, 27.7, 26.5, 25.7, 20.8, 19.3, 18.4, 17.1, 16.2, 14.5.

2-(2-(2-azidoethoxy)ethoxy)ethanamine (**49**). 1,2-bis(2-azidoethoxy)ethane **48** (4.8 g, 20.7 mmol), the side product from the synthesis of 2-(2-(2-azidoethoxy)ethoxy)ethanol **23**, was dissolved in a solution of Et_2O/EtOAc/5%HCl (30 mL/30 mL/30 mL) and cooled to 0 °C. Triphenylphosphine was added slowly, portion-wise to the solution over 1 h. The reaction was stirred overnight. The organic layer was discarded, and the water layered was basified to pH ~12. The product was extracted into DCM and then concentrated under reduced pressure yielding compound **49** (2.2 g, 64%) as a viscous oil. ^{1}H NMR (400 MHz, $CDCl_3$) δ 3.69 (t, J = 5.00 Hz, 2H), 3.63 - 3.70 (m, 4H), 3.52 (t, J = 5.27 Hz, 2H), 3.40 (t, J = 5.02 Hz, 2H), 2.87 (t, J = 5.14 Hz, 2H), 1.72 (br. s., 2H).

3-(2-(2-(2-azidoethoxy)ethoxy)ethylcarbamoyl)propanoic acid (**50**). Compound **49** (1.0 g, 4.85 mmol), succinic anhydride (1.84 g, 19.40 mmol), and Et_3N (0.5 mL) were dissolved in DCM (15 mL). The solution was stirred at room temperature overnight. The solution was washed with 1 N HCl, and then the organic layer was concentrated under reduced pressure. The resulting residue was purified by column chromatography (DCM/MeOH/AcOH: 95/5/0 to 92/7.9/0.1) giving compound **50** (400 mg, 30%) as a white solid. ^{1}H NMR (400 MHz, $CDCl_3$) δ 6.39 (br. s., 1H), 3.71 (t, J = 4.80 Hz, 2H), 3.63 - 3.68 (m, 4H), 3.57 (t, J = 5.00 Hz, 2H), 3.48 (q, J = 5.10 Hz, 2H), 3.42 (t, J = 5.00 Hz, 2H), 2.69 (t, J = 6.40 Hz, 2H), 2.53 (t, J = 6.40 Hz, 2H).

(1'S,2R,2'S,4'S,5R,7'S,8'R,9'S,12'S,13'R,16'S)-5,7',9',13'-tetramethyl-5'-oxaspiro[oxane-2,6'-pentacyclo[10.8.0.0^{2,9}.0^{4,8}.0^{13,18}]icosan]-18'-en-16'-yl 3-(2-[2-(2-azidoethoxy)ethoxy]ethylcarbamoyl)propanoate (**51**). Compound **50** (1.4 g, 4.89 mmol) was reacted with diosgenin **4** (2.23 g, 5.38 mmol) following Procedure D to give compound **51** (1.4 g, 42%) as a white solid. ^{1}H NMR (400 MHz, $CDCl_3$) δ 6.08 (br. s., 1H), 5.36 (d, J = 5.52 Hz, 1H), 4.54 - 4.67 (m, 1H), 4.41 (q, J = 7.50 Hz, 1H), 3.69 (t, J = 5.00 Hz, 2H), 3.62 - 3.66 (m, 4H), 3.56 (t, J = 5.14 Hz, 2H), 3.46 (q, J = 5.19 Hz, 2H), 3.40 (t, J = 5.02 Hz, 2H), 2.71 (s, 1H), 2.63 (t, J = 7.03 Hz, 2H), 2.47 (t, J = 7.03 Hz, 2H), 2.32 (d, J = 7.28 Hz, 2H), 1.94 - 2.05 (m, 2H), 1.81 - 1.90 (m, 3H), 1.56 - 1.77 (m, 10H), 1.41 - 1.53 (m, 3H), 1.28 (dt, J = 6.40, 12.86 Hz, 1H), 1.06 - 1.23 (m, 3H), 1.03 (s, 3H), 0.97 (d, J = 7.03 Hz, 4H), 0.79 (t, J = 3.14 Hz, 6H).

(1'S,2R,2'S,4'S,5R,7'S,8'R,9'S,12'S,13'R,16'S)-5,7',9',13'-tetramethyl-5'-oxaspiro[oxane-2,6'-pentacyclo[10.8.0.0^{2,9}.0^{4,8}.0^{13,18}]icosan]-18'-en-16'-yl 3-(2-[2-(2-(4-[(2Z,4E)-2-[(2E)-1-hydroxy-3-(4-hydroxy-3-methoxyphenyl)prop-2-en-1-ylidene]-5-(4-hydroxy-3-methoxyphenyl)-3-oxopent-4-en-1-yl]-1H-1,2,3-triazol-1-yl)ethoxy)ethoxy]ethylcarbamoyl)propanoate (**18**). Compound **51** (250 mg, 0.37 mmol) was reacted with compound **46** (167 mg, 0.41 mmol) following Procedure E to give compound **18** (158 mg, 40%) as a dark orange solid. ^{1}H NMR (400 MHz, $CDCl_3$) δ 7.70 (d, J = 15.06 Hz, 1H), 7.60 (d, J = 16.06 Hz, 1H), 7.09 (d, J = 8.28 Hz, 2H), 7.01 - 7.05 (m, 2H), 6.94 (s, 1H), 6.90 (d, J = 8.28 Hz, 2H), 6.71 (d, J = 15.81 Hz, 1H), 6.36 (br. s., 1H), 5.96 - 6.07 (m, 2H), 5.33 (br. s., 1H), 4.36 - 4.48 (m, 4H), 4.07 (s, 1H), 3.93 - 3.95 (m, 3H), 3.92 (s, 3H), 3.77 - 3.83 (m, 2H), 3.36 - 3.53 (m, 10H), 3.27 - 3.35 (m, 3H), 2.63 (t, J = 6.78 Hz, 2H), 2.44 - 2.53 (m, 2H), 2.29 (d, J = 8.53 Hz, 2H), 1.98 (dd, J = 6.02, 12.55 Hz, 2H), 1.60 - 1.89 (m, 10H), 1.42 - 1.53 (m, 4H), 1.05 - 1.29 (m, 5H), 1.01 (d, J = 2.76 Hz, 3H), 0.97 (d, J = 7.03 Hz, 4H), 0.76 - 0.81 (m, 6H); ^{13}C NMR (100 MHz, $CDCl_3$) δ 154.8, 149.1, 122.7, 109.3,

95.8, 80.8, 77.2, 74.7, 70.8, 70.5, 70.2, 68.8, 66.9, 62.1, 56.4, 49.9, 41.6, 40.3, 39.7, 39.2, 36.7, 32.0, 31.4, 30.3, 29.7, 29.2, 28.8, 20.8, 19.3, 17.1, 16.3, 14.5.

(1'S,2R,2'S,4'S,5R,7'S,8'R,9'S,12'S,13'R,16'S)-5,7',9',13'-tetramethyl-5'-oxaspiro[oxane-2,6'-pentacyclo[10.8.0.0^{2,9}.0^{4,8}.0^{13,18}]icosan]-18'-en-16'-yl 3-[2-(2-[2-(4-(4-[(1E,3Z,6E)-3-hydroxy-7-(4-hydroxy-3-methoxyphenyl)-5-oxohepta-1,3,6-trien-1-yl]-2-methoxyphenoxymethyl)-1H-1,2,3-triazol-1-yl)ethoxy]ethoxy)ethylcarbamoyl]propanoate (**19**). Compound **51** (250 mg, 0.37 mmol) was reacted with compound **47** (167 mg, 0.41 mmol) following Procedure E to give compound **19** (201 mg, 51%) as a dark orange solid. ^{1}H NMR (400 MHz, $CDCl_3$) δ 7.84 (s, 1H), 7.59 (dd, J = 5.40, 15.69 Hz, 2H), 7.11 (s, 2H), 7.12 (dd, J = 1.80, 7.90 Hz, 1H), 7.06 (dd, J = 1.38, 7.91 Hz, 2H), 6.93 (d, J = 8.28 Hz, 1H), 6.48 (dd, J = 4.27, 15.81 Hz, 2H), 6.11 (s, 1H), 5.79 - 5.87 (m, 2H), 5.33 (s, 2H), 4.55 (t, J = 5.02 Hz, 3H), 4.35 - 4.44 (m, 1H), 3.95 (s, 3H), 3.91 (s, 3H), 3.89 (t, J = 5.00 Hz, 3H), 3.50 - 3.59 (m, 5H), 3.44 - 3.50 (m, 4H), 3.33 - 3.44 (m, 4H), 2.68 (s, 1H), 2.61 (t, J = 6.78 Hz, 2H), 2.45 (t, J = 6.90 Hz, 2H), 2.30 (d, J = 6.78 Hz, 2H), 1.98 (d, J = 13.05 Hz, 2H), 1.58 - 1.88 (m, 10H), 1.27 (d, J = 5.02 Hz, 2H), 1.04 - 1.20 (m, 4H), 1.02 (s, 3H), 0.96 (d, J = 7.03 Hz, 4H), 0.76 - 0.80 (m, 6H); ^{13}C NMR (100 MHz, $CDCl_3$) δ 182.6, 181.9, 171.4, 170.6, 148.6, 146.9, 145.8, 142.6, 139.7, 139.1, 138.7, 126.7, 123.3, 121.9, 121.4, 121.3, 120.8, 113.9, 112.8, 109.5, 108.7, 108.3, 100.3, 79.8, 73.2, 69.5, 69.2, 68.9, 68.3, 65.8, 62.0, 61.1, 55.4, 55.0, 49.4, 48.9, 40.6, 39.2, 38.7, 38.3, 37.0, 35.9, 35.7, 31.0, 30.8, 30.4, 29.9, 29.3, 28.8, 27.8, 27.1, 26.7, 19.8, 18.3, 16.1, 15.2, 13.5.

(1'S,2R,2'S,4'S,5R,7'S,8'R,9'S,12'S,13'R,16'S)-5,7',9',13'-tetramethyl-5'-oxaspiro[oxane-2,6'-pentacyclo[10.8.0.0^{2,9}.0^{4,8}.0^{13,18}]icosan]-18'-en-16'-yl 3-(2-(2-(2-[4-(2-methylpropyl)-1H-1,2,3-triazol-1-yl]ethoxy)ethoxy)ethylcarbamoyl)propanoate (**20**). Compound **51** (110 mg, 0.16 mmol) was reacted with 4-methyl-1-pentyne (15 mg, 0.18 mmol) following Procedure E to give

compound **20** (100 mg, 81%) as a white solid. ^{1}H NMR (400 MHz, $CDCl_3$) δ 7.41 (s, 1H), 6.16 (br. s., 1H), 5.36 (d, J = 4.52 Hz, 1H), 4.54 - 4.66 (m, 1H), 4.52 (t, J = 5.27 Hz, 2H), 4.41 (q, J = 7.50 Hz, 1H), 3.89 (t, J = 5.14 Hz, 2H), 3.54 - 3.60 (m, 4H), 3.50 (t, J = 5.00 Hz, 2H), 3.43 (q, J = 5.50 Hz, 2H), 3.37 (t, J = 11.00 Hz, 1H), 2.64 (t, J = 7.00 Hz, 2H), 2.59 (d, J = 7.03 Hz, 2H), 2.48 (t, J = 7.00 Hz, 2H), 2.32 (d, J = 7.53 Hz, 2H), 1.91 - 2.02 (m, 3H), 1.81 - 1.89 (m, 3H), 1.66 - 1.80 (m, 3H), 1.64 (s, 6H), 1.40 - 1.56 (m, 4H), 1.06 - 1.34 (m, 5H), 1.03 (s, 3H), 0.97 (d, J = 7.03 Hz, 3H), 0.95 (s, 3H), 0.93 (s, 3H), 0.76 - 0.82 (m, 6H); ^{13}C NMR (100 MHz, $CDCl_3$) δ 172.4, 171.5, 147.1, 139.7, 122.4, 122.3, 109.3, 80.8, 74.3, 70.5, 70.3, 69.9, 69.7, 66.9, 62.1, 56.5, 50.1, 50.0, 41.6, 40.3, 39.8, 39.3, 38.1, 37.0, 36.8, 34.8, 32.1, 31.8, 31.4, 31.1, 30.3, 29.9, 28.8, 28.7, 27.7, 22.3, 20.8, 19.3, 17.1, 16.3, 14.5.

Methyl 3-(2-(2-(2-azidoethoxy)ethoxy)ethylcarbamoyl)propanoate (**54**). Compound **49** (1.0 g, 4.85 mmol) was reacted with 3-(methoxycarbonyl)propanoic acid **53** (700 mg, 5.33 mmol) following Procedure B to give compound **54** (1.26 g, 81%) as a white solid. ^{1}H NMR (400 MHz, $CDCl_3$) δ 6.12 (br. s., 1H), 3.69 (s, 3H), 3.70 (t, J = 4.80 Hz, 2H), 3.62 - 3.68 (m, 4H), 3.56 (t, J = 5.02 Hz, 2H), 3.46 (q, J = 5.20 Hz, 2H), 3.40 (t, J = 5.02 Hz, 2H), 2.67 (t, J = 7.03 Hz, 2H), 2.49 (t, J = 6.90 Hz, 2H).

Methyl 3-(2-[2-(2-(4-[(2Z,4E)-2-[(2E)-1-hydroxy-3-(4-hydroxy-3-methoxyphenyl)prop-2-en-1-ylidene]-5-(4-hydroxy-3-methoxyphenyl)-3-oxopent-4-en-1-yl]-1H-1,2,3-triazol-1-yl)ethoxy)ethoxy]ethylcarbamoyl)propanoate (**21**). Compound **54** (100 mg, 0.312 mmol) was reacted with compound **46** (127 mg, 0.312 mmol) following Procedure E to give compound **21** (100 mg, 44%) as an orange solid. ^{1}H NMR (400 MHz, $CDCl_3$) δ 7.70 (d, J = 15.31 Hz, 1H), 7.61 (d, J = 15.81 Hz, 1H), 7.00 - 7.12 (m, 2H), 7.09 (d, J = 7.80 Hz, 2H), 6.93 - 6.99 (m, 1H), 6.90 (d, J = 7.78 Hz, 2H), 6.71 (d, J = 15.81 Hz, 1H), 6.45 - 6.55 (m, 1H), 4.46 (q, J = 4.30 Hz,

2H), 4.07 (br. s., 1H), 3.91 (s, 3H), 3.88 (s, 3H), 3.80 (q, J = 5.27 Hz, 2H), 3.66 (s, 3H), 3.65 (s, 3H), 3.52 (s, 3H), 3.48 - 3.51 (m, 2H), 3.37 - 3.48 (m, 4H), 3.28 - 3.34 (m, 2H), 2.66 (t, J = 6.40 Hz, 2H), 2.50 (td, J = 6.93, 13.49 Hz, 2H); ^{13}C NMR (100 MHz, $CDCl_3$) δ 194.5, 183.2, 173.4, 148.8, 148.2, 147.0, 146.9, 145.2, 142.4, 127.8, 126.7, 124.1, 123.1, 122.1, 117.9, 114.9, 114.9, 110.1, 109.9, 70.5, 70.2, 70.0, 69.9, 69.7, 69.5, 56.1, 56.1, 51.7, 39.2, 30.9, 30.9, 29.3, 29.3.

5.1.2 Hybrid Compounds

Ethyl 4-(triphenylphosphoranylidene)acetoacetate (**70**). Triphenylphosphine (14.4 g, 55.3 mmol) was added to a solution of ethyl 4-chloroacetoacetate **69** (8.4 g, 60.8 mmol) in benzene (35 mL) and stirred for 24 h at 55 °C. The solution was then cooled to room temperature, and the precipitate was collected by filtration and washed with benzene. The solid precipitate was then dissolved in H_2O (10 mL). To this solution, a 1 N $NaHCO_3$ solution (10 mL) was added, and the resulting precipitate was collected by filtration, washed with H_2O, and then dried under reduced pressure to afford compound **70** (15.3 g, 71%) as a white solid. ^{1}H NMR (400 MHz, $CDCl_3$) δ 7.72 - 7.60 (m, 6H), 7.60 - 7.50 (m, 3H), 7.45 (m, 6H), 4.19 (q, J = 7.13 Hz, 2H), 3.81 (m, 1H), 3.35 (s, 2H), 1.28 (t, J = 7.13 Hz, 3H).

N-[2-(5-methoxy-1H-indol-3-yl)ethyl]-3-oxo-4-(triphenyl-λ^5-phosphanylidene) butanamide (**72**). Compound **70** (5.0 g, 13.0 mmol) and 5-methoxytryptamine **71** (2.6 g, 13.7 mmol) were added together in xylene (25 mL), and the solution was heated to reflux for 3 h. The solution was then cooled to room temperature and concentrated under reduced pressure. The crude residue was purified by column chromatography (MeOH/DCM: 2/98) to give compound **72** (3.9 g, 57%) as an off-white solid. ^{1}H NMR (400 MHz, $CDCl_3$) δ 8.32 (br. s., 1H), 7.89 (br.

s., 1H), 7.70 - 7.51 (m, 9H), 7.50 - 7.39 (m, 6H), 7.19 (d, J = 8.76 Hz, 1H), 7.04 (d, J = 2.42 Hz, 1H), 6.93 (d, J = 2.06 Hz, 1H), 6.82 (dd, J = 8.76, 2.42 Hz, 1H), 3.91 (m, 1H), 3.87 (s, 3H), 3.55 (m, 2H), 3.31 (s, 2H), 2.89 (t, J = 7.46 Hz, 2H); ^{13}C NMR (100 MHz, $CDCl_3$) δ 186.87, 169.47, 153.97, 133.07, 132.97, 132.37, 131.37, 129.06, 128.94, 127.89, 126.63, 125.73, 122.69, 113.28, 112.30, 111.77, 100.46, 100.00, 55.95, 39.45, 25.66.

Procedure F. 5-(4-hydroxy-3-methoxyphenyl)-N-[2-(5-methoxy-1H-indol-3-yl)ethyl]-3-oxopent-4-enamide (**54**). Compound **72** (0.25 g, 0.47 mmol) was added to a solution of NaH (0.075 g, 1.87 mmol) in DMPU/THF (2 mL/2.2 mL) and cooled to 0 °C for 30 min. To this, vanillin **73** (0.09 g, 0.56 mmol) in THF (0.5 mL) was added dropwise. The solution was heated to 40 °C for 3 h. The solution was then cooled to room temperature and stirred overnight. The reaction was then quenched using NH_4Cl (0.5 mL). The solvent was removed under reduced pressure, and the residual oil was purified by column chromatography (Hexanes/Acetone: 50/50) to give compound **54** (0.06 g, 31%) as a light yellow solid. ^{1}H NMR (400 MHz, $CDCl_3$) δ 8.03 (s, 1H), 7.56 (d, J = 16.04 Hz, 1H), 7.23 (d, J = 8.80 Hz, 1H), 7.09 (dd, J = 8.28 Hz, 1.84 Hz, 1H), 7.04-6.99 (m, 3H), 6.93 (d, J = 8.20 Hz, 1H), 6.85 (dd, J = 8.80 Hz, 2.4 Hz, 1H), 6.59 (d, J = 16.04 Hz, 1H), 3.92 (s, 3H), 3.86 (s, 3H), 3.63 (q, J = 5.76 Hz, 2H), 3.58 (s, 2H), 2.96 (t, J = 6.88 Hz, 2H); ^{13}C NMR (100 MHz, $CDCl_3$) δ 195.31, 165.96, 154.09, 149.00, 147.00, 145.68, 131.56, 127.73, 126.48, 124.18, 123.30, 122.89, 115.00, 112.62, 112.43, 111.95, 109.83, 100.54, 56.03, 55.96, 47.30, 39.79, 25.24.

N-[2-(5-methoxy-1H-indol-3-yl)ethyl]-5-(3-methoxyphenyl)-3-oxopent-4-enamide (**55**). 3-Methoxybenzaldehyde (0.076 g, 0.56 mmol) was reacted with **72** (0.25 g, 0.47 mmol) following Procedure F to give compound **55** (0.06 g, 33%). ^{1}H NMR (400 MHz, $CDCl_3$) δ 7.95 (br. s., 1H), 7.71 (d, J = 7.53 Hz, 1H), 7.60 (d, J = 12.80 Hz, 1H), 7.37 (t, J = 8.03 Hz, 1H), 7.32

(t, J = 8.00 Hz, 1H), 7.24 (d, J = 8.78 Hz, 1H), 7.14 (d, J = 8.28 Hz, 1H), 7.04 (s, 1H), 7.03 (br. s., 1H), 6.98 (d, J = 1.76 Hz, 1H), 6.85 (dd, J = 2.51, 8.78 Hz, 1H), 6.72 (d, J = 16.31 Hz, 1H), 3.86 (s, 6H), 3.60 - 3.67 (m, 4H), 2.97 (t, J = 7.03 Hz, 2H); ^{13}C NMR (100 MHz, $CDCl_3$) δ 195.5, 166.1, 159.9, 159.6, 154.0, 145.3, 135.3, 131.5, 130.0, 129.4, 127.7, 125.8, 122.9, 121.4, 120.1, 117.1, 113.4, 112.3, 111.9, 100.5, 55.9, 55.4, 55.3, 47.1, 39.8, 25.1.

Procedure G. 5-(4-hydroxyphenyl)-N-[2-(5-methoxy-1H-indol-3-yl)ethyl]-3-oxopent-4-enamide (**56**)**.** 4-Hydroxybenzaldehyde (0.035 g, 0.29 mmol) and **72** (0.25 g, 0.47 mmol) were added together in a DMSO/H_2O (5 mL/1 mL) solution, and then heated to 100 °C for 24 h. The reaction was cooled to room temperature, and the product was extracted into EtOAc. The EtOAc layer was washed extensively H_2O and then concentrated under reduced pressure. The residual was purified by column chromatography (1. MeOH/DCM: 5/95; 2. Hexanes/Acetone: 50/50) to give compound **56** (0.045 g, 41%). ^{1}H NMR (400 MHz, $CDCl_3$) δ 9.01 (br. s., 1H), 8.21 (br. s., 1H), 7.41 (d, J = 16.06 Hz, 1H), 7.24 (d, J = 8.53 Hz, 2H), 7.09 - 7.16 (m, 2H), 6.91 (dd, J = 2.26, 5.52 Hz, 2H), 6.74 (d, J = 8.78 Hz, 2H), 6.69 - 6.73 (m, 1H), 6.43 (d, J = 16.06 Hz, 1H), 3.73 (s, 3H), 3.49 (q, J = 6.78 Hz, 2H), 3.45 (s, 2H), 2.84 (t, J = 6.78 Hz, 2H); ^{13}C NMR (100 MHz, CD_3COCD_3) δ 194.7, 173.2, 168.2, 154.8, 154.8, 144.5, 135.0, 132.9, 131.3, 129.8, 128.5, 124.1, 121.1, 116.6, 113.1, 112.5, 101.2, 55.9, 55.9, 49.3, 40.3, 26.3.

N-[2-(5-methoxy-1H-indol-3-yl)ethyl]-3-oxo-5-phenylpent-4-enamide (**57**). Benzaldehyde (0.060 g, 0.56 mmol) was reacted with **72** (0.25 g, 0.47 mmol) following Procedure F to give compound **57** (0.05 g, 29%). ^{1}H NMR (400 MHz, $CDCl_3$) δ 8.15 (br. s., 1H), 7.59 (d, J = 16.06 Hz, 1H), 7.51 (dd, J = 1.80, 7.60 Hz, 2H), 7.29 - 7.45 (m, 3H), 7.21 (d, J = 8.78 Hz, 1H), 7.08 (br. s., 1H), 7.02 - 7.04 (m, 1H), 7.00 (d, J = 2.01 Hz, 1H), 6.84 (dd, J = 2.51, 8.78 Hz, 1H), 6.71 (d, J = 16.06 Hz, 1H), 3.84 (s, 3H), 3.61 (q, J = 6.80 Hz, 2H), 3.57 (s, 2H),

2.94 (t, J = 6.80 Hz, 2H); ^{13}C NMR (100 MHz, $CDCl_3$) δ 195.5, 165.6, 154.1, 145.3, 134.0, 131.5, 131.2, 129.1, 128.8, 128.7, 127.7, 127.4, 125.7, 122.9, 112.7, 112.5, 112.0, 100.5, 56.0, 47.4, 39.8, 25.2.

N-[2-(5-methoxy-1H-indol-3-yl)ethyl]-5-(4-methoxyphenyl)-3-oxopent-4-enamide (**58**). 4-Methoxybenzaldehyde (0.076 g, 0.56 mmol) was reacted with **72** (0.25 g, 0.47 mmol) following Procedure F to give compound **58** (0.07 g, 39%). ^{1}H NMR (400 MHz, $CDCl_3$) δ 7.96 (br. s., 1H), 7.59 (d, J = 16.06 Hz, 1H), 7.50 (d, J = 8.80 Hz, 2H), 7.24 (d, J = 9.03 Hz, 1H), 7.13 (br. s., 1H), 7.04 (s, 2H), 6.92 (d, J = 8.80 Hz, 2H), 6.85 (dd, J = 2.38, 8.91 Hz, 1H), 6.62 (d, J = 16.06 Hz, 1H), 3.86 (s, 3H), 3.85 (s, 3H), 3.59 - 3.65 (m, 4H), 2.96 (t, J = 6.90 Hz, 2H); ^{13}C NMR (100 MHz, $CDCl_3$) δ 195.4, 165.8, 162.2, 154.1, 145.2, 131.5, 130.5, 127.7, 126.6, 123.4, 122.8, 114.6, 112.7, 112.5, 111.9, 100.5, 55.9, 55.4, 47.2, 39.7, 25.3.

5-(2H-1,3-benzodioxol-5-yl)-N-[2-(5-methoxy-1H-indol-3-yl)ethyl]-3-oxopent-4-enamide (**59**). 1,3-Benzodioxole-5-carbaldehyde (0.070 g, 0.47 mmol) was reacted with **72** (0.25 g, 0.47 mmol) following Procedure F to give compound **59** (0.05 g, 26%). ^{1}H NMR (400 MHz, $CDCl_3$) δ 8.13 (br. s., 1H), 7.51 (d, J = 16.06 Hz, 1H), 7.22 (d, J = 8.78 Hz, 1H), 7.12 (br. s., 1H), 6.99 - 7.04 (m, 4H), 6.84 (dd, J = 2.51, 8.78 Hz, 1H), 6.81 (d, J = 8.53 Hz, 1H), 6.54 (d, J = 15.81 Hz, 1H), 6.01 (s, 2H), 3.85 (s, 3H), 3.61 (q, J = 6.78 Hz, 2H), 3.55 (s, 2H), 2.95 (t, J = 6.80 Hz, 2H); ^{13}C NMR (100 MHz, $CDCl_3$) δ 195.2, 165.8, 154.0, 150.4, 148.5, 145.1, 131.5, 127.7, 125.6, 123.7, 122.9, 112.6, 112.4, 111.9, 108.7, 106.7, 101.7, 100.5, 55.9, 47.3, 39.7, 25.2.

5-(3,4-dimethoxyphenyl)-N-[2-(5-methoxy-1H-indol-3-yl)ethyl]-3-oxopent-4-enamide (**60**). 3,4-Dimethoxybenzaldehyde (0.093 g, 0.56 mmol) was reacted with **72** (0.25 g, 0.47 mmol) following Procedure F to give compound **60** (0.075 g, 38%). ^{1}H NMR (400 MHz, $CDCl_3$) δ 8.15

(br. s., 1H), 7.58 (d, J = 13.55 Hz, 1H), 7.22 (d, J = 8.78 Hz, 1H), 7.14 (d, J = 8.28 Hz, 1H), 7.01 - 7.09 (m, 4H), 6.88 (d, J = 8.53 Hz, 1H), 6.84 (dd, J = 1.51, 8.78 Hz, 1H), 6.62 (d, J = 16.06 Hz, 1H), 3.92 (s, 3H), 3.91 (s, 3H), 3.86 (s, 3H), 3.58 - 3.65 (m, 4H), 2.96 (t, J = 6.90 Hz, 2H); ^{13}C NMR (100 MHz, $CDCl_3$) δ 195.3, 165.8, 154.0, 152.0, 149.3, 145.4, 131.5, 127.7, 126.9, 123.7, 123.6, 122.9, 112.5, 112.3, 111.9, 111.1, 110.0, 100.5, 55.9, 47.3, 39.7, 25.2.

5-(3,4-dihydroxyphenyl)-N-[2-(5-methoxy-1H-indol-3-yl)ethyl]-3-oxopent-4-enamide (**61**). 3,4-Dihydroxybenzaldehyde (0.077 g, 0.56 mmol) was reacted with **72** (0.25 g, 0.47 mmol) following Procedure G to give compound **61** (0.035 g, 19%). ^{1}H NMR (400 MHz, $CDCl_3$) δ 7.53 (d, J = 16.06 Hz, 1H), 7.20 (d, J = 8.78 Hz, 1H), 7.07 - 7.10 (m, 1H), 7.03 - 7.07 (m, 2H), 6.96 (d, J = 7.53 Hz, 1H), 6.78 (d, J = 8.03 Hz, 1H), 6.74 (dd, J = 2.26, 8.78 Hz, 1H), 6.60 (d, J = 15.81 Hz, 1H), 3.78 - 3.83 (m, 3H), 3.49 - 3.55 (m, 2H), 3.31 (s, 2H), 2.93 (t, J = 7.03 Hz, 2H); ^{13}C NMR (100 MHz, CD_3OD) δ 196.3, 169.7, 155.1, 150.7, 147.2, 147.1, 133.6, 129.2, 127.6, 124.5, 124.0, 123.5, 116.8, 115.6, 113.0, 112.7, 101.6, 56.6, 41.6, 31.0, 26.3.

5-(4-hydroxy-3,5-dimethoxyphenyl)-N-[2-(5-methoxy-1H-indol-3-yl)ethyl]-3-oxopent-4-enamide (**62**). 4-Hydroxy-3,5-dimethoxybenzaldehyde (0.129 g, 0.71 mmol) was reacted with **72** (0.25 g, 0.47 mmol) following Procedure G to give compound **62** (0.068 g, 33%). ^{1}H NMR (400 MHz, $CDCl_3$) δ 8.20 (br. s., 1H), 7.54 (d, J = 16.06 Hz, 1H), 7.23 (d, J = 8.53 Hz, 1H), 7.11 (t, J = 5.40 Hz, 1H), 7.03 (dd, J = 2.26, 6.53 Hz, 2H), 6.84 (dd, J = 2.51, 8.78 Hz, 1H), 6.78 (s, 2H), 6.61 (d, J = 16.06 Hz, 1H), 3.90 (s, 6H), 3.85 (s, 3H), 3.73 (s, 1H), 3.58 - 3.65 (m, 4H), 2.96 (t, J = 7.00 Hz, 2H); ^{13}C NMR (100 MHz, $CDCl_3$) δ 195.1, 165.9, 154.0, 147.3, 145.9, 138.1, 131.5, 127.7, 125.3, 123.5, 122.9, 112.4, 112.3, 111.9, 105.8, 100.5, 56.4, 55.9, 47.4, 43.4, 39.8, 25.2.

5-[4-(dimethylamino)phenyl]-N-[2-(5-methoxy-1H-indol-3-yl)ethyl]-3-oxopent-4-enamide (**63**). 4-(Dimethylamino)benzaldehyde (0.084 g, 0.56 mmol) was reacted with **72** (0.25 g, 0.47 mmol) following Procedure F to give compound **63** (0.047 g, 25%). ^{1}H NMR (400 MHz, $CDCl_3$) δ 8.15 (br. s., 1H), 7.59 (d, J = 15.81 Hz, 1H), 7.44 (d, J = 9.03 Hz, 2H), 7.32 (t, J = 5.77 Hz, 1H), 7.24 (d, J = 8.78 Hz, 1H), 7.05 (dd, J = 2.26, 9.54 Hz, 2H), 6.86 (dd, J = 2.51, 8.78 Hz, 1H), 6.63 - 6.69 (m, 2H), 6.55 (d, J = 15.81 Hz, 1H), 3.87 (s, 3H), 3.63 (q, J = 6.78 Hz, 2H), 3.58 (s, 2H), 3.04 (s, 6H), 2.97 (t, J = 6.90 Hz, 2H); ^{13}C NMR (100 MHz, $CDCl_3$) δ 195.2, 166.3, 154.0, 152.4, 146.2, 131.5, 130.7, 127.7, 122.9, 121.5, 120.4, 112.6, 112.3, 111.9, 111.8, 100.5, 55.9, 46.9, 40.0, 39.7, 25.2.

N-[2-(5-methoxy-1H-indol-3-yl)ethyl]-3-oxo-5-(pyridin-3-yl)pent-4-enamide (**64**). Nicotinaldehyde (0.055 g, 0.51 mmol) was reacted with **72** (0.25 g, 0.47 mmol) following Procedure F to give compound **64** (0.055 g, 32%). ^{1}H NMR (400 MHz, $CDCl_3$) δ 13.59 (s, 1H), 8.65 (s, 1H), 8.55 (d, J = 4.52 Hz, 1H), 8.13 (br. s., 1H), 7.76 (d, J = 8.03 Hz, 1H), 7.50 (d, J = 16.06 Hz, 1H), 7.23 - 7.27 (m, 1H), 7.15 (d, J = 8.80 Hz, 1H), 6.94 (s, 1H), 6.86 (br. s., 1H), 6.77 (dd, J = 2.50, 8.80 Hz, 1H), 6.71 (d, J = 16.31 Hz, 1H), 3.78 (s, 3H), 3.50 - 3.57 (m, 4H), 2.89 (t, J = 6.90 Hz, 2H); ^{13}C NMR (100 MHz, $CDCl_3$) δ 194.8, 154.1, 151.6, 150.3, 143.8, 141.3, 134.6, 133.7, 131.5, 127.3, 122.8, 112.6, 112.5, 111.9, 100.5, 94.4, 55.9, 39.8, 25.2.

N-[2-(5-methoxy-1H-indol-3-yl)ethyl]-3-oxo-5-(pyridin-4-yl)pent-4-enamide (**65**). Isonicotinaldehyde (0.060 g, 0.56 mmol) was reacted with **72** (0.25 g, 0.47 mmol) following Procedure F to give compound **65** (0.065 g, 38%). ^{1}H NMR (400 MHz, $CDCl_3$) δ 13.64 (br. s., 1H), 8.63 (d, J = 6.02 Hz, 1H), 8.54 (d, J = 5.77 Hz, 2H), 8.46 (br. s., 1H), 7.46 (d, J = 16.06 Hz, 1H), 7.32 (d, J = 6.02 Hz, 1H), 7.23 (s, 1H), 6.99 (d, J = 2.00 Hz, 1H), 6.92 (br. s., 1H), 6.86 (dd, J = 2.26, 8.53 Hz, 1H), 6.46 (d, J = 15.81 Hz, 1H), 3.83 (s, 3H), 3.55 - 3.65 (m, 4H), 2.97 (t, J =

7.00 Hz, 2H); ^{13}C NMR (100 MHz, $CDCl_3$) δ 194.8, 171.4, 165.9, 154.3, 150.4, 142.0, 132.4, 129.3, 127.0, 122.1, 121.4, 112.7, 112.5, 112.0, 100.5, 95.3, 56.0, 48.1, 39.5, 25.2.

5-(furan-2-yl)-N-[2-(5-methoxy-1H-indol-3-yl)ethyl]-3-oxopent-4-enamide (**66**). 2-Furaldehyde (0.054 g, 0.56 mmol) was reacted with **72** (0.25 g, 0.47 mmol) following Procedure F to give compound **66** (0.025 g, 15%). ^{1}H NMR (400 MHz, $CDCl_3$) δ 8.01 (br. s., 1H), 7.52 (d, J = 1.51 Hz, 1H), 7.37 (d, J = 15.81 Hz, 1H), 7.21 - 7.25 (m, 1H), 7.12 (br. s, 1H), 7.04 (d, J = 2.51 Hz, 2H), 6.85 (dd, J = 2.38, 8.66 Hz, 1H), 6.72 (d, J = 3.51 Hz, 1H), 6.62 (d, J = 15.81 Hz, 1H), 6.50 (dd, J = 1.88, 3.39 Hz, 1H), 3.86 (s, 1H), 3.58 - 3.65 (m, 2H), 3.55 (s, 2H), 2.96 (t, J = 7.03 Hz, 2H); ^{13}C NMR (100 MHz, $CDCl_3$) δ 195.0, 165.8, 154.1, 150.7, 145.7, 131.5, 130.9, 127.7, 122.9, 122.8, 117.2, 112.8, 112.7, 112.4, 111.9, 100.6, 55.9, 47.6, 39.7, 25.2.

5-(furan-3-yl)-N-[2-(5-methoxy-1H-indol-3-yl)ethyl]-3-oxopent-4-enamide (**67**). 3-Furaldehyde (0.054 g, 0.56 mmol) was reacted with **72** (0.25 g, 0.47 mmol) following Procedure F to give compound **67** (0.020 g, 12%). ^{1}H NMR (400 MHz, $CDCl_3$) δ 7.99 (br. s., 1H), 7.73 (s, 1H), 7.55 (d, J = 15.81 Hz, 1H), 7.46 (t, J = 1.38 Hz, 1H), 7.26 (d, J = 8.78 Hz, 1H), 7.12 (br. s., 1H), 7.05 (d, J = 2.26 Hz, 2H), 6.87 (dd, J = 2.26, 8.78 Hz, 1H), 6.61 (d, J = 1.76 Hz, 1H), 6.47 (d, J = 16.06 Hz, 1H), 3.87 (s, 3H), 3.60 - 3.66 (m, 2H), 3.57 (s, 2H), 2.97 (t, J = 6.90 Hz, 2H); ^{13}C NMR (100 MHz, $CDCl_3$) δ 165.8, 154.1, 146.0, 144.8, 135.4, 131.5, 125.6, 122.8, 122.6, 112.6, 112.5, 111.9, 107.3, 100.5, 55.9, 47.1, 39.8, 25.2.

5-(4-hydroxyphenyl)-N-[2-(5-methoxy-1H-indol-3-yl)ethyl]-3-oxopentanamide (**68**). Compound **56** (0.50 g, 1.32 mmol) was dissolved in MeOH (30 mL) under N_2. To this, Pd/C (0.050 g) was added. The solution was then stirred under H_2 at normal pressure overnight. The solution was then filtered to remove Pd/C, and the filtrate was concentrated under reduced

pressure. The residue was purified by column chromatography (MeOH/DCM: 2/98) to give compound **68** (0.360 g, 72%). ^{1}H NMR (400 MHz, $CDCl_3$) δ 8.37 (br. s., 1H), 7.75 (br. s., 1H), 7.22 (d, J = 8.78 Hz, 1H), 7.01 (d, J = 2.26 Hz, 1H), 6.91 - 6.98 (m, 4H), 6.83 (dd, J = 2.26, 8.78 Hz, 1H), 6.74 (d, J = 8.28 Hz, 2H), 3.83 (s, 0H), 3.55 (q, J = 6.61 Hz, 2H), 3.25 (s, 2H), 2.90 (t, J = 6.78 Hz, 2H), 2.67 - 2.78 (m, 4H); ^{13}C NMR (100 MHz, $CDCl_3$) δ 205.8, 165.8, 155.0, 153.9, 131.5, 131.3, 129.2, 127.6, 123.0, 115.5, 112.2, 112.0, 100.5, 55.9, 49.3, 45.2, 39.7, 28.5, 25.0.

5.1.3 NLRP3 Inhibitors

5-chloro-2-methoxy-*N*-phenethylbenzamide (**87**). 5-Chloro-2-methoxybenzoic acid **90** (2.0 g, 10.7 mmol) and 2-phenylethanamine **91** (1.3 g, 10.7 mmol) were reacted following Procedure B to give compound **87** (1.95 g, 63%) as a viscous oil. ^{1}H NMR (400 MHz, $CDCl_3$) δ 8.19 (d, J = 3.01 Hz, 1H), 7.82 (br. s., 1H), 7.36 (dd, J = 3.00, 8.80 Hz, 1H), 7.34 (d, J = 6.78 Hz, 2H), 7.27 (d, J = 7.03 Hz, 2H), 7.26 - 7.28 (m, 1H), 6.85 (d, J = 8.78 Hz, 1H), 3.77 (q, J = 6.20 Hz, 2H), 3.74 (s, 3H), 2.93 (t, J = 6.78 Hz, 2H); ^{13}C NMR (100 MHz, DMSO-d6) δ 163.4, 155.7, 139.4, 131.5, 129.6, 128.7, 128.3, 126.1, 124.7, 124.3, 114.1, 56.2, 40.7, 34.9.

4-(2-[(5-chloro-2-methoxyphenyl)formamido]ethyl)benzene-1-sulfonyl chloride (**71**). Compound **87** (0.50 g, 1.73 mmol) was dissolved in DCM (2 mL). To this, excess chlorosulfonic acid (1 mL) was added, and the solution stirred at 70 °C for 2 h. The reaction was cooled to room temperature, and then poured over crushed ice. The product was extracted into DCM, and then concentrated under reduced pressure. The product was purified by column chromatography (EtOAc/Hexanes: 20/80 to 50/50) yielding compound **71** (0.35 g, 52%) as a white solid. ^{1}H NMR (400 MHz, $CDCl_3$) δ 8.17 (d, J = 3.01 Hz, 1H), 8.00 (d, J = 8.28 Hz, 2H),

7.81 (br. s., 1H), 7.50 (d, J = 8.53 Hz, 2H), 7.39 (dd, J = 2.76, 8.78 Hz, 1H), 6.89 (d, J = 8.78 Hz, 1H), 3.81 (s, 3H), 3.77 (q, J = 6.50 Hz, 2H), 3.08 (t, J = 6.90 Hz, 2H); ^{13}C NMR (100 MHz, DMSO-d6) δ 163.5, 155.7, 146.1, 139.8, 131.5, 129.5, 128.0, 125.6, 124.7, 124.3, 114.2, 56.2, 40.6, 34.6.

4-(2-[(5-chloro-2-methoxyphenyl)formamido]ethyl)benzene-1-sulfonic acid (**73**). Compound **71** (61 mg, 0.16 mmol) was added to H_2O (5 mL) and refluxed overnight. The water layer was washed with DCM, and the product was collected by distillation affording **73** (17.0 mg, 29%). ^{1}H NMR (400 MHz, DMSO-d6) δ 8.21 (t, J = 5.65 Hz, 1H), 7.67 (d, J = 2.76 Hz, 1H), 7.53 - 7.57 (m, J = 8.28 Hz, 2H), 7.49 (dd, J = 2.76, 8.78 Hz, 1H), 7.19 - 7.23 (m, J = 8.03 Hz, 2H), 7.15 (d, J = 8.78 Hz, 1H), 4.61 (br. s., 1H), 3.80 (s, 3H), 3.50 (q, J = 6.50 Hz, 2H), 2.83 (t, J = 7.03 Hz, 2H); ^{13}C NMR (100 MHz, DMSO-d6) δ 163.5, 155.7, 146.1, 139.8, 131.5, 129.5, 128.0, 125.6, 124.7, 124.3, 114.2, 56.2, 40.6, 34.6.

5-chloro-2-methoxy-N-[2-(4-sulfamoylphenyl)ethyl]benzamide (**72**). Compound **71** (500 mg, 1.29 mmol) was added to aqueous NH_4OH (10 mL) and stirred at room temperature for 1 h. The solid precipitate was collected, filtered, and washed extensively with H_2O. The remaining solid was purified by recrystallization in EtOH affording compound **72** (324 mg, 68%) as a white solid. ^{1}H NMR (400 MHz, DMSO-d6) δ 8.25 (t, J = 5.52 Hz, 1H), 7.77 (d, J = 8.28 Hz, 2H), 7.65 (d, J = 3.01 Hz, 1H), 7.50 (dd, J = 2.89, 8.91 Hz, 1H), 7.45 (d, J = 8.28 Hz, 2H), 7.28 (s, 2H), 7.15 (d, J = 8.78 Hz, 1H), 3.81 (s, 3H), 3.54 (q, J = 6.30 Hz, 2H), 2.92 (t, J = 7.15 Hz, 2H); ^{13}C NMR (100 MHz, DMSO-d6) δ 163.6, 155.7, 143.6, 142.1, 131.5, 129.5, 129.2, 125.7, 124.8, 124.3, 114.1, 56.3, 40.3, 34.6.

N-(2-(4-[bis(propan-2-yl)sulfamoyl]phenyl)ethyl)-5-chloro-2-methoxybenzamide (**74**). Compound **71** (220 mg, 0.76 mmol) was added to excess diisopropylamine (2 mL) in DCM (5 mL) and stirred overnight. The solution was then washed with H_2O and concentrated under reduced pressure. The product was purified by column chromatography (DCM/MeOH: 100/0 to 97/3) yielding compound **74** (100 mg, 29%) as a white solid. ^{1}H NMR (400 MHz, $CDCl_3$) δ 8.13 (d, J = 2.76 Hz, 1H), 7.81 (d, J = 8.28 Hz, 2H), 7.32 - 7.38 (m, 3H), 6.87 (d, J = 9.03 Hz, 1H), 3.78 (s, 3H), 3.67 - 3.75 (m, 4H), 2.99 (t, J = 6.78 Hz, 2H), 1.27 (s, 6H), 1.25 (s, 6H); ^{13}C NMR (100 MHz, DMSO-d6) δ 163.6, 155.6, 144.1, 140.1, 131.4, 129.4, 126.7, 124.8, 124.3, 114.1, 56.2, 47.9, 40.1, 34.6, 21.5.

5-chloro-2-methoxy-N-(2-[4-(piperidine-1-sulfonyl)phenyl]ethyl)benzamide (**75**). Compound **71** (206 mg, 0.711 mmol) was added to excess piperidine (2 mL) in DCM (5 mL) and stirred overnight. The solution was then washed with H_2O and concentrated under reduced pressure. The product was purified by column chromatography (DCM/MeOH: 100/0 to 97/3) yielding compound **75** (126 mg, 41%) as a white solid. ^{1}H NMR (400 MHz, $CDCl_3$) δ 8.16 (d, J = 2.76 Hz, 1H), 7.78 (br. s., 1H), 7.71 (d, J = 8.28 Hz, 2H), 7.40 (d, J = 8.30 Hz, 1H), 7.38 (dd, J = 2.80, 8.80 Hz, 2H), 6.88 (d, J = 8.78 Hz, 1H), 3.79 (s, 3H), 3.76 (q, J = 6.78 Hz, 2H), 2.99 (t, J = 5.50 Hz, 2H), 3.01 (t, J = 6.80 Hz, 4H), 1.64 (quin, J = 5.71 Hz, 4H), 1.42 (quin, J = 5.96 Hz, 2H); ^{13}C NMR (100 MHz, DMSO-d6) δ 163.6, 155.6, 145.0, 133.3, 131.4, 129.6, 129.4, 127.4, 124.9, 124.3, 114.1, 56.2, 46.5, 40.1, 34.7, 24.6, 22.8.

5-chloro-N-(2-[4-(dimethylsulfamoyl)phenyl]ethyl)-2-methoxybenzamide (**76**). Dimethylamine HCl (105 mg, 1.29 mmol) and N-methylmorpholine (0.5 mL) were added to H_2O (3 mL). Compound **71** (400 mg, 1.03 mmol) was dissolved in DCM (2 mL) and then added to the reaction, and the solution was stirred overnight at room temperature. The product was

extracted into DCM, concentrated, and purified by column chromatography (EtOAc/Hexanes: 20/80 to 75/25) to give compound **76** (250 mg, 60%) as a white solid. ^{1}H NMR (400 MHz, DMSO-d6) δ 8.26 (br. s., 1H), 7.68 (d, J = 7.78 Hz, 2H), 7.59 (br. s., 1H), 7.53 (d, J = 7.78 Hz, 2H), 7.49 (d, J = 9.03 Hz, 1H), 7.15 (d, J = 9.29 Hz, 1H), 3.82 (s, 3H), 3.56 (q, J = 6.50 Hz, 2H), 2.95 (t, J = 6.65 Hz, 2H), 2.59 (s, 6H); ^{13}C NMR (100 MHz, DMSO-d6) δ 163.6, 155.6, 145.1, 132.6, 131.4, 129.6, 129.4, 127.6, 124.9, 124.3, 114.1, 56.2, 40.1, 37.5, 34.7.

5-chloro-2-methoxy-N-(2-[4-(methylsulfamoyl)phenyl]ethyl)benzamide (**77**). Methylamine HCl (44 mg, 0.644 mmol) and N-methylmorpholine (0.1 mL) were added to MeOH (1 mL). Compound **71** (50 mg, 0.129 mmol) was dissolved in DCM (2 mL) and then added to the reaction, and the solution was stirred overnight at room temperature. The reaction was concentrated, and then dissolved in DCM and H_2O. The product was extracted into DCM, concentrated, and purified by column chromatography (DCM/MeOH: 100/0 to 95/5) to give compound **77** (42 mg, 85%) as a white solid. ^{1}H NMR (400 MHz, $CDCl_3$) δ 8.17 (d, J = 2.76 Hz, 1H), 7.82 (d, J = 8.28 Hz, 2H), 7.41 (d, J = 8.53 Hz, 2H), 7.39 (dd, J = 2.89, 8.91 Hz, 1H), 6.88 (d, J = 8.78 Hz, 1H), 4.26 (q, J = 5.19 Hz, 1H), 3.80 (s, 3H), 3.75 (q, J = 6.70 Hz, 2H), 3.02 (t, J = 6.78 Hz, 2H), 2.68 (d, J = 5.52 Hz, 3H); ^{13}C NMR (100 MHz, DMSO-d6) δ 163.6, 155.7, 144.3, 137.2, 131.4, 129.5, 129.4, 126.7, 124.9, 124.3, 114.2, 56.2, 40.1, 34.6, 28.6.

5-chloro-N-(2-[4-(acetamidosulfonyl)phenyl]ethyl)-2-methoxybenzamide (**78**). Compound **72** (450 mg, 1.22 mmol) was added to excess acetic anhydride (1 mL) in DCM (5 mL) and stirred at 75 °C overnight. The solid precipitate was filtered off and washed with H_2O and DCM affording compound **78** (400 mg, 80%) as a white solid. ^{1}H NMR (400 MHz, DMSO-d6) δ 12.01 (s, 1H), 8.25 (t, J = 5.65 Hz, 1H), 7.85 (d, J = 8.53 Hz, 2H), 7.63 (d, J = 2.76 Hz, 1H), 7.47 - 7.53 (m, 3H), 7.15 (d, J = 8.78 Hz, 1H), 3.79 (s, 3H), 3.55 (q, J = 6.70 Hz, 2H), 2.94

(t, J = 7.03 Hz, 2H), 1.92 (s, 3H); ^{13}C NMR (100 MHz, DMSO-d6) δ 168.7, 163.6, 155.7, 145.8, 137.3, 131.5, 129.5, 129.4, 127.5, 124.9, 124.3, 114.1, 56.2, 40.1, 34.7, 23.2.

5-chloro-N-(2-[4-(hydrazinesulfonyl)phenyl]ethyl)-2-methoxybenzamide (**79**). Excess hydrazine (0.2 mL) was dissolved in DCM (8 mL) and cooled to 0 °C. To this, compound **71** (50 mg, 0.129 mmol) dissolved in DCM (2 mL) was added dropwise, slowly. The reaction was allowed to warm to room temperature and stirred overnight. The organic layer was washed with H_2O and concentrated to give compound **79** (41 mg, 85%) as a white solid. ^{1}H NMR (400 MHz, DMSO-d6) δ 8.32 (s, 1H), 8.28 (t, J = 5.65 Hz, 1H), 7.75 (d, J = 8.28 Hz, 2H), 7.64 (d, J = 2.76 Hz, 1H), 7.50 (dd, J = 2.80, 8.80 Hz, 0H), 7.48 (d, J = 8.30 Hz, 2H), 7.16 (d, J = 9.03 Hz, 1H), 4.06 (d, J = 3.01 Hz, 2H), 3.82 (s, 3H), 3.54 (q, J = 6.53 Hz, 2H), 2.93 (t, J = 6.90 Hz, 2H); ^{13}C NMR (100 MHz, DMSO-d6) δ 163.6, 155.7, 144.6, 136.0, 131.5, 129.5, 129.3, 127.7, 124.8, 124.3, 114.2, 56.3, 40.3, 34.7.

5-chloro-N-(2-[4-(hydroxysulfamoyl)phenyl]ethyl)-2-methoxybenzamide (**80**). Hydroxylamine HCl (441 mg, 6.44 mmol) and N-methylmorpholine (0.2 mL) were dissolved in MeOH (2 mL). To this, compound **71** (500 mg, 1.29 mmol) was added, and the solution was stirred for 4 h. H_2O was added, and the product was extracted into DCM and concentrated. The product was purified by column chromatography (DCM/MeOH: 100/0 to 94/6) to give compound **80** (90 mg, 18%) as a white solid. ^{1}H NMR (400 MHz, DMSO-d6) δ 9.56 (d, J = 3.26 Hz, 1H), 9.52 (d, J = 3.26 Hz, 1H), 8.27 (t, J = 5.40 Hz, 1H), 7.78 (d, J = 8.28 Hz, 2H), 7.64 (d, J = 2.76 Hz, 1H), 7.48 - 7.53 (m, 3H), 7.15 (d, J = 8.78 Hz, 1H), 3.81 (s, 3H), 3.55 (q, J = 6.70 Hz, 2H), 2.94 (t, J = 6.90 Hz, 2H); ^{13}C NMR (100 MHz, DMSO-d6) δ 163.6, 155.7, 145.2, 135.3, 131.5, 129.5, 129.2, 128.2, 124.8, 124.3, 114.2, 56.2, 40.2, 34.7.

3-chloro-N-[2-(4-sulfamoylphenyl)ethyl]benzamide (**81**). 3-Chlorobenzoic acid (1.0 g, 6.39 mmol) was added to thionyl chloride (20 mL) and 1 drop DMF. The solution was refluxed for 3 h, cooled to room temperature, and concentrated. The remaining residue was dissolved in ACN (40 mL). To this, a solution of 4-(2-aminoethyl)benzenesulfonamide **92** (1.60 g, 7.98 mmol) and N-methylmorpholine (1 mL) in ACN (9 mL) was added dropwise over 15 minutes. The reaction was stirred at room temperature overnight. The solution was concentrated, and cold H_2O was added. The resulting precipitate was collected, filtered, and washed with H_2O. The product was purified by recrystallization in EtOH to give compound **81** (1.4 g, 65%) as a white solid. ^{1}H NMR (400 MHz, DMSO-d6) δ 8.70 (br. s., 1H), 7.85 (s, 1H), 7.75 (d, J = 8.00 Hz, 2H), 7.72 - 7.79 (m, 1H), 7.59 (d, J = 7.53 Hz, 1H), 7.50 (t, J = 7.53 Hz, 1H), 7.43 (d, J = 8.03 Hz, 2H), 7.28 (s, 2H), 3.52 (q, J = 6.80 Hz, 2H), 2.93 (t, J = 7.15 Hz, 2H); ^{13}C NMR (100 MHz, DMSO-d6) δ 164.8, 143.6, 142.1, 136.4, 133.2, 131.0, 130.3, 129.1, 126.9, 125.9, 125.7, 40.5, 34.6.

2-methoxy-N-[2-(4-sulfamoylphenyl)ethyl]benzamide (**82**). 2-Methoxybenzoic acid (1.0 g, 6.57 mmol) was added to thionyl chloride (20 mL) and 1 drop DMF. The solution was refluxed for 3 h, cooled to room temperature, and concentrated. The remaining residue was dissolved in ACN (40 mL). To this, a solution of compound **92** (1.32 g, 6.57 mmol) and N-methylmorpholine (1 mL) in ACN (9 mL) was added dropwise over 15 minutes. The reaction was stirred at room temperature overnight. The solution was concentrated, and cold H_2O was added. The resulting precipitate was collected, filtered, and washed with H_2O. The product was purified by recrystallization in EtOH to give compound **82** (1.4 g, 62%) as a white solid. ^{1}H NMR (400 MHz, DMSO-d6) δ 8.17 (br. s., 1H), 7.77 (d, J = 7.03 Hz, 2H), 7.72 (d, J = 7.53 Hz, 1H), 7.46 (d, J = 7.53 Hz, 2H), 7.41 - 7.48 (m, 0H), 7.28 (s, 2H), 7.11 (d, J = 8.78 Hz, 1H), 7.02

(t, J = 7.40 Hz, 1H), 3.81 (s, 3H), 3.55 (q, J = 6.80 Hz, 2H), 2.92 (t, J = 6.65 Hz, 2H); ^{13}C NMR (100 MHz, DMSO-d6) δ 164.9, 156.9, 143.8, 142.1, 132.2, 130.4, 129.2, 125.7, 122.9, 120.5, 112.0, 55.8, 40.2, 34.7.

N-[2-(4-sulfamoylphenyl)ethyl]benzamide (**83**). Benzoic acid (0.61 g, 5.0 mmol) was added to thionyl chloride (20 mL) and 1 drop DMF. The solution was refluxed for 3 h, cooled to room temperature, and concentrated. The remaining residue was dissolved in ACN (40 mL). To this, a solution of compound **92** (1.0 g, 5.0 mmol) and N-methylmorpholine (1 mL) in ACN (9 mL) was added dropwise over 15 minutes. The reaction was stirred at room temperature overnight. The solution was concentrated, and cold H_2O was added. The resulting precipitate was collected, filtered, and washed with H_2O. The product was purified by recrystallization in EtOH to give compound **83** (0.83 g, 55%) as a white solid. ^{1}H NMR (400 MHz, DMSO-d6) δ 8.57 (br. s., 1H), 7.81 (d, J = 7.03 Hz, 2H), 7.75 (d, J = 7.78 Hz, 2H), 7.52 (t, J = 7.00 Hz, 1H), 7.41 - 7.48 (m, 4H), 7.29 (s, 2H), 3.52 (q, J = 6.20 Hz, 2H), 2.93 (t, J = 6.90 Hz, 2H); ^{13}C NMR (100 MHz, DMSO-d6) δ 166.3, 143.8, 142.0, 134.5, 131.1, 129.1, 128.2, 127.1, 125.7, 40.4, 34.8.

5-chloro-2-hydroxy-N-[2-(4-sulfamoylphenyl)ethyl]benzamide (**84**). 5-Chloro-2-hydroxybenzoic acid (1.0 g, 5.79 mmol) was dissolved in DMF (40 mL) and cooled to 0 °C. EDC (1.39 g, 7.24 mmol) and HOBt (0.78 g, 5.79 mmol) were added, and the solution was stirred for 1 h. Compound **92** (1.16 g, 5.79 mmol) and N-methylmorpholine (1.28 mL) were then added, and the solution was stirred overnight. The solution was then concentrated under reduced pressure. DCM was then added, and the resulting precipitate was filtered off and collected. The precipitate was purified by recrystallization in EtOH to yield compound **84** (165 mg, 8%) as a white solid. ^{1}H NMR (400 MHz, DMSO-d6) δ 12.47 (s, 1H), 8.93 (t, J = 5.52 Hz,

1H), 7.90 (d, J = 2.51 Hz, 1H), 7.75 (d, J = 8.53 Hz, 2H), 7.44 (d, J = 8.28 Hz, 2H), 7.43 (dd, J = 2.50, 8.80 Hz, 1H), 7.27 (s, 2H), 6.93 (d, J = 8.78 Hz, 1H), 3.56 (q, J = 6.80 Hz, 2H), 2.94 (t, J = 7.28 Hz, 2H); ^{13}C NMR (100 MHz, DMSO-d6) δ 167.3, 158.4, 143.4, 142.2, 133.2, 129.1, 127.3, 125.7, 122.3, 119.3, 116.9, 40.2, 34.4.

5-chloro-2-methoxy-N-[2-(4-sulfamoylphenyl)ethyl]pyridine-3-carboxamide (**85**). 5-Chloro-2-methoxypyridine-3-carboxylic acid (150 mg, 0.800 mmol) was added to thionyl chloride (5 mL) and 1 drop DMF. The solution was refluxed for 3 h, cooled to room temperature, and concentrated. The remaining residue was dissolved in ACN (5 mL). To this, a solution of compound **92** (121 mg, 0.60 mmol) and N-methylmorpholine (0.5 mL) in ACN (5 mL) was added dropwise over 15 minutes. The reaction was stirred at room temperature overnight. The solution was concentrated, and cold H_2O was added. The resulting precipitate was collected, filtered, and washed with H_2O. The product was purified by recrystallization in EtOH to give compound **85** (210 mg, 95%) as a white solid. ^{1}H NMR (400 MHz, DMSO-d6) δ 8.35 (d, J = 2.76 Hz, 1H), 8.35 (s, 0H), 8.06 (d, J = 2.76 Hz, 1H), 7.77 (d, J = 8.28 Hz, 2H), 7.45 (d, J = 8.03 Hz, 2H), 7.28 (s, 2H), 3.92 (s, 3H), 3.54 (q, J = 6.70 Hz, 2H), 2.92 (t, J = 7.03 Hz, 2H); ^{13}C NMR (100 MHz, DMSO-d6) δ 162.4, 158.8, 146.8, 143.5, 142.2, 138.9, 129.2, 125.7, 123.5, 118.9, 54.2, 40.4, 34.5.

5-chloro-2-(methylamino)-N-[2-(4-sulfamoylphenyl)ethyl]benzamide (**86**). 2-[(*tert*-butoxycarbonyl)(methyl)amino]-5-chlorobenzoic acid (125 mg, 0.44 mmol) was dissolved in DCM (5 mL) and DMF (0.25 mL), and cooled to 0 °C. EDC (150 mg, 0.78 mmol) and HOBt (105 mg, 0.78 mmol) were added, and the solution was stirred for 1 h. Compound **92** (75 mg, 0.374 mmol) and Et_3N (0.1 mL) were then added, and the reaction was stirred overnight. The solution was washed with acidic H_2O. The organic layer was then concentrated under reduced

pressure. The product was purified by column chromatography (DCM/MeOH: 100/0 to 95/5) to give compound **86** (79 mg, 49%) as a white solid. ^{1}H NMR (400 MHz, DMSO-d6) δ 8.53 (t, J = 5.27 Hz, 1H), 7.72 - 7.77 (m, 2H), 7.62 (q, J = 5.19 Hz, 1H), 7.53 (d, J = 2.51 Hz, 1H), 7.39 - 7.44 (m, J = 8.28 Hz, 2H), 7.28 (s, 2H), 7.30 (dd, J = 2.50, 8.80 Hz, 1H), 6.63 (d, J = 8.78 Hz, 1H), 3.46 (q, J = 6.80 Hz, 2H), 2.90 (t, J = 7.28 Hz, 2H), 2.76 (d, J = 5.02 Hz, 3H); ^{13}C NMR (100 MHz, DMSO-d6) δ 167.8, 148.8, 143.7, 142.1, 131.8, 129.1, 127.4, 125.7, 117.4, 116.0, 112.3, 40.1, 34.6, 29.3.

4-(2-([(5-chloro-2-methoxyphenyl)methyl]amino)ethyl)benzene-1-sulfonamide (**88**). Compound **92** (66 mg, 0.328 mmol) and 5-chloro-2-methoxybenzaldehyde **93** (50 mg, 0.293 mmol) were added together in DCE (9 mL) and stirred at room temperature for 30 min. Glacial acetic acid (16.4 mg, 0.328 mmol) in DCE (1 mL) was then added, and the reaction was stirred at room temperature for 1 h. The solution was cooled to 0 °C, and then $NaCNBH_3$ (25.5 mg, 0.39 mmol) in MeOH (3 mL) was added dropwise. The reaction was stirred at room temperature overnight. The solution was then concentrated under reduced pressure, and then DCM was added. The organic layer was washed with H_2O, and then concentrated again. The product was purified by column chromatography (DCM/MeOH/Et_3N: 100/0/0 to 90/8/2) to afford compound **88** (58 mg, 51%) as a white solid. ^{1}H NMR (400 MHz, $CDCl_3$) δ 7.84 (d, J = 8.53 Hz, 2H), 7.34 (d, J = 8.28 Hz, 2H), 7.15 - 7.22 (m, 2H), 6.72 - 6.77 (m, 1H), 4.72 (br. s., 2H), 3.75 (s, 2H), 3.74 (s, 3H), 2.87 - 2.90 (m, 4H); ^{13}C NMR (100 MHz, DMSO-d6) δ 155.7, 144.8, 141.8, 129.0, 128.1, 127.0, 125.6, 123.9, 112.1, 55.6, 49.9, 46.7, 35.5.

4-([(5-chloro-2-methoxyphenyl)formohydrazido]methyl)benzene-1-sulfonamide (**89**). 5-chloro-2-methoxybenzohydrazide **95** (200 mg, 1.00 mmol) and 4-formylbenzene-1-sulfonamide **94** (185 mg, 1.00 mmol) were added together in EtOH (5 mL). AcOH (0.1 mL) was then added

and the reaction was refluxed overnight. The solution was then cooled to room temperature, and the precipitate was filtered off and washed with EtOH. The solid precipitate was added to a THF/MeOH (50/50) solution (20 mL). To this, $NaCNBH_3$ (63 mg, 1.00 mmol) was added, and the suspension was stirred at room temperature overnight. Concentrated HCl (2 mL) was added to the suspension. When no more bubbles were formed, the solution was basified with a saturated $NaHCO_3$ solution. The solid precipitate was filtered off, washed with H_2O, and dried to give compound **89** (234 mg, 63%) as a white solid. ^{1}H NMR (400 MHz, DMSO-d6) δ 9.50 (d, J = 6.27 Hz, 1H), 7.76 - 7.80 (m, 2H), 7.54 - 7.58 (m, J = 8.28 Hz, 2H), 7.53 (d, J = 2.76 Hz, 1H), 7.48 (dd, J = 2.89, 8.91 Hz, 1H), 7.30 (s, 2H), 7.12 (d, J = 8.78 Hz, 1H), 5.69 (q, J = 5.50 Hz, 1H), 4.06 (d, J = 5.27 Hz, 2H), 3.77 (s, 3H); ^{13}C NMR (100 MHz, DMSO-d6) δ 163.3, 155.6, 142.8, 142.7, 131.4, 129.1, 128.8, 125.4, 124.4, 124.2, 114.0, 56.2, 53.8.

5.2 Biological Methods

5.2.1 *In Vitro* Assays

5.2.1.1 MC65 Cell Culture

MC65 cells (kindly provided by Dr. George M. Martin at the University of Washington, Seattle) were cultured in Dulbecco's Modified Eagle's Medium (DMEM) (Life Technologies, Inc., Grand Island, NY) supplemented with 10% of heat-inactivated fetal bovine serum (FBS) (Hyclone, Logan, UT), 1% Penicillin/Streptomycin (P/S) (Invitrogen), 1 μg/mL Tetracycline (TC) (Sigma Aldrich, St. Louis, MO), and 0.2 mg/mL G418 (Invitrogen). All assays were carried out in Opti-MEM Reduced Serum Medium (Life Technologies, Inc., Grand Island, NY).

Cells were maintained at 37 °C in a fully humidified atmosphere containing 5% CO_2. Cell controls were prepared in Opti-MEM with or without TC (+TC or -TC).

5.2.1.2 MC65 Viability Assay

MC65 cells were cells were washed twice with PBS, resuspended in Opti-MEM, and seeded in 96-well plates (4×10^4 cells/well). Indicated compounds were then added, and cells were incubated at 37 °C under +TC or -TC conditions for 72 h. MTT (5 mg/mL in PBS) were then added and the cells were incubated for another 4 h. Cell medium was then removed, and the remaining formazan crystals produced by the cellular reduction of MTT were dissolved in DMSO. Absorbance at 570 nm was immediately recorded using a FlexStation 3 plate reader (Molecular Devices, CA). Values are expressed as a percentage relative to those obtained in the +TC controls.

5.2.1.3 ROS Production Assay

MC65 cells were washed twice with PBS, resuspended in Opti-MEM, and seeded in 6-well plates (2×10^6 cells/well). Indicated compounds were then added, and cells were incubated at 37 °C under +TC and -TC conditions for 48 h. Cells were harvested, washed with cold PBS, then suspended in PBS and incubated with DCFH-DA (25 μM) in dark for 1 h. Fluorescence was analyzed by flow cytometry using a Millipore Guava easyCyte flow cytometer. Values are expressed as a percentage relative to those obtained in -TC controls.

5.2.1.4 Rotenone-Induced Toxicity Assay

MC65 cells were seeded in 96-well plates (4×10^4 cells/well) in growth medium and incubated at 37 °C for 24 h. Medium was then removed and compounds were added in fresh growth medium at the indicated concentrations, and the cells were incubated for another 2 h. Rotenone was then added at a final concentration of 10 μM, and the plates were then incubated for 48 h. Cell viability was assessed by MTT assay as previously described. Values are expressed as a percentage relative to the negative (rotenone-free) control.

5.2.1.5 Aß Western Blot

MC65 cells were washed twice with PBS, re-suspended in Opti-MEM, and seeded in 6-well plates (2×10^6 cells/well). Indicated compounds were then added, and cells were incubated at 37 °C under +TC and -TC conditions for 48 h. Cells were harvested, washed with cold PBS, then lysed by sonication in a Tricine buffer solution. Protein samples were collected from the supernatant after centrifugation at 12,800×g for 5 min, and then quantified using the Bradford method. Equal amounts of protein (20.0 μg) were separated by SDS-PAGE on a Tris-Tricine gel (Bio-Rad) and transferred onto a PVDF membrane (Bio-Rad). Blots were blocked with a 5% milk in TBS-Tween 20 (0.1%) solution at room temperature for 1 h, and then probed with the 6E10 antibody (Signet, Dedham, MA) overnight at 4 °C. Blots were washed twice in TBS-Tween 20 for 15 min, and then incubated with a 1:1000 dilution of horseradish peroxidase-conjugated secondary antibody in a 5% milk/PBS-Tween 20 solution at room temperature for 1 h. After washing twice in TBS-Tween 20 for 15 min, the proteins were visualized by a Western Blot Chemiluminescence Reagent following the manufacturer's instructions (Thermo Fischer

Scientific, Waltham, MA). Blots were also probed with antibodies against α-tubulin to ensure equal loading of proteins.

5.2.1.6 Aß$_{40}$ and Aß$_{42}$ ELISA

MC65 cells were cells were washed twice with PBS, re-suspended in Opti-MEM, and seeded in 96-well plates (4×10^4 cells/well). Indicated compounds were then added, and cells were incubated at 37 °C under +TC or -TC conditions for 48 h. The conditioned media was then added to ELISA plates precoated with BNT77 antibody (Wako, Richmond, VA) and incubated overnight at 4 °C. Plates were then washed 5 times and HRP-conjugated secondary antibodies were added, BA27 for Aß$_{40}$ or BC05 for Aß$_{42}$, and plates were incubated at room temperature for 1 h. Plates were washed once more. TMB was added to initiate the HRP reaction, and plates incubated in dark at room temperature for 30 min. Stop solution was then added to terminate the reaction. Absorbance at 450 nm was immediately recorded using a FlexStation 3 plate reader (Molecular Devices, CA). Values are expressed in pM and were calculated using calibration curves generated with Aß standard proteins.

5.2.1.7 Thioflavin T Binding Assay

A thioflavin T (ThT)-binding assay, used to measure Aß$_{42}$ aggregation, was conducted following published methods.[10] Aß$_{42}$ was obtained from American Peptide, Inc. (Sunnyvale, CA). Briefly, 1 μL of each compound solution in DMSO (0.01 μM to 100 μM) was added to

corresponding wells in a 96-well plate. Each concentration was prepared as independent triplicates, and a solvent control was included. To each well, 9 μL of 25 μM $Aß_{42}$ in PBS (pH 7.4) was added, and plates were then incubated in dark at room temperature for 48 h. Next, 200 μL of a 5 μM ThT in 50 mM glycine solution (pH 8.0) was added to each well. Fluorescence was immediately recorded using a FlexStation 3 plate reader (Molecular Devices, CA) at an excitation wavelength of 446 nm and an emission wavelength of 490 nm.

5.2.1.8 AFM Analysis of $Aß_{42}$ Fibril and Oligomer Formation

$Aß_{42}$ oligomers and fibrils were prepared based on reported procedures.[230] Indicated compounds were incubated with $Aß_{42}$ at a 1:1 ratio for 24 h. Samples were loaded on mica, washed extensively with water, and dried overnight at room temperature before AFM analysis. The morphology of the $Aß_{42}$ aggregates was assessed using an atomic force microscope (Dimension Icon, Bruker) operating in tapping mode in air. The scan rate was varied between 1 Hz and 0.5 Hz, depending on the tracking quality. The silicon tips (Bruker mpp2100-100) have a sharpness of less than 5 nm and a force constant between 3 and 5 N/m along with a resonant frequency rated between 60-90 Hz. All images were taken with 512 points per line, with a 1:1 ratio. Images were processed using Nanoscope analysis software v1.20 and Image-J (from the National Institutes of Health).

5.2.1.9 Biometal Chelation Assay

Compounds (50 μM) and $CuSO_4$, $FeCl_2$, or $ZnCl_2$ (50 μM) in water were incubated at room temperature for 10 min, and then UV absorption was recorded from 200 nm to 600 nm on a Flexstation 3 plate reader (Molecular Devices, CA).

5.2.1.10 HT22 Cell Culture

HT22 mouse hippocampal cells (graciously provided by Dr. Dave R. Schubert at the Salk Institute, La Jolla, CA) were cultured in DMEM supplemented with 10% FBS and 1% P/S. Cells were maintained at 37 °C in a fully humidified atmosphere containing 5% CO_2.

5.2.1.11 H_2O_2-Induced Toxicity Assay

HT22 cells were seeded in 96-well plates (4×10^3 cells/well) in growth medium and incubated at 37 °C for 24 h. Medium was then removed and compounds were added in fresh growth medium at the indicated concentrations, and the cells were incubated for another 1 h. H_2O_2 was then added at a final concentration of 500 μM, and the plates were then incubated for 24 h. Cell viability was assessed by MTT assay as previously described. Values were expressed as a percentage relative to the negative (H_2O_2-free) control.

5.2.1.12 J774.A1 Cell Culture

J774.A1 murine macrophage cells (ATCC, Manassas, VA) were cultured in DMEM supplemented with 10% FBS and 1% P/S, and filtered through a 0.2 micron membrane. Cells were maintained at 37 °C in a fully humidified atmosphere containing 5% CO_2.

5.2.1.13 HL-1 Cell Culture

HL-1 immortalized adult murine cardiomyocytes (a gift from Dr. Claycomb at Louisiana State University, New Orleans, LA) were cultured in Claycomb medium (Sigma-Aldrich) as suggested.[231] Cells were maintained at 37 °C in a fully humidified atmosphere containing 5% CO_2.

5.2.1.14 NLRP3 Inflammasome Activation and IL-1ß ELISA

J774.A1 cells were plated in ($5x10^4$ cells/well) 96-well plates for 24 h in growth medium. The cells were primed with *Escherichia coli* 0111:B4 lipopolysaccharide (LPS) (25 ng/mL; Sigma-Aldrich) (1 µg/mL) for 4 h. Next, compounds were added at the indicated concentrations for 30 min. Then, ATP (5 mM) was added to induce NLRP3 inflammasome formation, and cells were incubated another 30 min. The supernatants were collected and levels of IL-1ß were measured with a mouse IL-1ß ELISA kit (Thermo Fisher Scientific, Princeton, NJ) following the manufacturer's instructions. Values are expressed as a percentage relative to the positive (+LPS/ATP) control.

In separate experiments, HL-1 cells were plated and primed with LPS (25 ng/mL) for 2 h and then treated with ATP (5 mM) for 1 h. Cells were treated with compounds at the indicated

concentrations during the LPS priming phase, 30 min before ATP addition. The supernatants were collected and levels of IL-1ß were measured as previously described. Values are expressed as a percentage relative to the positive (+LPS/ATP) control.

5.2.1.15 ASC Aggregation Staining

HL-1 cells were plated on 24×24 mm glass covers pretreated with gelatin/plasma human-fibronectin (0.02–0.5%) at 2.5×10^5 in 35-mm dishes 24 h before the experiment. ASC expression was detected as circumscribed cytoplasmic perinuclear aggregates and expressed as ASC-positive cells over the total cells per field. ASC aggregates were quantified blindly by two different investigators.

5.2.1.16 Caspase-1 Activity

HL-1 cells (2×10^6 cells) were plated in 90-mm dishes and NLRP3 inflammasome formation was induced as described above. After treatment, cells were washed, harvested, and frozen. The pellet was then homogenized using RIPA buffer (Sigma-Aldrich) containing a mixture of protease inhibitors (Sigma-Aldrich) and centrifuged at 16,200×g for 20 min. The supernatants were collected and the protein contents were quantified using the Bradford method. The caspase-1 activity was determined by cleavage of CaspACE, a fluorogenic substrate (Promega, Madison, WI). The fluorescence was measured at an excitation wavelength of 360 nm and an absorbance wavelength of 460 nm. Data is reported as arbitrary fluorescence units produced by 1 μg of sample per min (fluorescence/μg/min).

5.2.1.17 Trypan Exclusion Method

HL-1 cells were treated as described above and also with LPS (25 ng/mL) and nigericin (20 μM) (Enzo Life Sciences Inc, Farmingdale, NY). Cells were then harvested, and re-suspended in 1 mL of Claycomb medium. Cells were treated with 100 μL of 0.4% Trypan blue stain (Gibco) and incubated at room temperature for 5 min. Trypan blue positive cells were deemed nonviable, and the percentage of cell death was measured as the ratio of trypan blue positive cells over total cell number per field.

5.2.1.18 NLRC4 and AIM2 Inflammasome Activation

HL-1 cells ($1x10^6$) were plated in 35 mm dishes and treated with flagellin or Poly-deoxyadenylic-deoxythymidylic acid sodium salt (Poly(dA:dT)) to induce NLRC4 and AIM2 inflammasome formation, respectively. Flagellin (0.7 μg/mL) (Enzo Life Sciences, Farmingdale, NY), isolated from *Salmonella typhimurium* strain 14028, was added to Claycomb medium without FBS. In order to induce the NLRC4 inflammasome, cells were first treated with flagellin for 4 h and then treated with LPS (25 ng/mL) for 1 h. In order to induce the AIM2 inflammasome, HL-1 cells were cultured in DMEM (Invitrogen) without FBS, treated with Poly(dA:dT) (4 μg/mL) for 6 h and then treated with LPS (25 ng/mL) for 1 h. Compounds were added at indicated concentrations at the same time as flagellin or Poly(dA:dT). Formation of the AIM2 and NLRC4 inflammasomes was determined and quantified by caspase-1 activity and cell death, as described above.

5.2.2 *In Vivo* Assays

5.2.2.1 BBB Penetration Assay

Ten week old CD1 male mice were purchased from Harlan Laboratories (Frederich, MD). Compound **68** was diluted to a concentration of 15 mg/mL in a solution with 2% DMSO and 10% Cremophor in PBS, and was administered via oral gavage at a final dosage of 50 mg/kg. Two groups of mice (n = 6/group) were used to determine the plasma and brain concentrations of the compound at various time points. Following administration of anesthetic (sodium pentobarbital 150 mg/kg, Sigma-Aldrich, Saint Louis, MO), blood samples were collected from the inferior vena cava to prepare the plasma. Afterward, the right atrium was removed to allow exsanguination, and the left ventricular apex was cannulated with a 24 G needle and perfused with 30 mL of warm (37 °C) heparinized normal saline solution to enable perfusion of all the organs and complete blood washout. The perfused brains were then collected, rapidly washed in normal saline, blot-dried, and frozen in liquid nitrogen. For brain samples, half a brain was weighed and diluted with 1.0 mL of acetonitrile and then homogenized well. For plasma samples, 0.01 mL of plasma was diluted with 0.99 mL of acetonitrile and then mixed well. After mixing, samples were centrifuged at 15,000 rpm, and the supernatant was transferred to a new tube and evaporated to dryness using a spin vacuum. The samples were then reconstituted with an 80:20 solution of 1% acetic acid in acetonitrile: 1% acetic acid in water, and a volume of 0.025 mL was then injected into a LC-MS/MS. The LC/MS/MS method employed positive electrospray ionization (ESI) with a selected reaction monitoring (SRM) mode. Compound **68** was monitored using the following SRM transitions: 381→174, 130, and

159. Chromatographic separation was achieved under gradient conditions using a Waters Acquity® UPLC, with a reversed phase column (Gemini 5 µm C18 110Å, 100 mm x 2.0 mm; 5 µm, Phenomenex Inc., Torrance, CA) with a mobile phase composition of 1% acetic acid in water (mobile phase A) and 1% acetic acid in acetonitrile (mobile phase B). The initial gradient consisted of 30% B for 1 min, 30% to 95% B from 1 to 3 min, hold for 1 min at 95% B, and then equilibrate at 30% B for 2.5 min. The total run time was 6.5 min. Results were processed using Analyst 1.5.2 software. Absolute recovery, precision and accuracy, and matrix effects experiments produced an efficient method to continue sample analysis. Calibration curves were made with freshly prepared samples and calculated using peak area versus concentration with a linear or quadratic regression.

5.2.2.2 Administration of Compound 72 in the Mouse

Compound **72** was dissolved in DMSO (0.05-0.1 mL). In order to determine whether treatment with **72** had any toxic effects *in vivo*, weight, appetite, and behavior were measured after single and repeated administrations intraperitoneally in healthy control mice. Adult male (12-16 weeks old) out-bred Institute of Cancer Research (CD1) mice were supplied by Harlan Laboratories (Charles River, MA). Capillary glucose levels were measured through prick stick of the tail and a point-of-care-testing glucometer. Transthoracic echocardiography (to measure cardiac function) was used after single and repeated injections, over a range of concentrations between 20 to 500 mg/kg (N=4-6 per group). All the experiments were conducted under the guidelines of the "Guide for the care and use of laboratory animals" published by National

Institutes of Health (revised 2011). The study protocol was approved by the Virginia Commonwealth University Institutional Animal Care and Use Committee.

5.2.2.3 Experimental Model of Acute Myocardial Infarction

Experimental acute myocardial infarction (AMI) was induced by transient myocardial ischemia for 30 min followed by reperfusion as described.[232] Briefly, mice were orotracheally intubated under anesthesia (pentobarbital 50 to 70 mg/kg), placed in the right lateral decubitus position, then subjected to left thoracotomy, pericardiectomy, and ligation of the proximal left coronary artery. The ligated coronary artery was released after 30 min before closure of the thorax. Sham operations were performed wherein animals underwent the same surgical procedure without coronary artery ligation (N=6-12 per group). To evaluate the effect of compound **72**, a group of mice were given **72** (100 mg/kg in 0.1 mL), DMSO solution (0.1 mL, vehicle), NaCl 0.9% solution (0.1 mL, control) 30 min prior to surgery, then repeated at time of reperfusion and every 6 h for 3 additional doses. Mice were then sacrificed at 24 h. The hearts were removed and processed for the assessment of caspase-1 in the tissue or infarct size measurement. Caspase-1 activity was measured on frozen hearts as previously described.

5.2.2.4 Infarct Size Measurement

Infarct size was measured using two different methods: using triphenyl tetrazolium chloride (TTC) (Sigma Aldrich) staining of viable myocardium,[232] and measuring serum troponin I levels (Life Diagnostic Inc., West Chester, PA), 24 h after surgery. Briefly, blood was

drawn from the heart and processed for troponin I levels determined by ELISA in the supernatant (following the manufacturer's protocol). The heart was quickly removed after sacrifice and mounted on a Langendorff apparatus. The coronary arteries were perfused with 0.9% NaCl containing 2.5 mM $CaCl_2$. After the blood was washed out, the coronary artery was again ligated, and approximately 2 mL of 1% Evans blue dye (Sigma Aldrich) was injected as a bolus into the aorta until the heart 'not-at-risk' turned blue. The heart was then removed, frozen, and cut into 5 to 7 transverse slices from apex to base of equal thickness (approximately 1 mm). The slices were then incubated in a 1% TTC isotonic phosphate buffer (pH 7.4) at room temperature for 30 min. The infarcted tissue (appearing white), the risk zone (red), and the non-risk zone (blue) were measured by computer morphometry using Image Pro Plus 6.0 software (Media Cybernetics, Silver Spring, MD).

5.2.2.5 Experimental Model of Acute Peritonitis in the Mouse

To determine the effects of **72** in the NLRP3 inflammasome *in vivo*, independent of other potential effects on heart viability or function, mice were injected with 1 mg (0.1 mL) of zymosan A (Sigma-Aldrich) freshly prepared in sterile saline solution (0.9% NaCl) into the peritoneum. After 6 h mice were sacrificed by anesthesia overdose. The peritoneal cavity was immediately washed with 7 mL of cold PBS to recover peritoneal cells. Treatment with **72** or an equal volume of DMSO (vehicle) was administered at different doses (5, 20, and 100 mg/kg in 0.1 mL) 30 min before stimulation with zymosan A to determine the inhibitory effects on leukocyte recruitment in the cavity (N=4-12 per group). In addition to **72**, glyburide (132.5

mg/kg) was used as a positive control. The total number of leukocytes in the peritoneal cavity was measured using a cell-counting Thoma chamber (Thermo Fisher Scientific).

6 Conclusion

Alzheimer's disease is a devastating neurodegenerative disorder and the leading cause of dementia. As of yet, there is no cure, and currently approved treatments only offer symptomatic relief. Utilizing a bivalent design strategy, a series of ligands based on curcumin and diosgenin were synthesized and evaluated for their neuroprotective abilities in MC65 cells. From this series, compounds **8** and **18** were discovered to have neuroprotective ability, antioxidative function, and anti-Aß oligomerization properties, all in the nM range. Interestingly, linker lengths of 17 and 21 atoms imparted the most potent protection, in agreement with previous publications. A hybridization strategy was also followed for the design of a second series of compounds. These ligands combined pharmacophoric features from two natural products known to have neuroprotective properties, curcumin and melatonin. From this series, representative compound **54** and analogs **56** and **68** all conferred neuroprotection to MC65 cells. Lead compound **68** was also shown to have antioxidative function, but interestingly, no strong effects on Aß oligomerization. Mechanistic studies suggest **68** works by disrupting interactions between AßOs and partner proteins in the mitochondria. Compound **68** was also shown to be able to pass the BBB, supporting its further investigation. Lastly, a series of NLRP3 inhibitors were designed based on glyburide, an anti-diabetic medication shown to have some anti-inflammatory activity. Synthesis of this series yielded compound **72**, which was able to successfully inhibit the NLRP3 inflammasome and reduce IL-1ß express without affecting blood glucose. Further studies demonstrated **72**'s ability to reduce adverse inflammation-related outcomes in *in vivo* models of peritonitis and acute myocardial infarction. Compounds **76** and **80** were also shown to prevent IL-1ß release at concentrations similar to **72**. Together, these results warrant further investigations of these analogs in other NLRP3-related pathologies, specifically AD.

References

1. 2013 Alzheimer's disease facts and figures. *Alzheimers Dement* **2013,** 9, 208-45.

2. Alzheimer's Disease Education & Referral Center. Alzheimer's Disease Fact Sheet In Aging, N. I. o., Ed. National Institutes of Health: 2012.

3. Alzheimer, A.; Stelzmann, R. A.; Schnitzlein, H. N.; Murtagh, F. R. An English translation of Alzheimer's 1907 paper, "Uber eine eigenartige Erkankung der Hirnrinde". *Clin Anat* **1995,** 8, 429-31.

4. Khachiyants, N.; Trinkle, D.; Son, S. J.; Kim, K. Y. Sundown syndrome in persons with dementia: an update. *Psychiatry Investig* **2011,** 8, 275-87.

5. Fu, C.; Chute, D. J.; Farag, E. S.; Garakian, J.; Cummings, J. L.; Vinters, H. V. Comorbidity in dementia: an autopsy study. *Arch Pathol Lab Med* **2004,** 128, 32-8.

6. Magaki, S.; Yong, W. H.; Khanlou, N.; Tung, S.; Vinters, H. V. Comorbidity in dementia: update of an ongoing autopsy study. *J Am Geriatr Soc* **2014,** 62, 1722-8.

7. Iqbal, K.; Gong, C. X.; Liu, F. Microtubule-associated protein tau as a therapeutic target in Alzheimer's disease. *Expert Opin Ther Targets* **2014,** 18, 307-18.

8. Nelson, P. T.; Head, E.; Schmitt, F. A.; Davis, P. R.; Neltner, J. H.; Jicha, G. A.; Abner, E. L.; Smith, C. D.; Van Eldik, L. J.; Kryscio, R. J.; Scheff, S. W. Alzheimer's disease is not "brain aging": neuropathological, genetic, and epidemiological human studies. *Acta Neuropathol* **2011,** 121, 571-87.

9. McGeer, P. L.; McGeer, E. G. The amyloid cascade-inflammatory hypothesis of Alzheimer disease: implications for therapy. *Acta Neuropathol* **2013,** 126, 479-97.

10. Foundation, B. F. Amyloid Plaques & Neurofibrillary Tangles. http://www.brightfocus.org/alzheimers/about/understanding/plaques-and-tangles.html (Nov 18).

11. Masters, C. L.; Simms, G.; Weinman, N. A.; Multhaup, G.; McDonald, B. L.; Beyreuther, K. Amyloid plaque core protein in Alzheimer disease and Down syndrome. *Proc Natl Acad Sci U S A* **1985,** 82, 4245-9.

12. Serpell, L. C. Alzheimer's amyloid fibrils: structure and assembly. *Biochim Biophys Acta* **2000,** 1502, 16-30.

13. Yin, Y. I.; Bassit, B.; Zhu, L.; Yang, X.; Wang, C.; Li, Y. M. {gamma}-Secretase Substrate Concentration Modulates the Abeta42/Abeta40 Ratio: IMPLICATIONS FOR ALZHEIMER DISEASE. *J Biol Chem* **2007,** 282, 23639-44.

14. Hartmann, T.; Bieger, S. C.; Bruhl, B.; Tienari, P. J.; Ida, N.; Allsop, D.; Roberts, G. W.; Masters, C. L.; Dotti, C. G.; Unsicker, K.; Beyreuther, K. Distinct sites of intracellular production for Alzheimer's disease A beta40/42 amyloid peptides. *Nat Med* **1997,** 3, 1016-20.

15. Shaw, L. M.; Korecka, M.; Clark, C. M.; Lee, V. M.; Trojanowski, J. Q. Biomarkers of neurodegeneration for diagnosis and monitoring therapeutics. *Nat Rev Drug Discov* **2007,** 6, 295-303.

16. Ghiso, J.; Frangione, B. Amyloidosis and Alzheimer's disease. *Adv Drug Deliv Rev* **2002,** 54, 1539-51.

17. Walsh, D. M.; Selkoe, D. J. A beta oligomers - a decade of discovery. *J Neurochem* **2007,** 101, 1172-84.

18. Greenberg, B. D.; Murphy, M. F. Toward an integrated discovery and development program in Alzheimer's disease: the amyloid hypothesis. *Neurobiol Aging* **1994,** 15 Suppl 2, S105-9.

19. Hardy, J.; Allsop, D. Amyloid deposition as the central event in the aetiology of Alzheimer's disease. *Trends Pharmacol Sci* **1991,** 12, 383-8.

20. Lue, L. F.; Kuo, Y. M.; Roher, A. E.; Brachova, L.; Shen, Y.; Sue, L.; Beach, T.; Kurth, J. H.; Rydel, R. E.; Rogers, J. Soluble amyloid beta peptide concentration as a predictor of synaptic change in Alzheimer's disease. *Am J Pathol* **1999,** 155, 853-62.

21. McLean, C. A.; Cherny, R. A.; Fraser, F. W.; Fuller, S. J.; Smith, M. J.; Beyreuther, K.; Bush, A. I.; Masters, C. L. Soluble pool of Abeta amyloid as a determinant of severity of neurodegeneration in Alzheimer's disease. *Ann Neurol* **1999,** 46, 860-6.

22. Deshpande, A.; Mina, E.; Glabe, C.; Busciglio, J. Different conformations of amyloid beta induce neurotoxicity by distinct mechanisms in human cortical neurons. *J Neurosci* **2006,** 26, 6011-8.

23. Hoshi, M.; Sato, M.; Matsumoto, S.; Noguchi, A.; Yasutake, K.; Yoshida, N.; Sato, K. Spherical aggregates of beta-amyloid (amylospheroid) show high neurotoxicity and activate tau protein kinase I/glycogen synthase kinase-3beta. *Proc Natl Acad Sci U S A* **2003,** 100, 6370-5.

24. Whalen, B. M.; Selkoe, D. J.; Hartley, D. M. Small non-fibrillar assemblies of amyloid beta-protein bearing the Arctic mutation induce rapid neuritic degeneration. *Neurobiol Dis* **2005,** 20, 254-66.

25. Kayed, R.; Head, E.; Thompson, J. L.; McIntire, T. M.; Milton, S. C.; Cotman, C. W.; Glabe, C. G. Common structure of soluble amyloid oligomers implies common mechanism of pathogenesis. *Science* **2003,** 300, 486-9.

26. Lesne, S. E.; Sherman, M. A.; Grant, M.; Kuskowski, M.; Schneider, J. A.; Bennett, D. A.; Ashe, K. H. Brain amyloid-beta oligomers in ageing and Alzheimer's disease. *Brain* **2013,** 136, 1383-98.

27. Benilova, I.; Karran, E.; De Strooper, B. The toxic Abeta oligomer and Alzheimer's disease: an emperor in need of clothes. *Nat Neurosci* **2012,** 15, 349-57.

28. Larson, M. E.; Lesne, S. E. Soluble Abeta oligomer production and toxicity. *J Neurochem* **2012,** 120 Suppl 1, 125-39.

29. Walsh, D. M.; Tseng, B. P.; Rydel, R. E.; Podlisny, M. B.; Selkoe, D. J. The oligomerization of amyloid beta-protein begins intracellularly in cells derived from human brain. *Biochemistry* **2000,** 39, 10831-9.

30. Klein, W. L. Synaptotoxic amyloid-beta oligomers: a molecular basis for the cause, diagnosis, and treatment of Alzheimer's disease? *J Alzheimers Dis* **2013,** 33 Suppl 1, S49-65.

31. Cordy, J. M.; Hooper, N. M.; Turner, A. J. The involvement of lipid rafts in Alzheimer's disease. *Mol Membr Biol* **2006,** 23, 111-22.

32. Kim, S. I.; Yi, J. S.; Ko, Y. G. Amyloid beta oligomerization is induced by brain lipid rafts. *J Cell Biochem* **2006,** 99, 878-89.

33. Watt, N. T.; Griffiths, H. H.; Hooper, N. M. Lipid rafts: linking prion protein to zinc transport and amyloid-beta toxicity in Alzheimer's disease. *Front Cell Dev Biol* **2014,** 2, 41.

34. Petersen, R. B.; Nunomura, A.; Lee, H. G.; Casadesus, G.; Perry, G.; Smith, M. A.; Zhu, X. Signal transduction cascades associated with oxidative stress in Alzheimer's disease. *J Alzheimers Dis* **2007,** 11, 143-52.

35. Choo-Smith, L. P.; Garzon-Rodriguez, W.; Glabe, C. G.; Surewicz, W. K. Acceleration of amyloid fibril formation by specific binding of Abeta-(1-40) peptide to ganglioside-containing membrane vesicles. *J Biol Chem* **1997,** 272, 22987-90.

36. Vetrivel, K. S.; Cheng, H.; Lin, W.; Sakurai, T.; Li, T.; Nukina, N.; Wong, P. C.; Xu, H.; Thinakaran, G. Association of gamma-secretase with lipid rafts in post-Golgi and endosome membranes. *J Biol Chem* **2004,** 279, 44945-54.

37. Lee, S. J.; Liyanage, U.; Bickel, P. E.; Xia, W.; Lansbury, P. T., Jr.; Kosik, K. S. A detergent-insoluble membrane compartment contains A beta in vivo. *Nat Med* **1998,** 4, 730-4.

38. Oda, A.; Tamaoka, A.; Araki, W. Oxidative stress up-regulates presenilin 1 in lipid rafts in neuronal cells. *J Neurosci Res* **2010,** 88, 1137-45.

39. Ariga, T.; McDonald, M. P.; Yu, R. K. Role of ganglioside metabolism in the pathogenesis of Alzheimer's disease--a review. *J Lipid Res* **2008,** 49, 1157-75.

40. Wakabayashi, M.; Okada, T.; Kozutsumi, Y.; Matsuzaki, K. GM1 ganglioside-mediated accumulation of amyloid beta-protein on cell membranes. *Biochem Biophys Res Commun* **2005,** 328, 1019-23.

41. Atwood, C. S.; Moir, R. D.; Huang, X.; Scarpa, R. C.; Bacarra, N. M.; Romano, D. M.; Hartshorn, M. A.; Tanzi, R. E.; Bush, A. I. Dramatic aggregation of Alzheimer abeta by Cu(II) is induced by conditions representing physiological acidosis. *J Biol Chem* **1998,** 273, 12817-26.

42. Liu, L.; Zhang, K.; Tan, L.; Chen, Y. H.; Cao, Y. P. Alterations in Cholesterol and Ganglioside GM1 Content of Lipid Rafts in Platelets From Patients With Alzheimer Disease. *Alzheimer Dis Assoc Disord* **2014**.

43. Harada, A.; Oguchi, K.; Okabe, S.; Kuno, J.; Terada, S.; Ohshima, T.; Sato-Yoshitake, R.; Takei, Y.; Noda, T.; Hirokawa, N. Altered microtubule organization in small-calibre axons of mice lacking tau protein. *Nature* **1994,** 369, 488-91.

44. Avila, J.; Lucas, J. J.; Perez, M.; Hernandez, F. Role of tau protein in both physiological and pathological conditions. *Physiol Rev* **2004,** 84, 361-84.

45. Grundke-Iqbal, I.; Iqbal, K.; Quinlan, M.; Tung, Y. C.; Zaidi, M. S.; Wisniewski, H. M. Microtubule-associated protein tau. A component of Alzheimer paired helical filaments. *J Biol Chem* **1986,** 261, 6084-9.

46. Grundke-Iqbal, I.; Iqbal, K.; Tung, Y. C.; Quinlan, M.; Wisniewski, H. M.; Binder, L. I. Abnormal phosphorylation of the microtubule-associated protein tau (tau) in Alzheimer cytoskeletal pathology. *Proc Natl Acad Sci U S A* **1986,** 83, 4913-7.

47. Bennecib, M.; Gong, C. X.; Grundke-Iqbal, I.; Iqbal, K. Role of protein phosphatase-2A and -1 in the regulation of GSK-3, cdk5 and cdc2 and the phosphorylation of tau in rat forebrain. *FEBS Lett* **2000,** 485, 87-93.

48. Gong, C. X.; Lidsky, T.; Wegiel, J.; Zuck, L.; Grundke-Iqbal, I.; Iqbal, K. Phosphorylation of microtubule-associated protein tau is regulated by protein phosphatase 2A in mammalian brain. Implications for neurofibrillary degeneration in Alzheimer's disease. *J Biol Chem* **2000,** 275, 5535-44.

49. Perrin, R. J.; Fagan, A. M.; Holtzman, D. M. Multimodal techniques for diagnosis and prognosis of Alzheimer's disease. *Nature* **2009,** 461, 916-22.

50. Bloom, G. S.; Ren, K.; Glabe, C. G. Cultured cell and transgenic mouse models for tau pathology linked to beta-amyloid. *Biochim Biophys Acta* **2005,** 1739, 116-24.

51. King, M. E.; Kan, H. M.; Baas, P. W.; Erisir, A.; Glabe, C. G.; Bloom, G. S. Tau-dependent microtubule disassembly initiated by prefibrillar beta-amyloid. *J Cell Biol* **2006,** 175, 541-6.

52. Kertesz, A. Frontotemporal dementia, Pick's disease. *Ideggyogy Sz* **2010,** 63, 4-12.

53. Schneider, A.; Mandelkow, E. Tau-based treatment strategies in neurodegenerative diseases. *Neurotherapeutics* **2008,** 5, 443-57.

54. Sahara, N.; Maeda, S.; Takashima, A. Tau oligomerization: a role for tau aggregation intermediates linked to neurodegeneration. *Curr Alzheimer Res* **2008,** 5, 591-8.

55. Gandy, S.; Ikonomovic, M. D.; Mitsis, E.; Elder, G.; Ahlers, S. T.; Barth, J.; Stone, J. R.; DeKosky, S. T. Chronic traumatic encephalopathy: clinical-biomarker correlations and current concepts in pathogenesis. *Mol Neurodegener* **2014,** 9, 37.

56. Hoyer, S. Intermediary metabolism disturbance in AD/SDAT and its relation to molecular events. *Prog Neuropsychopharmacol Biol Psychiatry* **1993,** 17, 199-228.

57. Minoshima, S.; Giordani, B.; Berent, S.; Frey, K. A.; Foster, N. L.; Kuhl, D. E. Metabolic reduction in the posterior cingulate cortex in very early Alzheimer's disease. *Ann Neurol* **1997,** 42, 85-94.

58. Fukuyama, H.; Ogawa, M.; Yamauchi, H.; Yamaguchi, S.; Kimura, J.; Yonekura, Y.; Konishi, J. Altered cerebral energy metabolism in Alzheimer's disease: a PET study. *J Nucl Med* **1994,** 35, 1-6.

59. Blass, J. P. The mitochondrial spiral. An adequate cause of dementia in the Alzheimer's syndrome. *Ann N Y Acad Sci* **2000,** 924, 170-83.

60. Castellani, R.; Hirai, K.; Aliev, G.; Drew, K. L.; Nunomura, A.; Takeda, A.; Cash, A. D.; Obrenovich, M. E.; Perry, G.; Smith, M. A. Role of mitochondrial dysfunction in Alzheimer's disease. *J Neurosci Res* **2002,** 70, 357-60.

61. Wang, X.; Wang, W.; Li, L.; Perry, G.; Lee, H. G.; Zhu, X. Oxidative stress and mitochondrial dysfunction in Alzheimer's disease. *Biochim Biophys Acta* **2014,** 1842, 1240-7.

62. Gibson, G. E.; Sheu, K. F.; Blass, J. P. Abnormalities of mitochondrial enzymes in Alzheimer disease. *J Neural Transm* **1998,** 105, 855-70.

63. Maurer, I.; Zierz, S.; Moller, H. J. A selective defect of cytochrome c oxidase is present in brain of Alzheimer disease patients. *Neurobiol Aging* **2000,** 21, 455-62.

64. Cottrell, D. A.; Blakely, E. L.; Johnson, M. A.; Ince, P. G.; Turnbull, D. M. Mitochondrial enzyme-deficient hippocampal neurons and choroidal cells in AD. *Neurology* **2001,** 57, 260-4.

65. Marcus, D. L.; Strafaci, J. A.; Freedman, M. L. Differential neuronal expression of manganese superoxide dismutase in Alzheimer's disease. *Med Sci Monit* **2006,** 12, Br8-14.

66. De Leo, M. E.; Borrello, S.; Passantino, M.; Palazzotti, B.; Mordente, A.; Daniele, A.; Filippini, V.; Galeotti, T.; Masullo, C. Oxidative stress and overexpression of manganese superoxide dismutase in patients with Alzheimer's disease. *Neurosci Lett* **1998,** 250, 173-6.

67. Perrin, R.; Briancon, S.; Jeandel, C.; Artur, Y.; Minn, A.; Penin, F.; Siest, G. Blood activity of Cu/Zn superoxide dismutase, glutathione peroxidase and catalase in Alzheimer's disease: a case-control study. *Gerontology* **1990,** 36, 306-13.

68. Manczak, M.; Anekonda, T. S.; Henson, E.; Park, B. S.; Quinn, J.; Reddy, P. H. Mitochondria are a direct site of A beta accumulation in Alzheimer's disease neurons: implications for free radical generation and oxidative damage in disease progression. *Hum Mol Genet* **2006,** 15, 1437-49.

69. Lustbader, J. W.; Cirilli, M.; Lin, C.; Xu, H. W.; Takuma, K.; Wang, N.; Caspersen, C.; Chen, X.; Pollak, S.; Chaney, M.; Trinchese, F.; Liu, S.; Gunn-Moore, F.; Lue, L. F.; Walker, D. G.; Kuppusamy, P.; Zewier, Z. L.; Arancio, O.; Stern, D.; Yan, S. S.; Wu, H. ABAD directly links Abeta to mitochondrial toxicity in Alzheimer's disease. *Science* **2004,** 304, 448-52.

70. Devi, L.; Prabhu, B. M.; Galati, D. F.; Avadhani, N. G.; Anandatheerthavarada, H. K. Accumulation of amyloid precursor protein in the mitochondrial import channels of human Alzheimer's disease brain is associated with mitochondrial dysfunction. *J Neurosci* **2006,** 26, 9057-68.

71. Behl, C.; Davis, J. B.; Lesley, R.; Schubert, D. Hydrogen peroxide mediates amyloid beta protein toxicity. *Cell* **1994,** 77, 817-27.

72. Greenough, M. A.; Camakaris, J.; Bush, A. I. Metal dyshomeostasis and oxidative stress in Alzheimer's disease. *Neurochem Int* **2013,** 62, 540-55.

73. Myhre, O.; Utkilen, H.; Duale, N.; Brunborg, G.; Hofer, T. Metal dyshomeostasis and inflammation in Alzheimer's and Parkinson's diseases: possible impact of environmental exposures. *Oxid Med Cell Longev* **2013,** 2013, 726954.

74. Lovell, M. A.; Robertson, J. D.; Teesdale, W. J.; Campbell, J. L.; Markesbery, W. R. Copper, iron and zinc in Alzheimer's disease senile plaques. *J Neurol Sci* **1998,** 158, 47-52.

75. Huang, X.; Cuajungco, M. P.; Atwood, C. S.; Hartshorn, M. A.; Tyndall, J. D.; Hanson, G. R.; Stokes, K. C.; Leopold, M.; Multhaup, G.; Goldstein, L. E.; Scarpa, R. C.; Saunders, A. J.; Lim, J.; Moir, R. D.; Glabe, C.; Bowden, E. F.; Masters, C. L.; Fairlie, D. P.; Tanzi, R. E.; Bush, A. I. Cu(II) potentiation of alzheimer abeta neurotoxicity. Correlation with cell-free hydrogen peroxide production and metal reduction. *J Biol Chem* **1999,** 274, 37111-6.

76. Hu, W. P.; Chang, G. L.; Chen, S. J.; Kuo, Y. M. Kinetic analysis of beta-amyloid peptide aggregation induced by metal ions based on surface plasmon resonance biosensing. *J Neurosci Methods* **2006,** 154, 190-7.

77. Rottkamp, C. A.; Raina, A. K.; Zhu, X.; Gaier, E.; Bush, A. I.; Atwood, C. S.; Chevion, M.; Perry, G.; Smith, M. A. Redox-active iron mediates amyloid-beta toxicity. *Free Radic Biol Med* **2001,** 30, 447-50.

78. Qian, L.; Flood, P. M.; Hong, J. S. Neuroinflammation is a key player in Parkinson's disease and a prime target for therapy. *J Neural Transm* **2010,** 117, 971-9.

79. Akiyama, H.; Barger, S.; Barnum, S.; Bradt, B.; Bauer, J.; Cole, G. M.; Cooper, N. R.; Eikelenboom, P.; Emmerling, M.; Fiebich, B. L.; Finch, C. E.; Frautschy, S.; Griffin, W. S.; Hampel, H.; Hull, M.; Landreth, G.; Lue, L.; Mrak, R.; Mackenzie, I. R.; McGeer, P. L.; O'Banion, M. K.; Pachter, J.; Pasinetti, G.; Plata-Salaman, C.; Rogers, J.; Rydel, R.; Shen, Y.; Streit, W.; Strohmeyer, R.; Tooyoma, I.; Van Muiswinkel, F. L.; Veerhuis, R.; Walker, D.; Webster, S.; Wegrzyniak, B.; Wenk, G.; Wyss-Coray, T. Inflammation and Alzheimer's disease. *Neurobiol Aging* **2000,** 21, 383-421.

80. Betmouni, S.; Perry, V. H.; Gordon, J. L. Evidence for an early inflammatory response in the central nervous system of mice with scrapie. *Neuroscience* **1996,** 74, 1-5.

81. Shie, F. S.; Woltjer, R. L. Manipulation of microglial activation as a therapeutic strategy in Alzheimer's disease. *Curr Med Chem* **2007,** 14, 2865-71.

82. Bonifati, D. M.; Kishore, U. Role of complement in neurodegeneration and neuroinflammation. *Mol Immunol* **2007,** 44, 999-1010.

83. Stewart, W. F.; Kawas, C.; Corrada, M.; Metter, E. J. Risk of Alzheimer's disease and duration of NSAID use. *Neurology* **1997,** 48, 626-32.

84. Leoutsakos, J. M.; Muthen, B. O.; Breitner, J. C.; Lyketsos, C. G. Effects of non-steroidal anti-inflammatory drug treatments on cognitive decline vary by phase of pre-clinical Alzheimer disease: findings from the randomized controlled Alzheimer's Disease Anti-inflammatory Prevention Trial. *Int J Geriatr Psychiatry* **2012,** 27, 364-74.

85. Jaturapatporn, D.; Isaac, M. G.; McCleery, J.; Tabet, N. Aspirin, steroidal and non-steroidal anti-inflammatory drugs for the treatment of Alzheimer's disease. *Cochrane Database Syst Rev* **2012,** 2, Cd006378.

86. Butterfield, D. A.; Griffin, S.; Munch, G.; Pasinetti, G. M. Amyloid beta-peptide and amyloid pathology are central to the oxidative stress and inflammatory cascades under which Alzheimer's disease brain exists. *J Alzheimers Dis* **2002,** 4, 193-201.

87. Kuznetsova, E.; Schliebs, R. beta-Amyloid, cholinergic transmission, and cerebrovascular system -- a developmental study in a mouse model of Alzheimer's disease. *Curr Pharm Des* **2013,** 19, 6749-65.

88. Pakaski, M.; Kalman, J. Interactions between the amyloid and cholinergic mechanisms in Alzheimer's disease. *Neurochem Int* **2008,** 53, 103-11.

89. Snyder, P. J.; Lim, Y. Y.; Schindler, R.; Ott, B. R.; Salloway, S.; Daiello, L.; Getter, C.; Gordon, C. M.; Maruff, P. Microdosing of scopolamine as a "cognitive stress test": rationale and test of a very low dose in an at-risk cohort of older adults. *Alzheimers Dement* **2014,** 10, 262-7.

90. Hardenacke, K.; Kuhn, J.; Lenartz, D.; Maarouf, M.; Mai, J. K.; Bartsch, C.; Freund, H. J.; Sturm, V. Stimulate or degenerate: deep brain stimulation of the nucleus basalis Meynert in Alzheimer dementia. *World Neurosurg* **2013,** 80, S27.e35-43.

91. Whitehouse, P. J.; Price, D. L.; Struble, R. G.; Clark, A. W.; Coyle, J. T.; Delon, M. R. Alzheimer's disease and senile dementia: loss of neurons in the basal forebrain. *Science* **1982,** 215, 1237-9.

92. Summers, W. K.; Tachiki, K. H.; Kling, A. Tacrine in the treatment of Alzheimer's disease. A clinical update and recent pharmacologic studies. *Eur Neurol* **1989,** 29 Suppl 3, 28-32.

93. Mayeux, R.; Sano, M. Treatment of Alzheimer's disease. *N Engl J Med* **1999,** 341, 1670-9.

94. Di Santo, S. G.; Prinelli, F.; Adorni, F.; Caltagirone, C.; Musicco, M. A meta-analysis of the efficacy of donepezil, rivastigmine, galantamine, and memantine in relation to severity of Alzheimer's disease. *J Alzheimers Dis* **2013,** 35, 349-61.

95. Anand, P.; Singh, B. A review on cholinesterase inhibitors for Alzheimer's disease. *Arch Pharm Res* **2013,** 36, 375-99.

96. Li, F.; Tsien, J. Z. Memory and the NMDA receptors. *N Engl J Med* **2009,** 361, 302-3.

97. Parsons, C. G.; Danysz, W.; Dekundy, A.; Pulte, I. Memantine and cholinesterase inhibitors: complementary mechanisms in the treatment of Alzheimer's disease. *Neurotox Res* **2013,** 24, 358-69.

98. Tsien, J. Z. Building a brainier mouse. *Sci Am* **2000,** 282, 62-8.

99. Kleckner, N. W.; Dingledine, R. Requirement for glycine in activation of NMDA-receptors expressed in Xenopus oocytes. *Science* **1988,** 241, 835-7.

100. Shah, R. S.; Lee, H. G.; Xiongwei, Z.; Perry, G.; Smith, M. A.; Castellani, R. J. Current approaches in the treatment of Alzheimer's disease. *Biomed Pharmacother* **2008,** 62, 199-207.

101. Dysken, M. W.; Guarino, P. D.; Vertrees, J. E.; Asthana, S.; Sano, M.; Llorente, M.; Pallaki, M.; Love, S.; Schellenberg, G. D.; McCarten, J. R.; Malphurs, J.; Prieto, S.; Chen, P.; Loreck, D. J.; Carney, S.; Trapp, G.; Bakshi, R. S.; Mintzer, J. E.; Heidebrink, J. L.; Vidal-Cardona, A.; Arroyo, L. M.; Cruz, A. R.; Kowall, N. W.; Chopra, M. P.; Craft, S.; Thielke, S.; Turvey, C. L.; Woodman, C.; Monnell, K. A.; Gordon, K.; Tomaska, J.; Vatassery, G. Vitamin E and memantine in Alzheimer's disease: clinical trial methods and baseline data. *Alzheimers Dement* **2014,** 10, 36-44.

102. Nakamura, Y.; Kitamura, S.; Homma, A.; Shiosakai, K.; Matsui, D. Efficacy and safety of memantine in patients with moderate-to-severe Alzheimer's disease: results of a pooled analysis of two randomized, double-blind, placebo-controlled trials in Japan. *Expert Opin Pharmacother* **2014,** 15, 913-25.

103. Zhu, C. W.; Livote, E. E.; Scarmeas, N.; Albert, M.; Brandt, J.; Blacker, D.; Sano, M.; Stern, Y. Long-term associations between cholinesterase inhibitors and memantine use and health outcomes among patients with Alzheimer's disease. *Alzheimers Dement* **2013,** 9, 733-40.

104. Reisberg, B.; Doody, R.; Stoffler, A.; Schmitt, F.; Ferris, S.; Mobius, H. J. Memantine in moderate-to-severe Alzheimer's disease. *N Engl J Med* **2003,** 348, 1333-41.

105. van Dyck, C. H.; Tariot, P. N.; Meyers, B.; Malca Resnick, E. A 24-week randomized, controlled trial of memantine in patients with moderate-to-severe Alzheimer disease. *Alzheimer Dis Assoc Disord* **2007,** 21, 136-43.

106. Tariot, P. N.; Farlow, M. R.; Grossberg, G. T.; Graham, S. M.; McDonald, S.; Gergel, I. Memantine treatment in patients with moderate to severe Alzheimer disease already receiving donepezil: a randomized controlled trial. *Jama* **2004,** 291, 317-24.

107. Allain, H.; Bentue-Ferrer, D.; Tribut, O.; Gauthier, S.; Michel, B. F.; Drieu-La Rochelle, C. Alzheimer's disease: the pharmacological pathway. *Fundam Clin Pharmacol* **2003,** 17, 419-28.

108. Schenk, D.; Barbour, R.; Dunn, W.; Gordon, G.; Grajeda, H.; Guido, T.; Hu, K.; Huang, J.; Johnson-Wood, K.; Khan, K.; Kholodenko, D.; Lee, M.; Liao, Z.; Lieberburg, I.; Motter, R.; Mutter, L.; Soriano, F.; Shopp, G.; Vasquez, N.; Vandevert, C.; Walker, S.; Wogulis, M.; Yednock, T.; Games, D.; Seubert, P. Immunization with amyloid-beta attenuates Alzheimer-disease-like pathology in the PDAPP mouse. *Nature* **1999,** 400, 173-7.

109. Holmes, C.; Boche, D.; Wilkinson, D.; Yadegarfar, G.; Hopkins, V.; Bayer, A.; Jones, R. W.; Bullock, R.; Love, S.; Neal, J. W.; Zotova, E.; Nicoll, J. A. Long-term effects of Abeta42 immunisation in Alzheimer's disease: follow-up of a randomised, placebo-controlled phase I trial. *Lancet* **2008,** 372, 216-23.

110. Doody, R. S.; Thomas, R. G.; Farlow, M.; Iwatsubo, T.; Vellas, B.; Joffe, S.; Kieburtz, K.; Raman, R.; Sun, X.; Aisen, P. S.; Siemers, E.; Liu-Seifert, H.; Mohs, R. Phase 3 Trials of Solanezumab for Mild-to-Moderate Alzheimer's Disease. *New England Journal of Medicine* **2014,** 370, 311-321.

111. Salloway, S.; Sperling, R.; Fox, N. C.; Blennow, K.; Klunk, W.; Raskind, M.; Sabbagh, M.; Honig, L. S.; Porsteinsson, A. P.; Ferris, S.; Reichert, M.; Ketter, N.; Nejadnik, B.; Guenzler, V.; Miloslavsky, M.; Wang, D.; Lu, Y.; Lull, J.; Tudor, I. C.; Liu, E.; Grundman, M.; Yuen, E.; Black, R.;

Brashear, H. R. Two Phase 3 Trials of Bapineuzumab in Mild-to-Moderate Alzheimer's Disease. *New England Journal of Medicine* **2014,** 370, 322-333.

112. Single Ascending Dose Study of BIIB037 in Participants With Alzheimer's Disease. In.

113. Multiple Dose Study of BIIB037 (Recombinant, Fully Human Anti-Aβ IgG1 mAb) in Participants With Prodromal or Mild Alzheimer's Disease. In.

114. Lannfelt, L.; Moller, C.; Basun, H.; Osswald, G.; Sehlin, D.; Satlin, A.; Logovinsky, V.; Gellerfors, P. Perspectives on future Alzheimer therapies: amyloid-beta protofibrils - a new target for immunotherapy with BAN2401 in Alzheimer's disease. *Alzheimers Res Ther* **2014,** 6, 16.

115. Panza, F.; Solfrizzi, V.; Imbimbo, B. P.; Giannini, M.; Santamato, A.; Seripa, D.; Logroscino, G. Efficacy and safety studies of gantenerumab in patients with Alzheimer's disease. *Expert Rev Neurother* **2014,** 14, 973-86.

116. Roberds, S. L.; Anderson, J.; Basi, G.; Bienkowski, M. J.; Branstetter, D. G.; Chen, K. S.; Freedman, S. B.; Frigon, N. L.; Games, D.; Hu, K.; Johnson-Wood, K.; Kappenman, K. E.; Kawabe, T. T.; Kola, I.; Kuehn, R.; Lee, M.; Liu, W.; Motter, R.; Nichols, N. F.; Power, M.; Robertson, D. W.; Schenk, D.; Schoor, M.; Shopp, G. M.; Shuck, M. E.; Sinha, S.; Svensson, K. A.; Tatsuno, G.; Tintrup, H.; Wijsman, J.; Wright, S.; McConlogue, L. BACE knockout mice are healthy despite lacking the primary beta-secretase activity in brain: implications for Alzheimer's disease therapeutics. *Hum Mol Genet* **2001,** 10, 1317-24.

117. Ghosh, A. K.; Kumaragurubaran, N.; Hong, L.; Koelsh, G.; Tang, J. Memapsin 2 (beta-secretase) inhibitors: drug development. *Curr Alzheimer Res* **2008,** 5, 121-31.

118. A Safety Study of LY2811376 Single Doses in Healthy Subjects. In.

119. Study of LY2886721 in Mild Cognitive Impairment Due to Alzheimer's Disease or Mild Alzheimer's Disease. In.

120. An Efficacy and Safety Trial of MK-8931 in Mild to Moderate Alzheimer's Disease (P07738). In.

121. Imbimbo, B. P. Therapeutic potential of gamma-secretase inhibitors and modulators. *Curr Top Med Chem* **2008,** 8, 54-61.

122. Barten, D. M.; Meredith, J. E., Jr.; Zaczek, R.; Houston, J. G.; Albright, C. F. Gamma-secretase inhibitors for Alzheimer's disease: balancing efficacy and toxicity. *Drugs R D* **2006,** 7, 87-97.

123. Milano, J.; McKay, J.; Dagenais, C.; Foster-Brown, L.; Pognan, F.; Gadient, R.; Jacobs, R. T.; Zacco, A.; Greenberg, B.; Ciaccio, P. J. Modulation of notch processing by gamma-secretase inhibitors causes intestinal goblet cell metaplasia and induction of genes known to specify gut secretory lineage differentiation. *Toxicol Sci* **2004,** 82, 341-58.

124. Radke, A. L.; Reynolds, L. E.; Melo, R. C.; Dvorak, A. M.; Weller, P. F.; Spencer, L. A. Mature human eosinophils express functional Notch ligands mediating eosinophil autocrine regulation. *Blood* **2009,** 113, 3092-101.

125. van Es, J. H.; van Gijn, M. E.; Riccio, O.; van den Born, M.; Vooijs, M.; Begthel, H.; Cozijnsen, M.; Robine, S.; Winton, D. J.; Radtke, F.; Clevers, H. Notch/gamma-secretase inhibition turns proliferative cells in intestinal crypts and adenomas into goblet cells. *Nature* **2005,** 435, 959-63.

126. Wong, G. T.; Manfra, D.; Poulet, F. M.; Zhang, Q.; Josien, H.; Bara, T.; Engstrom, L.; Pinzon-Ortiz, M.; Fine, J. S.; Lee, H. J.; Zhang, L.; Higgins, G. A.; Parker, E. M. Chronic treatment with the gamma-secretase inhibitor LY-411,575 inhibits beta-amyloid peptide production and alters lymphopoiesis and intestinal cell differentiation. *J Biol Chem* **2004,** 279, 12876-82.

127. Coric, V.; van Dyck, C. H.; Salloway, S.; et al. Safety and tolerability of the γ-secretase inhibitor avagacestat in a phase 2 study of mild to moderate alzheimer disease. *Archives of Neurology* **2012,** 69, 1430-1440.

128. Doody, R. S.; Raman, R.; Farlow, M.; Iwatsubo, T.; Vellas, B.; Joffe, S.; Kieburtz, K.; He, F.; Sun, X.; Thomas, R. G.; Aisen, P. S.; Siemers, E.; Sethuraman, G.; Mohs, R. A phase 3 trial of semagacestat for treatment of Alzheimer's disease. *N Engl J Med* **2013,** 369, 341-50.

129. Arvanitakis, Z.; Grodstein, F.; Bienias, J. L.; Schneider, J. A.; Wilson, R. S.; Kelly, J. F.; Evans, D. A.; Bennett, D. A. Relation of NSAIDs to incident AD, change in cognitive function, and AD pathology. *Neurology* **2008,** 70, 2219-25.

130. Beeri, M. S.; Schmeidler, J.; Lesser, G. T.; Maroukian, M.; West, R.; Leung, S.; Wysocki, M.; Perl, D. P.; Purohit, D. P.; Haroutunian, V. Corticosteroids, but not NSAIDs, are associated with less Alzheimer neuropathology. *Neurobiol Aging* **2012,** 33, 1258-64.

131. Hoozemans, J. J.; Veerhuis, R.; Rozemuller, J. M.; Eikelenboom, P. Soothing the inflamed brain: effect of non-steroidal anti-inflammatory drugs on Alzheimer's disease pathology. *CNS Neurol Disord Drug Targets* **2011,** 10, 57-67.

132. Cole, G. M.; Frautschy, S. A. Mechanisms of action of non-steroidal anti-inflammatory drugs for the prevention of Alzheimer's disease. *CNS Neurol Disord Drug Targets* **2010,** 9, 140-8.

133. Martinon, F.; Burns, K.; Tschopp, J. The inflammasome: a molecular platform triggering activation of inflammatory caspases and processing of proIL-beta. *Mol Cell* **2002,** 10, 417-26.

134. Pedra, J. H.; Cassel, S. L.; Sutterwala, F. S. Sensing pathogens and danger signals by the inflammasome. *Curr Opin Immunol* **2009,** 21, 10-6.

135. Martinon, F.; Mayor, A.; Tschopp, J. The inflammasomes: guardians of the body. *Annu Rev Immunol* **2009,** 27, 229-65.

136. Aachoui, Y.; Sagulenko, V.; Miao, E. A.; Stacey, K. J. Inflammasome-mediated pyroptotic and apoptotic cell death, and defense against infection. *Curr Opin Microbiol* **2013,** 16, 319-26.

137. Kigerl, K. A.; de Rivero Vaccari, J. P.; Dietrich, W. D.; Popovich, P. G.; Keane, R. W. Pattern recognition receptors and central nervous system repair. *Exp Neurol* **2014,** 258, 5-16.

138. Bauernfeind, F.; Ablasser, A.; Bartok, E.; Kim, S.; Schmid-Burgk, J.; Cavlar, T.; Hornung, V. Inflammasomes: current understanding and open questions. *Cell Mol Life Sci* **2011,** 68, 765-83.

139. Leemans, J. C.; Cassel, S. L.; Sutterwala, F. S. Sensing damage by the NLRP3 inflammasome. *Immunol Rev* **2011,** 243, 152-62.

140. Boyden, E. D.; Dietrich, W. F. Nalp1b controls mouse macrophage susceptibility to anthrax lethal toxin. *Nat Genet* **2006,** 38, 240-4.

141. Mariathasan, S.; Newton, K.; Monack, D. M.; Vucic, D.; French, D. M.; Lee, W. P.; Roose-Girma, M.; Erickson, S.; Dixit, V. M. Differential activation of the inflammasome by caspase-1 adaptors ASC and Ipaf. *Nature* **2004,** 430, 213-8.

142. Sutterwala, F. S.; Mijares, L. A.; Li, L.; Ogura, Y.; Kazmierczak, B. I.; Flavell, R. A. Immune recognition of Pseudomonas aeruginosa mediated by the IPAF/NLRC4 inflammasome. *J Exp Med* **2007,** 204, 3235-45.

143. Hornung, V.; Ablasser, A.; Charrel-Dennis, M.; Bauernfeind, F.; Horvath, G.; Caffrey, D. R.; Latz, E.; Fitzgerald, K. A. AIM2 recognizes cytosolic dsDNA and forms a caspase-1-activating inflammasome with ASC. *Nature* **2009,** 458, 514-8.

144. Fernandes-Alnemri, T.; Yu, J. W.; Datta, P.; Wu, J.; Alnemri, E. S. AIM2 activates the inflammasome and cell death in response to cytoplasmic DNA. *Nature* **2009,** 458, 509-13.

145. Bauernfeind, F. G.; Horvath, G.; Stutz, A.; Alnemri, E. S.; MacDonald, K.; Speert, D.; Fernandes-Alnemri, T.; Wu, J.; Monks, B. G.; Fitzgerald, K. A.; Hornung, V.; Latz, E. Cutting edge: NF-kappaB activating pattern recognition and cytokine receptors license NLRP3 inflammasome activation by regulating NLRP3 expression. *J Immunol* **2009,** 183, 787-91.

146. Allen, I. C.; Scull, M. A.; Moore, C. B.; Holl, E. K.; McElvania-TeKippe, E.; Taxman, D. J.; Guthrie, E. H.; Pickles, R. J.; Ting, J. P. The NLRP3 inflammasome mediates in vivo innate immunity to influenza A virus through recognition of viral RNA. *Immunity* **2009,** 30, 556-65.

147. Lechtenberg, B. C.; Mace, P. D.; Riedl, S. J. Structural mechanisms in NLR inflammasome signaling. *Curr Opin Struct Biol* **2014,** 29c, 17-25.

148. Cheng, J.; Waite, A. L.; Tkaczyk, E. R.; Ke, K.; Richards, N.; Hunt, A. J.; Gumucio, D. L. Kinetic properties of ASC protein aggregation in epithelial cells. *J Cell Physiol* **2010,** 222, 738-47.

149. Boini, K. M.; Xia, M.; Abais, J. M.; Li, G.; Pitzer, A. L.; Gehr, T. W.; Zhang, Y.; Li, P. L. Activation of inflammasomes in podocyte injury of mice on the high fat diet: Effects of ASC gene deletion and silencing. *Biochim Biophys Acta* **2014,** 1843, 836-45.

150. Fernandes-Alnemri, T.; Wu, J.; Yu, J. W.; Datta, P.; Miller, B.; Jankowski, W.; Rosenberg, S.; Zhang, J.; Alnemri, E. S. The pyroptosome: a supramolecular assembly of ASC dimers mediating inflammatory cell death via caspase-1 activation. *Cell Death Differ* **2007,** 14, 1590-604.

151. Lu, A.; Wu, H. Structural mechanisms of inflammasome assembly. *Febs j* **2014**.

152. Sutterwala, F. S.; Haasken, S.; Cassel, S. L. Mechanism of NLRP3 inflammasome activation. *Ann N Y Acad Sci* **2014,** 1319, 82-95.

153. Netea, M. G.; Nold-Petry, C. A.; Nold, M. F.; Joosten, L. A.; Opitz, B.; van der Meer, J. H.; van de Veerdonk, F. L.; Ferwerda, G.; Heinhuis, B.; Devesa, I.; Funk, C. J.; Mason, R. J.; Kullberg, B. J.; Rubartelli, A.; van der Meer, J. W.; Dinarello, C. A. Differential requirement for the activation of the inflammasome for processing and release of IL-1beta in monocytes and macrophages. *Blood* **2009,** 113, 2324-35.

154. Piccini, A.; Carta, S.; Tassi, S.; Lasiglie, D.; Fossati, G.; Rubartelli, A. ATP is released by monocytes stimulated with pathogen-sensing receptor ligands and induces IL-1beta and IL-18 secretion in an autocrine way. *Proc Natl Acad Sci U S A* **2008,** 105, 8067-72.

155. Asgari, E.; Le Friec, G.; Yamamoto, H.; Perucha, E.; Sacks, S. S.; Kohl, J.; Cook, H. T.; Kemper, C. C3a modulates IL-1beta secretion in human monocytes by regulating ATP efflux and subsequent NLRP3 inflammasome activation. *Blood* **2013,** 122, 3473-81.

156. Sharma, A. A.; Jen, R.; Kan, B.; Sharma, A.; Marchant, E.; Tang, A.; Gadawski, I.; Senger, C.; Skoll, A.; Turvey, S. E.; Sly, L. M.; Cote, H. C.; Lavoie, P. M. Impaired NLRP3 inflammasome activity during fetal development regulates IL-1beta production in human monocytes. *Eur J Immunol* **2014**.

157. Liao, P. C.; Chao, L. K.; Chou, J. C.; Dong, W. C.; Lin, C. N.; Lin, C. Y.; Chen, A.; Ka, S. M.; Ho, C. L.; Hua, K. F. Lipopolysaccharide/adenosine triphosphate-mediated signal transduction in the regulation of NLRP3 protein expression and caspase-1-mediated interleukin-1beta secretion. *Inflamm Res* **2013,** 62, 89-96.

158. Choi, A. J.; Ryter, S. W. Inflammasomes: molecular regulation and implications for metabolic and cognitive diseases. *Mol Cells* **2014,** 37, 441-8.

159. Heneka, M. T.; Kummer, M. P.; Latz, E. Innate immune activation in neurodegenerative disease. *Nat Rev Immunol* **2014,** 14, 463-77.

160. Glass, C. K.; Saijo, K.; Winner, B.; Marchetto, M. C.; Gage, F. H. Mechanisms underlying inflammation in neurodegeneration. *Cell* **2010,** 140, 918-34.

161. Esser, N.; Legrand-Poels, S.; Piette, J.; Scheen, A. J.; Paquot, N. Inflammation as a link between obesity, metabolic syndrome and type 2 diabetes. *Diabetes Res Clin Pract* **2014,** 105, 141-50.

162. Akama, K. T.; Van Eldik, L. J. Beta-amyloid stimulation of inducible nitric-oxide synthase in astrocytes is interleukin-1beta- and tumor necrosis factor-alpha (TNFalpha)-dependent, and involves a TNFalpha receptor-associated factor- and NFkappaB-inducing kinase-dependent signaling mechanism. *J Biol Chem* **2000,** 275, 7918-24.

163. Halle, A.; Hornung, V.; Petzold, G. C.; Stewart, C. R.; Monks, B. G.; Reinheckel, T.; Fitzgerald, K. A.; Latz, E.; Moore, K. J.; Golenbock, D. T. The NALP3 inflammasome is involved in the innate immune response to amyloid-beta. *Nat Immunol* **2008,** 9, 857-65.

164. Heneka, M. T.; Kummer, M. P.; Stutz, A.; Delekate, A.; Schwartz, S.; Vieira-Saecker, A.; Griep, A.; Axt, D.; Remus, A.; Tzeng, T. C.; Gelpi, E.; Halle, A.; Korte, M.; Latz, E.; Golenbock, D. T. NLRP3 is activated in Alzheimer's disease and contributes to pathology in APP/PS1 mice. *Nature* **2013,** 493, 674-8.

165. Simons, J. P.; Baril, D. T.; Goodney, P. P.; Bertges, D. J.; Robinson, W. P.; Cronenwett, J. L.; Messina, L. M.; Schanzer, A. The effect of postoperative myocardial ischemia on long-term survival after vascular surgery. *J Vasc Surg* **2013,** 58, 1600-8.

166. Christia, P.; Frangogiannis, N. G. Targeting inflammatory pathways in myocardial infarction. *Eur J Clin Invest* **2013,** 43, 986-95.

167. Kawaguchi, M.; Takahashi, M.; Hata, T.; Kashima, Y.; Usui, F.; Morimoto, H.; Izawa, A.; Takahashi, Y.; Masumoto, J.; Koyama, J.; Hongo, M.; Noda, T.; Nakayama, J.; Sagara, J.; Taniguchi, S.; Ikeda, U. Inflammasome activation of cardiac fibroblasts is essential for myocardial ischemia/reperfusion injury. *Circulation* **2011,** 123, 594-604.

168. Pomerantz, B. J.; Reznikov, L. L.; Harken, A. H.; Dinarello, C. A. Inhibition of caspase 1 reduces human myocardial ischemic dysfunction via inhibition of IL-18 and IL-1beta. *Proc Natl Acad Sci U S A* **2001,** 98, 2871-6.

169. Hwang, M. W.; Matsumori, A.; Furukawa, Y.; Ono, K.; Okada, M.; Iwasaki, A.; Hara, M.; Miyamoto, T.; Touma, M.; Sasayama, S. Neutralization of interleukin-1beta in the acute phase of myocardial infarction promotes the progression of left ventricular remodeling. *J Am Coll Cardiol* **2001,** 38, 1546-53.

170. Suzuki, K.; Murtuza, B.; Smolenski, R. T.; Sammut, I. A.; Suzuki, N.; Kaneda, Y.; Yacoub, M. H. Overexpression of interleukin-1 receptor antagonist provides cardioprotection against ischemia-reperfusion injury associated with reduction in apoptosis. *Circulation* **2001,** 104, I308-i3.

171. Abbate, A.; Van Tassell, B. W.; Seropian, I. M.; Toldo, S.; Robati, R.; Varma, A.; Salloum, F. N.; Smithson, L.; Dinarello, C. A. Interleukin-1beta modulation using a genetically engineered antibody prevents adverse cardiac remodelling following acute myocardial infarction in the mouse. *Eur J Heart Fail* **2010,** 12, 319-22.

172. Lenhart, J. A.; Ling, X.; Gandhi, R.; Guo, T. L.; Gerk, P. M.; Brunzell, D. H.; Zhang, S. "Clicked" bivalent ligands containing curcumin and cholesterol as multifunctional abeta oligomerization inhibitors: design, synthesis, and biological characterization. *J Med Chem* **2010,** 53, 6198-209.

173. Liu, K.; Guo, T. L.; Chojnacki, J.; Lee, H. G.; Wang, X.; Siedlak, S. L.; Rao, W.; Zhu, X.; Zhang, S. Bivalent ligand containing curcumin and cholesterol as fluorescence probe for Abeta plaques in Alzheimer's disease. *ACS Chem Neurosci* **2012,** 3, 141-146.

174. Liu, K.; Gandhi, R.; Chen, J.; Zhang, S. Bivalent ligands targeting multiple pathological factors involved in Alzheimer's disease. *ACS Med Chem Lett* **2012,** 3, 942-946.

175. Viegas-Junior, C.; Danuello, A.; da Silva Bolzani, V.; Barreiro, E. J.; Fraga, C. A. Molecular hybridization: a useful tool in the design of new drug prototypes. *Curr Med Chem* **2007,** 14, 1829-52.

176. Govindarajan, V. S. Turmeric--chemistry, technology, and quality. *Crit. Rev. Food Sci. Nutr.* **1980,** 12, 199-301.

177. Frautschy, S. A.; Cole, G. M. Why pleiotropic interventions are needed for Alzheimer's disease. *Mol. Neurobiol.* **2010,** 41, 392-409.

178. Hatcher, H.; Planalp, R.; Cho, J.; Torti, F. M.; Torti, S. V. Curcumin: from ancient medicine to current clinical trials. *Cell. Mol. Life Sci.* **2008,** 65, 1631-52.

179. Papadopoulos, V.; Lecanu, L. Caprospinol: discovery of a steroid drug candidate to treat Alzheimer's disease based on 22R-hydroxycholesterol structure and properties. *J Neuroendocrinol* **2012,** 24, 93-101.

180. Lecanu, L.; Yao, W.; Teper, G. L.; Yao, Z. X.; Greeson, J.; Papadopoulos, V. Identification of naturally occurring spirostenols preventing beta-amyloid-induced neurotoxicity. *Steroids* **2004,** 69, 1-16.

181. Dixon, R.; Furutachi, T.; Lieberman, S. The isolation of crystalline 22R-hydroxycholesterol and 20 alpha, 22R-dihydroxycholesterol from bovine adrenals. *Biochem Biophys Res Commun* **1970,** 40, 161-5.

182. Yao, Z. X.; Brown, R. C.; Teper, G.; Greeson, J.; Papadopoulos, V. 22R-Hydroxycholesterol protects neuronal cells from beta-amyloid-induced cytotoxicity by binding to beta-amyloid peptide. *J Neurochem* **2002,** 83, 1110-9.

183. Portoghese, P. S. From models to molecules: opioid receptor dimers, bivalent ligands, and selective opioid receptor probes. *J Med Chem* **2001,** 44, 2259-69.

184. Arnatt, C. K.; Zhang, Y. Bivalent ligands targeting chemokine receptor dimerization: molecular design and functional studies. *Curr Top Med Chem* **2014,** 14, 1606-18.

185. Akgun, E.; Javed, M. I.; Lunzer, M. M.; Smeester, B. A.; Beitz, A. J.; Portoghese, P. S. Ligands that interact with putative MOR-mGluR5 heteromer in mice with inflammatory pain produce potent antinociception. *Proc Natl Acad Sci U S A* **2013,** 110, 11595-9.

186. Cavalli, A.; Bolognesi, M. L.; Minarini, A.; Rosini, M.; Tumiatti, V.; Recanatini, M.; Melchiorre, C. Multi-target-directed ligands to combat neurodegenerative diseases. *J Med Chem* **2008,** 51, 347-72.

187. Staudinger, H.; Meyer, J. Über neue organische Phosphorverbindungen III. Phosphinmethylenderivate und Phosphinimine. *Helvetica Chimica Acta* **1919,** 2, 635-646.

188. Neises, B.; Steglich, W. Simple Method for the Esterification of Carboxylic Acids. *Angewandte Chemie International Edition in English* **1978,** 17, 522-524.

189. Sopher, B. L.; Fukuchi, K.; Kavanagh, T. J.; Furlong, C. E.; Martin, G. M. Neurodegenerative mechanisms in Alzheimer disease. A role for oxidative damage in amyloid beta protein precursor-mediated cell death. *Mol Chem Neuropathol* **1996,** 29, 153-68.

190. Maezawa, I.; Hong, H. S.; Wu, H. C.; Battina, S. K.; Rana, S.; Iwamoto, T.; Radke, G. A.; Pettersson, E.; Martin, G. M.; Hua, D. H.; Jin, L. W. A novel tricyclic pyrone compound ameliorates cell death associated with intracellular amyloid-beta oligomeric complexes. *J Neurochem* **2006,** 98, 57-67.

191. Hong, H. S.; Maezawa, I.; Yao, N.; Xu, B.; Diaz-Avalos, R.; Rana, S.; Hua, D. H.; Cheng, R. H.; Lam, K. S.; Jin, L. W. Combining the rapid MTT formazan exocytosis assay and the MC65 protection assay led to the discovery of carbazole analogs as small molecule inhibitors of Abeta oligomer-induced cytotoxicity. *Brain Res* **2007,** 1130, 223-34.

192. Gomes, A.; Fernandes, E.; Lima, J. L. Fluorescence probes used for detection of reactive oxygen species. *J Biochem Biophys Methods* **2005,** 65, 45-80.

193. Kim, J.; Lee, H. J.; Lee, K. W. Naturally occurring phytochemicals for the prevention of Alzheimer's disease. *J Neurochem* **2010,** 112, 1415-30.

194. Yang, F.; Lim, G. P.; Begum, A. N.; Ubeda, O. J.; Simmons, M. R.; Ambegaokar, S. S.; Chen, P. P.; Kayed, R.; Glabe, C. G.; Frautschy, S. A.; Cole, G. M. Curcumin inhibits formation of amyloid beta oligomers and fibrils, binds plaques, and reduces amyloid in vivo. *J Biol Chem* **2005,** 280, 5892-901.

195. Frautschy, S. A.; Cole, G. M. Why pleiotropic interventions are needed for Alzheimer's disease. *Mol Neurobiol* **2010,** 41, 392-409.

196. Pevet, P. Melatonin and biological rhythms. *Biol Signals Recept* **2000,** 9, 203-12.

197. Rosales-Corral, S. A.; Acuna-Castroviejo, D.; Coto-Montes, A.; Boga, J. A.; Manchester, L. C.; Fuentes-Broto, L.; Korkmaz, A.; Ma, S.; Tan, D. X.; Reiter, R. J. Alzheimer's disease: pathological mechanisms and the beneficial role of melatonin. *J Pineal Res* **2012,** 52, 167-202.

198. Carpentieri, A.; Diaz de Barboza, G.; Areco, V.; Peralta Lopez, M.; Tolosa de Talamoni, N. New perspectives in melatonin uses. *Pharmacol Res* **2012,** 65, 437-44.

199. Zhou, J. N.; Liu, R. Y.; Kamphorst, W.; Hofman, M. A.; Swaab, D. F. Early neuropathological Alzheimer's changes in aged individuals are accompanied by decreased cerebrospinal fluid melatonin levels. *J Pineal Res* **2003,** 35, 125-30.

200. Hatfield, C. F.; Herbert, J.; van Someren, E. J.; Hodges, J. R.; Hastings, M. H. Disrupted daily activity/rest cycles in relation to daily cortisol rhythms of home-dwelling patients with early Alzheimer's dementia. *Brain* **2004,** 127, 1061-74.

201. Pandi-Perumal, S. R.; BaHammam, A. S.; Brown, G. M.; Spence, D. W.; Bharti, V. K.; Kaur, C.; Hardeland, R.; Cardinali, D. P. Melatonin antioxidative defense: therapeutical implications for aging and neurodegenerative processes. *Neurotox Res* **2013,** 23, 267-300.

202. Wang, X. The antiapoptotic activity of melatonin in neurodegenerative diseases. *CNS Neurosci Ther* **2009,** 15, 345-57.

203. Rosales-Corral, S.; Acuna-Castroviejo, D.; Tan, D. X.; Lopez-Armas, G.; Cruz-Ramos, J.; Munoz, R.; Melnikov, V. G.; Manchester, L. C.; Reiter, R. J. Accumulation of exogenous amyloid-beta peptide in hippocampal mitochondria causes their dysfunction: a protective role for melatonin. *Oxid Med Cell Longev* **2012,** 2012, 843649.

204. Hardeland, R. Melatonin in aging and disease -multiple consequences of reduced secretion, options and limits of treatment. *Aging Dis* **2012,** 3, 194-225.

205. Lane, E. A.; Moss, H. B. Pharmacokinetics of melatonin in man: first pass hepatic metabolism. *J Clin Endocrinol Metab* **1985,** 61, 1214-6.

206. Wittig, G.; Geissler, G. Zur Reaktionsweise des Pentaphenyl-phosphors und einiger Derivate. *Justus Liebigs Annalen der Chemie* **1953,** 580, 44-57.

207. Chojnacki, J. E.; Liu, K.; Yan, X.; Toldo, S.; Selden, T.; Estrada, M.; Rodriguez-Franco, M. I.; Halquist, M. S.; Ye, D.; Zhang, S. Discovery of 5-(4-hydroxyphenyl)-3-oxo-pentanoic acid [2-(5-methoxy-1H-indol-3-yl)-ethyl]-amide as a neuroprotectant for Alzheimer's disease by hybridization of curcumin and melatonin. *ACS Chem Neurosci* **2014,** 5, 690-9.

208. Bush, A. I. Drug development based on the metals hypothesis of Alzheimer's disease. *J Alzheimers Dis* **2008,** 15, 223-40.

209. Esatbeyoglu, T.; Huebbe, P.; Ernst, I. M.; Chin, D.; Wagner, A. E.; Rimbach, G. Curcumin--from molecule to biological function. *Angew Chem Int Ed Engl* **2012,** 51, 5308-32.

210. Aruoma, O. I.; Halliwell, B.; Hoey, B. M.; Butler, J. The antioxidant action of N-acetylcysteine: its reaction with hydrogen peroxide, hydroxyl radical, superoxide, and hypochlorous acid. *Free Radic Biol Med* **1989,** 6, 593-7.

211. Atkuri, K. R.; Mantovani, J. J.; Herzenberg, L. A.; Herzenberg, L. A. N-Acetylcysteine--a safe antidote for cysteine/glutathione deficiency. *Curr Opin Pharmacol* **2007,** 7, 355-9.

212. McClain, D. E.; Kalinich, J. F.; Ramakrishnan, N. Trolox inhibits apoptosis in irradiated MOLT-4 lymphocytes. *Faseb j* **1995,** 9, 1345-54.

213. Ishimura, A.; Ishige, K.; Taira, T.; Shimba, S.; Ono, S.; Ariga, H.; Tezuka, M.; Ito, Y. Comparative study of hydrogen peroxide- and 4-hydroxy-2-nonenal-induced cell death in HT22 cells. *Neurochem Int* **2008,** 52, 776-85.

214. Lezoualc'h, F.; Skutella, T.; Widmann, M.; Behl, C. Melatonin prevents oxidative stress-induced cell death in hippocampal cells. *Neuroreport* **1996,** 7, 2071-7.

215. Hirst, J.; King, M. S.; Pryde, K. R. The production of reactive oxygen species by complex I. *Biochem Soc Trans* **2008,** 36, 976-80.

216. Reale, M.; Pesce, M.; Priyadarshini, M.; Kamal, M. A.; Patruno, A. Mitochondria as an easy target to oxidative stress events in Parkinson's disease. *CNS Neurol Disord Drug Targets* **2012,** 11, 430-8.

217. Martin, L. J. Olesoxime, a cholesterol-like neuroprotectant for the potential treatment of amyotrophic lateral sclerosis. *IDrugs* **2010,** 13, 568-80.

218. Nazarewicz, R. R.; Dikalova, A.; Bikineyeva, A.; Ivanov, S.; Kirilyuk, I. A.; Grigor'ev, I. A.; Dikalov, S. I. Does scavenging of mitochondrial superoxide attenuate cancer prosurvival signaling pathways? *Antioxid Redox Signal* **2013,** 19, 344-9.

219. De Felice, F. G.; Wu, D.; Lambert, M. P.; Fernandez, S. J.; Velasco, P. T.; Lacor, P. N.; Bigio, E. H.; Jerecic, J.; Acton, P. J.; Shughrue, P. J.; Chen-Dodson, E.; Kinney, G. G.; Klein, W. L. Alzheimer's

disease-type neuronal tau hyperphosphorylation induced by A beta oligomers. *Neurobiol Aging* **2008,** 29, 1334-47.

220. Jin, M.; Shepardson, N.; Yang, T.; Chen, G.; Walsh, D.; Selkoe, D. J. Soluble amyloid beta-protein dimers isolated from Alzheimer cortex directly induce Tau hyperphosphorylation and neuritic degeneration. *Proc Natl Acad Sci U S A* **2011,** 108, 5819-24.

221. Aumuller, W.; Bander, A.; Heerdt, R.; Muth, K.; Pfaff, W.; Schmidt, F. H.; Weber, H.; Weyer, R. [A new highly-active oral antidiabetic]. *Arzneimittelforschung* **1966,** 16, 1640-1.

222. Prendergast, B. D. Glyburide and glipizide, second-generation oral sulfonylurea hypoglycemic agents. *Clin Pharm* **1984,** 3, 473-85.

223. Nieland, T. J.; Chroni, A.; Fitzgerald, M. L.; Maliga, Z.; Zannis, V. I.; Kirchhausen, T.; Krieger, M. Cross-inhibition of SR-BI- and ABCA1-mediated cholesterol transport by the small molecules BLT-4 and glyburide. *J Lipid Res* **2004,** 45, 1256-65.

224. Terao, Y.; Ayaori, M.; Ogura, M.; Yakushiji, E.; Uto-Kondo, H.; Hisada, T.; Ozasa, H.; Takiguchi, S.; Nakaya, K.; Sasaki, M.; Komatsu, T.; Iizuka, M.; Horii, S.; Mochizuki, S.; Yoshimura, M.; Ikewaki, K. Effect of sulfonylurea agents on reverse cholesterol transport in vitro and vivo. *J Atheroscler Thromb* **2011,** 18, 513-30.

225. Koh, G. C.; Maude, R. R.; Schreiber, M. F.; Limmathurotsakul, D.; Wiersinga, W. J.; Wuthiekanun, V.; Lee, S. J.; Mahavanakul, W.; Chaowagul, W.; Chierakul, W.; White, N. J.; van der Poll, T.; Day, N. P.; Dougan, G.; Peacock, S. J. Glyburide is anti-inflammatory and associated with reduced mortality in melioidosis. *Clin Infect Dis* **2011,** 52, 717-25.

226. Hamon, Y.; Luciani, M. F.; Becq, F.; Verrier, B.; Rubartelli, A.; Chimini, G. Interleukin-1beta secretion is impaired by inhibitors of the Atp binding cassette transporter, ABC1. *Blood* **1997,** 90, 2911-5.

227. Lamkanfi, M.; Mueller, J. L.; Vitari, A. C.; Misaghi, S.; Fedorova, A.; Deshayes, K.; Lee, W. P.; Hoffman, H. M.; Dixit, V. M. Glyburide inhibits the Cryopyrin/Nalp3 inflammasome. *J Cell Biol* **2009,** 187, 61-70.

228. Marchetti, C.; Chojnacki, J.; Toldo, S.; Mezzaroma, E.; Tranchida, N.; Rose, S. W.; Federici, M.; Van Tassell, B. W.; Zhang, S.; Abbate, A. A novel pharmacologic inhibitor of the NLRP3 inflammasome limits myocardial injury after ischemia-reperfusion in the mouse. *J Cardiovasc Pharmacol* **2014,** 63, 316-22.

229. Strowig, T.; Henao-Mejia, J.; Elinav, E.; Flavell, R. Inflammasomes in health and disease. *Nature* **2012,** 481, 278-86.

230. Stine, W. B., Jr.; Dahlgren, K. N.; Krafft, G. A.; LaDu, M. J. In vitro characterization of conditions for amyloid-beta peptide oligomerization and fibrillogenesis. *J Biol Chem* **2003,** 278, 11612-22.

231. Claycomb, W. C.; Lanson, N. A., Jr.; Stallworth, B. S.; Egeland, D. B.; Delcarpio, J. B.; Bahinski, A.; Izzo, N. J., Jr. HL-1 cells: a cardiac muscle cell line that contracts and retains phenotypic characteristics of the adult cardiomyocyte. *Proc Natl Acad Sci U S A* **1998,** 95, 2979-84.

232. Toldo, S.; Seropian, I. M.; Mezzaroma, E.; Van Tassell, B. W.; Salloum, F. N.; Lewis, E. C.; Voelkel, N.; Dinarello, C. A.; Abbate, A. Alpha-1 antitrypsin inhibits caspase-1 and protects from acute myocardial ischemia-reperfusion injury. *J Mol Cell Cardiol* **2011,** 51, 244-51.

Vita

Jeremy Edward Chojnacki was born February 15, 1986 in Portsmouth, Virginia to parents, John and Rebecca Chojnacki. He spent his childhood in Chesapeake, Virginia, where he graduated from Deep Creek High School in 2004. From there, he attended Virginia Polytechnic and State University, eventually earning his bachelor of science in chemical engineering with a minor in chemistry in 2009. He joined the Department of Medicinal Chemistry at Virginia Commonwealth University in the fall of 2010 to pursue his Ph.D. He is first author of two publications and holds co-authorship on three additional publications. In 2011, he was the recipient of the Werner Lowenthal Award, given for his research in the area of genetically-based neurodegenerative disorders. In 2014, he was awarded the prestigious J. Doyle Smith Award, for excellence and distinction in the Department of Medicinal Chemistry.